NON-LINEAR ANALYSIS

OF

REINFORCED CONCRETE

PLANE FRAMES

BY

JONN MARK KENYON

B.E.(Adel.)

A THESIS SUBMITTED FOR THE DEGREE OF

DOCTOR OF PHILOSOPHY

University of Adelaide

Department of Civil and Environmental Engineering

Australia

November 1993

To my maternal grandparents :

Harold John Hynes (1900-1979)

and

Marie Eleanor Hynes (1904-1993)

Contents

List of Figures

List of Tables

ABSTRACT

An investigation has been made of an existing non-linear method of analysis for reinforced concrete frames which takes into account material and geometric non-linearities. To check the adequacy and accuracy of this method, comparisons have been made between analytical results and published results for test beams and frames.

Although poor correlation was achieved in some cases it was also noted that additional effects due to tension stiffening and joint flexibility had not been taken into account. Analytic models for these effects have proposed and incorporated in the non-linear method of frame analysis. The method of analysis has also been modified to allow for sequential non-proportional loading, as well as proportional loading. Good correlation has been achieved between analytical results and test data.

An analytical study of frames using the improved method of analysis has shown that tension stiffening has a beneficial effect on stiffness, and a minor influence on strength. However, frame performance is highly dependent on the nature of the joint detailing. Flexibility and reduction of strength in joints can adversely affect both frame behaviour under load and load capacity. A study of several multi-storey frames for proportional and non-proportional loading has shown that stiffness can be influenced by the method of load application.

The accurate method of analysis has also been used to check the adequacy of the simplified analysis and design procedures for slender columns of the Australian Standard AS 3600. A series of unbraced sway frames were investigated by the bottom-tier moment magnifier method and a middle-tier second order elastic approach. The simplified approaches were found to give quite conservative results.

Several isolated pin-ended columns were analysed by the moment magnifier method and also by a method of analysis for columns in non-sway frames mentioned in the draft code Eurocode 2. Both these bottom-tier approaches gave accurate results for

column capacities for stocky columns. Results for slender columns were more conservative.

STATEMENT OF ORIGINALITY

This work contains no material which has been accepted for the award of any other degree or diploma in any university or other tertiary institution and, to the best of my knowledge and belief, contains no material previously published or written by another person, except where due reference has been made in the text.

I give consent to this copy of my thesis, when deposited in the University Library, being available for loan and photocopying.

SIGNED:.   DATE:....12/11/93

The work undertaken in this thesis marks the end of a 3 year commitment under the supervision of Professor Robert F. Warner at the University of Adelaide. The author wishes to acknowledge the steadfast guidance and direction given by Prof. Warner throughout the research project. The author also wishes to thank Prof. Warner for his continual interest and his advice and suggestions in the review of the thesis.

Special thanks must be given to the Departmental Computing Officers for their invaluable advice from consultations. The author wishes also to commend the sharing of knowledge with fellow postgraduates.

Finally, the author wishes to give praise to two special people. He is deeply indebted to his wife Fiona and daughter Chantel Simone for their love and support throughout this project. Their continual encouragement has made an enormous difference during the difficult times.

Chapter 1

Introduction

1.1 Background

Non-linear behaviour of reinforced concrete frames is evident at all stages of loading,
including the working load range and up to the high overload levels. To study this
behaviour, accurate, rigorous methods of analysis must be developed, which serve an
additional important purpose: results from non-linear analyses can be used to calibrate
the more popular simplified linear elastic methods.

Essential to the development of a non-linear method of frame analysis are material
stress-strain relationships and experimental results for individual frame components,
i.e. beams, columns and beam-column connections. This allows for the development
of individual numerical models which also form the basis for a general method of
frame analysis. Hence, the influence of the non-linear behaviour of these components
on overall frame performance can be studied.

1.2   Objectives and Scope

Described in this thesis is an investigation of the accuracy and adequacy of a non-linear method of frame analysis, SAFRAME, proposed earlier by Wong (1989). Advantages of this method, in terms of computational efficiency and storage requirements, are discussed, and comparisons with experimental results are made. In particular, where poor correlation was achieved it was noted that additional non-linear effects, due to tension stiffening and deformations within beam-column joints, were not taken into account in the method of analysis. To study the influence of these non-linear effects on frame behaviour, the following work has been undertaken in the present study:

1. a study for the behaviour of flexural (beam) elements and isolated beam-column connections and the performance of various test frames.

2. modifications to SAFRAME to include analytic models for tension stiffening in the beam elements, deformations in the beam-column joints, and sequential non-proportional application of the vertical and horizontal loads.

3. a study of unbraced slender frames for non-linear behaviour, including the influence of the non-linear effects mentioned at point 2. Analysis for post-peak behaviour and modes of frame failure were investigated.

4. an investigation of the adequacy and accuracy of the simplified methods for analysis and design of slender columns in AS 3600.

1.3   Layout and Content of Thesis

Chapter 2 is a review of non-linear methods of analysis for reinforced concrete frames. Included in this review are details of a segmental method of frame analysis proposed

by Wong (1989). Comparisons with test data are made and suggested improvements to this method are discussed. These areas of improvement also form the basis for investigations of reinforced concrete test beams and frames in Chapters 3, 4 and 5.

Tension stiffening is described in Chapter 3 and, following a review of previous methods, a model for tension stiffening in flexural elements is proposed. This model has been incorporated in the segmental method of analysis and a study of the behaviour of various single span and two-span beams is carried out.

Chapter 4 investigates the performance of isolated L-, T-, and X-joints for various types of detailing. A simplified model to predict the reduction in strength and stiffness of opening L-joints and top floor T-joints is proposed.

In Chapter 5, a method for non-proportional loading is developed. The validity of this method is checked by comparing analytical predictions and experimental results for a number of test frames. Typically, a set of vertical loads is applied to the structure, followed by horizontal loading to failure.

Chapter 6 investigates the accuracy and adequacy of the moment magnifier method and the second order elastic method of AS 3600. Various sway frames are analysed by these simplified methods and results are compared with results determined from rigorous non-linear analyses. The effects of tension stiffening and joint flexibility are also investigated in a number of single storey frames.

In most real situations, dead loads are applied to the structure followed by the application of horizontal wind loads. The assumption of applying these loads proportionally is checked in Chapter 6 in a study of several multi-storey frames. Results from non-linear analyses with proportional loading are compared with predictions assuming non-proportional loading.

Several isolated pin-ended columns are also analysed by two simplified approaches in Chapter 6. Predicted column capacities by the moment magnifier method are compared with predictions made by a method described in the draft Eurocode 2.

A number of conclusions are drawn from the work carried out in the present study and are summarised in Chapter 7. Recommendations for further work are also outlined in Chapter 7.

Chapter 2

Non-linear Methods of Frame Analysis

2.1 Introduction

In this chapter, various non-linear methods of analysis for reinforced concrete frames are reviewed. The two sources of non-linearity, material and geometric effects, are described in general terms in Section 2.2. As sectional behaviour depends on the level of moment and axial thrust, procedures for developing M-κ-N relations are discussed in Section 2.3.

Techniques for solving the load-displacement relations are described in Section 2.4, and analytical procedures for frame behaviour beyond the peak load are described in Section 2.5. Although the behaviour of reinforced concrete is influenced by creep, shrinkage and thermal effects, these are outside the scope of the present study. The review of methods of frame analysis for material effects in Section 2.6 and for

5

geometric effects in Section 2.7 assumes the load application is short term, proportional and static.

Section 2.8 reviews a segmental method of frame analysis proposed by Wong (1989). Computational time and storage requirements are discussed and comparisons are made between analytical and experimental results.

2.2   Non-linearities

2.2.1   Material Non-linearity

Non-linear material effects in reinforced concrete are attributed to the stress-strain relationships for concrete and the reinforcing steel and also the bond breakdown between steel and concrete. Although behaviour at sections within frames is often characterised by multiaxial stress conditions, it is usual for non-linear frame analysis to predict behaviour by assuming uniaxial stress-strain relationships. These may also take into account the effect of confinement by reinforcing stirrups.

Most often an elasto-plastic stress-strain relationship describes the tensile and compressive behaviour of reinforcing steel. Strain hardening at higher strains is allowed for by including further linear or curvilinear segments. Stress-strain relationships for uniaxial compressive concrete have been proposed by various investigators and will be mentioned in this chapter where appropriate. In addition, stress-strain curves have been developed for tensile concrete in the vicinity of cracks, but these will be discussed in Chapter 3, Tension Stiffening.

2.2.2   Geometric Non-linearity

A second type of non-linearity which influences frame behaviour is due to geometric effects. As a frame deforms under increasing load, changes in geometry may induce additional second order moments within members. These changes in geometry may be

due to the movement at the ends of columns and also lateral deflections within the length of columns. Non-linear geometric effects in a slender column may lead to a stability failure which can occur well before material strength has been reached.

2.3 Moment-Curvature-Thrust Relations

2.3.1 Methods for Determining Moment-Curvature-Thrust Relations

When reinforced concrete framed structures are subjected to increasing levels of load, the flexural behaviour at sections within the structure is determined from moment-curvature-thrust relations. The development of these theoretical $(M - \kappa - N)$ curves is based on assumed stress-strain curves for concrete and steel and a linear distribution of strain at each section. Usually, the influence of shear deformations is ignored and a uniaxial stress-strain relationship is used. Figure 2.1 shows a rectangular section of width, b, and depth, D, subjected to a moment and thrust. A linear strain distribution is assumed to exist across the section and the internal actions, thrust, N, and moment, M, are found by solving Equations 2.1 and 2.2.
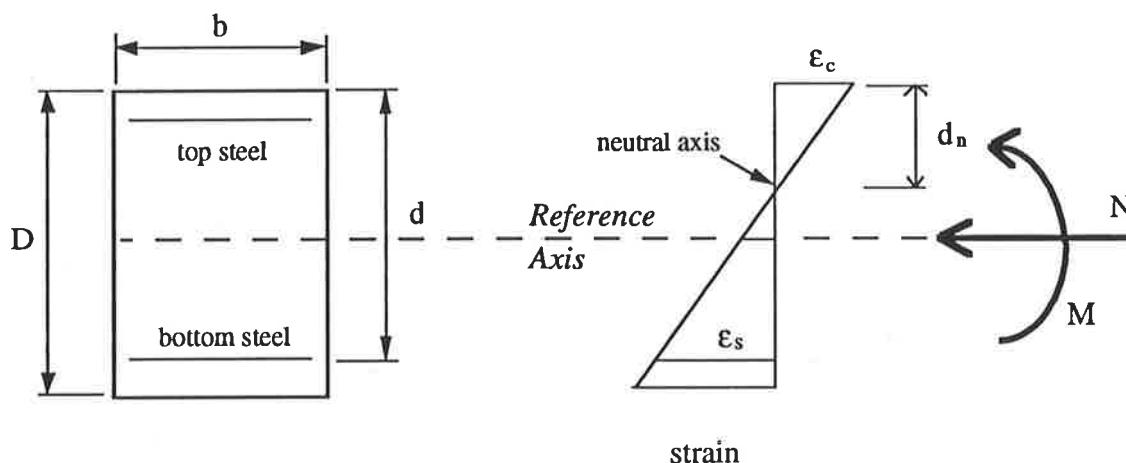
Figure 2.1: Assumed strain distribution for rectangular section subjected to moment and axial thrust

$$N = b \int_0^y \sigma(y)dy \qquad (2.1)$$

$$M = b \int_0^y \sigma(y)ydy \qquad (2.2)$$

From Figure 2.1, curvature is related to strain by the following expression:

$$\kappa = \frac{\varepsilon_c}{d_n} = \frac{\varepsilon_c + \varepsilon_s}{d} \qquad (2.3)$$

For a given strain distribution, Equations 2.1 and 2.2 are solved by one of two methods:

(1) Direct integration
(2) Integration using numerical techniques

The early approach by Broms and Viest (1958) involves direct integration to yield analytical expressions for moment and axial force in a rectangular section. Based on these expressions, Pfrang *et al.* (1964) obtained moment-curvature-thrust relations, which were also used in a frames study by Breen (1964).

Kroenke *et al.* (1973) extended the approach by Broms and Viest (1958) to allow for the more general case of unequal areas of unsymmetrically placed compression and tension steel. The strain hardening portion of the steel stress-strain curve was also included. Berwanger (1975) found from experimental results that strain hardening can have a significant effect on the load carrying capacity of columns.

Figure 2.2 shows the assumed strain distribution used by Kroenke *et al.*, with concrete strains ε_1 and ε_4 and the steel strains ε_2 and ε_3. The stress-strain relationship for concrete proposed by Hognestad (1951) and shown in Figure 2.3 is also used.
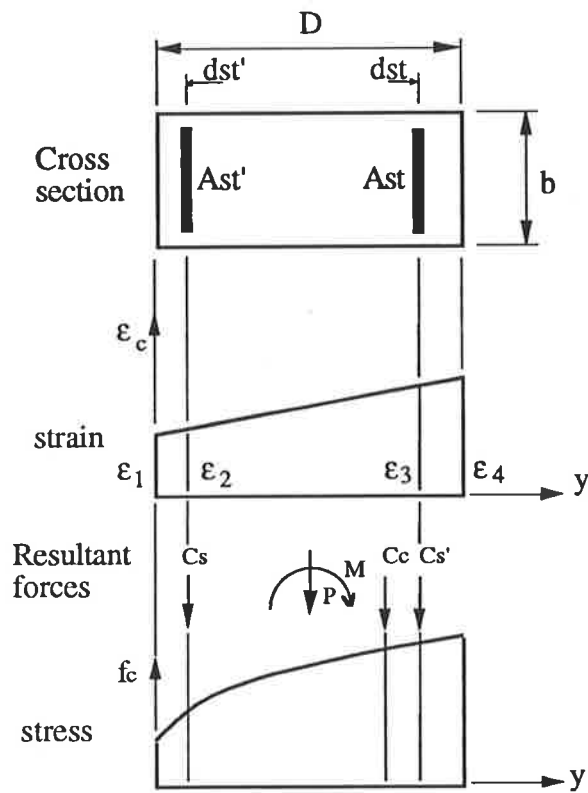
Figure 2.2: Cross-section with strain and stress configurations (Kroenke *et al.*, 1973)
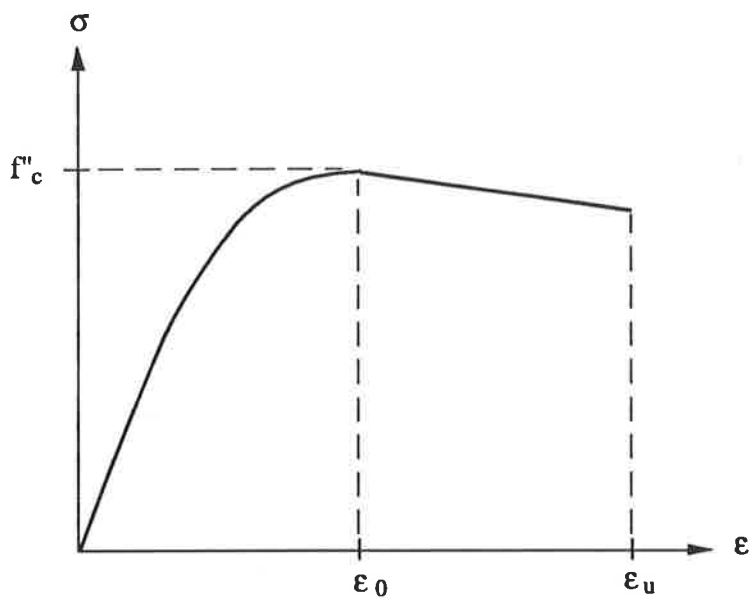
Figure 2.3: Stress-strain relationship for concrete proposed by Hognestad (1951)

Depending on the level of concrete strain, concrete compressive stress in Hognestad's model is evaluated from either of the following expressions:

$$f_c = f_c'' \left[2\frac{\varepsilon_c}{\varepsilon_o} - \left(\frac{\varepsilon_c}{\varepsilon_o}\right)^2 \right] \quad \text{for } 0 \leq \varepsilon_c \leq \varepsilon_o \tag{2.4}$$

$$f_c = f_c'' \left[1 - 0.15\left(\frac{\varepsilon_c - \varepsilon_o}{\varepsilon_u - \varepsilon_o}\right) \right] \quad \text{for } \varepsilon_o < \varepsilon_c \leq \varepsilon_u \tag{2.5}$$

where ε_o is the concrete strain corresponding to maximum stress and equal to 0.002; ε_u is the ultimate concrete strain and equal to 0.0038; $f''_c = f'_c =$ ultimate concrete compressive strength; $f_c =$ stress in concrete; and $\varepsilon_c =$ strain in concrete. The stress-strain curve includes the following keypoints:

$$f_s = E_s \varepsilon_s \quad \text{for} \quad 0 \leq \varepsilon_s \leq \varepsilon_y \tag{2.6}$$

$$f_s = f_y \quad \text{for} \quad \varepsilon_y < \varepsilon_s \leq \varepsilon_{SH} \tag{2.7}$$

$$f_s = E_s \varepsilon_y + E_{SH}(\varepsilon_s - \varepsilon_{SH}) \quad \text{for} \quad \varepsilon_{SH} < \varepsilon_s \tag{2.8}$$

where f_s and ε_s are the stress and strain in the steel; f_y and ε_y are the yield stress and yield strain; ε_{SH} is the steel strain at the start of strain hardening, and greater than 0.0038; E_S is the elastic modulus of steel; and E_{SH} is the strain hardening modulus of steel.

To allow for ease of integration, strain distributions are divided into ten discrete regions. The four regions for the values of concrete strains ε_1 and ε_4, and shown in Figure 2.2, are given by:

1. Concrete Region 1 for $0 \leq \varepsilon_1 \leq \varepsilon_0$ and $0 \leq \varepsilon_4 < \varepsilon_0$
2. Concrete Region 2 for $\varepsilon_1 < 0$ and $0 \leq \varepsilon_4 < \varepsilon_0$
3. Concrete Region 3 for $0 \leq \varepsilon_1 \leq \varepsilon_0$ and $\varepsilon_0 \leq \varepsilon_4 \leq \varepsilon_u$
4. Concrete Region 4 for $\varepsilon_1 < 0$ and $\varepsilon_0 \leq \varepsilon_4 \leq \varepsilon_u$

Kroenke *et al.* defined the following six regions for the steel strains ε_2 and ε_3 shown in Figure 2.2:

1. Steel Region 1 for $\varepsilon_2 < \varepsilon_y$ and $\varepsilon_3 < \varepsilon_y$
2. Steel Region 2 for $\varepsilon_2 < \varepsilon_y$ and $\varepsilon_y \leq \varepsilon_3$
3. Steel Region 3 for $\varepsilon_y \leq \varepsilon_2 < \varepsilon_{SH}$ and $\varepsilon_3 < \varepsilon_y$
4. Steel Region 4 for $\varepsilon_y \leq \varepsilon_2 < \varepsilon_{SH}$ and $\varepsilon_y \leq \varepsilon_3$
5. Steel Region 5 for $\varepsilon_{SH} \leq \varepsilon_2$ and $\varepsilon_3 < \varepsilon_y$
6. Steel Region 6 for $\varepsilon_{SH} \leq \varepsilon_2$ and $\varepsilon_y \leq \varepsilon_3$

Expressions for the resultant concrete force, C_c, and its location in the section, $\bar{y}$, for each of the four concrete strain regions can be found in the paper by Kroenke *et al.* The total resultant axial force, P, on a cross-section is given by the sum of the resultant concrete force, C_c, and the force in each layer of steel, C_s and C'_s:

$$P = C_c + C_s + C'_s \qquad (2.9)$$

There are a number of disadvantages with this approach. Inelastic behaviour which can arise from strain reversal in the concrete and steel is not accounted for. The analytical expressions only apply to Hognestad's stress-strain relationship and the concrete is assumed to have no tensile capacity. Hence, the beneficial effect of tension stiffening is ignored. However, for ultimate strength calculations this may be a reasonable assumption.

Sved (1988) also proposed a method of direct integration to solve for the moment and curvature for a given axial force and concrete strain in the outermost (compressive) fibre. The stress-strain relationship for concrete is represented by cubic splines. Hence, any relationship can be used. The method involves developing expressions for the total compression force in the concrete, C_c, and the moment of the concrete forces, M_c, about the neutral axis.

Shown in Figure 2.4 is the stress-strain curve for concrete in compression, and moment and thrust is evaluated for the level of strain shown. The strain in the outermost fibre is ε_a and the depth to the neutral axis is Y, as shown in Figure 2.5. The strain axis is drawn vertically to a scale so that ε_a equals Y.
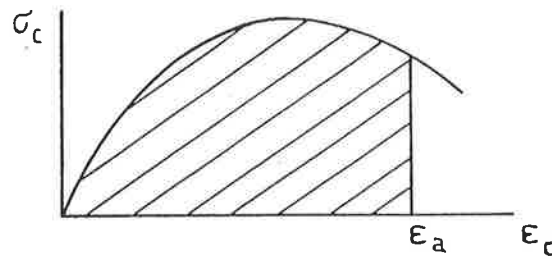
Figure 2.4: Stress-strain curve for concrete in compression
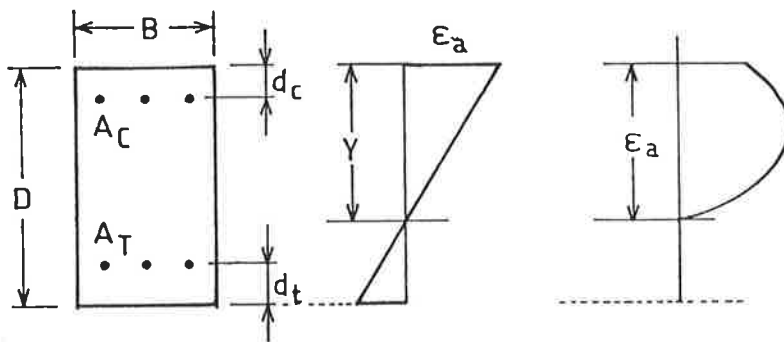
Figure 2.5: Strain distribution

The expressions for axial force, C_c, and moment, M_c, are given by:

$$C_c = B\int_0^Y \sigma(y)dy = B\frac{Y}{\varepsilon_a}\int_0^{\varepsilon_a} \sigma(\varepsilon)d\varepsilon \qquad (2.10)$$

$$M_c = B\int_0^Y y\sigma(y)dy = B\left(\frac{Y}{\varepsilon_a}\right)^2 \int_0^{\varepsilon_a} \varepsilon\sigma(\varepsilon)d\varepsilon \qquad (2.11)$$

The integrals expressed in terms of y are replaced by integrals with ε_a as the independent variable. To obtain C_c and M_c, the following integrals are solved:

$$I_1(\varepsilon_a) = \int_0^{\varepsilon_a} \sigma(\varepsilon)d\varepsilon \qquad (2.12)$$

$$I_2(\varepsilon_a) = \int_0^{\varepsilon_a} \varepsilon.\sigma(\varepsilon)d\varepsilon \qquad (2.13)$$

The first integral expresses the shaded area under the stress-strain curve in Figure 2.4 up to the value ε_a, the strain in the outermost fibre. The second integral is the first moment of area of this shaded region about the vertical (σ_c) axis. To find the depth to the neutral axis, Y, a quadratic equation is solved. The evaluation of the integrals $I_1(\varepsilon_a)$ and $I_2(\varepsilon_a)$ are given in the paper by Sved.

Warner (1969) noted that the analytical expressions for moment and thrust used by Pfrang *et al.* are not feasible in the general case of a column in biaxial bending. A direct summation technique for determining moment and thrust was proposed, but the description here is for the particular case of a column in a plane frame with moment applied about a single axis.

A section is divided into a sufficient number of thin layers of concrete and steel as in Figure 2.6. From a given strain distribution across the section the average stress in each layer can be evaluated from assumed stress-strain relationships for concrete and steel. Stress in the concrete layers is calculated at mid-depth.
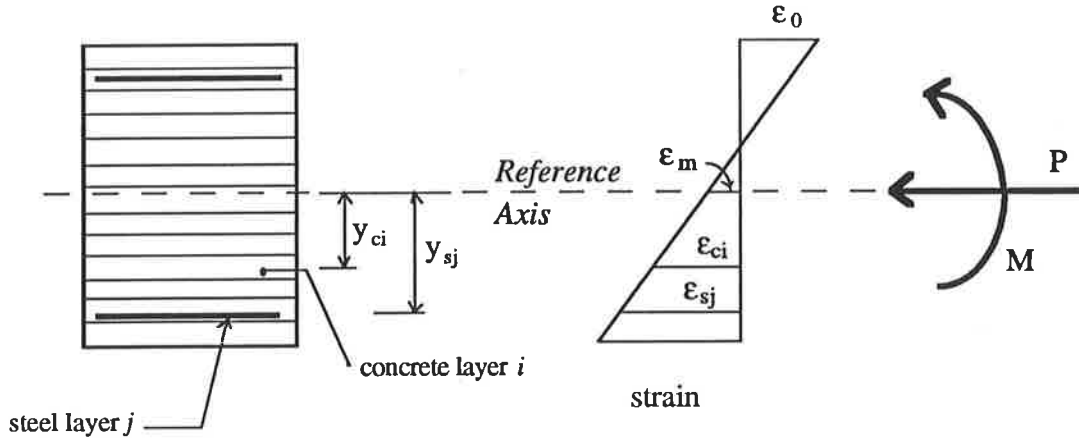
Figure 2.6: Layered cross-section

By summing the axial force in each layer, a resultant axial force, P, is found, which is given by:

$$P = \sum_{i=1}^{nconc} f_{ci}A_{ci} + \sum_{j=1}^{nsteel} f_{sj}A_{sj} \qquad (2.14)$$

where

f_{ci} = stress at mid-level of the i-th concrete layer;

A_{ci} = area of the i-th concrete layer;

f_{sj} = stress at mid-level of the j-th steel layer; and

A_{sj} = area of the j-th steel layer.

The bending moment at the section is then given by:

$$M = \sum_{i=1}^{nconc} f_{ci}A_{ci}y_{ci} + \sum_{j=1}^{nsteel} f_{sj}A_{sj}y_{sj} \qquad (2.15)$$

where

y_{ci} = distance from the mid-level of the i-th concrete layer from the reference axis;

y_{sj} = distance from the mid-level of the j-th steel layer from the reference axis;

$nconc$ = total number of concrete layers; and

$nsteel$ = total number of steel layers.

For assumed values of curvature κ and axial strain ε, flexural and axial stiffnesses EI and EA are given by the following:

$$EI = M / \kappa \qquad\qquad (2.16)$$

$$EA = P / \varepsilon \qquad\qquad (2.17)$$

Alternatively, the direct summation method can be used to formulate these stiffness terms directly, which are given by the following:

$$EA = \sum_{i=1}^{nconc} E_{ci}A_{ci} + \sum_{j=1}^{nsteel} E_{sj}A_{sj} \qquad\qquad (2.18)$$

$$EI = \sum_{i=1}^{nconc} E_{ci}y_{ci}{}^2 A_{ci} + \sum_{j=1}^{nsteel} E_{sj}y_{sj}{}^2 A_{sj} \qquad\qquad (2.19)$$

where E_{ci} and E_{sj} are the material moduli for concrete and steel respectively.

The direct summation method of determining moment and thrust is both easy to understand and to implement in a computer program. There are also other major advantages with this approach. Compressive and tensile curves for both steel and concrete can be used and inelastic unloading curves can easily be incorporated. Unlike the direct integration method used by Broms and Viest, Pfrang *et al.* and Kroenke *et al.*, the summation approach is not limited to any one particular stress-strain relationship for concrete.

Many investigators have since used direct summation in a section analysis routine of a non-linear frame analysis, including Aas-Jakobsen and Grenacher (1974), Bazant *et al.* (1987a), Kang and Scordelis (1980), McAdie *et al.* (1987) and Wong (1989). In the approach by McAdie *et al.*, an additional stiffness term, the shear rigidity, was calculated. This is given by:

$$GA = \sum_{i=1}^{nconc} G_{ci} A_{ci} \qquad (2.20)$$

The shear modulus, G, is related to the Young's modulus by the following expression:

$$G = \frac{E}{2(1+\upsilon)} \qquad (2.21)$$

where υ is the poisson's ratio.

Both Bazant *et al.* (1987a) and Kang and Scordelis (1980) introduced a stiffness term to take into account the shift in the centroidal axis. This is given by:

$$ES = \sum_{i=1}^{nconc} E_{ci} y_{ci} A_{ci} + \sum_{j=1}^{nsteel} E_{sj} y_{sj} A_{sj} \qquad (2.22)$$

In the section analyses used by these investigators, three stiffness terms are calculated. These are EA, ES and EI, which are sometimes referred as the zero, first and second order stiffnesses.

Finally, M-κ-N relationships can be developed by numerical integration using Gaussian quadrature. Virdi (1977) proposed a method for columns in biaxial bending, but the description here is for the particular case of uniaxial bending of columns in plane frames.

Gaussian integration involves the use of transformed coordinates so the function to be integrated is between the limits +1 and -1. The definite integral is then replaced with a weighted sum of the values of the integrand at two or more sampling points. The formula is expressed as:

$$\int_{-1}^{+1} f(\xi)d\xi = \sum_{i=1}^{m} w_i f(a_i) \qquad (2.23)$$

where

w_i = weight factors

a_i = Gaussian sampling points

Values of w_i and a_i can be found in suitable texts on numerical methods, (Chapra and Canale, 1988; Isaacson and Keller, 1966). The size of concrete elements can be chosen to locate a Gauss point level at the elevation of the steel layers. Alternatively, the area of reinforcement can be distributed to adjacent Gauss points which represent the concrete, (Balakrishnan *et al.*, 1988).

Virdi found when the method is applied to biaxial bending computational time is reduced by a factor of one third compared to the direct summation method. However, no comparison was made for the uniaxial bending case. The approach has been used in non-linear methods of frame analysis by Aldstedt and Bergan (1974), Ghoneim and Ghali (1982) and Holzer *et al.* (1978).

2.3.2 Methods to Obtain Strain Distribution and Moment-Curvature-Thrust Relations

In the determination of moment-curvature-thrust relations from a given strain distribution, usually two variables are assigned values and numerical procedures calculate values for the remaining two variables. The starting variables are progressively updated with each iteration until a solution is obtained for moment, thrust, curvature and strain distribution.

The Newton method has been used by Virdi and Dowling (1976) and El-Metwally and Chen (1989a). The method as described by the latter, requires the following steps:

1. From an initial distribution of strain and curvature and using an integration technique, determine an incremental load vector and the total load vector given by:

$$\left| \begin{matrix} P_1 \\ M_1 \end{matrix} \right| = \left| \begin{matrix} P_0 + \Delta P \\ M_0 + \Delta M \end{matrix} \right|$$

(2.24)

P_0 and M_0 are thrust and moment from the previous load step, and ΔP and ΔM are the increment in load for the current cycle of the current step.

2. Using the central difference method, calculate the tangent stiffness matrix, $[K_t]$, given by:

$$[K_t] = \begin{bmatrix} \dfrac{\Delta P}{\Delta \varepsilon} & \dfrac{\Delta P}{\Delta \phi} \\ \dfrac{\Delta M}{\Delta \varepsilon} & \dfrac{\Delta M}{\Delta \phi} \end{bmatrix} \qquad (2.25)$$

The off-diagonal terms define the increase in curvature caused by an increment of axial load and the increase in centroidal strain caused by an increment of bending moment. The influence of the off-diagonal terms becomes more significant as the section approaches the plastic state.

3. Determine the incremental deformation vector given by:

$$\begin{vmatrix} \Delta \varepsilon \\ \Delta \phi \end{vmatrix} = \begin{bmatrix} K_t^{-1} \end{bmatrix} \begin{vmatrix} \Delta P \\ \Delta M \end{vmatrix} \qquad (2.26)$$

4. Obtain the following sectional deformation vector:

$$\begin{vmatrix} \varepsilon_1 \\ \phi_1 \end{vmatrix} = \begin{vmatrix} \varepsilon_0 \\ \phi_0 \end{vmatrix} + \begin{vmatrix} \Delta \varepsilon \\ \Delta \phi \end{vmatrix} \qquad (2.27)$$

5. Calculate the load vector which corresponds to the deformation vector obtained from Step 4. Compare this vector with the load vector obtained from Step 1.

If the difference is within an acceptable tolerance, a solution is obtained for this load increment. Otherwise, add the difference vector obtained from Step 5 to the incremental load vector, and repeat Steps 3 through 5.

To obtain the load-deformation relationship at Step 3, the tangent stiffness matrix must be inverted. Hobbs and Jowharzedeh (1978) formulated an incremental method directly in terms of a flexibility matrix, which avoids a computational step requiring the stiffness matrix to be inverted.

Warner and Lambert (1974) developed a nested search procedure to find the extreme fibre concrete compressive strain, E_0, and tensile strain E_1. In the outer procedure, called SEEKE1 (see Figure 2.7), E_0 is fixed and E_1 is progressively adjusted until upper and lower bounds, E_1^U and E_1^L, are found. These bounds correspond to positive and negative values of $\overline{P}$, which is the normalised thrust and equal to P_{tar}/P. The target thrust is P_{tar} and the value of axial thrust, P, is determined by the direct summation method from an assumed strain distribution with values of E_1^U and E_1^L.

The inner routine, called SEEKE0, uses a halving procedure to reduce the size of these bounds by replacing either E_1^U or E_1^L with the midpoint, E_1. A solution is found when the difference between the desired thrust, P_{tar}, and calculated thrust, P, agree to an acceptable tolerance.

Although the nested search procedure is not optimal it was found to be efficient and reliable. It is also an easy method to implement in a computer program because of its simple structure. Another advantage with this approach is that it can be implemented in either a tangent or secant stiffness type of analysis. This search method has been used by Ahmad and Warner (1984), Kgoboko (1987) and Wong (1989).

2.3.3 M-κ-N Relations in Frame Analysis

Two different approaches have been used to develop *M-κ-N* relations for use in frame analysis. In one approach, *M-κ-N* relations are generated at each step during frame analysis, and in the other approach pre-generated values of *M-κ-N* form part of the input to a computerised frame analysis.

In the first approach, which uses automatic generation of *M-κ-N* relations, a section analysis forms part of the frame analysis program. The section analysis uses any of the integration methods described in Section 2.3.1, and an additional technique to update the strain distribution as described in Section 2.3.2.

Automatic generation of *M-κ-N* values is more accurate than using pre-generated values, but consumes a significant portion of the overall program execution time in a frame analysis. Automatic generation also requires large amounts of storage space. Data usually stored are keypoints which define the history of stress and strain. Keypoints are stored for all sections and take into account inelastic behaviour and points of unloading and reloading along the stress-strain curves.

In the second approach, pre-generated values of moment-curvature-thust are used as input to a computerised frame analysis. Previous studies have used pre-generated curves from two sources: (1) experimental results; and (2) *M-κ-N* relations determined from a section analysis program separate from the main structural analysis program.

Often a moment-curvature curve is defined by a large number of data points which are then read as input for a structural analysis computer program. A family of moment-curvature curves can be generated for a number of different levels of axial thrust. To reduce the storage demands required for each data point, the curves can be fitted to curvilinear equations or piecewise linear equations.

The Ramberg-Osgood polynomial, given by Equation 2.28, has also been used by Gunnin *et al.* (1977) to represent moment-curvature relations in a frame analysis.

$$\phi = \frac{M}{EI}\left(1 + a\left|\frac{M}{M_y}\right|^{r-1}\right) \tag{2.28}$$

In this equation, ϕ is the curvature; a and r are curve constants; M is the moment; EI is flexural stiffness; and M_y (or M_p) is the yield moment or plastic moment capacity.

E_o fixed

$E_1 = E_1(n-1)$

Calculate $\overline{P}$

is $\overline{P} > 0$?

NO   YES

$E_1 = E_1 + \Delta L$ $E_1 = E_1 + \Delta L$

Calculate $\overline{P}$ Calculate $\overline{P}$

is $\overline{P} > 0$?   is $\overline{P} > 0$?

NO   YES   NO   YES

$E_1^U = E_1$
$E_1^L = E_1 - \Delta E$

$E_1^U = E_1^U + \Delta L$
$E_1^L = E_1$
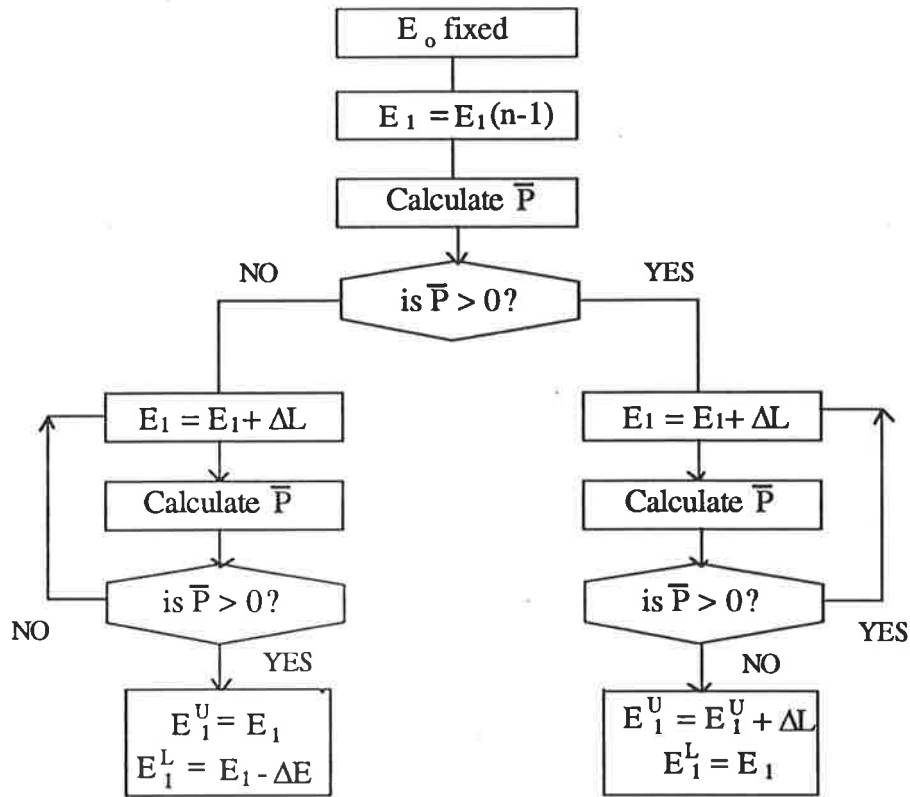
(a) SEEKE1: Bounds for strain E_1

E_o fixed
$E_1^U \quad E_1^L$ found

$E_1 = 0.5[\, E_1^U + E_1^L \,]$

Calculate $\overline{P}$

is $|\overline{P}| < t_n$?

YES

is $\overline{P} > 0$?

NO   YES

$E_1^L = E_1$ $E_1^U = E_1$

Search Complete
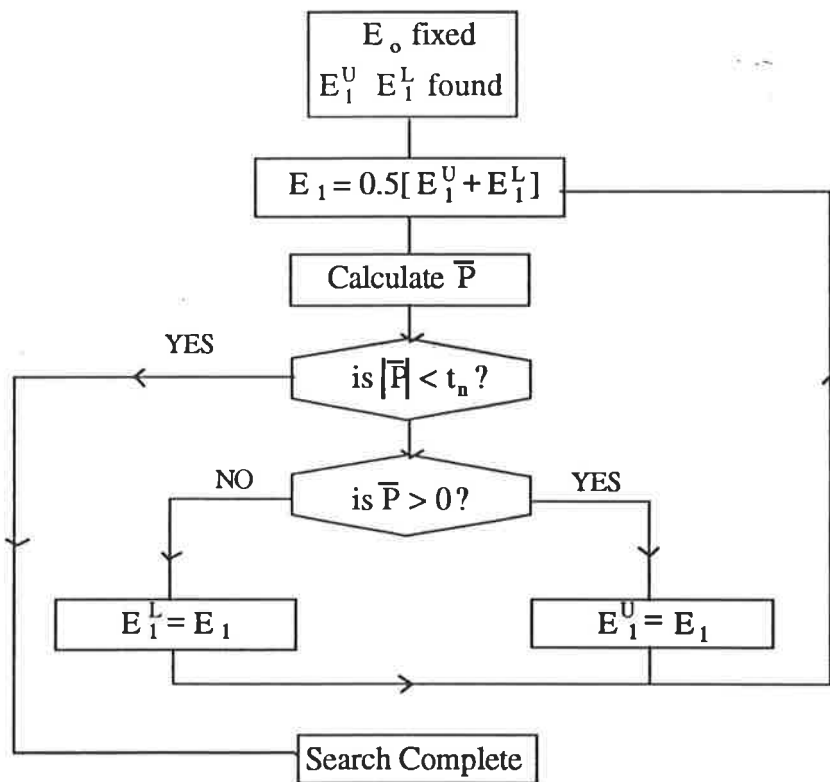
(b) SEEKE0: Halving procedure

Figure 2.7: Search procedure proposed by Warner and Lambert (1974)

Shown in Figure 2.8 is a family of curves derived from Equation 2.28.
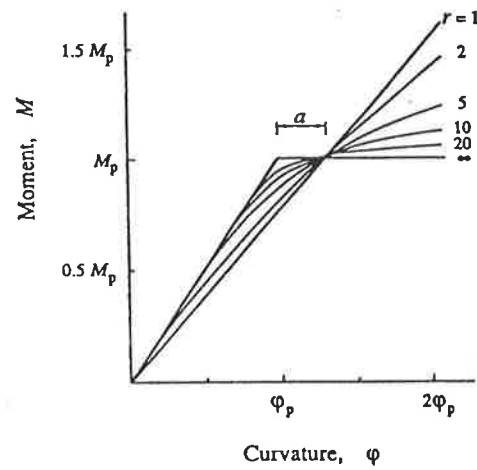
Figure 2.8: Ramberg-Osgood moment-curvature relationship (Gunnin *et al.*, 1977)

The Ramberg-Osgood M-κ relationship has also been refined to include inelastic unloading portions, Equation 2.29. The unloading or secondary curve is included in Figure 2.9.

$$\phi = \phi_0 + \frac{M - M_0}{EI}\left(1 + a\left|\frac{M - M_0}{2M_y}\right|^{r-1}\right)$$

(2.29)

where (M_0, ϕ_0) are moment and curvature at the reversal point.
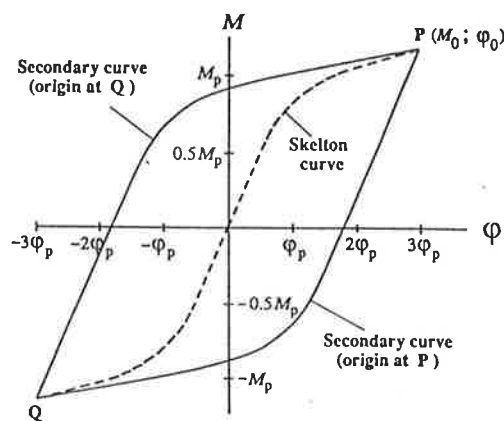
Figure 2.9: Ramberg-Osgood moment-curvature relationship for moment reversal

(Graff and Eisenberger, 1991)

An alternative to using curvilinear equations is to fit moment-curvature curves to piecewise linear equations. Shown in Figure 2.10 are three possible representations for M-κ curves (Darvall and Mendis, 1985). The change in slope between the first two linear segments of Figure 2.10c indicates that stiffness is influenced by tension stiffening. In Figures 2.10a and 2.10b, the linear portion up to the plastic moment describes moment and curvature for an over-reinforced section. In these cases, tension stiffening has little effect on stiffness. Note also the post-peak softening curve is influenced by the percentage of reinforcement.

Darvall (1982) noted that the softening portion of the moment-curvature curves is important when determining the collapse load of indeterminate structures. The term softening parameter, a, was used to express the softening slope in terms of the initial elastic slope, Figure 2.11. For softening, the value for a is a small negative number, but for strain hardening the slope of the third line is positive. A steep softening slope reduces both the number of hinges formed before collapse and the collapse load, (Mendis and Darvall, 1988). Hsu *et al.* (1981) included both hardening and softening portions for pre-generated M-κ curves in a non-linear method of frame analysis.

Softening curves have been obtained experimentally by Mendis (1986) and Tse and Darvall (1988) using a deformation controlled test system for single and two-span reinforced concrete beams. Softening behaviour can also be predicted from M-κ-N curves using a section analysis procedure. However, such curves are idealised.

Piecewise linear M-κ curves based on experimental beam results had been obtained earlier by Monnier (1970), but these curves do not include softening. Hence, they may have limited application for determining collapse loads for indeterminate structures subjected to high axial loads.

Pre-generated M-κ-N curves can be built up by section analyses in a computer program separate from the main structural analysis program. M-κ curves are generated for a range of values of compressive and tensile thrust. Accuracy of this

approach depends on the number of levels of thrust and also the method adopted for curve fitting.

Pre-generated curves can be used to advantage in analysis when the structure has a large number of members with uniform properties and section details. Sets of M-κ-N curves can also be used when a large number of frames are to be analysed.
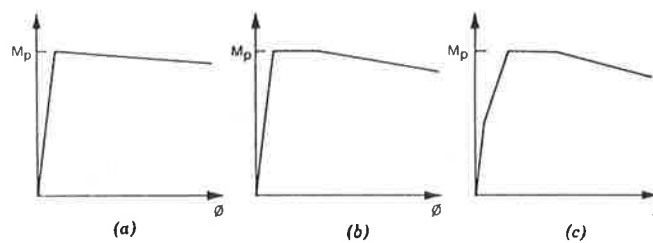
Figure 2.10: Approximations for moment-curvature curves: (a) Elastic-Softening; (b) Elastic-Plastic Softening; and (c) Elastic-Reduced Elastic-Plastic-Softening

(Darvall and Mendis, 1985)
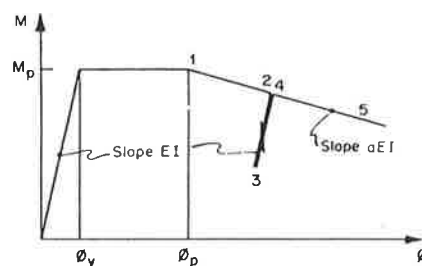
Figure 2.11: Assumptions for moment-curvature curve

(Darvall and Mendis, 1985)

2.4 Solution Techniques for Non-Linear Frame Analysis

Frame analysis for non-linear behaviour can be made either by simulating a load control or deformation control test set-up. In the latter approach, a set of deformations is incremented to the structure and the corresponding set of loads is calculated. In an analysis for load control, a load pattern is incremented to the structure up to a peak value. It should be noted that analysis beyond the peak load can only be made by employing additional special techniques. Usually, iterative procedures are required to achieve convergence for the load-deformation relationships and one of the following three techniques can be used:

(1) Tangent Stiffness method (also referred to as the Newton-Raphson method)

(2) Initial Stiffness method (also referred to as the modified Newton-Raphson method)

(3) Secant Stiffness method

A typical load step in the tangent stiffness approach is illustrated in Figure 2.12. This approach has been summarised by Zienkiewicz (1977) and de Araujo (1989).

Element stiffness matrices in local member coordinates are transformed into a global reference system, and using standard procedures (Coates, Coutie and Kong, 1980; Zienkiewicz, 1977) the global structural stiffness matrix, K_0, is formed. At the start of the load step, element stiffnesses are set to the values from the end of the previous step. For commencement of the initial load step, element stiffnesses must have assumed values. These are usually based on gross-sectional values. The incremental load vector ΔP is applied to the structure and the global deformations ΔD_1 are found by solving the following equation:

$$[K_0]|\Delta D_1| = |\Delta P| \tag{2.30}$$
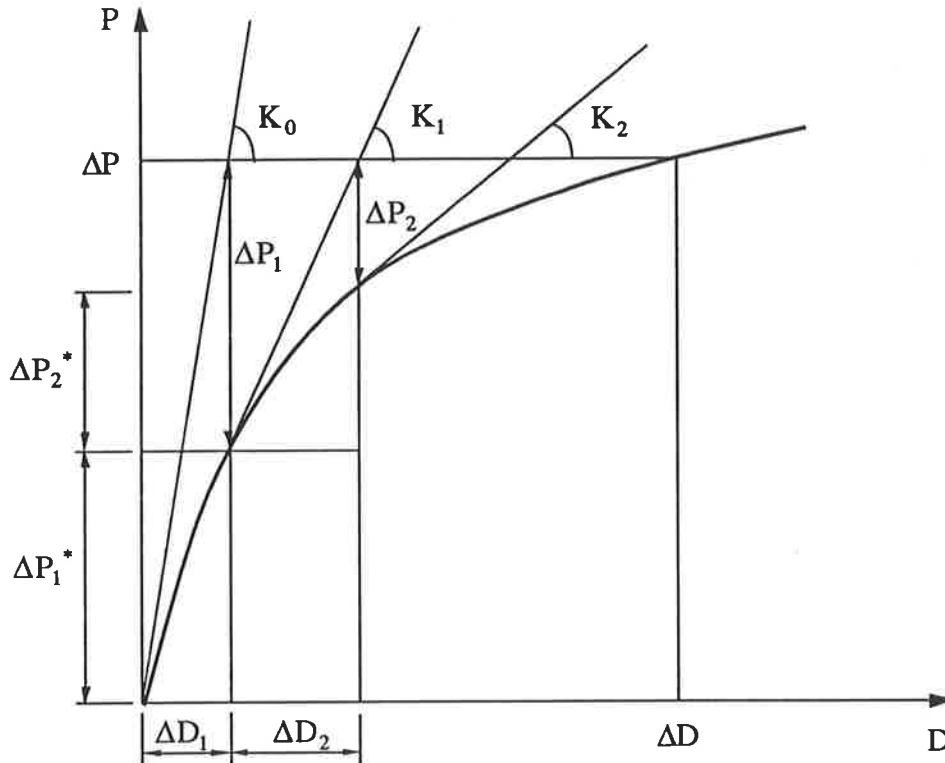
Figure 2.12: Tangent Stiffness method

From the current deformed state of the structure, the nodal load vector, ΔP^*, is calculated. By considering existing non-linear effects a new tangent stiffness matrix, K_1, is assembled. Various methods for modelling material and geometric non-linear behaviour in frame analysis will be discussed in Sections 2.6 and 2.7. The out-of-balance load vector ΔP_1 is calculated, which is the difference between the load vector at the start of the first iterative cycle and the system of loads from the current deformed configuration. This difference vector is given by:

$$\Delta P_1 = \Delta P - \Delta P_1^* \qquad (2.31)$$

A second iterative cycle commences by applying the out-of-balance loads, ΔP_1, to the structure and the incremental deformations, ΔD_2, are found by solving Equation 2.32.

$$[K_1]|\Delta D_2| = |\Delta P_1| \qquad (2.32)$$

A new tangent stiffness matrix K_2 is assembled and the out-of-balance load vector is given by:

$$\Delta P_2 = \Delta P_1 - \Delta P_2^*$$ (2.33)

At the end of the second and subsequent cycles, a check is made to see if the out-of-balance loads are within an acceptable tolerance. When convergence has been achieved after n cycles, the set of total deformations, which correspond to the total load increment ΔP, is given by:

$$\Delta D = \sum_{i=1}^{n} \Delta D_i$$ (2.34)

The values of ΔP and ΔD are added to existing quantities to give the total amount of load and deformation in the structure. Structural analysis is carried out by incrementing a system of loads up to a maximum load level, where the tangent stiffness becomes zero. To analyse the structure beyond the limit point, additional procedures must be adopted, which are discussed in the following section.

The initial stiffness method, which is also referred to as Newton-Raphson's modified method, is shown in Figure 2.13. Two cycles are shown, where ΔP_1 and ΔP_2 are the out-of-balance forces at the end of these cycles. Structural stiffness K_0 is held constant for the load step.

Calculation procedures for the initial stiffness method are the same as for the tangent stiffness method, except the stiffnesses for the first cycle are held constant for each iterative cycle of that particular load step. This reduces the amount of computational time required to assemble each element stiffness matrix into a global stiffness matrix. However, the number of iterative cycles required for convergence may be greater than for the tangent stiffness method and has an additional disadvantage that the solution may be less accurate.
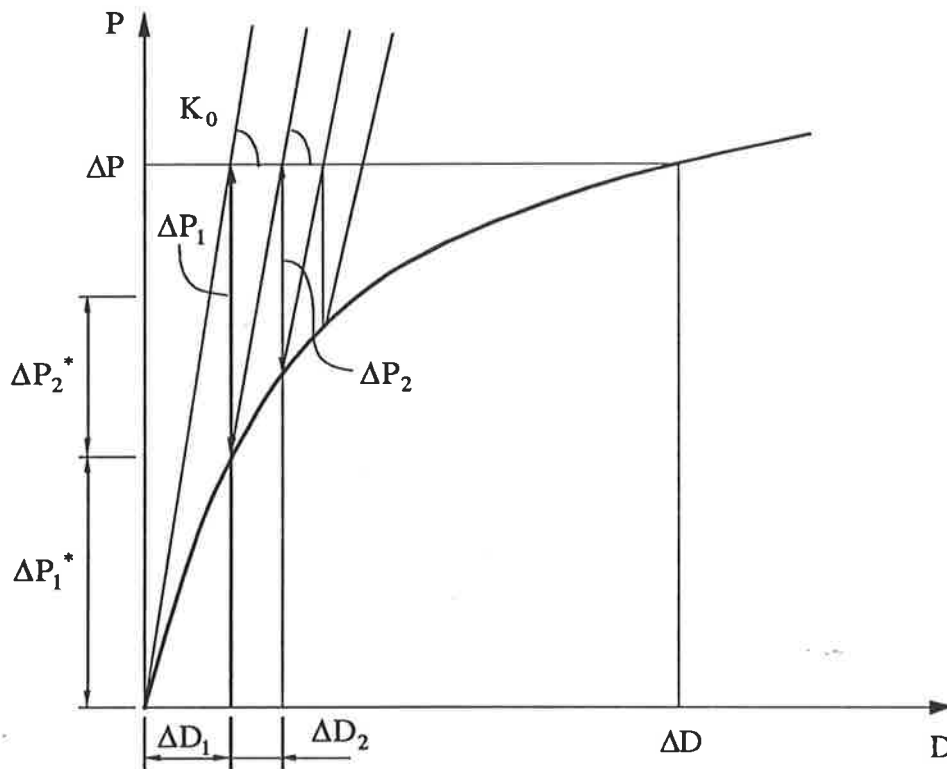
Figure 2.13: Initial Stiffness method

The secant stiffness method, shown in Figure 2.14, requires secant flexural and axial stiffnesses to be updated with each iterative cycle of the load step. This method differs to the tangent and initial stiffness methods by applying a total load at each step. When the method is used to simulate a deformation control control test system, rather than load control, behaviour beyond the peak load can be investigated. The set of forces

$F_{1,2...A}$ correspond to direct values for deformations $D_{1,2...A}$. In this method, the stiffnesses are updated with each iteration.
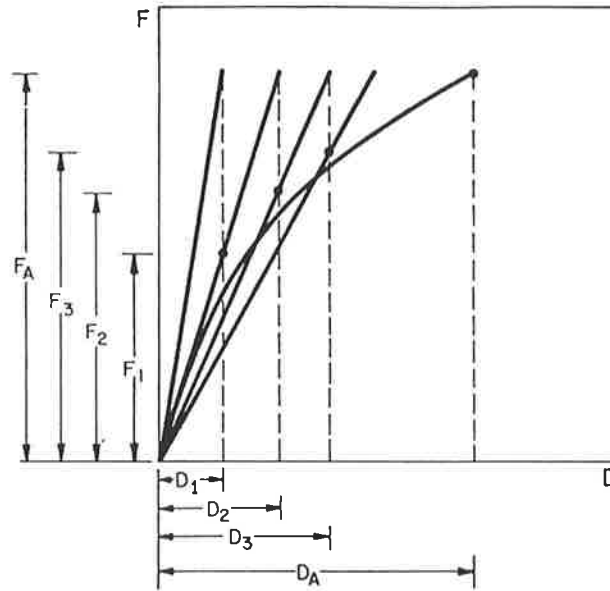
Figure 2.14: Secant Stiffness method (Chajes and Churchill, 1987)

A number of investigators have proposed mixed-modified Newton-Raphson methods of analysis, (de Araujo, 1989; Kao, 1974; Ma and May, 1986). In this type of approach, the initial stiffness and tangent stiffness methods are combined to improve the rate of convergence while maintaining accuracy of solution.

In the method proposed by Ma and May, the tangent stiffness matrix is updated at the end of the first iteration, which is then used for each subsequent iterative cycle until convergence is achieved. It was noted that formation of cracks also influenced the change in stiffness of a member, which is usually predicted in the first cycle. If more cracks are predicted, the tangential stiffness matrix is recalculated at the end of that iteration.

To improve the rate of convergence, Ma and May compared methods of analysis with and without the use of acceleration techniques. It was found that mixed-modified Newton-Raphson methods with accelerators gave much improved rates of convergence.

Crisfield's acceleration technique (1980) was investigated, and in this method the displacements $\{\Delta u\}_i$ are updated by an iterative change such that:

$$\{u\}_{i+1} = \{u\}_i + \{\Delta u^*\}_i \tag{2.35}$$

where

$$\{\Delta u^*\}_i = \alpha_i \{\Delta u^*\}_{i-1} + \beta_i \{\Delta u\}_i \tag{2.36}$$

and

$$\{\Delta u\}_i = [K_T]^{-1} \{R\}_i \tag{2.37}$$

In these expressions, $[K_T]$ is the tangent stiffness matrix and $\{R\}_i$ is the out-of-balance nodal load vector and α_i and β_i are acceleration scalars. Note that $\{u\}_i$ is the set of total displacements at the end of the *i*-th load step. If $\alpha_i=0$ and $\beta_i=1$, Equation 2.37 becomes the solution obtained by the tangent stiffness (or Newton-Raphson) method.

An automatic increment size method proposed by Crisfield (1980) was also examined by Ma and May. This expression is given by:

$$\Delta P_i = \Delta P_{i-1}(I_d / I_{d-1}) \tag{2.38}$$

where I_d = the desired number of iterations;

I_{d-1} = the number of iterations from the previous increment; and

ΔP_{i-1} = the size of load increment from the previous load step.

This approach gave a 3% improvement in the predicted collapse load, but there was no improvement in computational time. The use of Crisfield's accelerator was most efficient when applied with the initial stiffness method; computational time was reduced by 50% and rate of convergence was good.

de Araujo (1989) proposed a Newton-Raphson mixed method by using extrapolation formulae to accelerate convergence. Tangent stiffness matrices are updated at the end of the first cycle and held constant during further iterative cycles. For the first cycle, extrapolation is not required, but for subsequent cycles the extrapolation formulae are intended to give a better approximation of the amount of load required for each iteration. de Araujo found that efficiency of this approach increases with problems with increasing degrees of freedom.

2.5 Techniques for Post Peak Analysis

As the peak load value in frame analysis is reached, convergence problems may occur. For post-peak analysis, an approximation can be made by inserting a plastic hinge when a section has reached its yield strength, (Lazaro and Richards, 1973). Hence, overall load-displacement response analysis is also characterised by a horizontal plateau at the peak load. However, to predict softening after the peak load, additional numerical techniques are required which are more complicated to implement in a computerised frame analysis. Two approaches, which are based on the tangent stiffness and the initial stiffness methods, are described in the following.

Bergan (1980) described the "current stiffness parameter", S_p, which quantifies the overall non-linear response of a structure as it undergoes loading. This dimensionless scalar quantity is given by the following:

$$S_p = \frac{\Delta p_i}{\Delta p_1} \frac{\|\Delta r_1\|}{\|\Delta r_i\|}$$

(2.39)

where Δp_1 is the load increment which gives rise to the set of displacements Δr_1 for the first load step. The load increment and change in displacements at the current load level are given by Δp_i and Δr_i respectively. Displacement terms in Equation 2.39 are expressed in the Euclidean norm.

The current stiffness parameter is useful for detecting limit points and changes sign when passing such limit points. A typical load-displacement diagram of a snap-through problem is shown in Figure 2.15, with $\|r\|$ used as a measure of the displacements. The corresponding curve for S_p is also shown.

The initial value for the parameter S_p is always set to unity. The current stiffness parameter decreases in magnitude until its value becomes zero, which corresponds to the first limit point. The sign of the parameter S_p then becomes negative until the second second limit point is reached. At each limit point, the current stiffness parameter becomes zero. For a linear elastic system, S_p is always set to unity for analysis.

A limit point is reached when the determinant of the tangent stiffness matrix changes sign, which relies on very small increments of loads near the limit point. Negative load increments are then applied until the next extremum point is reached. The size of a new load increment is estimated from the following formula:

$$\Delta p_{i+1} = \Delta p_i \left(\frac{\Delta S_p}{\Delta S_{p,i}} \right)^2 \tag{2.40}$$

where ΔS_p is a prescribed constant and Δp_i and $\Delta S_{p,i}$ are the most recent load increment and associated current stiffness parameter.

Crisfield (1981) also proposed a method for traversing limit points which is based on a solution procedure developed earlier by Riks (1979). A constraint equation which fixes the size of the load increment is added to the equilibrium equations. The procedure is used in conjunction with the initial stiffness method (or modified Newton-Raphson method), but as noted by Bazant *et al.* (1987b), this approach is complicated to program, particularly as a second limit point is traversed.

Both approaches by Bergan and Crisfield use load control rather than displacement control and efficiency depends on the size of the load increment. Small increments are

required as the peak load is approached. After the peak load, inaccuracies in the tangent stiffness terms may occur, particularly if softening is characterised by a very gradual slope.
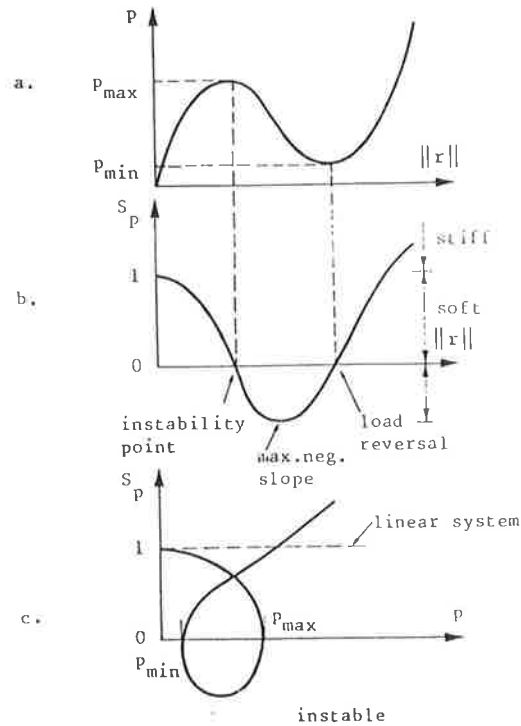
Figure 2.15: Variation of the current stiffness parameter (Bergan, 1980)

It should be noted that deformation controlled processes can be used to perform frame analysis beyond the peak load. In the approach by Kayal (1984), analysis switches from load control to strain control when the compressive strain at any Gaussian sampling point reaches a value of 0.002. However, concrete is assumed to have no tensile capacity and the stress-strain curve for concrete in compression is elastic. These simplifications, although not accurate, are likely to improve the search for the section with the maximum strain.

In the secant stiffness method of analysis by Aas-Jakobsen and Grenacher (1974), a switch is also made from load to deformation control prior to the peak load. Displacement is chosen as the controlling parameter, but relies on predetermining where displacement is expected to be a maximum. Hence, this approach is only suitable for simple frame or beam type problems.

Warner and Yeo (1984, 1986) describe a secant method of analysis which increments a set of curvatures to the structure. A linear elastic frame analysis determines the forces and deformations throughout the structure and a search is made for the "key segment" where curvature is a maximum, absolute value. The curvature in this segment is scaled to equal a predetermined target value. Hence, forces and deformations throughout the structure are scaled by the same factor.

This method has also been incorporated in the segmental method of analysis proposed by Wong (1989) and is discussed in further detail in Section 2.8.

2.6 Frame Analysis for Non-linear Material Behaviour

Most methods of non-linear analysis for reinforced concrete frames formulate the load-displacement relationships by employing a one dimensional straight beam element. Methods based on two dimensional finite elements, (Phillips and Zienkiewicz, 1976), model multi-directional cracking and the influence of shear deformations and provide more accurate solutions. However, relatively large demands on storage and computational time are required and these methods are more suitable for analysing local behaviour, e.g. at beam-column joints.

Although the flexibility approach by Cranston (1965) was a popular method of analysis for some years, it is limited to frames with a low order of indeterminacy. By far the most common approach to solving the load-displacement relationships for a structure is by the matrix displacement method. In many of these cases, the conventional first order linear elastic stiffness matrix, k_e, given by Equation 2.41 has formed the basis for non-linear methods of frame analysis.

$$\begin{vmatrix} \dfrac{EA}{L} & 0 & 0 & -\dfrac{EA}{L} & 0 & 0 \\[2mm] & \dfrac{12EI}{L^3} & \dfrac{6EI}{L^2} & 0 & -\dfrac{12EI}{L^3} & \dfrac{6EI}{L^2} \\[2mm] & & \dfrac{4EI}{L} & 0 & -\dfrac{6EI}{L^2} & \dfrac{2EI}{L} \\[2mm] & & & \dfrac{EA}{L} & 0 & 0 \\[2mm] & & & & \dfrac{12EI}{L^3} & -\dfrac{6EI}{L^2} \\[2mm] SYMMETRIC & & & & & \dfrac{4EI}{L} \end{vmatrix} \qquad (2.41)$$

In a first order linear elastic frame analysis, the stiffness terms EI and EA of this matrix are assumed to be constant throughout the analysis. When this matrix is used in a non-linear frame analysis, stiffness terms are progressively updated. This also implies that M-κ-N relationships can be built up as loads are incremented to the structure.

In the approach by Aas-Jakobsen and Grenacher (1974), each structural member is divided into a sufficient number of elements so that variations in flexural stiffness along the member can be calculated. Each element in the non-linear method is then divided into a number of thin layers and section analyses determine M-κ-N relations by the direct summation method for a given strain distribution. Secant stiffnesses EI and EA are updated by the section analyses, where $EI = M/\kappa$ and $EA = N/\varepsilon_m$. The moment, M, axial thrust, N, and curvature, κ, are average values for the element. The axial strain, ε_m, is taken at the centroid of the section. By using the direct summation method, described earlier in Section 2.3.1, the influence of axial force on flexural stiffness and the effect, if any, of bending moment on axial stiffness are taken into account.

A major disadvantage with the method by Aas-Jakobsen and Grenacher is that each member must be represented by a number of elements, where the length of each element should presumably represent the length of a potential hinge. Note also that only nodal loads can be represented. Frame analysis requires the storage and

manipulation of a large number of structural matrices, hence, this is an inefficient approach and likely to increase program execution time. However, since frame analysis is based on the fundamental first order linear elastic approach it is relatively simple to understand and to implement in a computer program. The method proposed by Aas-Jakobsen and Grenacher has also been used by Corderoy (1978) to study non-linear frame behaviour.

Kang and Scordelis (1980) and Bazant *et al.* (1987a) proposed non-linear method methods of analysis which also use the standard first order member stiffness matrix k_e, but with modifications. Additional stiffness terms are included in the off-diagonal positions which take into account the change in position of the centroidal axis. These terms are given by *ES*, where *E* is the Young's modulus and *S* is the first moment of area of the section. The method developed by Kang and Scordelis is formulated differently and the beam element and the unusual order of labelling the degrees of freedom are shown in Figure 2.16. This method has been summarised in more detail by Hellesland *et al.* (1985).
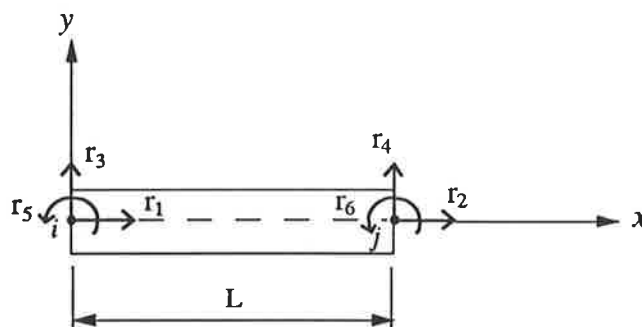
Figure 2.16: Beam element used by Kang and Scordelis (1980)

The element stiffness matrix used by Kang and Scordelis (1980) is given by:

$$
\begin{vmatrix}
\dfrac{EA}{L} & -\dfrac{EA}{L} & 0 & 0 & \dfrac{ES}{L} & -\dfrac{ES}{L} \\[2ex]
 & \dfrac{EA}{L} & 0 & 0 & -\dfrac{ES}{L} & -\dfrac{ES}{L} \\[2ex]
 & & \dfrac{12EI}{L^3} & -\dfrac{12EI}{L^3} & \dfrac{6EI}{L^2} & \dfrac{6EI}{L^2} \\[2ex]
 & & & \dfrac{12EI}{L^3} & -\dfrac{6EI}{L^2} & -\dfrac{6EI}{L^2} \\[2ex]
 & SYMMETRIC & & & \dfrac{4EI}{L} & \dfrac{2EI}{L} \\[2ex]
 & & & & & \dfrac{4EI}{L}
\end{vmatrix}
\qquad (2.42)
$$

Note that the axial stiffness terms are clustered in the top left hand corner. It has been shown by Graff and Eisenberger (1991) that problems with large axial stiffnesses combined with small flexural stiffnesses can sometimes result in loss of numerical accuracy. It is possible the order of the degrees of freedom was chosen by Kang and Scordelis so that axial stiffness terms would be positioned on or adjacent to the main diagonal. This may reduce inaccuracies in the solution which can arise from matrix manipulation.

The non-linear methods of analysis by Bazant *et al.* and Kang and Scordelis both require discretising each structural member into a number of elements. Hence, accuracy of solution depends on the number of elements taken. Riva and Cohn (1990) noted the benefit of using variable element lengths. At critical sections, shorter lengths should be used and as distance increases from the critical sections, elements with larger lengths can be used.

The length of the critical section is often called the hinge length, but its predicted value varies considerably for each type of reinforced concrete structure. The following have proposed hinge length formulae based on experimental results: Cohn and Petcu (1963), from tests on two-span continuous beams; Corley (1966) and Baker and Amarakone (1964), based on tests of simply supported beams; and Park *et al.* (1982)

who tested reinforced concrete columns. However, each formula yields different results for hinge length.

Both approaches by Bazant *et al.* (1987a) and Kang and Scordelis (1980) employ a layered element with a direct summation method to develop M-κ-N relations and updated values of the stiffnesses, *EI*, *ES* and *EA*. These terms are sometimes referred as second, first and zero order stiffness terms respectively, and are given by Equations 2.18, 2.19 and 2.22.

The advantage with the approach by Kang and Scordelis is that, in addition to integrating stress and strain over the depth of the section, integration at three Gauss points along the element is also performed. This allows for fewer elements to be taken to represent each member and reduces the size of the global storage matrix. Aldstedt and Bergan (1974) also employed Gaussian integration at two to four points along the element.

It should be noted the derivation of the conventional first order stiffness matrix, given by Equation 2.41, is based on an element with six degrees of freedom (d.o.f.). The shape functions describing the displacement field of this element are third order polynomials for the transverse displacement, *v*, and a first order polynomial for the longitudinal displacement, *u*. A number of investigators have developed stiffness matrices using beam elements with additional degrees of freedom and shape functions of higher order polynomials.

Both Blaauwendraad (1972) and Aldstedt and Bergan (1974) introduced a seven d.o.f. element as shown in Figure 2.17. The tangential displacement at mid-length of the beam element raises the order of both the transverse and longitudinal displacement fields.

Espion (1986) developed a nine d.o.f. beam element, shown in Figure 2.18, which takes into account non-linear geometric effects. In this element formulation, and also the methods by Blaauwendraad (1972) and Aldstedt and Bergan (1974), the equations

of equilibrium can be reduced to a system of equations represented by a 6x6 element stiffness matrix. This reduces the amount of storage required for a global stiffness matrix and also the size of the problem to be solved. However, as pointed out by Espion, these storage and time savings are offset by the number of operations required for static condensation of the 9x9 stiffness matrix into a reduced 6x6 matrix.
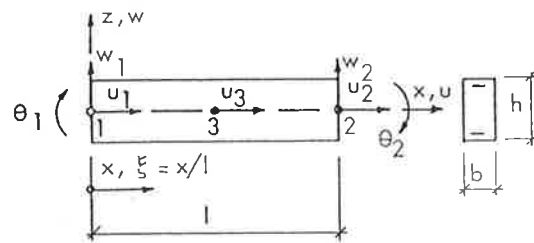
Figure 2.17: Beam element used by Aldstedt and Bergan (1974)
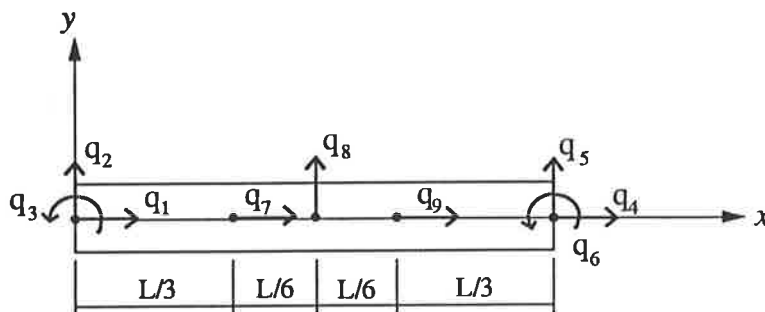
Figure 2.18: Beam element developed by Espion (1986)

The equilibrium equations for the method proposed by Blaauwendraad (1972) are given by Equation 2.43. The terms, θ_i and θ_j, in the displacement vector are the rotations at the ends of the element and Δl and u_K are the axial extension and transverse displacements at mid-length of the element.

$$\begin{bmatrix} S_{11} & S_{12} & S_{13} & S_{14} \\ & S_{22} & S_{23} & S_{24} \\ & & S_{33} & S_{34} \\ & & & S_{44} \end{bmatrix} \begin{bmatrix} u_k \\ \Delta l \\ \theta_i \\ \theta_j \end{bmatrix} = \begin{bmatrix} 0 \\ N \\ M_i \\ M_j \end{bmatrix} \tag{2.43}$$

The terms comprising the stiffness matrix, $\mathbf{S_e^0}$, are evaluated by solving the following integrals, where $y = x/l$:

$$S_{11} = \frac{1}{L} \int_0^1 (4 - 8\phi)^2 D_{11} d\phi \tag{2.44}$$

$$S_{12} = \frac{1}{L} \int_0^1 (4 - 8\phi) D_{11} d\phi \tag{2.45}$$

$$S_{13} = \frac{1}{L} \int_0^1 (4 - 8\phi)(4 - 6\phi) D_{12} d\phi \tag{2.46}$$

$$S_{14} = \frac{1}{L} \int_0^1 (4 - 8\phi)(2 - 6\phi) D_{12} d\phi \tag{2.47}$$

$$S_{22} = \frac{1}{L} \int_0^1 D_{11} d\phi \tag{2.48}$$

$$S_{23} = \frac{1}{L} \int_0^1 (4 - 6\phi) D_{12} d\phi \tag{2.49}$$

$$S_{24} = \frac{1}{L} \int_0^1 (2 - 6\phi) D_{12} d\phi \tag{2.50}$$

$$S_{33} = \frac{1}{L} \int_0^1 (4 - 6\phi)^2 D_{22} d\phi \tag{2.51}$$

$$S_{34} = \frac{1}{L} \int_0^1 (2 - 6\phi)(4 - 6\phi) D_{22} d\phi \tag{2.52}$$

$$S_{44} = \frac{1}{L} \int_0^1 (2 - 6\phi)^2 D_{22} d\phi \tag{2.53}$$

where

$$D_{11} = EA \tag{2.54}$$

$$D_{21} = y_z EA \tag{2.55}$$

$$D_{12} = D_{21} \tag{2.56}$$

$$D_{22} = EI + y_z^2 EA \tag{2.57}$$

The matrix $S_e{}^0$ is formulated as a 4x4, but is reduced to a 3x3 matrix. It is important to note each element stiffness matrix is symmetrical and therefore stored as a 3x3 matrix and not the usual 6x6. To assemble the element stiffness matrices into a structural stiffness matrix, S^e, in local coordinates, the matrix multiplication is given by Equation 2.58. Additional standard procedures are required to transform these element matrices into a global coordinate system.

$$S^e = C^T S_e{}^0 C \tag{2.58}$$

In this equation, C is a combination matrix and given by:

$$C = \begin{vmatrix} -1 & 0 & 0 & 1 & 0 & 0 \\ 0 & \frac{1}{L} & 1 & 0 & -\frac{1}{L} & 0 \\ 0 & \frac{1}{L} & 0 & 0 & -\frac{1}{L} & 1 \end{vmatrix} \tag{2.59}$$

The combination matrix remains unchanged for the entire analysis and requires that the displacements be small for member chord rotation. This form of matrix manipulation can be implemented in any structural analysis program where symmetrical stiffness matrices exist.

Another popular approach for modelling non-linear material behaviour is the use of the stability functions of Livesley and Chandler (1956). Equation 2.60 is the standard first order stiffness matrix with coefficients, ϕ_1, ϕ_2, ϕ_3 and ϕ_4, which modify the flexural stiffness terms. These stability functions, or coefficients, are in fact a modification to the first order matrix, k_e, to take into account the influence of axial forces upon flexural behaviour. These coefficients depend on the current load level and corresponding flexural stiffness in each element. By ignoring this effect, Equation 2.60 reduces to the first order matrix given by Equation 2.41. Expressions for these stability functions can be found in standard textbooks on structural analysis, (Coates, Coutie and Kong, 1980).

$$
\begin{bmatrix}
\dfrac{EA}{L} & 0 & 0 & -\dfrac{EA}{L} & 0 & 0 \\[2ex]
 & \dfrac{EI\phi_1}{L^3} & \dfrac{EI\phi_2}{L^2} & 0 & -\dfrac{EI\phi_1}{L^3} & \dfrac{EI\phi_2}{L^2} \\[2ex]
 & & \dfrac{EI\phi_4}{L} & 0 & -\dfrac{EI\phi_2}{L^2} & \dfrac{EI\phi_3}{L} \\[2ex]
 & & & \dfrac{EA}{L} & 0 & 0 \\[2ex]
\text{SYMMETRIC} & & & & \dfrac{EI\phi_1}{L^3} & -\dfrac{EI\phi_2}{L^2} \\[2ex]
 & & & & & \dfrac{EI\phi_4}{L}
\end{bmatrix}
\qquad (2.60)
$$

El-Metwally and Chen (1989b) used the stiffness matrix given by Equation 2.60 to describe the load-deformation relationship in a non-linear method of frame analysis. Stiffness terms are updated by performing section analyses. A tangent stiffness approach was adopted and the method can only be used up to the peak load. Special techniques, such as those described earlier, would have to be implemented to allow analysis in the post-peak region.

Goto and Chen (1987) noted the coefficients quoted above become indefinite as the axial force approaches zero, which causes numerical instability in a structural analysis. They introduced a power series to replace the trigonometric functions which express the stiffness coefficients. It was found that the use of a power series avoids numerical instability and is more convenient because the expressions by the series are the same for all values of axial force.

Mendis (1986), also Mendis and Darvall (1988), modified the stability functions to allow for softening at the ends of members. An element subjected to softening is shown in Figure 2.19.

The terms, s and c, are the stiffness factor and carry-over factor respectively, which depend on the axial load. The rotational stiffness is $k = EI/L$, and the modifying factor is $t = sc$. The symbols s and c are the stability functions, which have been derived by integrating compatibility equations in terms of curvature. At the ends of the member

are the potential hinge forming regions of length l_{p_1} and l_{p_2} which are determined by experiment. The slope of the softening curve is given by the parameter a, which has been described earlier. At critical softening, given by the value a_{cr}, the structure cannot sustain further increases of load. This value has been calculated for a number of cases by Darvall (1982, 1984).
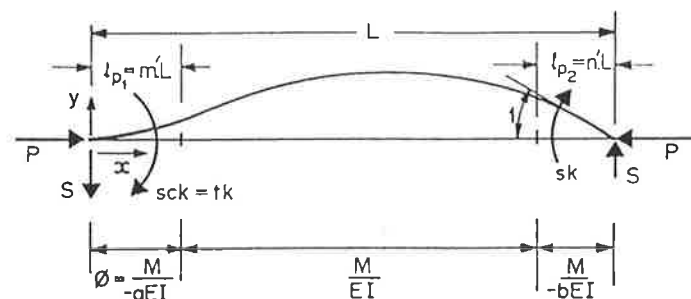
Figure 2.19: Member with softening at each end (Mendis and Darvall, 1988)

A major advantage with this approach is that each member does not have to be divided into a number of elements for frame analysis. Terms comprising the element stiffness matrix depend on the change in stiffness at the ends of the member, while the stiffness along the member and between the hinges is assumed to be constant. This is a reasonable assumption which relies on the accurate prediction of hinge locations within the structure.

Moment and curvature in the hinge forming regions depends on the level of axial thrust. The value of a_{cr} at far advanced curvature can be determined from a simple relationship, as shown in Figure 2.20.

Note that in the initial elastic range, or where $m'=0$ and $n'=0$, the stability functions proposed by Mendis (1986) reduce to the conventional stability functions of Livesley and Chandler.
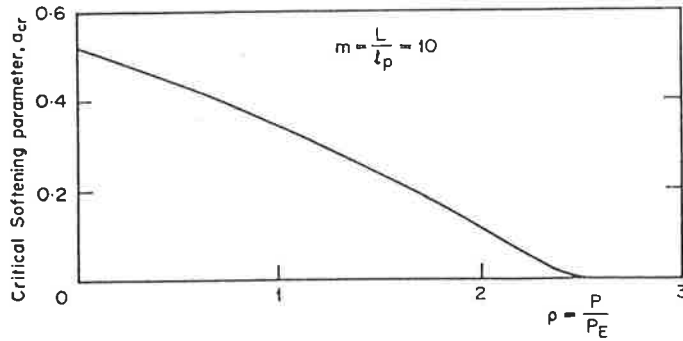
Figure 2.20: Critical softening parameter at various levels of axial load, (Mendis and Darvall, 1988)

2.7 Frame Analysis for Non-linear Geometric Behaviour

The influence of deformed geometry on structural behaviour was the subject of early investigations, including (Argyris, 1966; Turner, 1966). Non-linear load-deformation relationships were developed using finite element techniques and many studies have since followed, employing various member coordinates to formulate the equilibrium equations. Shown in Figure 2.21 are the configurations AB and A*B* respectively of a plane beam element before and after deformation.
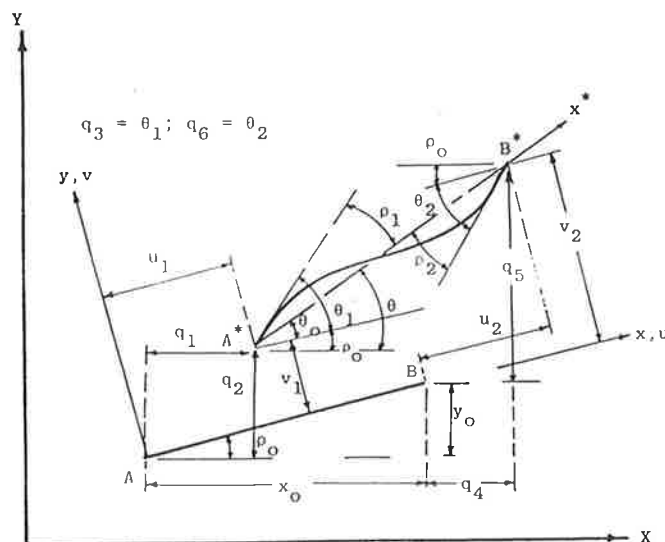
Figure 2.21: Geometry of beam element in Euler Member Coordinates, Lagrange Member Coordinates and Global Coordinates (Wen and Rahimzadeh, 1983)

The quantities $(q_1, q_2,....q_6)$ are taken to be the generalised displacements in global coordinates. The initial member coordinates are given by x and y. Euler coordinate axes are denoted by x^* and y^* and the generalised displacements ρ_1, ρ_2, and Δ are defined with reference to the chord of the deformed member. The terms ρ_1 and ρ_2 are angular rotations and the change of chord length is Δ. Lagrange member coordinates are defined with reference to the chord before deformation and are given by the quantities u_1, v_1, q_1, u_2, v_2, q_2. The Lagrange system of coordinates has the disadvantage that additional computations are required to transform the element matrices into a global matrix. However, an approach using Lagrange coordinates should give similar results as an approach using Euler coordinates.

Lagrange coordinates for small rotations (Lagrange-SR coordinates for short) assume the chord rotation (q_0 in Figure 2.21) is small. Hence, transformation of the stiffness matrices to the global coordinates is made through a fixed angle.

Wen and Rahimzadeh (1983) noted there are two approaches for representing the non-linear geometric stiffness problem: the geometric stiffness matrix (also referred as the initial stiffness matrix; and the incremental stiffness matrix.

Argyris (1966) formulated a tangent incremental stiffness matrix in Euler coordinates. The tangent stiffness matrix is evaluated at the initial position and behaviour is assumed to be linear within the increment. Jennings (1968) and Powell (1969) also developed incremental stiffness matrices in Euler coordinates. Mallett and Marcal (1968) formulated incremental matrices in Lagrange-SR coordinates.

Large deflection analysis of elastic frames received early attention by Turner *et al.* (1960) followed by Oran and Kassimali (1976). Analysis of inelastic frames based on the assumption of small deflections has been made by Oran (1973) and Saafan (1963). However, the problem of large deflection analysis for inelastic frames appears to be treated only recently (Bathe and Ozdemir, 1975; Cichon, 1984; Kam, 1988).

It is interesting to note that stiffness expressions, including geometric matrices, corresponding to beam-column theory have been formulated in Euler coordinates by Oran (1973), Oran and Kassimali (1976), Saafan (1963) and in Lagrange-SR coordinates by Connor *et al.* (1968). The developments by Oran (1973) improved earlier work by including the influence of flexure (bowing action) on member axial strains and modifying stability functions to take into account members subjected to compressive and tensile axial forces.

A popular approach for modelling geometric non-linearity in reinforced concrete frame analysis is to augment the standard first order stiffness matrix, k_e, with the geometric stiffness matrix, k_g, given by Equation 2.61.

$$k_g = N \begin{bmatrix} 0 & 0 & 0 & 0 & 0 & 0 \\ 0 & \dfrac{6}{5L} & \dfrac{1}{10} & 0 & -\dfrac{6}{5L} & \dfrac{1}{10} \\ 0 & \dfrac{1}{10} & \dfrac{2L}{15} & 0 & -\dfrac{1}{10} & -\dfrac{l}{30} \\ 0 & 0 & 0 & 0 & 0 & 0 \\ 0 & -\dfrac{6}{5L} & -\dfrac{1}{10} & 0 & \dfrac{6}{5L} & -\dfrac{1}{10} \\ 0 & \dfrac{1}{10} & -\dfrac{l}{30} & 0 & -\dfrac{1}{10} & \dfrac{2L}{15} \end{bmatrix} \qquad (2.61)$$

where

N = current level of element axial load; and

L = length of the element.

This matrix is also referred to as the initial stress matrix and its derivation can be found in a number of texts, including Przemieniecki (1985) and Martin and Carey (1973). Derivation of the force-displacement equations yields both the geometric stiffness matrix and the standard first order linear elastic matrix. Hence, both matrices are often

included in a non-linear frame analysis. Such studies include Aas-Jakobsen and Grenacher (1974), Blaauwendraad (1972), Corderoy (1978), Kang and Scordelis (1980), and Kulicki and Kostem (1974).

The derivation of Equation 2.61 is based on the conventional element with six degress of freedom, i.e. longitudinal and transverse displacements and rotations at each end of the element. Displacement fields within the element are also assumed. When an average constant slope is assumed over the element, this geometric stiffness matrix reduces to the following:

$$
\begin{bmatrix}
0 & 0 & 0 & 0 & 0 & 0 \\
0 & \dfrac{N}{L} & 0 & 0 & -\dfrac{N}{L} & 0 \\
0 & 0 & 0 & 0 & 0 & 0 \\
0 & 0 & 0 & 0 & 0 & 0 \\
0 & -\dfrac{N}{L} & 0 & 0 & \dfrac{N}{L} & 0 \\
0 & 0 & 0 & 0 & 0 & 0
\end{bmatrix}
\tag{2.62}
$$

Equation 2.62 is sometimes referred as the string stiffness matrix. Blaauwendraad (1972) used the string stiffness and the following 3x3 matrix to model geometric non-linearities in a frame analysis.

$$
S_e^{\,n} =
\begin{bmatrix}
0 & 0 & 0 \\
0 & \dfrac{2NL}{15} & -\dfrac{NL}{30} \\
0 & -\dfrac{NL}{30} & \dfrac{2NL}{15}
\end{bmatrix}
\tag{2.63}
$$

Blaauweendraad adopted this approach so that variations in stiffness and shifting centroidal axis could be confined to the 3x3 matrix, S_e^n. By performing the matrix multiplication, $C^T S_e^n C + \Delta S^{nn}$, the geometric stiffness matrix k_g is obtained. The symbol ΔS^{nn} denotes the string stiffness matrix and C is the combination matrix described earlier. This approach improves both convergence and computational time.

Chajes and Churchill (1987) summarised a non-linear method of frame analysis which includes higher order geometric terms. Figure 2.22 summarises typical steps in the analysis. The matrix $[k_p]$ is the initial stiffness matrix given by Equation 2.61 and $[k_1]$ and $[k_2]$ are geometric stiffness matrices originally developed by Mallett and Marcal (1968). The matrices $[k_1]$ and $[k_2]$ are linear and quadratic functions of the incremental element displacements and are updated during each iterative cycle.

The matrices $[k_0]$ and $[k_p]$ are only updated at the start of a given load step and are used to determine the first estimate of the incremental displacements during that load step. An obvious disadvantage with this method of analysis is the increase in storage and computational time required for the additional geometric matrices.

Some of the problems encountered with frame analysis for large deformation are the demands on computational time and storage for additional stiffness matrices. Some investigators have overcome these problems with geometric non-linearity by updating the nodal geometry as the structure deforms. Hence, terms comprising the transformation matrices are based on the most recent nodal deformations. This approach has been used successfully by Aldstedt and Bergan (1974) and El-Metwally and Chen (1989b). To ensure accuracy of solution, a sufficient number of node points must be chosen to represent the structure.

```
┌─────────────────────────────────────────┐
│        Form [k₀] for each element         │
└─────────────────────────────────────────┘
                     │
                     ▼
┌─────────────────────────────────────────┐
│        Specify increment loads ΔF         │◄──────────┐
└─────────────────────────────────────────┘           │
                     │                                  │
                     ▼                                  │
┌─────────────────────────────────────────┐           │
│            Form [kₚ] and [T]              │           │
│  from existing geometry and axial forces  │           │
└─────────────────────────────────────────┘           │
                     │                                  │
                     ▼                                  │
┌─────────────────────────────────────────┐           │
│     Assemble element stiffness matrices   │           │
│           [kᵢ] = [k₀]+[kₚ]                │           │
└─────────────────────────────────────────┘           │
                     │                                  │
                     ▼                                  │
┌─────────────────────────────────────────┐           │
│     Assemble global stiffness matrix      │           │
│        [Kᵢ]₀ = [T]ᵀ[k₀][T]               │           │
└─────────────────────────────────────────┘           │
                     │                                  │
                     ▼                                  │
┌─────────────────────────────────────────┐           │
│      i = 0 and Let [ΔF]₀ =[ΔF]           │           │
└─────────────────────────────────────────┘           │
                     │                                  │
          ┌──────────▼──────────────────────┐          │
     ┌───►│             i = i+1              │          │
     │    └─────────────────────────────────┘          │
     │                │                                 │
     │                ▼                                 │
     │    ┌─────────────────────────────────┐          │
     │    │       Solve displacements        │          │
     │    │   [Kᵢ]ᵢ₋₁[ΔD]ᵢ =[ΔF]ᵢ₋₁       │          │
     │    └─────────────────────────────────┘          │
     │                │                                 │
     │                ▼                                 │
     │    ┌─────────────────────────────────┐          │
     │    │     Obtain total displacements   │          │
     │    │     [ΔD]ᵢ = Σⁱₙ₌₁[ΔD]ₙ         │          │
     │    └─────────────────────────────────┘          │
     │                │                                 │
     │                ▼                                 │
     │    ┌─────────────────────────────────┐          │
     │    │  Obtain local displacements [Δd] │          │
     │    │    and form [k₁] and [k₂]        │          │
     │    └─────────────────────────────────┘          │
     │                │                                 │
     │                ▼                                 │
     │    ┌─────────────────────────────────┐          │
     │    │     Form element stiffness matrix│          │
     │    │  [kᵢ]=[k₀]+[kₚ]+[k₁]+[k₂]       │          │
     │    └─────────────────────────────────┘          │
     │                │                                 │
     │                ▼                                 │
     │    ┌─────────────────────────────────┐          │
     │    │  Assemble global stiffness matrix│          │
     │    │            [Kᵢ]ᵢ                 │          │
     │    └─────────────────────────────────┘          │
     │                │                                 │
     │                ▼                                 │
     │    ┌─────────────────────────────────┐          │
     │    │ Solve for the force imbalance [ΔF]ᵢ │       │
     │    │ using [Kᵢ]ᵢ[ΔD]ᵢ =[ΔF]−[ΔF]ᵢ   │        │
     │    └─────────────────────────────────┘          │
     │                │                                 │
  No │      ◄─────────▼─────────►  Yes                  │
     └──┤ Is [ΔF]−[ΔF]ᵢ ≤ tolerance ? ├─────────────────────┐
        └─────────────────────────────┘                  │
                     │                                    │
                     ▼                                    │
┌─────────────────────────────────────────┐             │
│  Calculate values [D], [P], [F] by adding │◄────────────┘
│       increments to existing quantities   │
└─────────────────────────────────────────┘
```

Figure 2.22: Non-linear analysis for first and second order incremental displacements

2.8   Segmental Method of Frame Analysis

2.8.1   General Description

The segmental method of frame analysis developed by Wong (1989), and reported in Wong, Yeo and Warner (1987, 1988) is a secant stiffness approach which allows full range behaviour to be investigated. Analysis for two types of non-linearity can be made. These are full geometric effects and material effects due to the stress-strain relationships for concrete and steel.

The segmental method is based on an earlier idea by Warner (1975) in which structural members are represented by a number of short segments. Typically, segment lengths are between $0.5D$ and $1.0D$, where D is the depth of the element. This follows recommendations by Bazant *et al.* (1987a) and Warner and Yeo (1984) and ensures that strain softening occurs over a finite length, often referred to as the hinge length.

In an earlier study of continuous beams by Warner and Yeo (1984, 1986) each segment was represented by an individual element. This requires the storage and manipulation of large matrices which is undesirable for plane frame problems and led to the development of the segmental element matrix. The derivation can be found in several publications, (Wong, 1989; Wong, Yeo and Warner; 1987, 1988), and has been reproduced in Appendix B of this study. The segmental element matrix takes into consideration deformations within each segment in the element. To formulate the problem, expressions for fixed end moments and shear forces are based on the area-moment method for an elastic member with a non-uniform section, (Bull and Sved, 1964). In this case, non-uniformity is also associated with variation in bending stiffness along the element. Derivations for the fixed end forces are also given in Appendix C of this study.

Frame analysis is performed by applying a unit load pattern to find forces and displacements at the ends of all elements. Deformations within all segments are found

by integrating curvature along the element from the set of most recent secant flexural stiffnesses. Hence, a set of unit curvatures is obtained.

A search is made of the unit curvatures to locate the segment with the maximum absolute value which is designated as the "key segment". The search is carried out assuming gross-sectional properties and also assuming the structure to be uncracked. It was found in the present study that the segment with the maximum absolute curvature can change at various stages of loading. To avoid numerical instabilities and convergence problems, the search for the key segment is carried out at the commencement of each computational step and, if necessary, the key segment is changed.

A deformation control test is simulated by imposing a set of increments in target curvature, $\kappa_{Key}(1),...\kappa_{Key}(ISTEP),...\kappa_{Key}(NSTEP)$, on the key segment, where *NSTEP* is a computational step in the post-collapse region. This approach has also been used in studies of prestressed concrete continuous beams, (Campbell and Kodur, 1990; Moucessian and Campbell, 1988). All segmental forces and deformations are scaled so that the unit curvature in the key segment equals the target curvature.

A major advantage with this method of deformation control is that full range analysis for loading up to and including the post-collapse (softening) region can be made. In some frames analysed by Wong, snapback instability was observed.

2.8.2 Section Analysis Procedures

Secant stiffnesses for frame analysis are updated by a sectional analysis, using the direct summation technique. This is done by assuming values of axial thrust, P, and curvature, κ, which are obtained from the frame analysis and segmental method of analysis respectively. An extreme fibre axial strain, ε_o, and sectional moment, M, are then calculated. The value of ε_o is updated by the search technique proposed by Warner and Lambert (1974) and described earlier in this chapter. Moment-thrust-curvature relationships are generated automatically to avoid the otherwise tedious

process of pre-generating a range of moment-thrust-curvature relationships each time a frame analysis is performed.

The section is divided into a number of thin layers of concrete and reinforcing steel as was shown in Figure 2.1. It was found that 15 layers could produce moment-thrust-curvature relationships of acceptable accuracy. The stress-strain relationship for concrete in compression and shown in Figure 2.23 is that proposed by Warner (1969), and includes a suitable unloading portion which is parallel to the initial loading curve. The advantage with this type of curve is that the strain at peak stress is independent of the concrete modulus, and the strain on the post-peak softening curve corresponding to zero stress can be varied.

An elasto-plastic stress-strain relationship for steel is assumed and is shown in Figure 2.24. Unloading curves are assumed to be parallel to the initial loading curve.
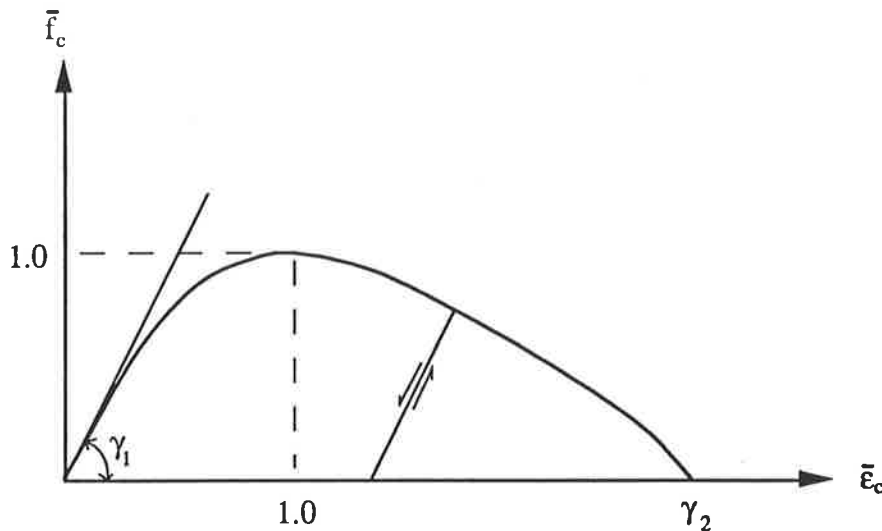
Figure 2.23: Stress-strain relationship for concrete in compression (Warner, 1969)

The following equations define the concrete stress-strain relationship:

$$\bar{\varepsilon}_c \leq 0.0 \quad : \quad \bar{f}_c = 0.0 \tag{2.64}$$

$$0.0 < \bar{\varepsilon}_c \leq 1.0 \quad : \quad \bar{f}_c = \gamma_1 E_c + (3 - 2\gamma_1)E_c^2 + (\gamma_1 - 2)E_c^3 \tag{2.65}$$

$$1.0 < \bar{\varepsilon}_c \leq \gamma_2 \quad : \quad \bar{f}_c = 1 - (1 - 2E_c + E_c^2)/(1 - 2\gamma_2 - \gamma_2^2) \tag{2.66}$$

$$\bar{\varepsilon}_c > \gamma_2 \quad : \quad \bar{f}_c = 0.0 \tag{2.67}$$

where

$\bar{\varepsilon}_c$ = normalised strain equal to $\varepsilon_c/\varepsilon_{cmax}$;

$\bar{f}_c$ = normalised stress equal to f_c/f_{cmax};

γ_1 = $E_0\varepsilon_{cmax}/f_{cmax}$;

E_0 = modulus of elasticity for concrete;

f_{cmax} = strength of concrete in a member; and

ε_{cmax} = strain corresponding to stress f_{cmax}.
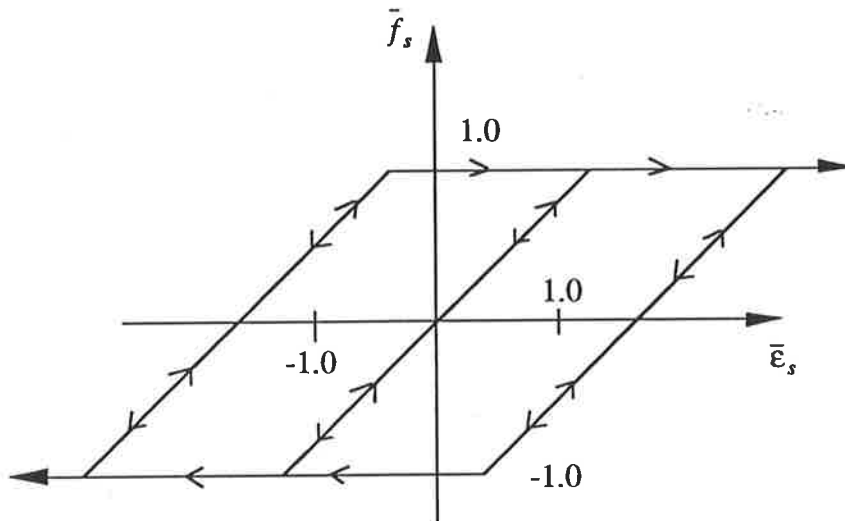
Figure 2.24: Elasto-plastic relationship for reinforcing steel

The following terms describe the steel stress-strain curve:

$\bar{\varepsilon}_s$ = normalised strain equal to $\varepsilon_s/\varepsilon_{sy}$;

$\bar{f}_s$ = normalised stress equal to f_s/f_{sy};

ε_{sy} = steel yield strain; and

f_{sy} = steel yield stress.

2.8.3 Structural Analysis

A typical computational step *ISTEP* commences with trial segmental stiffnesses $EI_{trial}(ISTEP,n)$ in all segments, n, and trial axial stiffnesses for the members, m, $EA(ISTEP,m)$ set to the values at the end of the previous step. Steps for a typical cycle (also shown in Figure 2.26) are described as follows :

1. Form the segmental element stiffness matrices from the most recent secant stiffness values. Using standard procedures, (Coates, Coutie and Kong, 1980; Meek, 1991; Vanderbilt, 1974), assemble the global stiffness matrix $[K]$ by transforming the element matrices from local coordinates to global coordinates.

2. Apply a unit load pattern to the structure and form the nodal load matrix $\{Q_{unit}\}$. Nodal loads from unit load patterns within the elements are based on fixed end moments which depend on the segmental stiffnesses.

3. Determine nodal deformations Δ_{unit} by solving the following matrix equation with Gauss-Jordan elimination and partial pivoting:

$$\{Q_{unit}\} + \{Q_{out-of-bal}\} = [K]\{\Delta_{unit}\} \tag{2.68}$$

$\{Q_{out-of-bal}\}$ is the set of residual forces which is the difference in nodal loads on the undeformed frame and the nodal loads compatible with the displacements allowing for changes in frame geometry.

4. From the nodal deformations of the frame, and using standard procedures, obtain deformations and forces at the ends of all the members. Based on these and the unit load patterns within the members, determine the unit curvatures $\kappa_{unit}(ISTEP,n)$ in all segments due to the unit load pattern.

$$\kappa_{unit}(ISTEP,n) = \frac{M_{unit}(ISTEP,n)}{EI_{trial}(ISTEP,n)} \qquad (2.69)$$

5. Calculate the scaling factor $SF(ISTEP)$ from the target curvature and the curvature of the key segment due to the unit load pattern.

$$SF(ISTEP) = \frac{\kappa_{key}(ISTEP)}{\kappa_{unit}(ISTEP,key)} \qquad (2.70)$$

6. Obtain a set of trial segmental curvatures, $\kappa_{trial}(ISTEP,n)$, by multiplying $\kappa_{unit}(ISTEP,n)$ by the scaling factor $SF(ISTEP)$.

$$\kappa_{trial}(ISTEP,n) = SF \times \kappa_{unit}(ISTEP,n) \qquad (2.71)$$

The trial curvature in the key segment is always equal to the target curvature, $\kappa_{key}(ISTEP)$.

7. Store the previous flexural stiffnesses :

$$OLDEI(ISTEP,n) = EI_{trial}(ISTEP,n) \qquad (2.72)$$

8. Perform sectional analyses for all segments to determine segmental moments $M_{trial}(ISTEP,n)$ which correspond to $\kappa_{trial}(ISTEP,n)$. Calculation of the stiffness EI for a typical segment is shown in Figure 2.25. New flexural stiffnesses are found :

$$EI_{trial}(ISTEP,n) = \frac{M_{trial}(ISTEP,n)}{\kappa_{trial}(ISTEP,n)} \qquad (2.73)$$

The total axial deformation along the centroidal axis for each member is obtained. New trial axial stiffnesses $EA(ISTEP,m)$ are then determined from the element axial thrust $N(ISTEP,m)$ and axial strain $\delta(m)$.

$$EA(ISTEP,m) = N(m)/\delta(m) \qquad\qquad (2.74)$$

$$\delta(m) = \sum_{i=1}^{nseg} \varepsilon(n)l(n) \qquad\qquad (2.75)$$

where $\delta(m)$ = total axial deformation along member m;

$\varepsilon(n)$ = axial strain of segment n along the reference axis; and

$l(n)$ = length of segment n.

9. At the end of each iterative cycle, the change in flexural stiffness for all segments is checked and convergence is achieved if the following relationship is satisfied :

$$\frac{EI_{trial}(ISTEP,n) - OLDEI(ISTEP,n)}{OLDEI(ISTEP,n)} \le \varepsilon \qquad\qquad (2.76)$$

where ε is a specified tolerance, e.g. 1×10^{-2}. Further cycles are required if convergence is not achieved.

It was found in the present study that a maximum number of fifteen iterative cycles could give sufficient accuracy, even though convergence may not be guaranteed in all segments. Non-convergence can occur for a segment at a point of contraflexure. However, this has a minor effect on the overall accuracy of solution.

Generally, convergence problems can be avoided by choosing a target curvature increment for the early stages of loading which is not too large, e.g. using an increment size $< 0.001 \text{ m}^{-1}$. As analysis is carried out into the post-peak region, which corresponds to the formation of one or more hinge forming segments, the increment size for the target curvature can be increased.
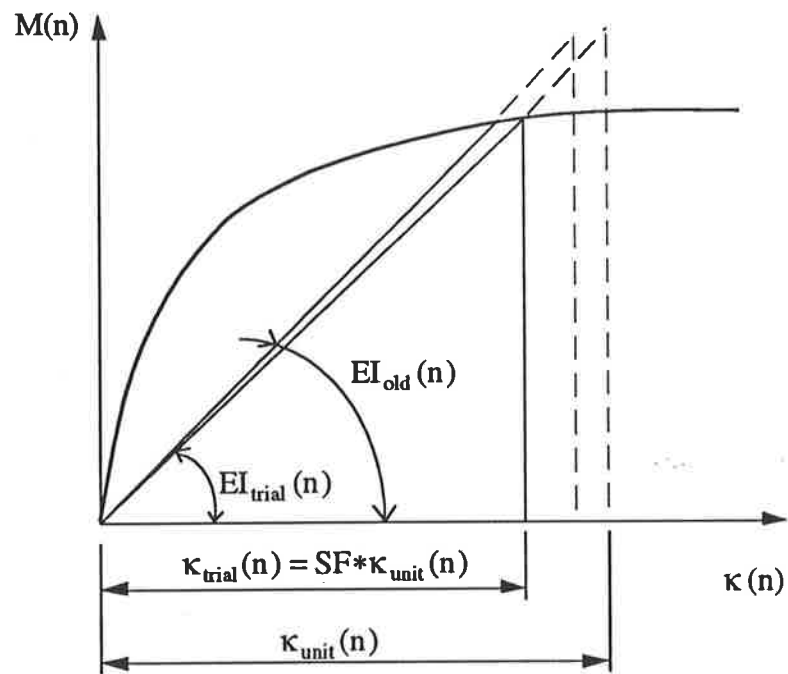
Figure 2.25: Trial curvature

```
                    ┌─────────────────────────────────────┐
              ┌────►│        Commence Step ISTEP          │
              │     └─────────────────────────────────────┘
              │                      │
              │     ┌─────────────────────────────────────┐
              │     │    Set curvature of key segment to   │
              │     │            κ_key(ISTEP)              │
              │     └─────────────────────────────────────┘
              │                      │
              │     ┌─────────────────────────────────────┐
              │     │    Set    EI(n) = OLDEI(n)          │
              │     └─────────────────────────────────────┘
              │                      │
              │     ┌─────────────────────────────────────┐
              │     │           CYCLE = 0                  │
              │     └─────────────────────────────────────┘
              │                      │
              │     ┌─────────────────────────────────────┐◄──────┐
              │     │        CYCLE = CYCLE + 1            │        │
              │     └─────────────────────────────────────┘        │
              │                      │                             │
              │     ┌─────────────────────────────────────┐        │
              │     │  Linear elastic analysis:            │        │
              │     │  Obtain from unit load pattern       │        │
              │     │  curvatures   κ_unit(n)             │        │
              │     └─────────────────────────────────────┘        │
```

Commence Step ISTEP

↓

Set curvature of key segment to $\kappa_{key}(ISTEP)$

↓

Set $EI(n) = OLDEI(n)$

↓

$CYCLE = 0$

↓

$CYCLE = CYCLE + 1$

↓

Linear elastic analysis:
Obtain from unit load pattern curvatures $\kappa_{unit}(n)$

↓

Calculate scaling factor
$SF(ISTEP) = \kappa_{key}(ISTEP) / \kappa_{unit}(n)$

↓

Obtain trial curvatures
$\kappa_{trial}(n) = SF(ISTEP) \times \kappa_{unit}(n)$

↓

Obtain updated deformed nodal positions and calculate out-of-balance nodal forces

↓

Section analyses:
Determine $M_{trial}(n)$ for each $\kappa_{trial}(n)$
Obtain updated flexural stiffnesses
$EI_{trial}(n) = M_{trial}(n) / \kappa_{trial}(n)$
and axial stiffnesses $EA(m)$

↓

Check Convergence:
Is $\dfrac{EI_{trial}(n) - OLDEI(n)}{OLDEI(n)} < \varepsilon$?　　Yes / No

↓ (No)

$OLDEI(n) = EI_{trial}(n)$ (loops back to $CYCLE = CYCLE + 1$)

↓ (Yes)

$ISTEP = ISTEP + 1$ (loops back to Commence Step ISTEP)

Figure 2.26: Typical computational step

2.8.4 Comparisons with Test Results

To check the accuracy of the segmental method of analysis, an investigation of test beams and frames was carried out in the present study. For discussion purposes, only three frames have been chosen, and represent three areas of concern: (1) good correlation, (2) poor correlation with stiffness underestimated; and (3) poor correlation with strength and stiffness overestimated.

Shown in Figure 2.27 is frame F6 which was tested by Furlong (1963). The tensile yield strength of the main reinforcing steel for this frame is 350 MPa, and the average concrete compressive strength from test cylinders is 24.5 MPa. Note the area of beam steel is considerably higher than the area of column steel, and it can be expected the beams to be much stronger and stiffer than the columns.

$Ast(BEAM) = 506 \text{ mm}^2$

$Ast(COLUMN) = 142 \text{ mm}^2$

$\alpha = 0.0555$
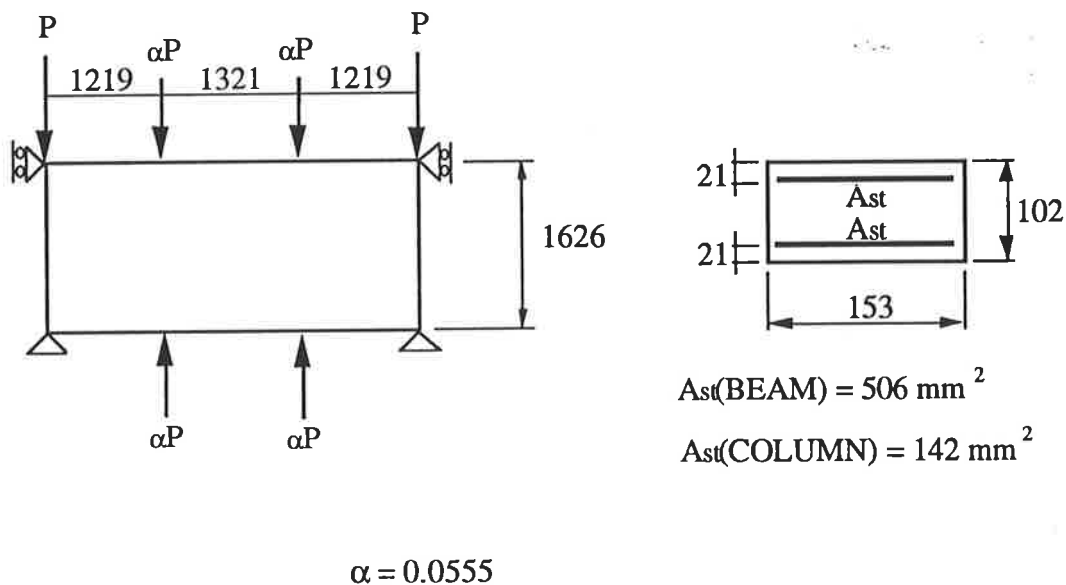
Figure 2.27: Test configuration and section details for frame F6 tested by

Furlong (1963)

Under the given load pattern, the columns are bent in single curvature, and for analysis, four elements have been chosen to represent the columns. This is done in order to model non-linear effects due to overall changes in geometry along the column lengths as the frame is subjected to increasing levels of applied load. The beams, which are not likely to be subjected to geometric non-linearities, are represented by single elements.

Analytical and experimental results for load versus lateral deflection at column mid-height are shown in Figure 2.28. Deflection was measured for both columns of the test frame, but as the magnitude of deflection at each level of load is very similar only a single line is shown to represent experimental results.
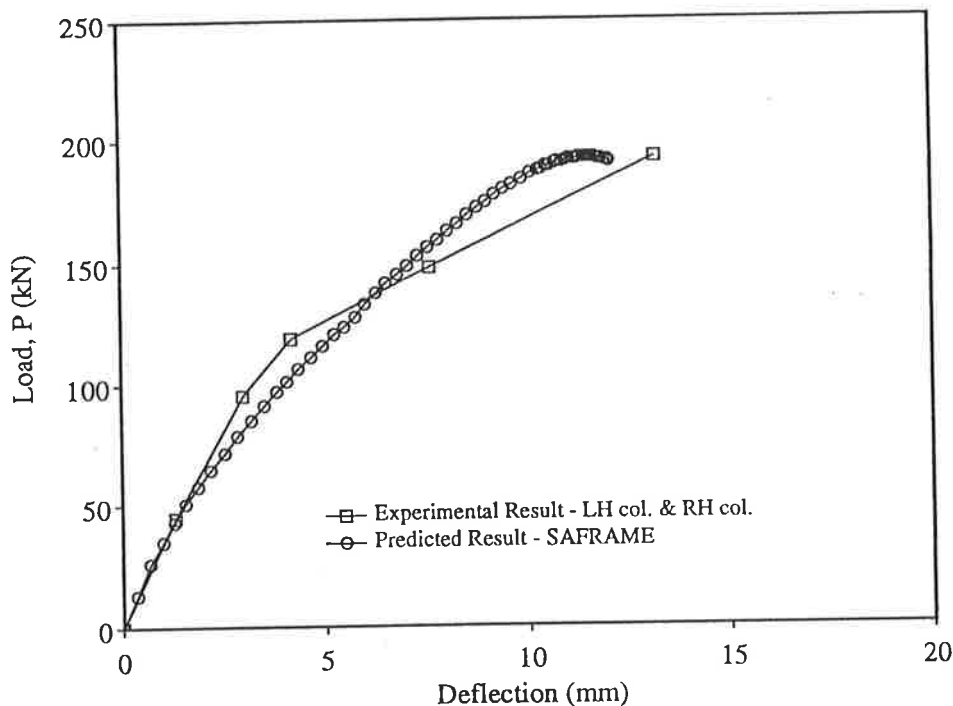
Figure 2.28: Comparison between experimental and analytical results
- good correlation

Frame failure corresponds to crushing of the concrete on the inside of the right hand column at the peak load, P, of 193 kN, and a similar failure occurred shortly after at mid-height of the left hand column. Analytical results compare very well up to a load of 50 kN, and as load increases up to a value of about 140 kN, stiffness is slightly

underestimated. From this load level up to the peak load, stiffness is slightly overestimated, but the peak failure load compares very well and the predicted critical sections also correspond to segments at mid-height of both columns.

The second type of comparison for analytical and experimental results is shown in Figure 2.29. Beam 4, tested by Clark and Spiers (1978), was subjected to symmetrical loading under a load control test situation. A primary flexural crack first developed at a midspan moment of approximately 19 kNm, and with increasing levels of applied load beyond the cracking load, there is a reduction in beam stiffness. The beam failed suddenly at a moment of 51.5 kNm.

Although the analytical results show a good prediction of the peak load value, stiffness is clearly underestimated. It should also be noted if a deformation control test set-up been employed, continuing deformation after the peak load could be expected.
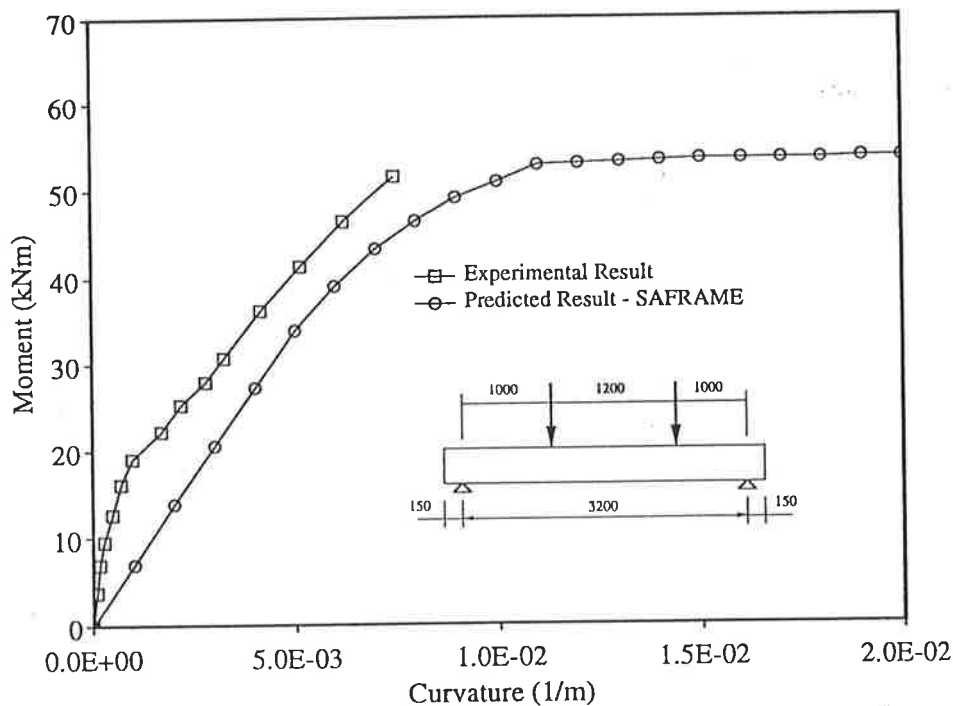
Figure 2.29: Comparison between experimental and analytical results
- stiffness underestimated

The third example of comparison for analytical and experimental results is for frame L2 tested by Ferguson and Breen (1966), and shown in Figure 2.30. A vertical load was applied to the top of the left hand and right hand columns and a lateral load was applied to the top of the right hand column. The section details are shown in Figure 2.31.

The beams are relatively stronger and stiffer than the columns, and failure can be expected to occur in the columns. Under the given load pattern, the columns are also bent in double curvature and failure is likely to occur at column ends, rather than within the column lengths.

Experimental and predicted results for load versus sway deflection are shown in Figure 2.32. This frame failed at a load, P, equal to 112 kN, when concrete crushed at the outside face at the top of the left hand column, i.e. at corner C. In comparison, the analytical results predicted the formation of hinges at the ends of all four columns prior to a peak load of 149 kN. The analysis overestimates the actual peak load by 33% and frame stiffness is also clearly overestimated.
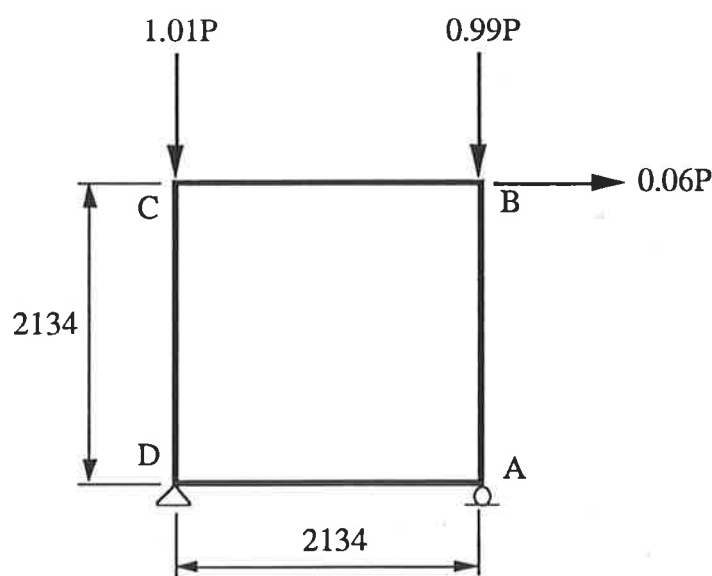
Figure 2.30: Test set-up for frame L2 tested by Ferguson and Breen (1966)
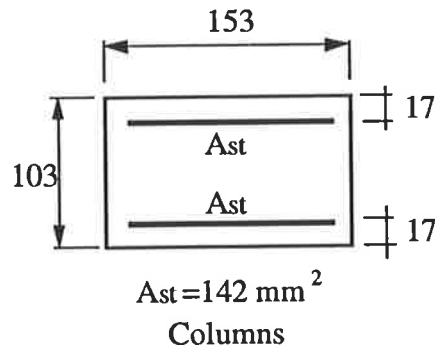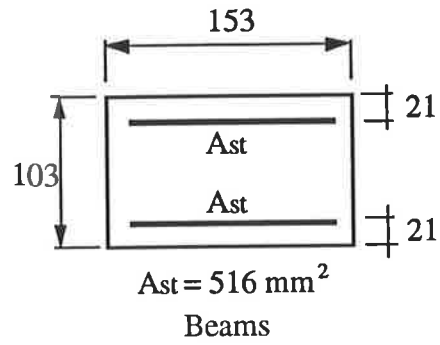
Figure 2.31: Section details for frame L2 tested by Ferguson and Breen (1966)
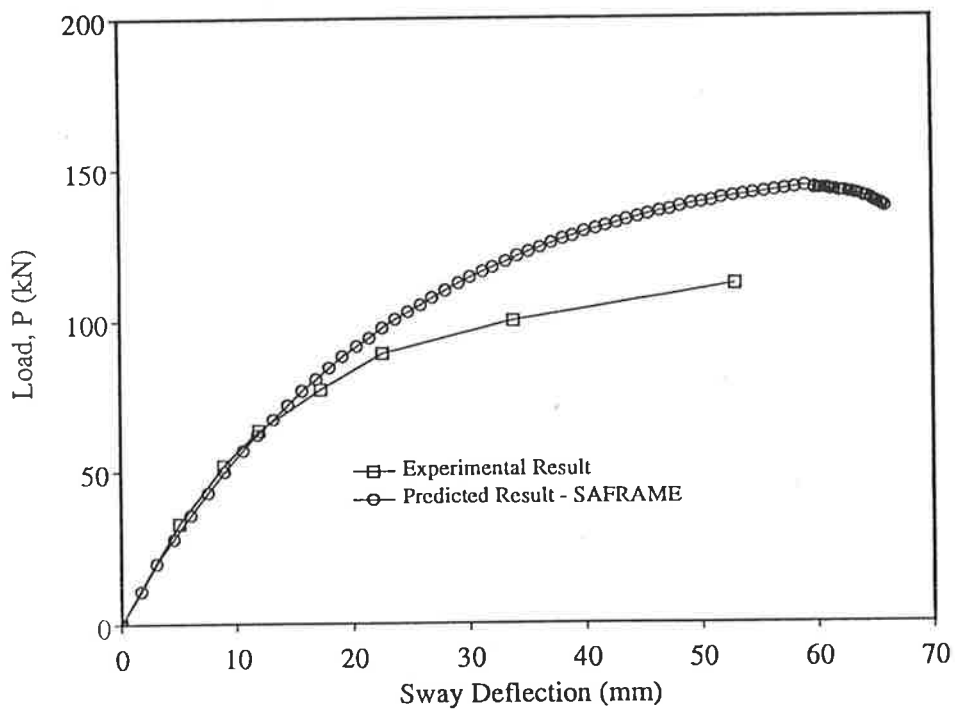
Figure 2.32: Comparison between experimental and analytical results

- strength and stiffness overestimated

2.8.5 Summary of Analytical Predictions by SAFRAME

Three different types of analytical prediction have been described in Section 2.8.4. In two cases, analytical results compared poorly with actual test results, and in the third case good correlation was achieved between analytical and experimental results. However, in making these observations it should be noted that accuracy of solution depends on limitations of the method of analysis. As pointed out by Wong (1989), the method does not take into account shear deformations or the beneficial effect of tension stiffening, and predicted deformations at any cross-section of a structure under load are due to primary flexural cracks. Crack growth may also be assisted or restrained by the presence of a tensile or compressive axial force respectively.

In the analysis of test beam 4 by Clark and Spiers, predicted strength compared well with actual strength, and flexural cracking at midspan was accurately predicted. However, stiffness was underestimated, and it was likely the tensile concrete had contributed to flexural stiffness in the pre-cracking range and additional stiffness was provided by concrete between cracks. However, the method of analysis ignores the tensile capacity of concrete.

Both strength and stiffness have been overestimated in the analysis of test frame L2 by Ferguson and Breen. Although tensile concrete may have contributed to stiffness of the column and beam elements, performance of this frame may have been controlled by joint behaviour. The analysis predicts the formation of four hinges, one at each column end, but actual frame failure corresponds to an insufficient number of hinges.

Finally, strength and stiffness and also the number and location of hinges compare well for test frame F6 by Furlong. In contrast to frame L2 by Ferguson and Breen, it appears that joint behaviour may not have adversely affected frame performance in this case. However, when assessing the performance of a beam-column connection, a number of factors must be considered, including the type of detailing within the connection, adequate anchorage of the reinforcement, and the direction of loading in the beam and column elements.

2.9 Summary and Conclusions

Various non-linear methods of analysis have been reviewed in this chapter, concluding with a description of the segmental method of analysis, SAFRAME, proposed by Wong (1989). A major advantage with the method is that full range behaviour, up to and including the post-collapse region, can be investigated. This is done by simulating a deformation control test set-up by incrementing curvature to a 'key segment' and performing a secant stiffness type of frame analysis. Most previous methods of frame analysis reviewed in this chapter simulate a load control test set-up in a tangent stiffness approach and analysis is terminated when the peak load is reached. These methods could be modified to include special techniques, such as those described in Section 2.5, but they are complicated to program and additional storage space is required.

Another advantage with SAFRAME is the treatment of geometric non-linearities by updating the nodal geometry and the transformation matrices as the structure deforms under load. Only one stiffness matrix per element is required in the formulation of the force-displacement relationships for material and geometric non-linear behaviour. Previous methods, some which have been described in this chapter, generally require additional matrices in the formulation for geometric non-linear effects. This increases the amount of storage and computational time for solution.

Although the method of section analysis in SAFRAME uses an elasto-plastic stress-strain relationship for steel, the strain hardening curve can easily be incorporated. Note also that any stress-strain relationship for concrete in compression and tension can be implemented.

To test the accuracy of the method of frame analysis, a number of comparisons were made between analytical predictions and actual results for test structures. Poor correlation was achieved in some cases, although it was noted that additional effects due to tension stiffening and deformations within beam-column connections had not

been taken into account. These non-linearities are investigated in Chapter 3 and Chapter 4 respectively of the present study, and numerical models for these effects are also proposed. These improvements to the segmental method of frame analysis have also been summarised elsewhere, (Kenyon and Warner; 1992, 1993).

Finally, the segmental method of frame analysis proposed by Wong assumes that loads are applied proportionally. In Chapter 5 of this thesis, the method of load application is modified to allow for sequential, non-proportional loading. Test frames with this type of loading are also investigated and the effects of tension stiffening and joint behaviour are noted.

Chapter 3

Tension Stiffening

3.1 Introduction

Tension stiffening in a flexural member is the additional stiffness provided by the tensile stress in the concrete between primary flexural cracks. The tensile force in the concrete is transferred to the reinforcing steel until the breakdown of bond between the concrete and steel occurs. As more primary cracks form, the region of concrete tensile stress diminishes.

Although tension stiffening has a minor influence on flexural strength, additional stiffness is provided at all sections, except right at the cracks, and this has a significant effect in decreasing deflections. Consequently, an analysis which ignores the uniaxial tensile strength of concrete and the effect of tension stiffening can overestimate deflections in the pre-cracking and post-cracking range.

Furthermore, tension stiffening influences frame behaviour by providing additional bending stiffness within beam and column elements and at beam-column connections. Following a review of previous work, a tension stiffening model is presented in this

chapter which uses a simplified stress-strain relationship for concrete in tension. This is based on experimental results of beams tested by Clark and Spiers (1978). The model is based on the results of beams which isolate the tension stiffening effect. Shear deformations are not considered in the tension stiffening model.

To check the accuracy of the model in a section analysis, results were compared with further simply supported beams tested by Healey (1993), Mendis (1986) and Monnier (1970). The behaviour of two-span continuous beams tested by Bachmann and Thürlimann (1965) and Tse and Darvall (1988), were also investigated.

3.2 Behaviour of Concrete Between Cracked Sections

Tension stiffening is only effective if a bond mechanism can transfer a tensile force between the steel and surrounding tensile concrete. The nature of the bond mechanism also changes at various stages of loading.

At initial stages of loading, chemical adhesion at the concrete-steel interface assists force transfer from concrete to steel, and vice versa. A radial compressive stress also exists at the interface, caused by shrinkage of the concrete on drying. Lutz and Gergely (1967) estimated a free shrinkage of 0.0003 produces a compressive interfacial stress of 80 psi (0.6 MPa).

When a primary flexural crack forms and crosses the reinforcing steel, the concrete adjacent to the crack slips against the steel. Slip, or bond-slip, is defined as the relative movement between the steel and surrounding concrete. However, the concrete in tension does not undergo immediate and rapid unloading. Tests by Goto (1971) and Jiang *et al.* (1984) show that shortly after the formation of a primary crack, secondary inclined cracks form at the surface of the reinforcement, (Figure 3.1a). Concrete between secondary cracks is a comb-like structure which wedges behind the

ribs. It offers frictional resistance to further slippage and assists the transfer of the tensile force in the concrete to the steel.
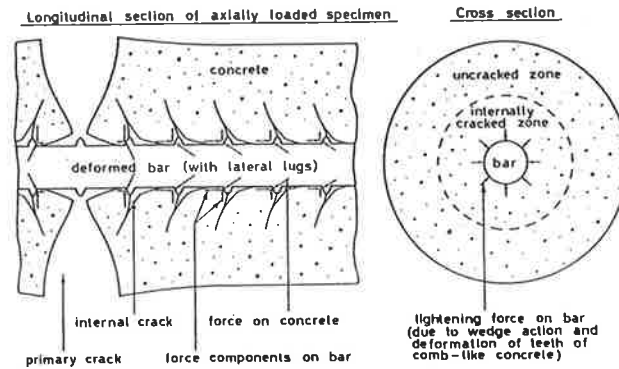
Figure 3.1: Cracked region around reinforcing steel, (a) longitudinal section; and (b) cross-section (Goto,1971)

Bond-slip is also influenced by the growth of longitudinal cracks near the steel and by crushing at points where concrete bears on the steel ribs. Ingraffea *et al.* (1984) modelled secondary cracking as the most significant effect on bond-slip and Lutz (1970) noted that secondary cracking inhibits the progress of splitting cracks.

As loading increases, extensive microcracking intersects primary and secondary cracks and may create a cracked zone as in Figure 3.1b. Eventually, transfer of a tensile concrete force to the steel becomes ineffective.

A relationship can be expressed between slip and the bond stress, u, at the bar-concrete interface. Bond stress is defined as the shear force per unit area of bar surface given by:

$$u = \frac{q}{\Sigma o} \tag{3.1}$$

where q = change of bar force over unit length

            Σo = nominal surface area of a bar of unit length

Shown in Figure 3.2 are curves of bond stress versus slip measured at four different locations in an embedded reinforced bar tested by Nilson (1972). The curves typify the non-linear and variable nature of bond-slip. In a more comprehensive study, Mirza and Houde (1979) found the amount of slip is dependent on the concrete strength, embedment length and concrete cover.
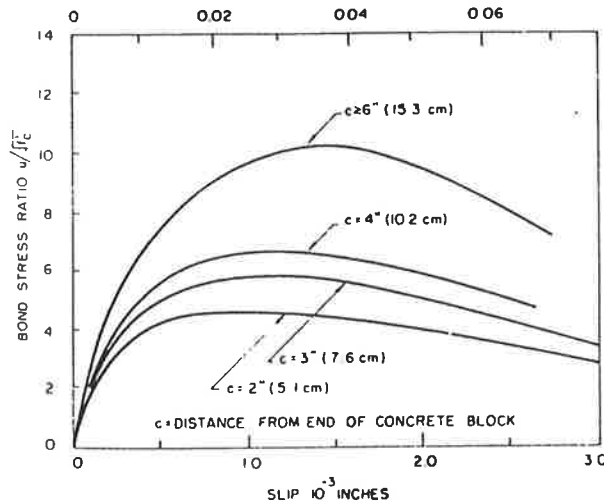
Figure 3.2: Bond stress-slip curves (Nilson, 1972)

3.3 Literature Review

3.3.1 Tensile Strength of Concrete

Essential to any tension stiffening model is an estimate of the tensile strength of concrete in uniaxial tension and the post-peak softening response. Although this strength is only 10-15% of the value for compressive strength, it is an important parameter in any tension stiffening model because it determines the load level at which a flexural crack forms. Tests for the tensile strength of plain concrete fall into one of three classifications, each with its own characteristic set of results: (1) direct tension, (2) flexural tension or modulus of rupture, and (3) indirect tension or splitting test.

There are no standard tests for direct tension, but it has been the subject of previous investigations partly because it is the only method which has allowed the post-peak response to be investigated. Hence, a stress-strain relationship based on the behaviour

of plain concrete in direct tension often forms the basis for modelling tension stiffening in a reinforced concrete member. The ascending and descending branches of the stress-strain curve can be obtained by using a testing machine in which the strain rate is controlled.

Specimen failure is caused by one crack propagating across the cross-section. A major problem with this method of testing is the difficulty in applying a pure tensile force to plain concrete. Hence, tests results can be affected by secondary bending stresses which may be induced by the grips. Prior to testing, the specimen is also allowed to dry and tensile stresses are created by shrinkage strains. The stress-strain curve is also affected by the location of the crack with respect to the length of strain gauge.

Evans and Marathe (1968) used a strain-controlled testing machine and the curves shown in Figure 3.3 are typical of the non-linear shape for the stress-strain response they obtained for concrete in tension. Hughes and Chapman (1966) and Gopalaratnam and Shah (1985) obtained curves of similar shape. Figure 3.4 shows unloading portions for specimens tested under cyclic loading by the latter.
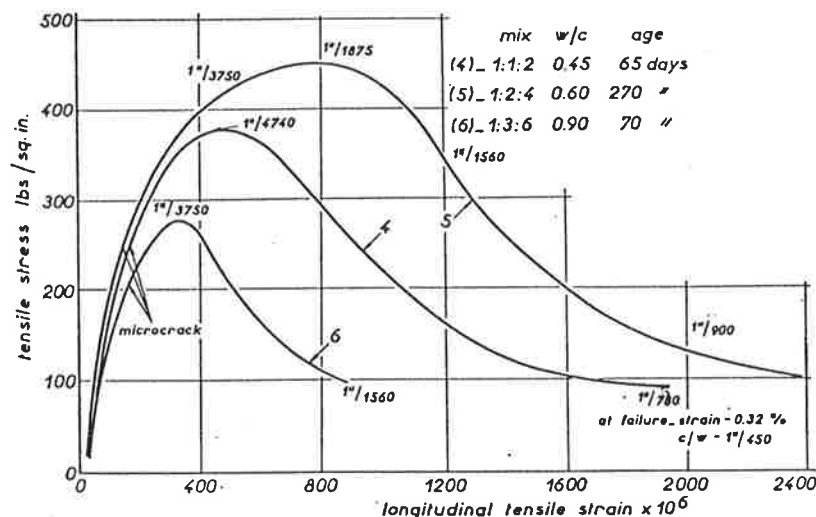
Figure 3.3: Stress-strain curves of plain concrete in tension

(Evans and Marathe, 1968)
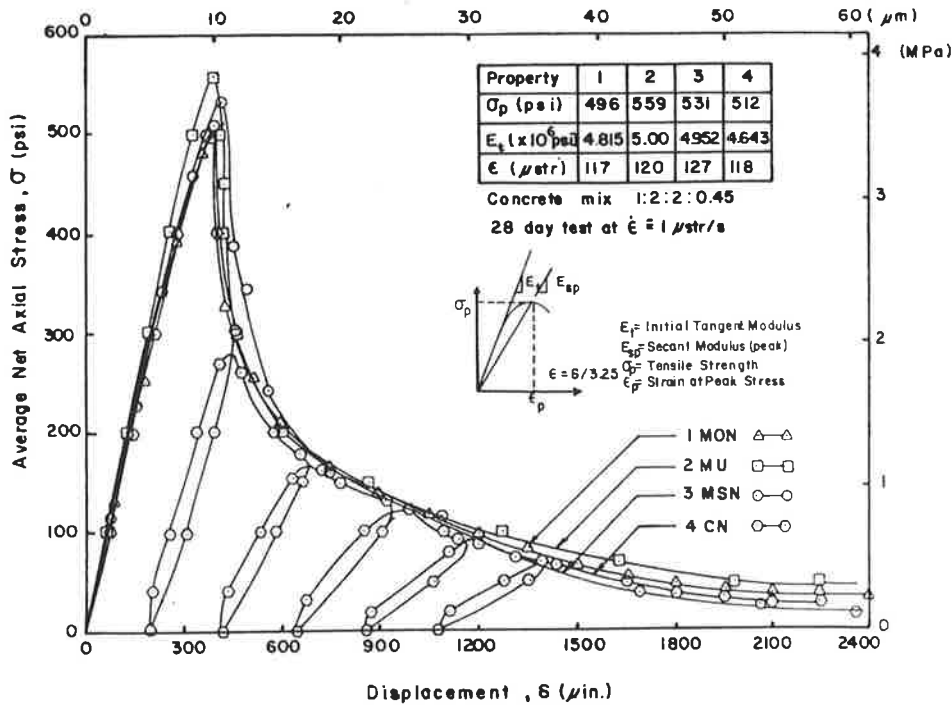
Figure 3.4: Stress-strain curves of plain concrete in tension
(Gopalaratnam and Shah, 1985)

In the modulus of rupture test, a simply supported beam is tested with either central point loading or third point loading. Test results depend on the dimensions of the beam and the arrangement of the loading. The modulus of rupture is the maximum tensile stress reached in the bottom fibre of the test beam and calculations are based on elastic theory. Stress is assumed to be proportional to the distance from the neutral axis of the beam, although the actual stress distribution is likely to be parabolic in shape. Modulus of rupture has been said to give the highest estimate of tensile strength and is the least preferred in analysis.

In the splitting test, a cylinder is loaded in compression on two diametrically opposite pads, as in Figure 3.5. The concrete is in a biaxial (compression-tension) state of stress and tensile failure occurs on the plane between the loaded pads. Tensile strength is measured indirectly. The splitting test gives more uniform results than other tension tests and is believed to give a strength which is closer to the true tensile strength of concrete than the modulus of rupture, (Neville, 1981). However, like the modulus of

rupture test, failure of the test specimen is sudden and a post-peak descending curve cannot be measured.
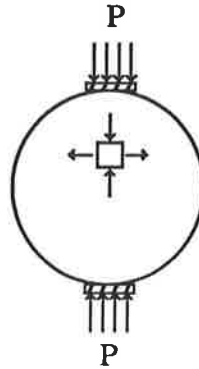
Figure 3.5: The splitting test

Tensile strength is often expressed mathematically as a function of compressive strength, and depends on the test method for obtaining the tensile strength. In the following Equations 3.2 to 3.6, the characteristic concrete compressive strength by cylinder test is given by f_c.

For an estimate of direct tensile strength (in MPa), ACI Committee 209 (1982) suggest the following for normal weight concrete:

$$f_t = 0.33\sqrt{f_c} \text{ , in MPa} \tag{3.2}$$

The following formulae have also been suggested to estimate the modulus of rupture, f_r:

ACI 318 Building Code (normal weight concrete):

$$f_r = 0.62\sqrt{f_c} \text{ , in MPa} \tag{3.3}$$

Raphael (1984):

$$f_r = 0.44 f_c^{2/3} \text{ , in MPa} \tag{3.4}$$

Raphael (1984) proposed the following relationship between the tensile strength from the splitting test, f_t, and the compressive strength, f_c :

$$f_t = 0.324 \, f_c{}^{2/3}, \text{ in MPa} \tag{3.5}$$

To account for concrete shrinkage before external load is applied, Collins and Mitchell (1987) proposed the following:

$$f_t = 0.33\sqrt{f_c} \tag{3.6}$$

Raphael (1984) analysed results from several hundred tests for compressive strength by cylindrical specimens and for tensile strength by the splitting, modulus of rupture and direct tension tests. It was found that modulus of rupture gave results 30-50% higher than the splitting test, compared to 40-80% as reported in ACI Committee 224 (1986). Raphael also found the direct tension test gave results 50% lower than the splitting test.

3.3.2 Methods of Analysis for Tension Stiffening

An analysis for the effect of tension stiffening can be performed at any of three different levels of complexity :

(1) at a microscopic level finite element methods of analysis are used to investigate the local state of stress in reinforcing steel and surrounding concrete;

(2) at a macroscopic level a modified stiffness approach uses "smeared" moment-curvature relationships by ignoring interactive effects between steel and concrete. The relationships are often empirically based; and

(3) an intermediate layered element approach commonly treats tension stiffening as properties of either the concrete or steel. It employs either a modified steel stress-strain relationship or a stress-strain curve for tensile concrete.

Investigations at the first level have contributed to an understanding of crack development and propagation. Early approaches by Lutz (1970), Ngo and Scordelis (1967), Nilson (1968) involved the idealisation of concrete and steel by a two dimensional system of triangular finite elements. To take into account bond-slip between the steel and concrete, Ngo and Scordelis used linkage elements to connect steel and concrete elements. The linkage elements, which have no physical dimensions, consist of two orthogonal linear springs. A disadvantage with these approaches is that cracks must be predefined so that manual mesh adjustments can be made.

Ingraffea *et al.* (1984) assumed that the bond-slip relationship at the location where a bar crosses a primary crack to be independent of the overall structural geometry. Interface elements model the effect of bond-slip and crack formation, and an updated deformed mesh is generated as cracks propagate, (Figure 3.6).
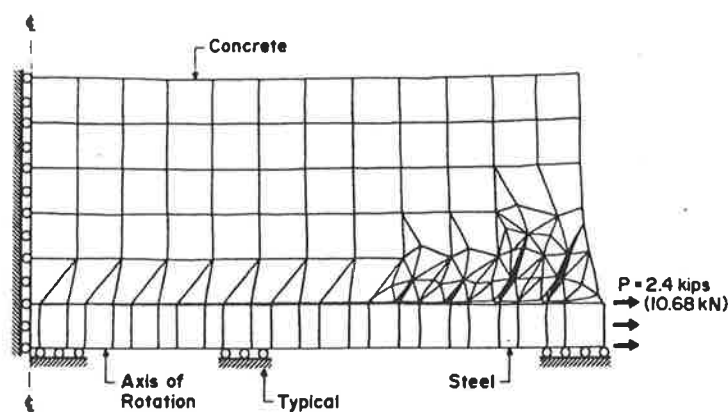
Figure 3.6: Deformed mesh from analysis by Ingraffea *et al.* (1984)

The second method of treating tension stiffening is by a modified stiffness method. It is concerned with load and deformation in the global sense. A typical example of this

approach is the trilinear moment-curvature curve proposed by Alwis (1990) and shown in Figure 3.7.
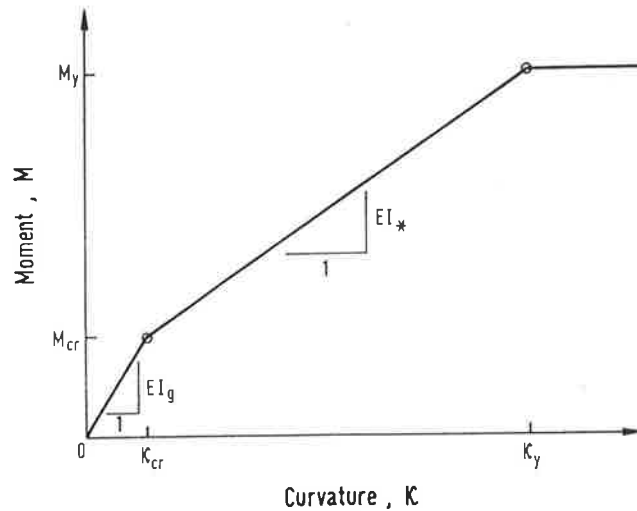
Figure 3.7: Trilinear moment-curvature curve (Alwis, 1990)

The first point which defines the curve corresponds to the first crack. From bending theory:

$$\frac{M_{cr}}{I_g} = \kappa_{cr}E_c = \frac{f_t}{y_t} \tag{3.7}$$

where f_t = tensile strength; E_c = elastic modulus; I_g = moment of inertia of the uncracked section, including the area of steel; and y_t = the distance from the neutral axis to the extreme concrete tensile fibre. The second coordinate point on the curve, (M_y, κ_y), corresponds to yielding of the tensile steel, and calculations are based on a fully cracked section. The response after yield is assumed to be perfectly plastic.

The trilinear M-κ curve in Figure 3.7 describes behaviour up to the post-yield region. At sections other than the hinge forming region, it is not uncommon for inelastic unloading to occur. Trilinear curves can also be modified to include a suitable unloading portion so that behaviour at all sections can be analysed.

Pre-generated M-κ curves have been used in investigations by others. Jofriet and McNiece (1971) used a bilinear moment-curvature relation for slabs based on flexural rigidities derived from effective and cracked moments of inertia of beams. In a similar approach, Bell and Elms (1971) assumed a rectangular bond stress-slip relationship to determine moment and curvature in the behaviour range between cracking and yield of the steel. Trilinear M-κ-N curves were used by Aguado *et al.* (1981) in a non-linear method of frame analysis.

The third method of modelling tension stiffening incorporates a tensile stress-strain relationship for concrete or steel and is commonly described as a smeared crack approach. A stress-strain curve for concrete in tension comprises an ascending portion which describes the uncracked behaviour of the concrete. The post-peak descending portion of the curve takes into account the effects of secondary cracking and bond-slip.

The most simplified approach to modelling tension stiffening is the bilinear curve proposed by Bazant and Oh (1984) and shown in Figure 3.8. The first segment of this curve corresponds to the pre-cracking range and is followed by a strain softening portion.
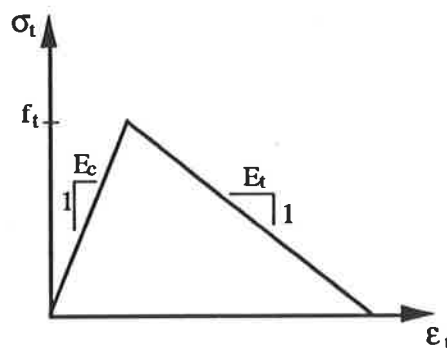
Figure 3.8: Uniaxial stress-strain curve for plain concrete in tension, (Bazant and Oh, 1984)

It is common in analysis to represent stress-strain up to the peak stress as a linear relationship of slope E_c, the Young's modulus for concrete in compression. The direct

tensile strength, in psi, is given by f_t. The tangent strain-softening modulus, E_t (in psi) is given by:

$$E_t = \frac{-70E_c}{57 + f_t}$$

(3.8)

The curve is derived from direct tension tests, (Bazant and Oh, 1983). The area under the curve is the strain energy released from the crack per unit width of fracture zone. The strain energy can be measured from the testing device for tensile strength and the width of fracture zone is simply estimated from the specimen. This type of relationship models the non-linear fracture zone as a smeared crack band. Accuracy of this approach was compared with Branson's formula for two theoretical cases: beams with 2% and 4% tensile reinforcement.

Tension stiffening models for reinforced concrete bars have been developed by Carreira and Chu (1986), Gupta and Maestrini (1990), Massicotte *et al.* (1990). These models are based on a single reinforcing bar embedded in a concrete specimen. A disadvantage with this approach is that the effects of bar spacing and embedment depth are not considered.

Gupta and Maestrini (1990) derived a tension stiffening curve for reinforced concrete bars and shown in Figure 3.9. A bilinear bond stress-slip relationship was included as a constitutive property based on a normalised bond stress-slip curve from the experimental curves obtained by Nilson (1972). Due to its high variability, bond-stress slip was eliminated from the formulation. Two assumptions were made: (1) when a primary crack forms, the bond force is relatively high; and (2) when the steel has yielded, bond between the steel and surrounding concrete is almost completely lost.

Keypoints on the tension stiffening curve are given by A, B, C and D. The curve is linear up to point A, where the first crack forms. At point A the bond force is relatively much larger than the tensile concrete cracking force. Tensile stress decays to point B. Between point B and point C, further cracks form along the bar and a

uniform bond stress is assumed. At point C all bond is assumed to be completely lost and tensile stress decays rapidly to point D where the steel yields. At point D, tension stiffening is assumed to have diminished.

The accuracy of this tension stiffening model was compared with load-deformation and stress-strain results of reinforced concrete bars tested in uniaxial tension. Although good correlation was obtained, no comparisons were made with the performance of test beams.
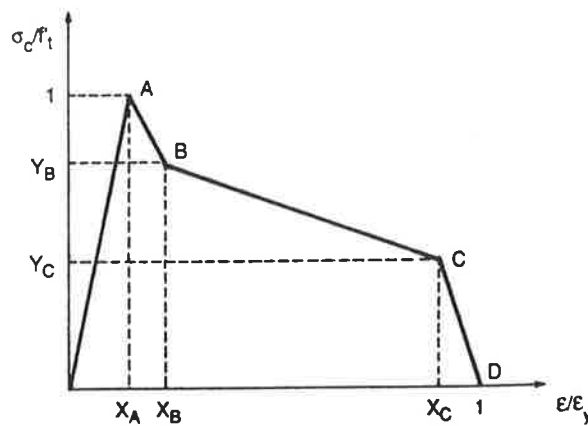
Figure 3.9: Tension stiffening model proposed by Gupta and Maestrini (1990)

Key points shown on the curve are:

$$X_A = \frac{nf_t'}{f_y}, \ Y_A = 1; \ X_B = \frac{nf_t'}{f_y}\left(1 + \frac{1+n\rho}{10n\rho}\right), \ Y_B = 1 - \frac{1+n\rho}{10};$$

$$X_C = 1 - \frac{1}{2n\rho}\frac{nf_t'}{f_y}, \ Y_C = \frac{1}{2} \tag{3.9}$$

where n is the modular ratio $= E_s/E_c$, and ρ is the ratio of area of steel to area of concrete. The yield strain and yield stress are ε_y and f_y, respectively, and the direct tensile strength of the concrete is f_t.

The concrete tensile stress-strain relationship proposed by Massicotte *et al.* (1990) is based on experimental results for plain concrete tested in direct tension. From this

relationship, a tension stiffening curve was developed and is shown in Figure 3.11. The tension stiffening model assumes that a member consists of uncracked regions between the cracks (region I) and fully cracked regions adjacent to the cracks (region II), which are shown in Figure 3.10. In region I, both the concrete and steel behave as if the concrete had an infinite tensile strength, i.e. linear elastic behaviour is assumed. In region II, the reinforcing steel carries all the tensile force in the member after cracking. The relative length of the two regions is given by a distribution coefficient :

$$\zeta = 1 - \beta_1 \beta_2 (f_{scr}/f_s)^2 \tag{3.10}$$

where $\beta_1 = 1.0$ for deformed bars; and $\beta_2 = 1.0$ for first loading and 0.5 for long-tem or cyclic loading. The terms f_{scr} and f_s are the steel stresses in region II at cracking and after cracking, respectively, assuming no stress in the concrete for both cases. The average strains in the steel over the length s_m are:

$$\varepsilon_m = (1 - \zeta)\varepsilon_1 + \zeta\varepsilon_2 \tag{3.11}$$

where ε_1 and ε_2 are the reinforcement strains in regions I and II, respectively.

The tension stiffening curve is linear up to a cracking strain ε_{cr} and peak stess f_{cr}. After a primary crack forms, stress in the concrete decreases to point a, where stabilised cracking is reached. The rate of decay of stress and strain depends on the effective reinforcement ratio, $\rho_{eff} = A_s/A_{cef}$, where A_s = the area of tensile steel and A_{cef} is the effective concrete-embedment zone in the vicinity of a reinforcing bar and is defined as the area of concrete of width and height equal to 15 times the bar diameter. If the effective reinforcing ratio ρ_{eff} is greater than $\rho_{stbl} = \frac{1}{6n}$, where $n = E_s/E_c$, the modular ratio, then the strain in region II remains equal to ε_{cr} at the cracking load level. This corresponds to a heavily reinforced section. If the value of ρ_{eff} is less than a limiting value ρ_{lim}, which is equal to $\frac{1}{15n}$, then the strain at stabilised cracking is given by:

$$\varepsilon_2 = \varepsilon_{cr}\left(1+\frac{1}{n\rho}\right) \tag{3.12}$$

When the effective reinforcing ratio is within the bounds, $\rho_{lim} \leq \rho \leq \rho_{stbl}$, the tensile concrete stabilises at a strain value given by the following:

$$\varepsilon_2 = \varepsilon_{cr}\frac{17+33n\rho}{33n\rho-1} \tag{3.13}$$

When ε_2 is evaluated by Equations 3.12 or 3.13, the average strain and stress, which correspond to point a in Figure 3.11, are given by:

$$\varepsilon_{TScr} = (1-\zeta_{cr})\varepsilon_{cr} + \zeta_{cr}\varepsilon_2 \geq \varepsilon_{cr} \tag{3.14}$$

$$f_{TScr} = (1-\zeta_{cr})f_t' + \zeta_{cr}f_{so} \geq f_{so} \tag{3.15}$$

for the condition

$$\zeta_{cr} = 1-\beta_1\beta_2 \geq \frac{w_c}{s_m} \tag{3.16}$$

In this expression, the post-cracking distribution factor is ζ_{cr}, the width of the fracture zone, w_c, is taken to be three times the aggregate size and the crack spacing is s_m. The concrete stress in region II is f_{so} and the maximum tensile stress of the plain concrete is f_t. Point b in Figure 3.11 is the average strain and average stress at the onset of yielding in region II and are given by:

$$\varepsilon_{TSy} = \frac{n\rho+\zeta_y}{1+n\rho}\varepsilon_y \tag{3.17}$$

$$f_{TSy} = n\rho E_c(\varepsilon_y - \varepsilon_{TSy}) \tag{3.18}$$

where the distribution factor ζ_y is obtained by substituting f_s for f_{sy} in Equation 3.10, i.e. :

$$\zeta_y = 1 - \beta_1\beta_2 \left(\frac{f_{scr}}{f_y}\right)^2 \qquad (3.19)$$

A second order relationship defines the stress-strain relationship between points *a* and *b* and is given by:

$$f_{TS} = f_{TSy} + (f_{TScr} - f_{TSy})\left(1 - \frac{\varepsilon_m - \varepsilon_{TScr}}{\varepsilon_{TSy} - \varepsilon_{TScr}}\right)^2 \qquad (3.20)$$

where ε_m = the average strain at which the concrete stress f_{TS} is evaluated. A linear relationship describes the average stress and strain between points *b* and *c* in Figure 3.11. Tension stiffening becomes ineffective when the strain ε_m equals the yield strain in the steel, ε_y. The tension stiffening model was compared with results of direct tension tests on reinforced concrete bars.
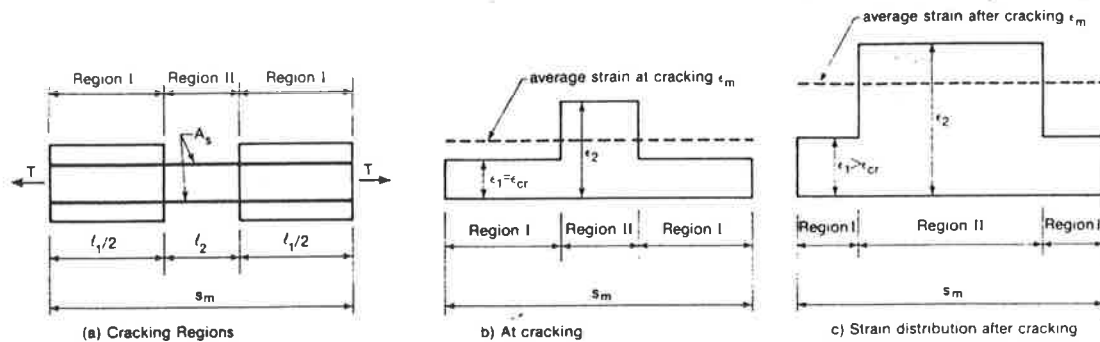
Figure 3.10: Cracked regions for tension stiffening model by Massicotte *et al.* (1990)
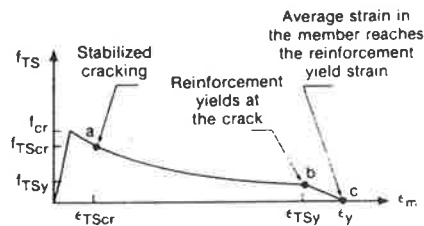
Figure 3.11: Tension stiffening model proposed by Massicotte *et al.* (1990)

The model by Massicotte *et al.* (1990) determines the relative weight of a cracked and an uncracked region by a distribution factor. The length over which softening is smeared can also be determined by a simple method proposed by Braam (1990). Figure 3.12 shows a cracked section with a height of h_{cr} and the smeared length is given by:

$$l_1 = 2(h_{cr} - y) \qquad (3.21)$$
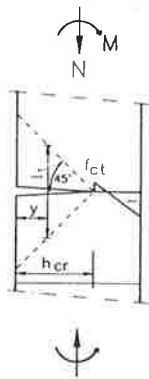
Figure 3.12: Section through cracked region, (Braam, 1990)

The shape of the curve by Massicotte *et al.* (1990) is similar to the curve proposed by Link *et al.* (1989) and shown in Figure 3.13. The stress-strain curve for concrete in tension comprises two second order polynomials after the peak tensile strength. An immediate drop in stress occurs if the strain at the level of the steel reaches the steel yield strain. In each model by Gupta and Maestrini (1990), Link *et al.* (1989) and Massicotte *et al.* (1990), tension stiffening is assumed to have diminished when the steel has yielded.

Carreira and Chu (1986) proposed the relationship given by Equation 3.22 to represent the overall behaviour of reinforced concrete in tension. This exponential expression takes into account the combined effects of cracking and slippage at cracks along the reinforcement.
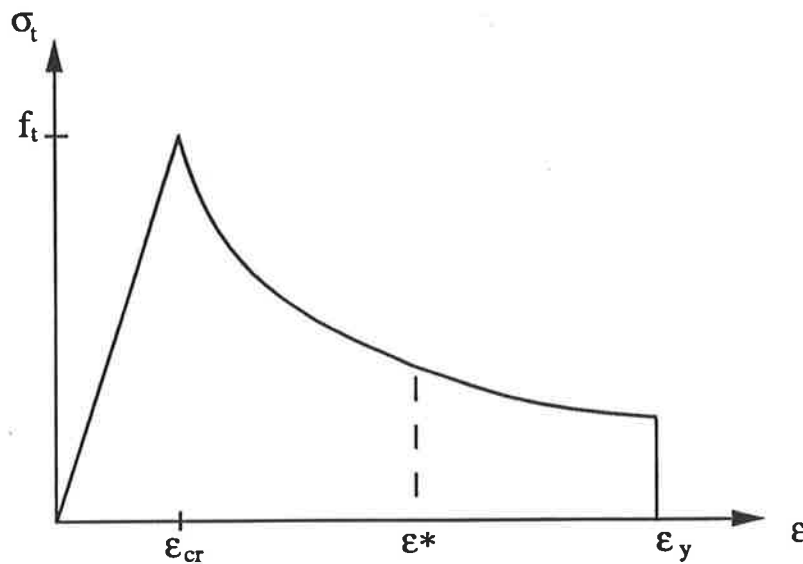
Figure 3.13: Tension stiffening model proposed by Link *et al.* (1989)

$$\frac{f_t}{f_t'} = \frac{\beta\left(\dfrac{\varepsilon}{\varepsilon_t'}\right)}{\beta - 1 + \left(\dfrac{\varepsilon}{\varepsilon_t'}\right)^{\beta}}$$

(3.22)

where

f_t = the stress corresponding to the strain ε

f_t' = the point of maximum stress, considered as the tensile strength

ε_t' = the strain corresponding to the maximum stress f_t'

β = a parameter that depends on the shape of the stress-strain diagram

Equation 3.22 is similar to a relationship for plain concrete in compression also developed by Carreira and Chu. Predicted values of β were found to be in the range 1.56 to 2.26 and it is convenient to use a value of β which is the same for tension as for compression. An average value of ε_t' equal to 0.00018 is recommended for normal weight concrete.

Various types of tension stiffening models were compared in a study by Gilbert and Warner (1978). Three different concrete tensile stress-strain diagrams were examined in a layered finite element study of slab deflections. Each stress-strain diagram in Figure 3.14a,b,c assumes a separate curve for the layer containing the tensile steel and cracked concrete layers once and twice removed from the tensile steel. Layers more than twice removed are assumed not to carry any tensile stress. The curve shown in Figure 3.14a is similar to the stepped diagram used in an analysis of slab deflections by Scanlon and Murray (1974). However, the method by Scanlon and Murray assumes the same stress-strain relationship for all concrete layers.

The curves in Figure 3.14b are similar to the curve used by Lin and Scordelis (1975) to analyse reinforced concrete shells. Gilbert and Warner also used a shear retention factor, similar to that used in layered element approaches by Hand *et al.* (1973) and Lin and Scordelis (1975). The shear retention factor modifies the concrete shear modulus and accounts for aggregate interlock and dowel action from slippage at the surface of the reinforcement.

Also considered by Gilbert and Warner are the piecewise linear diagrams with a discontinuity at the initial cracking stress, as shown in Figure 3.14c. The types of curves for concrete in tension proposed by Gilbert and Warner (1978) are well suited to a sectional analysis routine. Each curve can be represented by a simple mathematical formula and suitable unloading portions can be incorporated.

Gilbert and Warner also examined tension stiffening with a modified stress-strain relationship for tensile steel which is assumed to carry the additional stress when the concrete has cracked, (Figure 3.15). It was noted that results for the discontinuous unloading response stress-strain diagram, shown in Figure 3.14c, required an average number of 8.3 iterations per load increment. This is compared to 2.7 iterations for the modified stress-strain curve for steel. A likely reason for the large difference in the rates of convergence is that the modified steel curve requires stress and strain to be evaluated at a single layer, whereas the modified concrete curves require stress and strain to be evaluated at three layers. Both approaches include sudden changes in the

stress-strain curves which may also affect the rate of convergence and accuracy of solution.
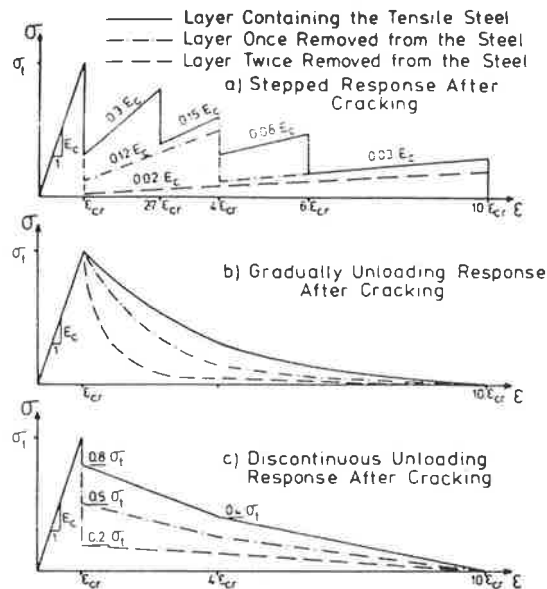
Figure 3.14: Stress-strain diagrams for concrete in tension,

(Gilbert and Warner, 1978)

Figure 3.15: Modified stress-strain diagrams for tension steel after cracking,

(Gilbert and Warner, 1978)

3.3.3 Summary and Conclusions

As described in this section, analysis for the effects of tension stiffening in a flexural member can be carried out at any of three levels. The finite element approach is best suited to the analysis for localised behaviour. It is not a practical option in a non-linear frame analysis because large numbers of elements and computer storage demands are required. Hence, a finite element approach was considered unsuitable for use in the present study for overall structural behaviour.

The intermediate level which treats tension stiffening effects in a smeared crack approach is well suited to the present method of frame analysis. A tensile stress-strain curve for either steel or concrete can be incorporated in the section analysis routine. This allows for the influence of tension stiffening on moment and curvature to be investigated. The global approach which involves pre-generated moment-curvature curves is recommended for further studies. Such curves need to be generated for different levels of axial thrust.

Several tension stiffening models have been reviewed, including those based on a tensile stress-strain curve for concrete in plain tension. However, there has been limited comparison between predicted results from the analytical models and the results from actual test beams. To determine a suitable tension stiffening model for the present method of frame analysis, comparisons are made between predicted analytical results and test results in the following section.

3.4 Experimental Basis for Proposed Model

A series of beams tested by Clark and Spiers (1978) was chosen for analysis. Fourteen beams with percentages of tensile reinforcement ranging from 0.44% to 1.99% were tested. Seven beams were designed with different section and material properties, and each of these initial test beams had repeat test beams using the same concrete mixes. All seven main beams were analysed plus three repeat beams, which

had significantly different mean compressive strengths from their corresponding main beams. Figure 3.16 shows the test set-up for all beams and section details and material properties for beam 4 and beam 6R. Note that the loading configuration creates a constant moment region.
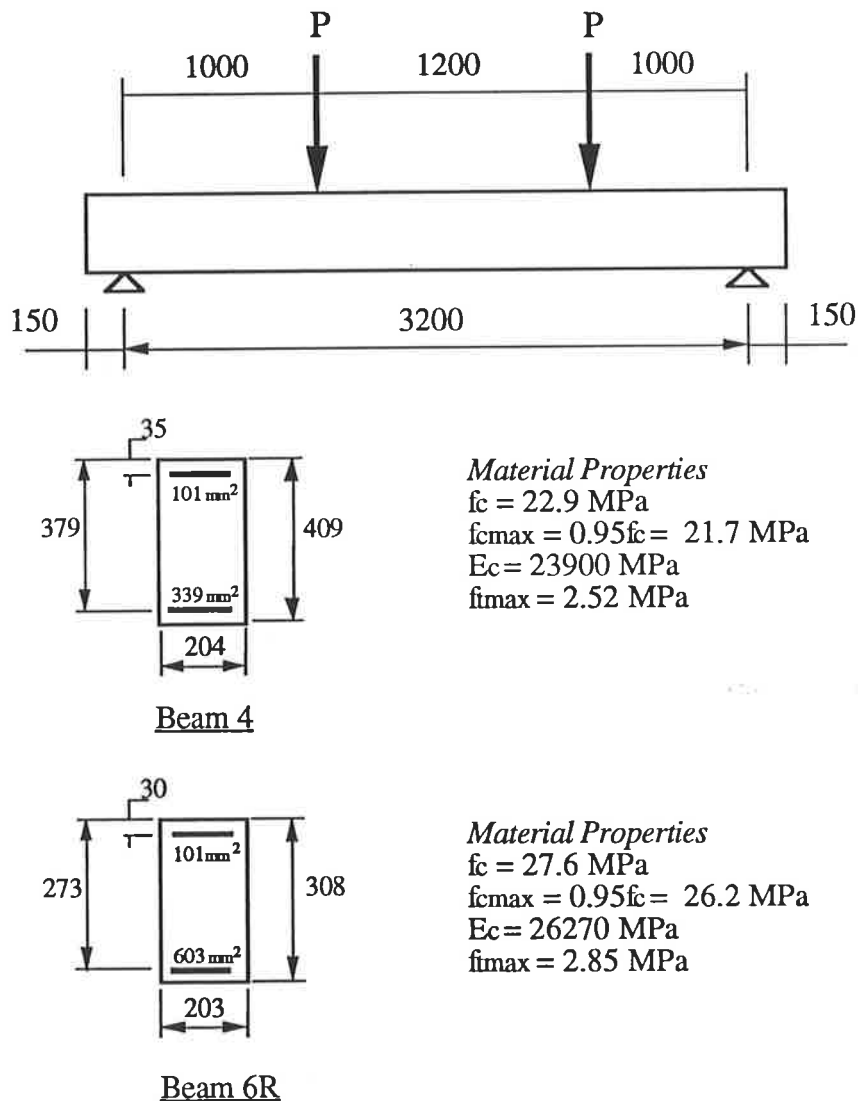
Figure 3.16: Test set-up for beams tested by Clark and Spiers (1978)

Materials

Reinforcing Steel

12, 16, 20 and 25 mm GK torbar deformed reinforcement was used by the investigators and Figure 3.17 shows the stress-strain plots obtained from testing. The steel becomes non-linear at a strain of 1400 to 1600 microstrain. For the present

study, steel stress is assumed to reach a maximum value at a strain of 0.0035 and with increasing strain the corresponding steel stress remains constant.
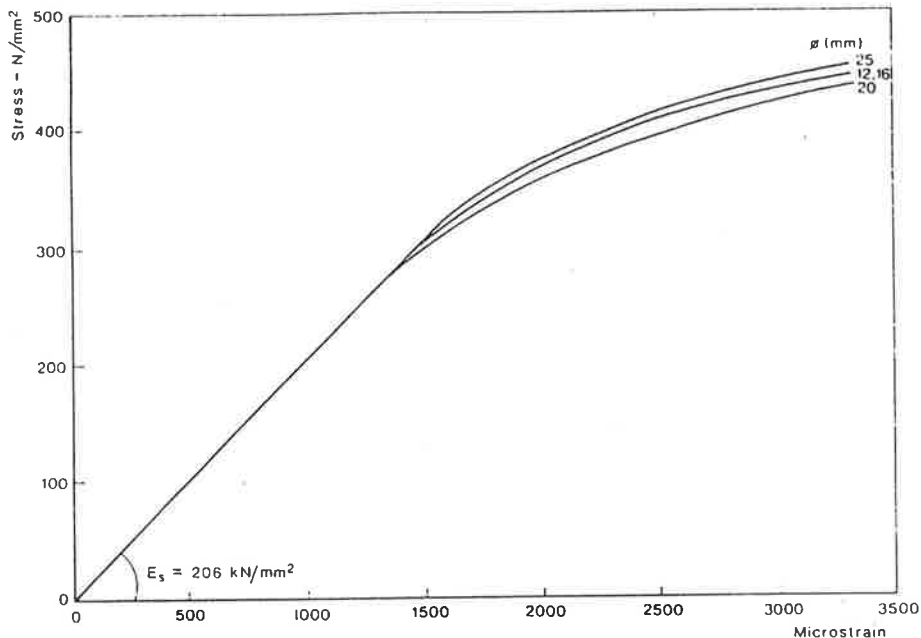
Figure 3.17: Stress-strain curves for reinforcing steel used by Clark and Spiers (1978)

Concrete - Compressive Strength

The compressive strength for test samples was determined from cube specimens. These samples were taken for each beam on the day of testing and the values reported by the investigators are assumed to be average compressive strengths. An equivalent cylinder compressive strength was determined from the ratio of cylinder-strength to cube-strength suggested by L'Hermite (1955) and cited by Neville (1981):

$$\frac{\sigma_{cyl}}{\sigma_{cube}} = 0.76 + 0.2log_{10}(\frac{\sigma_{cu}}{2840}) \tag{3.23}$$

where σ_{cu} is the strength of the cube in pounds per square inch.

It is also common practice to assume that the cylinder strength is equal to four-fifths of the cube strength, which is an approximation within 5 to 8% of the ratio suggested by

L'Hermite. All beams analysed were assumed to have a peak compressive stress, f_{cmax}, equal to 0.95 times the mean cylinder strength. A factor of 0.95 to convert concrete strength from a test sample to strength in a horizontally cast structural member has also been used by Ford, Chang and Breen (1981a). This value is used throughout the present study in the investigations for test beams and frames. Although a factor of 0.85, which was proposed by Hognestad (1951), is used more widely, this value is believed to be more applicable to vertically cast members.

The value for the concrete modulus, E_c, used throughout this study is assumed to be equal to $5000\sqrt{f_{cm}}$, where f_{cm} is the mean cylinder strength. Carse and Behan (1980) showed the concrete modulus expressed as a function of the concrete compressive strength has a 40% variation. Klink (1985) noted the modulus varies considerably across the section of the test specimen and the actual value is 50% higher than the value obtained from a standard empirical formula. Nevertheless, the value for the modulus in the present study is based on a conservative empirical formula.

Concrete - Tensile Strength

Indirect tensile (splitting) tests were also carried out on three samples for each beam. However, for the present study to determine the tensile strength, f_{tmax}, in a structural member the following equation, based on Raphael's study, was used.

$$f_{tmax} = 0.324(f_{cmax})^{2/3}, \text{ in MPa} \tag{3.24}$$

where $f_{cmax} = 0.95 \times f_c$, in MPa

3.5 Application of Previous Tension Stiffening Model in the Section Analysis

Initially, the simplified bilinear stress-strain curve for concrete in tension proposed by Bazant and Oh (1984) was included in the section analysis routine. This tension stiffening model is based on a maximum tensile stress in the concrete equal to the

strength obtained from a direct tension test. For the present study, the strength determined by the splitting test was chosen because it is believed to give a better estimate of the strength in a structural member.

The results for moment-curvature plotted at midspan for beam 4, with 0.44% tensile steel, are shown in Figure 3.18. Analytical results do not compare well with the experimental results. Other test beams by Clark and Spiers were examined and similar trends were observed. However, it was found that good correlation could be obtained by adjusting the softening portion of the model by Bazant and Oh. Such modifications led to the development of a tension stiffening model which is described in the following section. This model is based on previous investigations, including Gilbert and Warner (1978), Gupta and Maestrini (1990) and Massicotte *et al.* (1990).
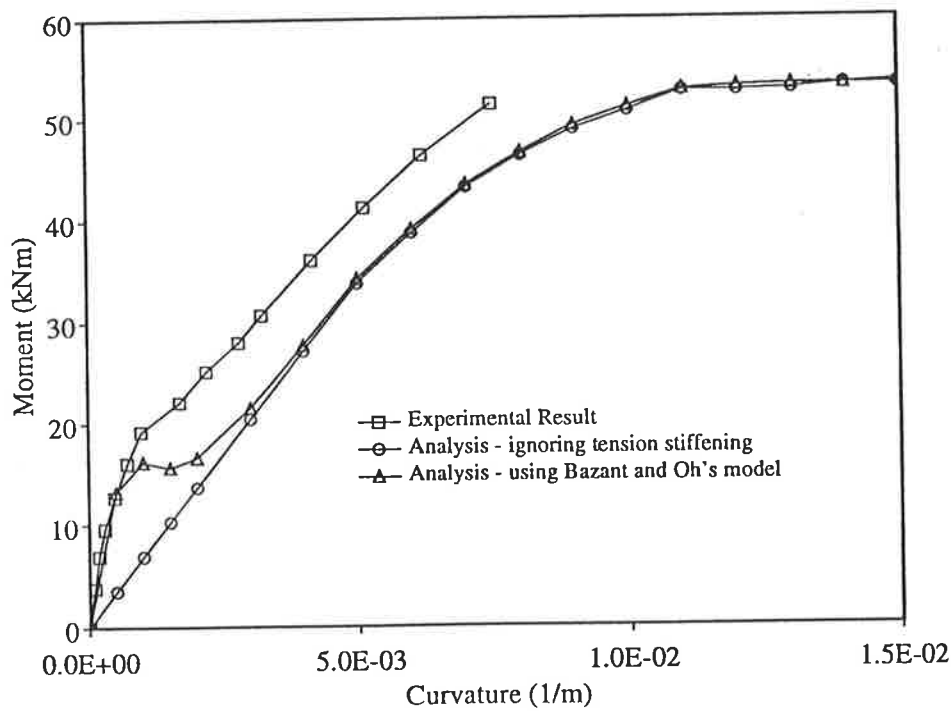
Figure 3.18: Analysis of test beam using concrete tension curve by

Bazant and Oh (1984)

3.6 Development of Proposed Model

The tension stiffening model developed in this study uses a simplified stress-strain relationship for tensile concrete, where each tensile layer has the same stress-strain response. The stress-strain relationship for concrete in compression is that proposed by Warner (1969) and has been discussed in Chapter 2. A suitable unloading portion has also been included. The stress-strain relationship for the reinforcing steel was modelled by a piecewise linear curve with four linear segments. It was found that by modelling the section with 20 layers, including concrete and reinforcing steel, that sufficient accuracy in analytical results could be achieved.

Beam analyses were carried out by dividing a member into a number of segments. The length of each segment is assumed to be equal to the depth of the beam, and tension stiffening effects are assumed to be smeared over the segment length.

Initially, a piecewise linear curve (Figure 3.19) for concrete in tension, was chosen for analysis, with an ascending portion of slope E_c, similar to that in Figure 3.8. A primary crack forms at a strain of ε_{cr} and corresponding maximum tensile stress f_{tmax}. This is followed by a discontinuity where the concrete tensile stress drops to a value of $0.4 f_{tmax}$. A softening portion then follows.

The commencement of tension softening is similar to the point of stabilised cracking termed by Massicotte *et al.* (1990). It was also found in the present study that the slope of the softening portion depends on the percentage of tensile reinforcement. Beams with high percentages of tensile steel are characterised by steeper softening portions.

The strain at which tension stiffening diminishes is given by $\gamma_t \varepsilon_{cr}$. In previous studies, tension stiffening is assumed to become ineffective at a strain which is either a multiple of the tensile concrete cracking strain or a strain equal to the yield strain of the tensile steel. Since the stress-strain curves for steel used by Clark and Spiers are non-linear

with no obvious yield point, it is more convenient to select a strain corresponding to a multiple of the cracking strain ε_{cr}.

The tension stiffening curve in Figure 3.19 also includes an unloading portion which is parallel to the initial tangent modulus. This is a reasonable assumption and is based on the test curves obtained by Gopalaratnam and Shah (1985) and shown in Figure 3.4.
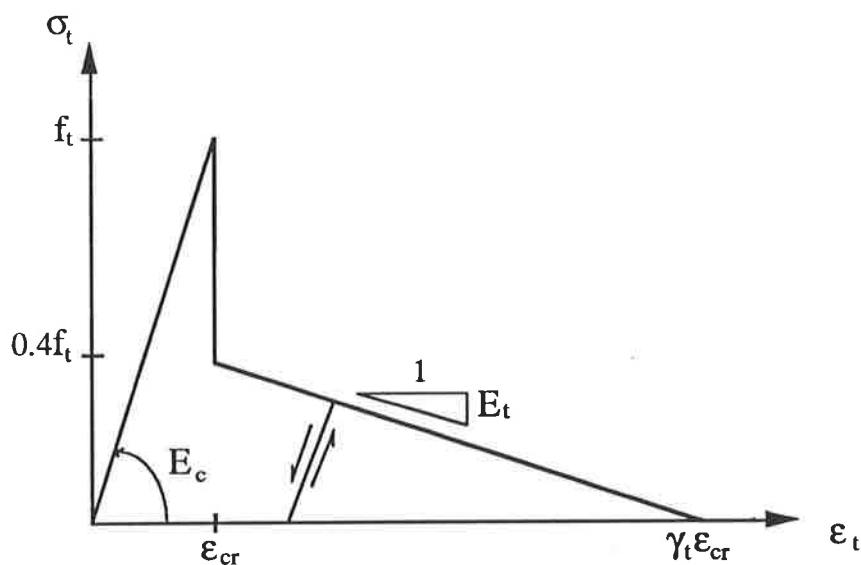
Figure 3.19: A preliminary tension stiffening curve

Figure 3.20 shows the relationship between γ_t and percentage of steel, p, for the ten beams analysed. A simplified equation representing the line of best fit has been adopted for the present study, where

$$\gamma_t = 41 - 17p \quad , \text{ for } 0.44\% \leq p \leq 2.0\% \qquad (3.25)$$
$$\gamma_t = 7 \quad , \text{ for } p > 2.0\% \qquad (3.26)$$

or in terms of a tangent softening modulus :

$$E_t = \frac{-E_c}{100 - 43p} \quad , \text{ for } 0.44\% \leq p \leq 2.0\% \qquad (3.27)$$

$$E_t = \frac{-E_c}{15} \qquad \text{, for } p > 2.0\% \tag{3.28}$$
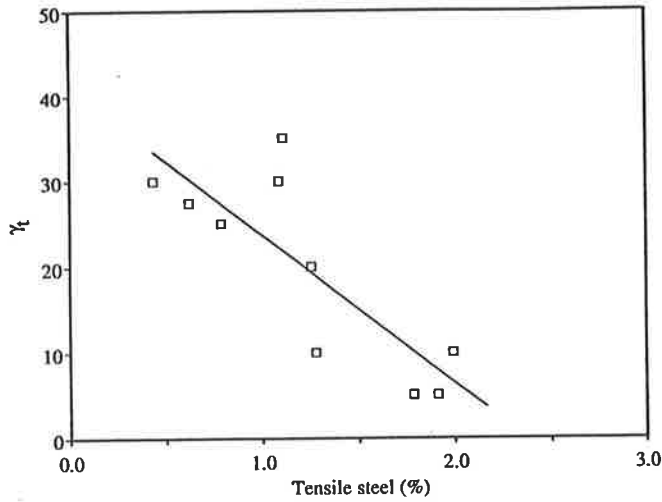
Figure 3.20: Tension stiffening parameters for proposed model
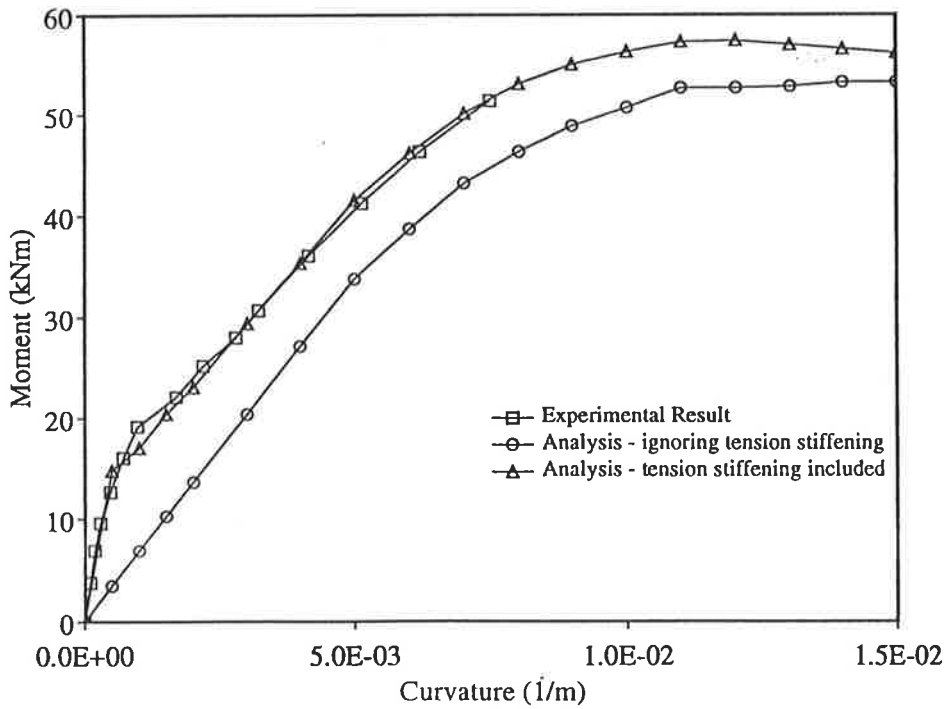
Figure 3.21: Moment versus curvature for beam 4 using the preliminary tension stiffening model

Figure 3.22 shows the experimental results for beam 4 and the results from two non-linear analyses. The analysis with tension stiffening shows there is some contribution from the tensile concrete to the strength of the member. It is doubtful whether this occurs, and the proposed model has been modified to include a discontinuity at a strain value of $10\varepsilon_{cr}$, (Figure 3.22). Although the softening curve could be modelled with further linear segments, the modifications were considered unnecessary.
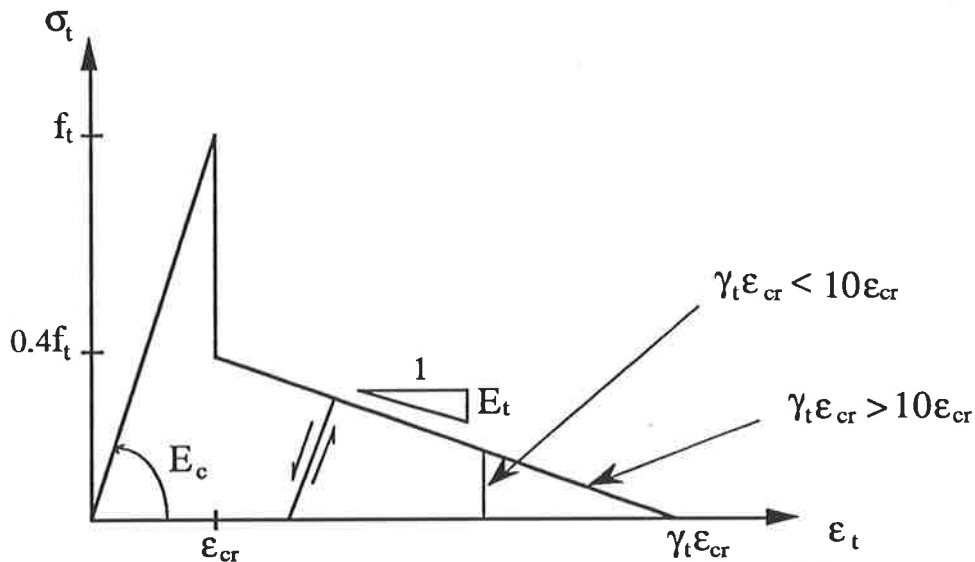
Figure 3.22: Proposed tension stiffening model

The proposed tension stiffening model was used to analyse ten of the fourteen beams tested by Clark and Spiers. Figures 3.23 and 3.24 compare experimental and analytical results for beam 4 and beam 6R respectively. Analytical results compare well with experimental results in the pre-cracking range and post-cracking range up to the maximum moment.

It should be noted that test results for moment and curvature were only published up to a corresponding level of steel strain of 0.002. Tests were based on a load control testing device but published results show no indication of a maximum failure load having been reached. In some cases, the analytical results predict a much higher failure moment and in all cases continuing deformation after the peak moment is predicted. Refer to Appendix D for beam details and analytical results of remaining

test beams by Clark and Spiers. The present method of analysis simulates a deformation control test set-up, hence continuing deformation after the maximum moment has also been predicted.
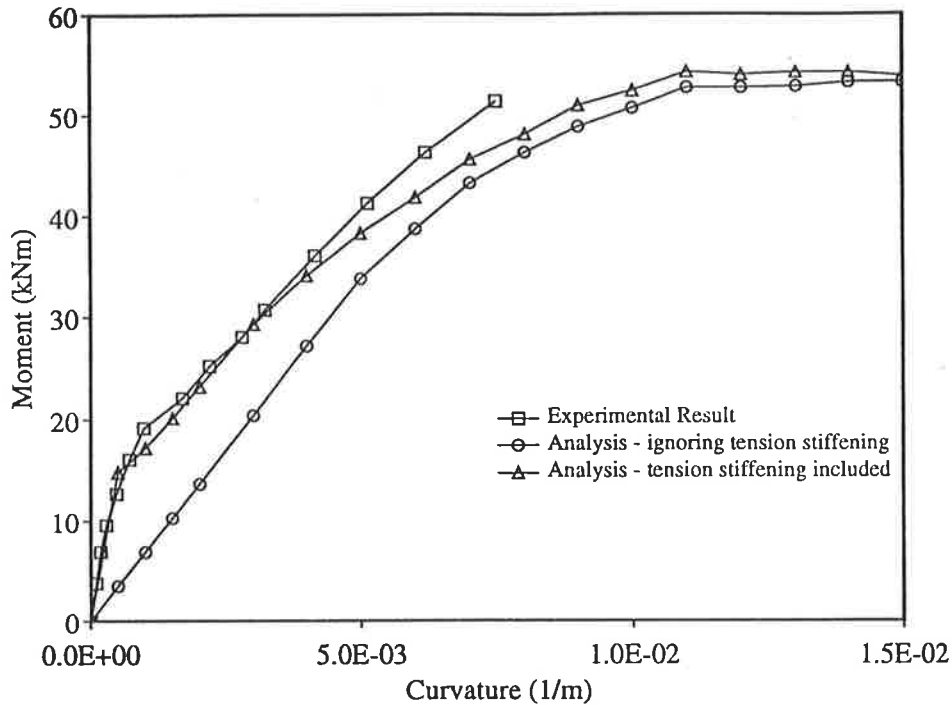
Figure 3.23: Moment versus curvature for beam 4 tested by Clark and Spiers (1978)
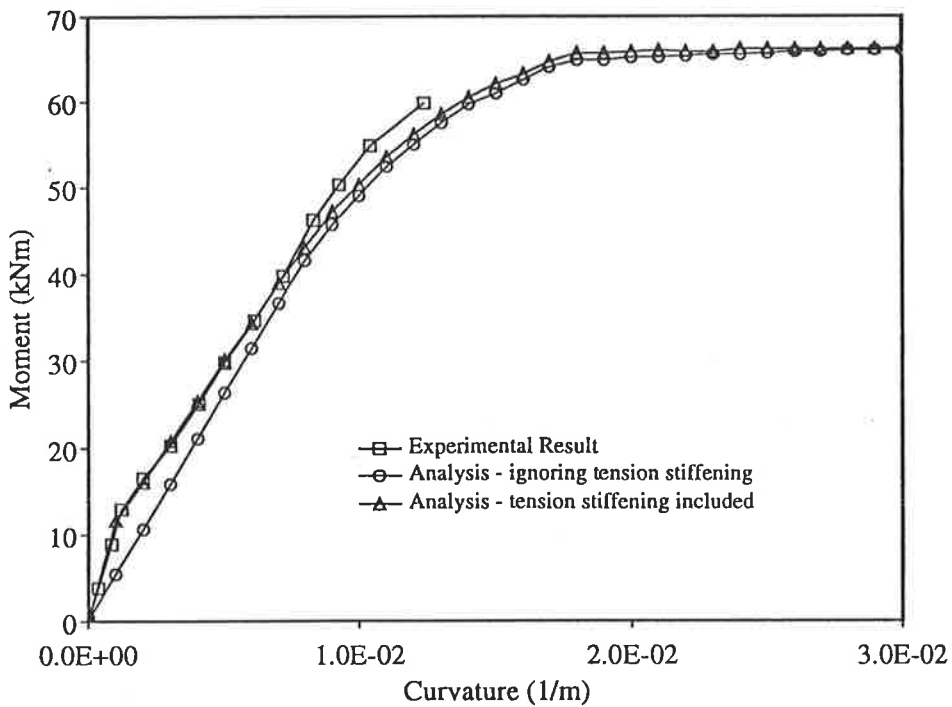
Figure 3.24: Moment versus curvature for beam 6R tested by Clark and Spiers (1978)

It is worth noting the amount of time to run an analysis for tension stiffening. The computer runs for both analyses in Figure 3.24 were made on a Sun 4/280 system. The total CPU time for the analysis ignoring tension stiffening effects was 26.6 secs with an average of 3.5 iterations per load step. The analysis including tension stiffening effects required 43.7 secs of CPU time with an average of 4.5 iterations per load step. A total of sixty load steps were carried out for each case.

A factor influencing the increase in computational time to run the problem for tension stiffening effects is the shape of the tension stiffening curve. As strain increases beyond the cracking strain, an instantaneous drop in stress occurs at the peak stress. It can be appreciated that such a change can affect convergence of the moment and axial force during a sectional analysis.

3.7 Comparisons with Experimental Beam Results

3.7.1 Introduction

To test the validity of the proposed tension stiffening model, beams tested by other investigators were examined. The main parameters considered were type of loading and percentage of steel. The non-linear behaviour of both single span and two-span continuous beams was also examined.

3.7.2 Comparisons with Single-Span Beams

Three simply supported beams tested under double point loading by Monnier (1970) were examined. The beams were subjected to cyclic loading at various stages prior to yielding of the tensile steel and each test was performed over a period of three days. The test set-up and section details are shown in Figure 3.25.

Reinforcing details are given in Table 3.1 and two types of reinforcing bar were used. Figure 3.26a shows the type of bar used in beam III, which becomes non-linear at a stress of 3000 kg/cm² (295 MPa). The stress-strain relationship for this type of bar was modelled with four piecewise linear segments. Figure 3.26b shows the stress-strain curves for bars used as main reinforcement in beams VIII and IX. These bars are characterised by the more common elasto-plastic shape followed by a strain hardening portion at higher strains.

Compressive strength for concrete in each test beam was determined from 20x20x20 mm cubes. For the present study, equivalent cylinder strength values were determined from Equation 3.23. Concrete material properties for all three beams analysed are given in Table 3.2.
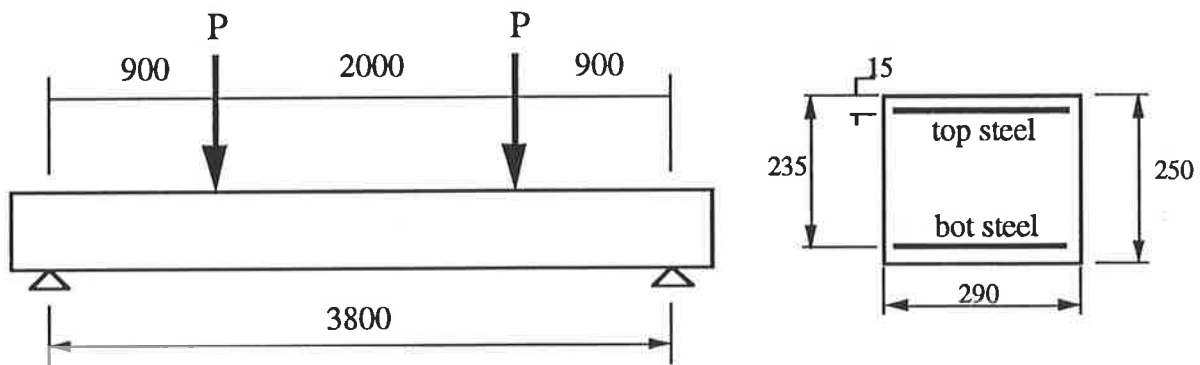
Figure 3.25 Test set-up and section details for beams tested by Monnier (1970)
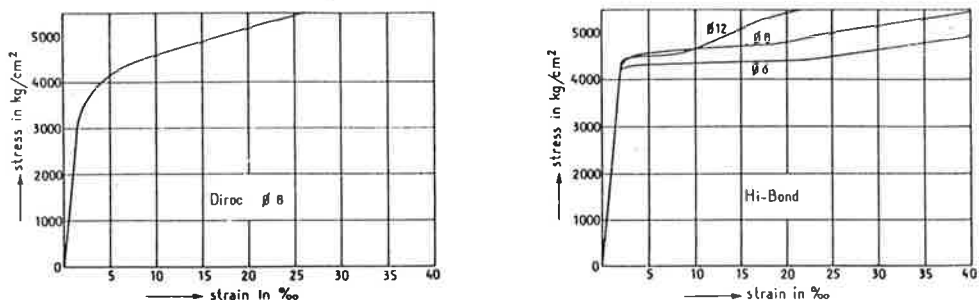
Figure 3.26 Stress-strain curves for reinforcing steel for: (a) beam III; and (b) beams VIII and IX tested by Monnier (1970)

Table 3.1: Reinforcing details for beams tested by Monnier (1970)

Beam	Type of bar	Top reinforcement			Bottom reinforcement			
		No.	Diam (mm)	Area (mm²)	No.	Diam (mm)	Area (mm²)	p (%)
III	Diroc	3	8	151	6	8	302	0.44
VIII	Hi-bond	3	8	151	3	12	339	0.5
IX	Hi-bond	3	8	151	6	12	678	1.0

Table 3.2: Material properties of beams tested by Monnier (1970)

Beam	Concrete details					
	f_c (MPa)	f_{cmax} (MPa)	f_{tmax} (MPa)	E_c (MPa)	γ_1	E_t
III	25.8	24.5	2.73	25390	2.07	-313
VIII	31.9	24.3	2.71	25300	2.08	-322
IX	25.8	24.5	2.73	25390	2.07	-445

Beam III has 0.44% tensile steel with a non-linear stress-strain relationship as shown in Figure 3.26a. By ignoring the effects of tension stiffening, stiffness is obviously underestimated, as shown in Figure 3.27. Analysis with tension stiffening effects included, predicts a cracking moment of 8.4 kNm. With further loading, cracks develop and beam behaviour is characterised by a loss of flexural stiffness. Tension stiffening also has some influence on ultimate strength. Beam III was also subjected to unloading and reloading at two separate load levels, but the test results show that the level of moment prior to unloading is uncoverable.

The effect of tension stiffening on beam VIII, with $p = 0.5\%$, is shown in Figure 3.28. It was shown in the analyses of beams tested by Clark and Spiers that tension stiffening is most beneficial with low percentages of tensile steel. Tension stiffening

has a noticeable improvement on bending stiffness for beam VIII. Moment and curvature compare well up to 20 kNm where tension stiffening begins to diminish. There also appears to be some contribution by tension stiffening to the moment at yield for this beam.

Beam IX has a percentage of steel, $p = 1.0\%$, and results are shown in Figure 3.29. The analysis, with tension stiffening included, predicts moment-curvature quite well up to the maximum moment. This beam has good ductility which is also predicted by the analysis.
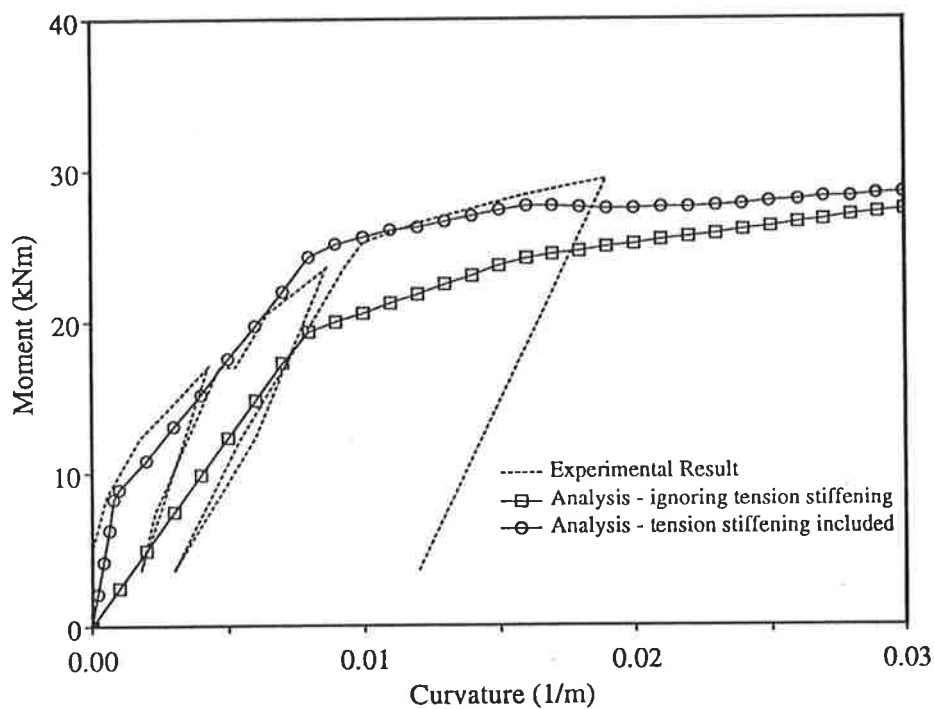
Figure 3.27: Moment versus curvature for beam III tested by Monnier (1970)
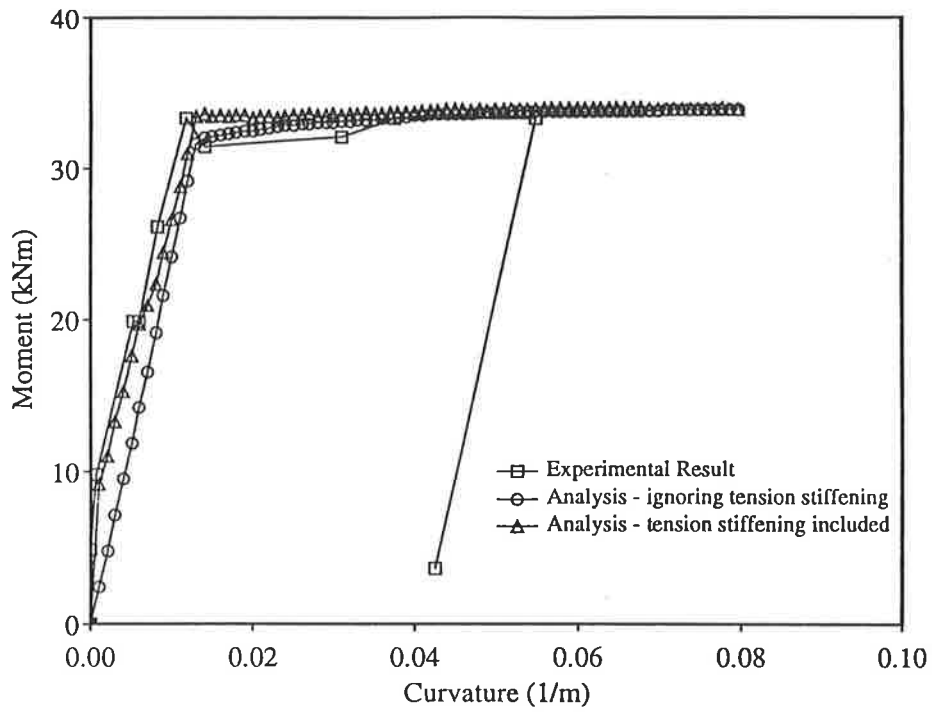
Figure 3.28: Moment versus curvature for beam VIII tested by Monnier (1970)
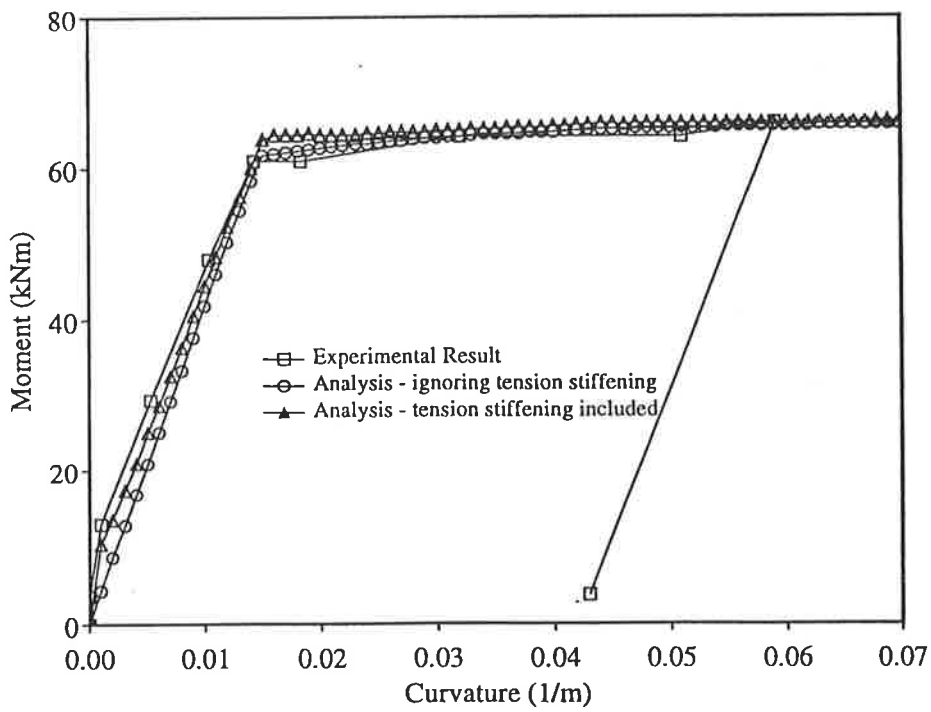
Figure 3.29: Moment versus curvature for beam IX tested by Monnier (1970)

Analytical results for beams with tension stiffening generally compare well with experimental results for beams tested by Monnier. Both strength and stiffness show good correlation for all three cases. However, the analytical results show a higher amount of ductility compared to the test results for moment and curvature. Although tests were conducted under deformation control conditions, it is difficult to judge whether tests were carried out into the collapse region. It is worth noting that beams tested by Monnier, and also Clark and Spiers, were subjected to loading which creates a constant moment region. An advantage with this method of testing is that the load plattens, under which disturbances are most significant, are located at a distance removed from the measuring instruments.

Tests of beams subjected to single point loading have been carried out by many investigators. The beams chosen for analysis in the present study have been tested by Healey (1993) and Mendis (1986).

Mendis (1986) tested simply supported beams under single point loading at midspan. Four beams were selected for analysis, and in general, the results did not compare well. Only the results for beam A1 are reported here, to illustrate particular areas of concern.

The configuration and section details for beam A1 are shown in Figure 3.30 and the stress-strain relationship for the reinforcing steel is shown in Figure 3.31. The area of two Y12 bars is assumed to be 225 mm^2 and and this amount of steel is placed at three separate depths. For the analysis for tension stiffening effects, beam A1 has an equivalent percentage of tensile steel, $p = 3.6\%$, which is based on an area of steel of 440 mm^2 and an effective depth, d, of 153 mm. For beam A1, concrete compressive strength, f_c, is 37.4 MPa and f_{cmax} is assumed to be 35.5 MPa, i.e. $0.95 f_{cmax}$. The value of E_c is assumed to be 30560 MPa and the remaining concrete parameters are: $f_{tmax} = 3.49$ MPa, $\gamma_1 = 1.64$, $\gamma_2 = 3.0$, $\gamma_t = 7.0$.
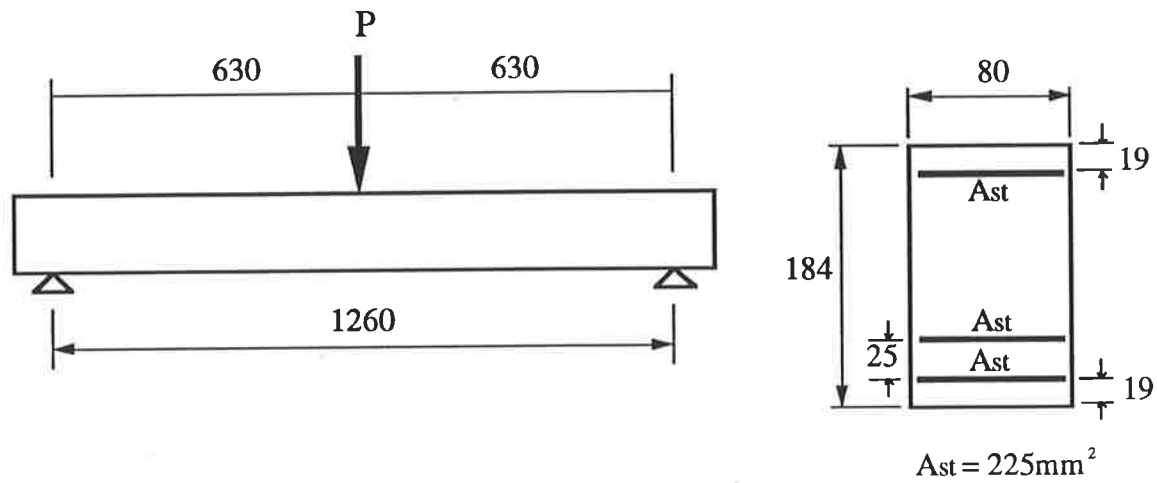
Figure 3.30: Test set-up and section details for beam A1 tested by Mendis (1986)
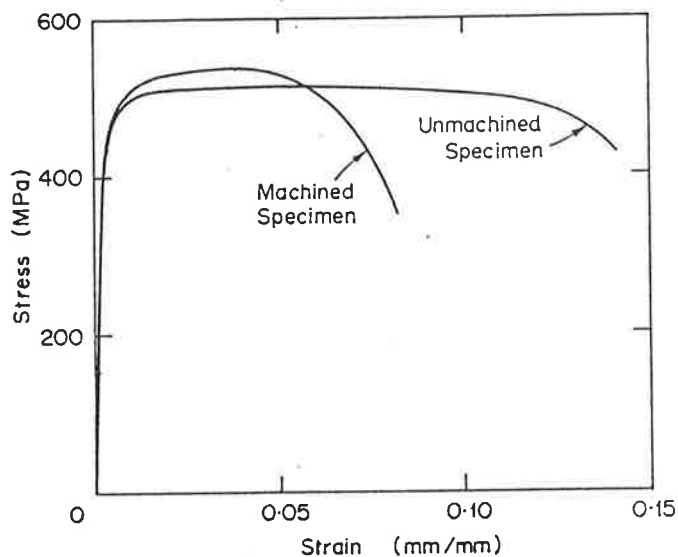
Figure 3.31 Stress-strain relationship for reinforcing steel for beam A1 tested by Mendis (1986)

Figures 3.32 and 3.33 compare moment versus curvature and load versus deflection respectively for beam A1. Tension stiffening has no noticeable effect on stiffness and suggests that tension stiffening can be ignored in an analysis for heavily reinforced members.
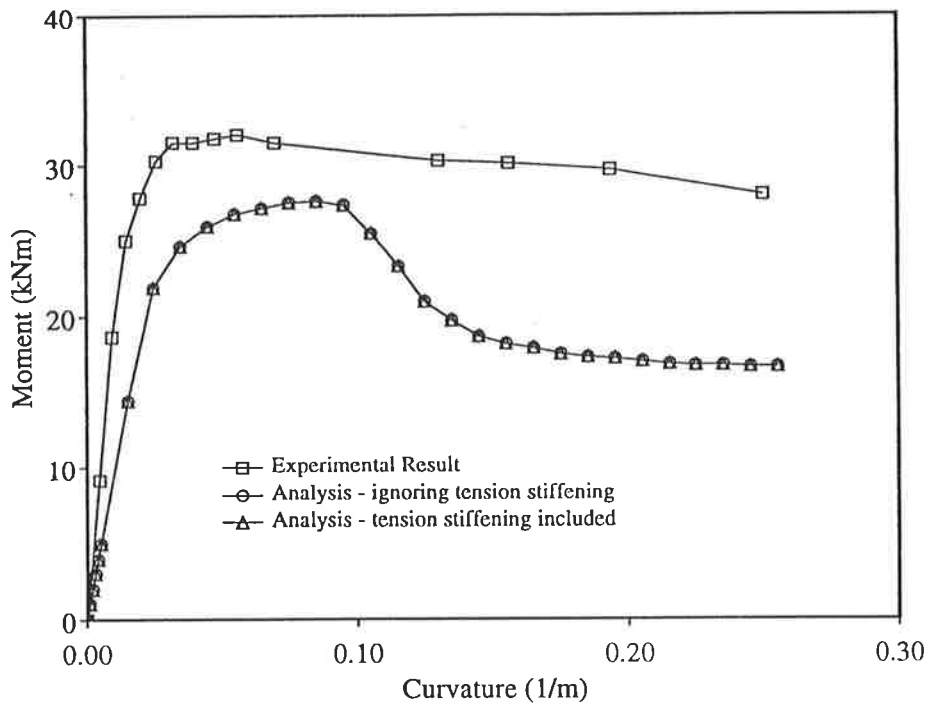
Figure 3.32: Moment versus curvature for beam A1 tested by Mendis (1986)
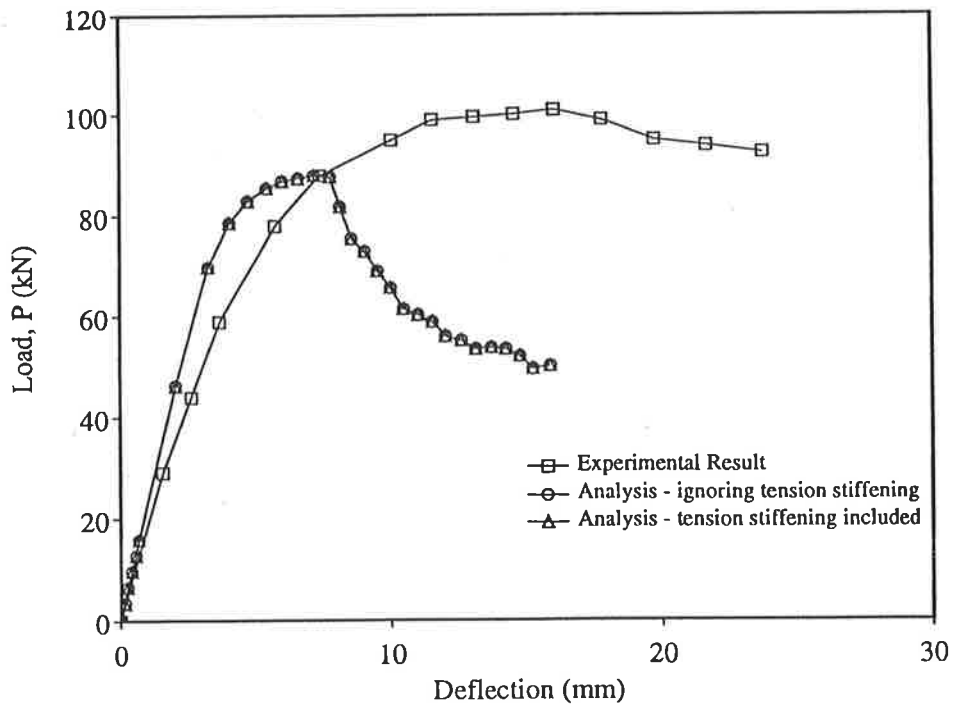
Figure 3.33: Load versus deflection for beam A1 tested by Mendis (1986)

In general, the analytical and test results for this beams do not compare well. It is also interesting to note that comparisons between analytical and experimental results for load versus deflection show that stiffness is overestimated. This is in contrast to the underestimation of stiffness shown for moment and curvature, (Figure 3.32). When considering the poor correlation between results, there are three areas of potential concern: (1) the reliability of the test measurements; (2) additional confinement effects created by the load platten; and (3) the adequacy of the method of analysis.

Firstly, the reliability of the test measurements is given consideration. Figure 3.34, from Burnett and Yu (1964), shows that for a beam under single point loading measurement of curvature becomes non-linear at early stages of loading. Curvature is the change in rotation over a distance between the two points where rotation is measured. Therefore, the magnitude of curvature depends highly on the chosen locations to measure rotation. In particular, curvature at midspan is most sensitive to the location of rotation measuring devices. Measurement of curvature near the loading platten can also be affected by disturbances during the application of load. These considerations may explain the difference in stiffness between analytical and test results.

Comparison of results for load versus deflection show that stiffness is underestimated. Investigations by Al-Zaid *et al.* (1990) show that stiffness depends on the distribution of loading. Typical results are shown in Figure 3.35. The case for midspan loading shows a noticeable loss of stiffness after the formation of the first crack, i.e. where M_a equals M_{cr}, whereas the case for third-point loading shows the best post-cracking response. Analyses of beams tested by Monnier, which also had constant moment regions, showed good correlation for stiffness. It is also apparent the present method of analysis does not predict additional loss of stiffness due to the method of loading. Unfortunately, some details relating to the test beams by Al-Zaid *et al.* were not published and these beams have not been analysed in the present study.
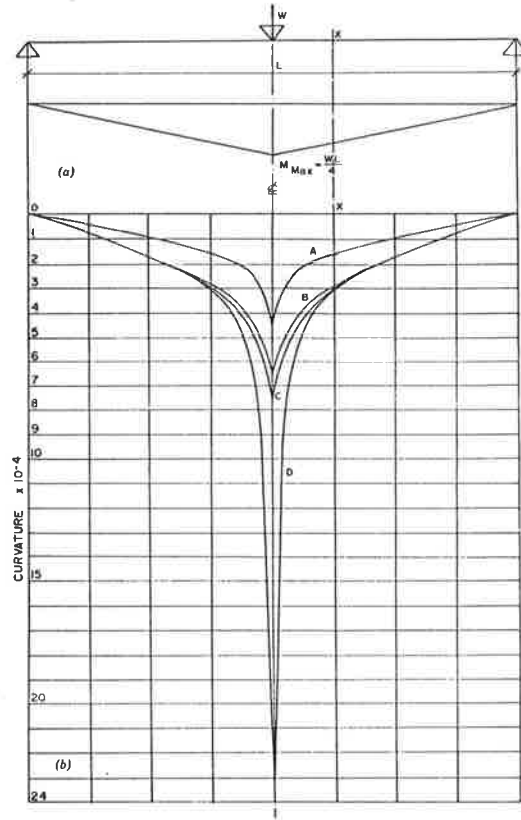
Figure 3.34: Typical distribution of curvature for a beam with single point loading, (Burnett and Yu, 1964)
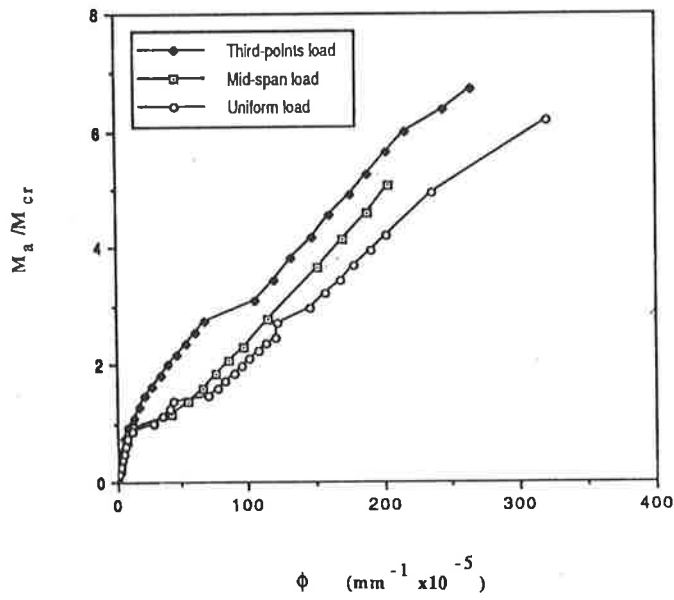
Figure 3.35: Typical moment-curvature curves obtained by Al-Zaid *et al.* (1990)

Although there is some inconsistency in the predicted results for stiffness, the predicted peak load and peak moment for beam A1 by Mendis are both underestimated. An earlier study of beams by Somes (1966) concluded that an apparent increase in beam strength may be due to confinement effects by the loading platten. Under these conditions, a triaxial state of stress develops, although confinement effects diminish with increasing distance from the point of load application. It has been shown that large increases in uniaxial compressive strength can result from small confinement pressures, (Kotsovos, 1987). Bearing pressures also depend on the stiffness of the load platten, (Hawkins, 1970).

A number of investigators, including Kupfer *et al.* (1973) and Liu *et al.* (1972), have proposed biaxial strength envelopes which can be used to determine the increase in uniaxial stress and the influence of shear stress. Kupfer and Gerstle (1969) developed strength envelopes for restrained and unrestrained specimens to take into account friction between bearing plattens and the concrete surface.

To further investigate the behaviour of single span beams under mid-span loading, a series of beams tested by Healey (1993) was chosen for analysis. Figure 3.36 shows the test configuration and section details. The main reinforcing steel for these beams has a yield stress of f_{sy} = 502 MPa. Concrete compressive strength, f_c, is 42.6 MPa and f_{cmax} is assumed to be 40.5 MPa, i.e. $0.95 f_{cmax}$. The value of E_c is assumed to be 32630 MPa and the remaining concrete parameters are: γ_1 = 1.61, γ_2 = 3.0. The percentage of steel for tension stiffening analyses is assumed to be 1.3%.

Results for load versus deflection for beam 15 are shown in Figure 3.37. Both analyses overestimate stiffness and underestimate the peak load. The amount of continuing deformation after the peak load is also not well predicted. Similar trends were observed in the analyses of beam A1 by Mendis. The observed failure of beam 15 was not under the load platten, which corresponds to the peak moment region, but adjacent to the platten. However, crushing was only observed to one side of the load platten and suggests some variability in the beam properties.

P

* Beam 4 : L = 3.0 m
   Beam 15 : L = 1.5 m
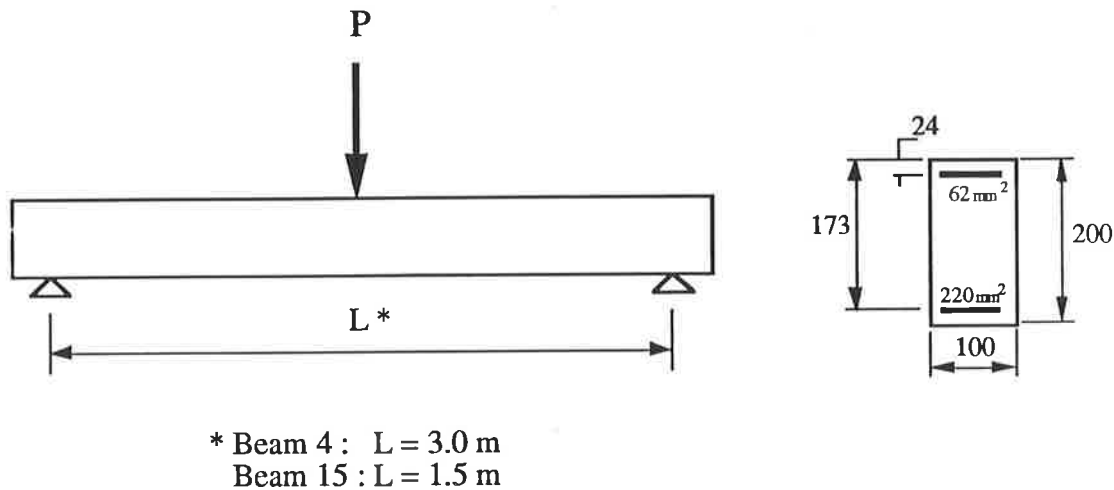
Figure 3.36: Test set-up and section details for beam tested by Healey (1993)

Inclined flexure-shear cracks were also observed at failure of beam 15. This beam has a relatively small shear span ratio, a/d, where a is distance to the point load and d is the effective depth. Shear deformations are ignored in the proposed tension stiffening model, although Balakrishnan and Murray (1988) proposed a relationship between the shear modulus and the concrete uniaxial stress-strain curve. However, this type of plane stress element increases the number of degrees of freedom for analysis, hence, additional storage and computational demands are required.

Results for load versus deflection for beam 4 are shown in Figure 3.38. The analysis for tension stiffening shows good correlation for stiffness, but the maximum load is overestimated by 8%. Preliminary checks for beam 15 and beam 4 showed that variations of ±15% for the peak compressive stress f_{cmax} had very little effect on the predicted strength and stiffness. However, it was found that predicted peak load is sensitive to the value for effective depth.
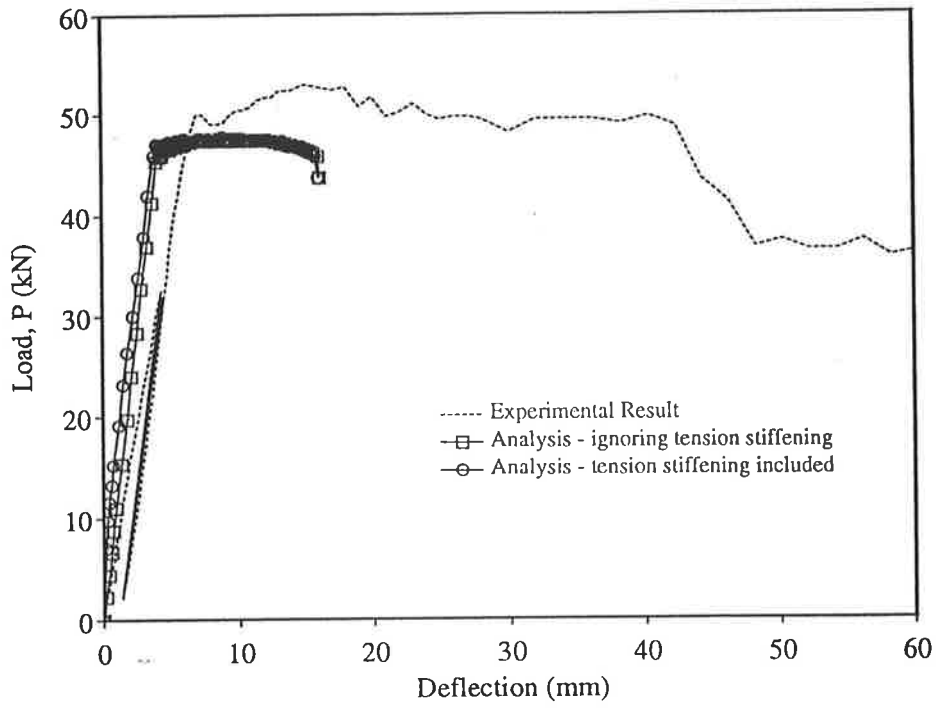
Figure 3.37: Load versus deflection for beam 15 tested by Healey (1993)
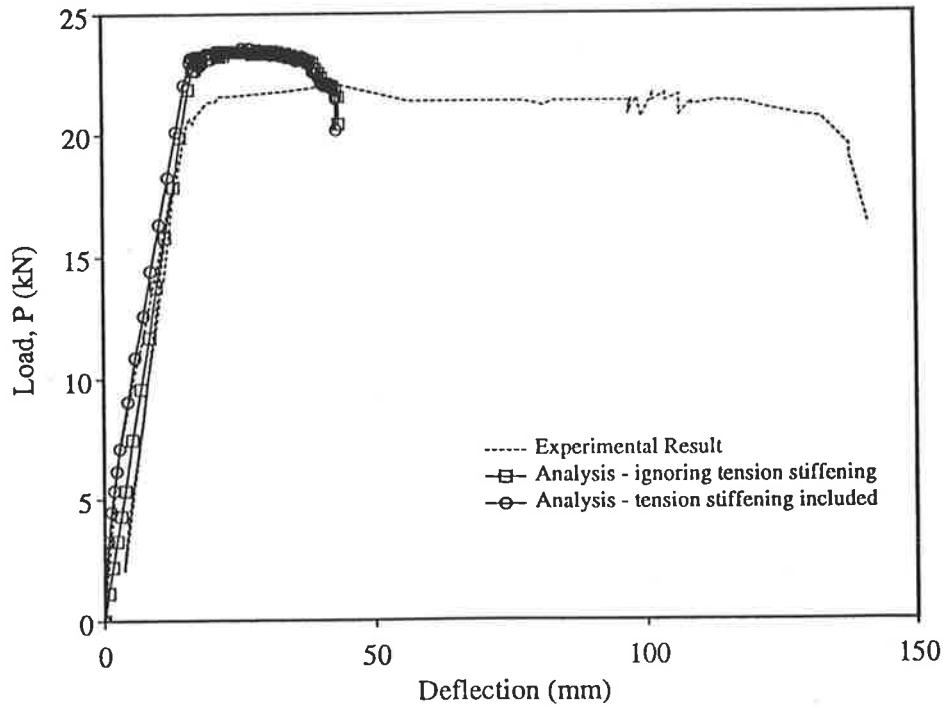
Figure 3.38: Load versus deflection for beam 4 tested by Healey (1993)

3.7.3   Comparisons with Two-Span Beams

A study of tension stiffening effects in two-span continuous beams tested by Bachmann and Thürlimann (1965) and Tse and Darvall (1988) has also been carried out.

Several beams tested by Bachmann and Thürlimann (1965) have been analysed and the results for beam A3, which are representive for these beams, are summarised. Figure 3.40 shows the test set-up and details for beam A3. Concrete compressive strength, f_c, is 37.1 MPa and f_{cmax} is assumed to be 35.2 MPa, i.e. $0.95 f_{cmax}$. The value of E_c is assumed to be 29680 MPa. Elasto-plastic stress-strain relationships are assumed for the reinforcing steel. For the steel in region A, the yield stress for the top steel is 461 MPa and the yield stress for the bottom steel is 400 MPa. The main reinforcement for region B has a yield stress of 400 MPa for both layers.

Figure 3.41 plots moment and curvature at the middle support. The analysis with tension stiffening taken into account some improvement in stiffness, but the maximum moment is underestimated by about 20%.

Experimental and analytical results for moment and curvature (Figure 3.41) and load versus deflection (Figure 3.42) compare more favourably. Moment and curvature was measured at a location 1.625 m from the middle support and load versus deflection was measured at a position 2.0 m from the middle support.

Results for load and deflection show that stiffness compares well, although the right hand span is slightly more ductile. These experimental results are not typical for the series and significant variation in the load-deflection response for adjacent spans was observed in some of the remaining test beams.

Figure 3.42 shows the experimental peak load is 140 kN compared to the analytical predicted load of 130 kN; the difference is only 9%. There may be some influence on peak load by confinement under the loading plates, but of particular interest is the

influence the interior support has on confining the beam. Improvements to strength and stiffness in two span beams were noted by Tse and Darvall (1988) in an investigation of test beams. Results for beam 22, which has been chosen for analysis in the present study, is representative of these beams. Beam 22 has 1.7% reinforcement in the top face and 5.0% steel in the bottom face. Figure 3.43 shows that by taking tension stiffening into account, there is some improvement in stiffness, but the overall correlation between strength and stiffness is not good.

Tse and Darvall noted that restraint provided by the interior support may improve the moment capacity at the support. It should be noted that as well as an increase in strength due to the triaxial state of stress, an increase in stiffness may also be achieved. The effectiveness of confinement depends on the area of contact between the support and the member and the relative depth of the member, (Niyogi, 1974; Kotsovos and Newman, 1981). These conditions may also develop under loading plates due to localised bearing pressures.
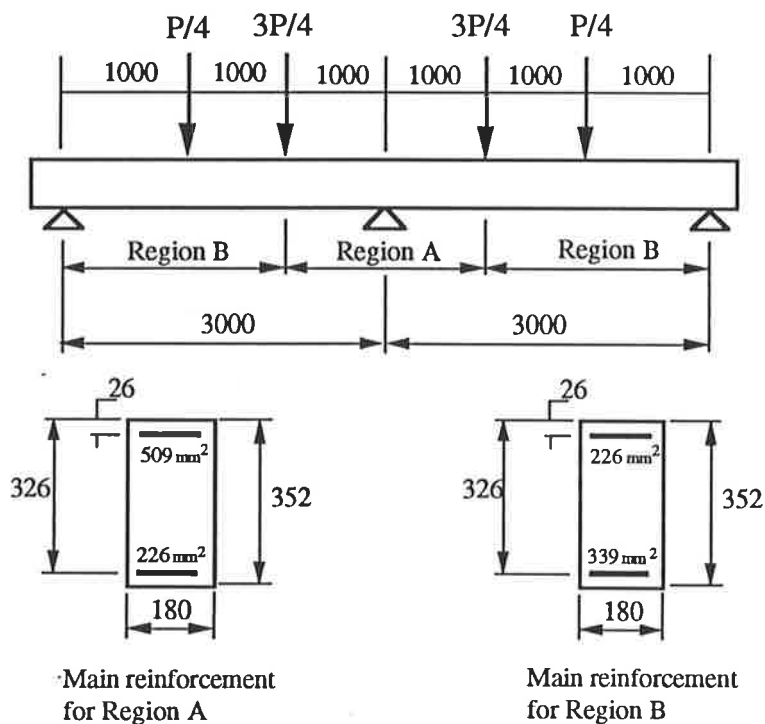
Figure 3.39: Test set-up and details for beam A3 tested by Bachmann and Thürlimann (1965)
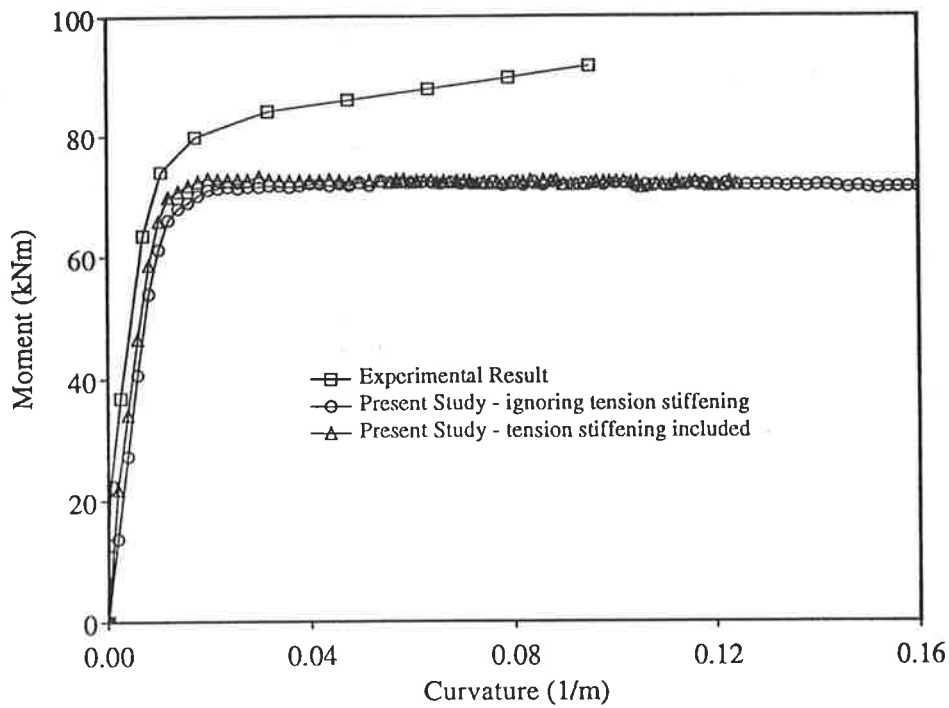
Figure 3.40: Moment versus curvature at middle support for beam A3
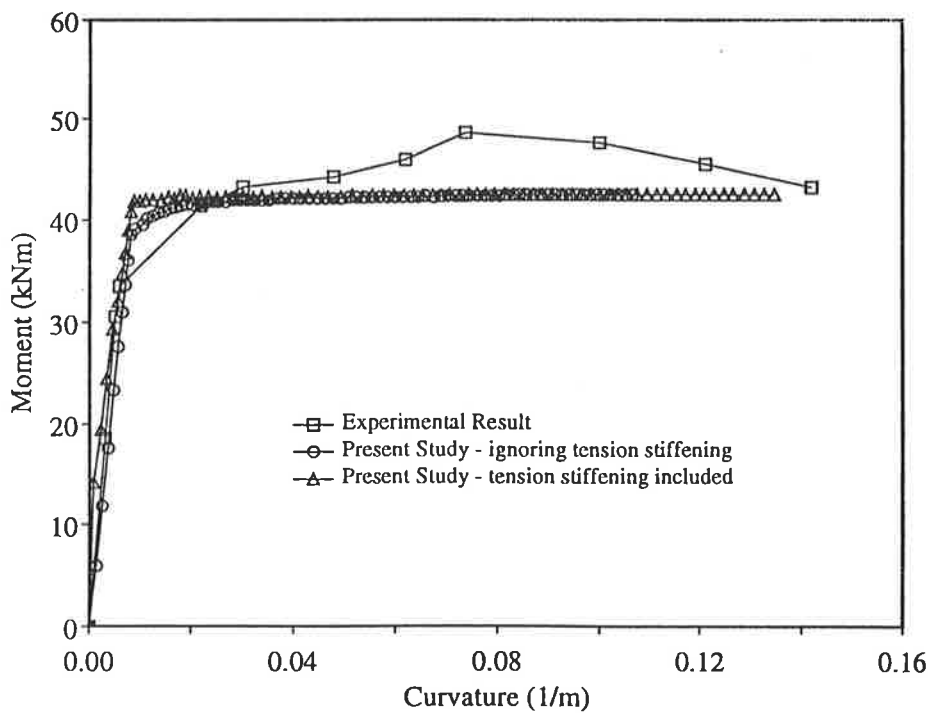
Figure 3.41: Moment versus curvature measured within the span for beam A3
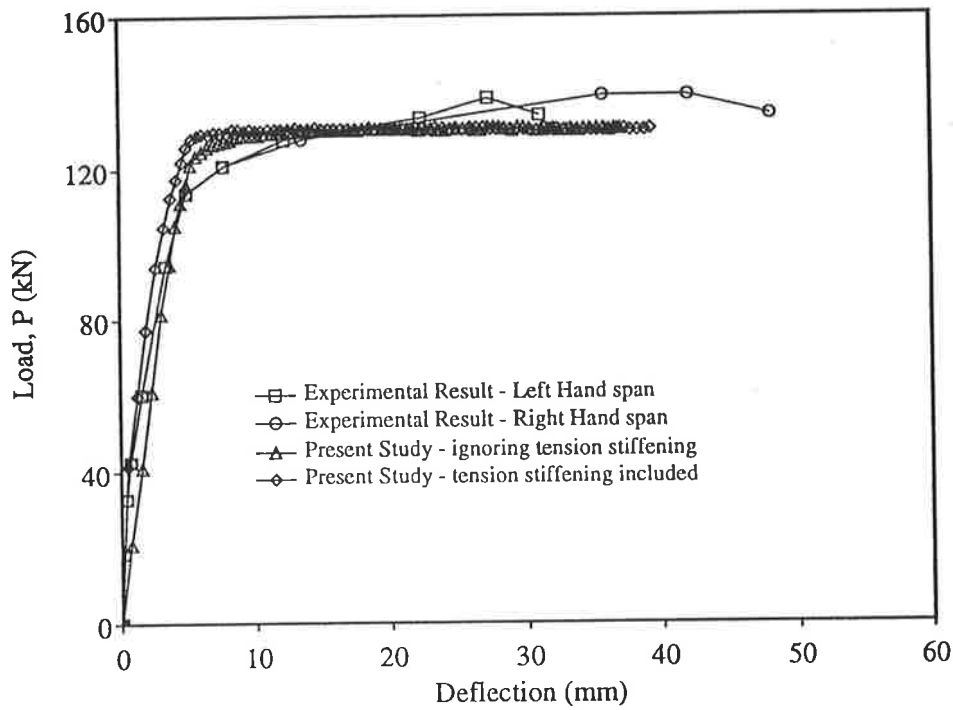
Figure 3.42: Load versus deflection measured within the span for beam A3
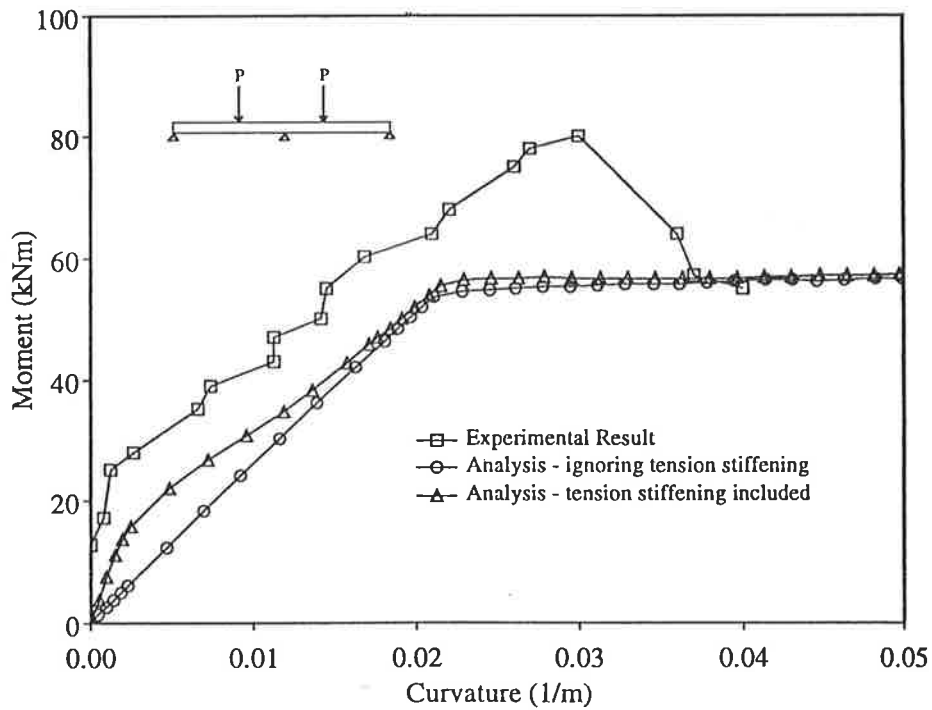
Figure 3.43: Moment versus curvature for beam 22 tested by Tse and Darvall (1988)

3.8 Summary and Conclusions

A simplified tension stiffening model has been developed which is based on previous investigations for tensile behaviour of reinforced concrete. The model is based on the concrete tensile strength determined by a splitting test and includes a suitable post peak softening curve. The stress-strain curve for tension stiffening has been implemented in the section analysis routine for the non-linear frame analysis computer program and the accuracy of the model has been checked with the performance of test beams.

Good correlation was achieved in some cases, but results have also indicated that, in addition to the concrete tensile capacity of concrete, strength and stiffness are influenced by bearing pressures in local regions such as interior supports of multi-span beams and under loading plates. The prediction of beam performance was best achieved with simply supported test beams with constant moment regions. In these cases, disturbance regions do not appear to affect overall structural behaviour.

The performance of single span beams under midspan loading and two-span continuous beams was also investigated. For these cases, the results do not compare well. The present method of analysis can be modified to take into account additional effects from shear deformation and confinement. These areas of improvement to the method of analysis have not been made and are recommended for further research. A simple and economical solution is the use of modified moment-curvature relationships for those regions where beam behaviour is affected by support restraint and the type of loading distribution.

While it has been shown that tension stiffening has a minor influence on the strength of flexural members, the tension stiffening model will be used to predict the performance of reinforced concrete plane frames. Column strength is not only influenced by the relative strength of adjoining members, but also the cracked and uncracked stiffness of beam elements.

The implementation of the proposed tension stiffening model into the general analysis for plane frames also allows for the investigation of joint deformations and its effect on frame performance. This type of non-linearity is examined in the following chapter.

Chapter 4

Joint   Modelling

4.1   Introduction

The strength and ductility of a concrete frame structure depend not only on the properties of the component beams and columns, but also on the manner in which the beam-to-column joints transfer forces between adjacent members.   Extensive laboratory tests have shown that strength and stiffness of joints vary considerably and when premature failure occurs, the type of reinforcement detailing at the joint is usually inadequate.   Strength is also adversely affected by reinforcement which is fabricated poorly or placed improperly.

Although joint detailing had been investigated in the decades prior to the 1960's, the tests examined in this chapter have all been carried out following investigations by Nilsson (1965).   That study showed a common form of detailing for joints had inadequate strength and ductility and this prompted a more comprehensive study of L-, T- and X-joints, (Nilsson, 1968, 1969a, 1969b, 1973).   Alternative designs for a

116

range of joint types were tested with noticeable improvements in some cases. Several studies followed by other investigators, including Balint and Taylor (1972), Burnett and Jajoo (1971), Burnett and Trenberth (1972), Mayfield *et al.* (1971, 1972), Skettrup *et al.* (1984), Swann (1969), Taylor (1974) and Yuan *et al.* (1982).

The discussion of joint behaviour in this chapter is restricted to those cases where the loading is short-term and monotonic. Similarly, the review of methods of analysis for joint behaviour is only for those methods which consider short-term loading. Finally, a method for modelling joint deformations is proposed, which can be incorporated in the segmental method of frame analysis.

4.2 Joint Efficiency

For statically loaded test joints, the assessment of joint performance is more often made in terms of strength rather than stiffness. This is usually done by evaluating joint efficiency, η, as given by Equation 4.1. The symbol η is used for the present study.

$$\text{efficiency, } \eta = \frac{M_{test}}{M_{calc}} \times 100 \ (\%) \tag{4.1}$$

This expression refers to the ratio of actual ultimate moment, M_{test}, from experiment to the theoretical ultimate moment of the adjoining member determined from an analysis, M_{calc}. The moment capacity, M_{calc}, is determined for a section taken through the beam element and a second calculation is performed on a section taken through the column. The predicted moment at failure is then taken as the lower of the two values.

It should be noted that each analysis is usually performed by assuming there is no axial thrust on the section and that moment only is acting. This is a simplified, approximate approach which allows moment capacity to be calculated directly rather than an iterative solution which considers the level of axial thrust.

4.3 Behaviour of Test Joints

4.3.1 Introduction

Frame behaviour depends not only on the type of loading conditions, but also the nature of the detailing within the corners. Tests on isolated L-, T- and X- joints with various types of joint detailing have been the subject of many investigations, but only those test joints with detailing which are found in common practice will be reviewed here.

4.3.2 Behaviour of L-joints

The L-joint can be classified into two types: the closing corner and the opening corner. A closing corner is created when the bending moments in the beam and column elements tend to reduce the inside angle of the joint, and an opening corner is created when the bending moments increase the inside angle of the joint. Illustrated in Figure 4.1 are two frames with different combinations of opening and closing corners. Figure 4.1a shows a frame subjected to a lateral load in which both an opening corner and a closing corner are created. The frame shown in Figure 4.1b is subjected to vertical loading and closing corners are created at the ends of the beam element. Assuming similar properties and detailing for the frames, the presence of the opening corner in Figure 4.1a may have an adverse affect on frame behaviour.
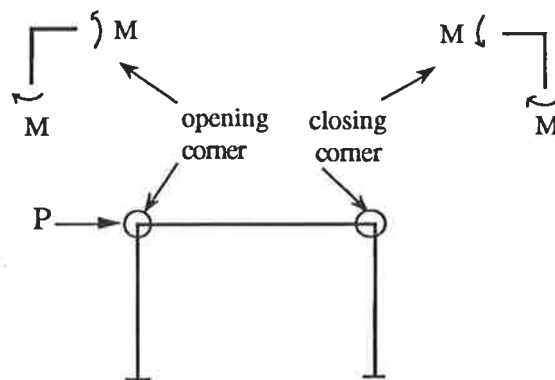
Figure 4.1a: Portal frame with an opening corner and a closing corner
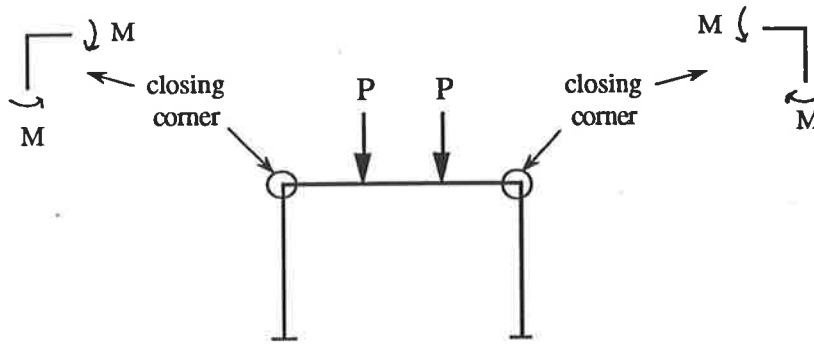
Figure 4.1b: Portal frame with two closing corners

Swann (1969) and Mayfield *et al.* (1971, 1972) tested L-shaped corners with various detailing under two load conditions, one tending to open the corner, and the other tending to close the corner. The test configuration for both studies is shown in Figure 4.2. The applied load, P_{open}, opens the corner and the load given by P_{close} will close the corner. In these tests, when the applied load creates an opening corner there is a tensile axial thrust in the column, and when the applied load creates a closing corner a compressive axial thrust is present in the column. In neither case, is an axial force present in the beam.
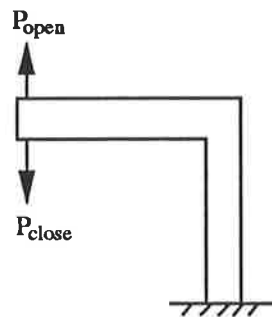
Figure 4.2: Test configuration for corners tested by Mayfield *et al.* and Swann

In all the tests by Swann (1969), the specimens had 3% tensile steel. Table 4.1 summarises the corner reinforcement layout, crack patterns and efficiency, η, for two types of detailing which are similar to those reported by Nilsson (1968, 1973).

Table 4.1 shows that the crack patterns at failure for an opening corner are quite different to the crack patterns of a closing corner at failure. The closing test corners 103 and 104 by Swann both developed flexural type cracks in the beam and column.

In the opening test corners 3 and 4, a tensile crack formed at the inside corner at an early stage of loading. This was followed by the formation of an inclined (diagonal splitting) crack across the corner which spread to the main steel in the outside face. Specimen failure was precipitated when concrete split from the beam and column steel. This is shown by the longitudinal (splitting) cracks and are likely to have been caused by the transfer of high radial tensile stresses to the surrounding concrete. A study by Kemp and Wilhelm (1979) showed this premature type of failure depends on bar spacing and concrete cover and that splitting cracks can be delayed by providing stirrups. Similar longitudinal splitting cracks patterns at failure were observed in frames with this type of detailing and tested by Nilsson (1968). In some cases, outside corners actually spalled off completely, corresponding to a brittle failure.
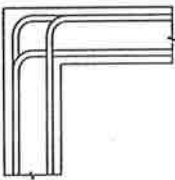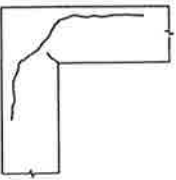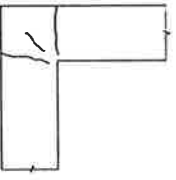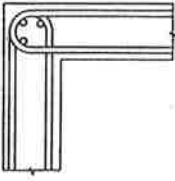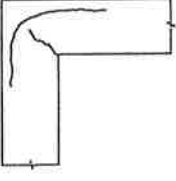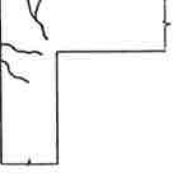
The results in Table 4.1 show that each closing corner is more efficient than its opening corner counterpart, i.e. the closing corner failed at a higher load. Corners with other types of detailing were also tested, and in each case the closing corner was more efficient than the opening corner.

While most investigations for joint performance concentrate on strength, it is also useful to compare predictions of both strength and stiffness. Test corners 3 and 103 were selected in the present study for analysis by the segmental method of frame analysis.

Two types of non-linear analysis were carried out for each test corner: an analysis which ignores the effect of tension stiffening, and an analysis which includes the proposed tension stiffening model. Only the results for the case which includes tension stiffening are presented here because there was no observed difference between the two sets of results. It was shown in Chapter 3 that tension stiffening

effects are less significant with increasing amounts of tensile steel and, for clarity, results are presented here for the analysis which includes tension stiffening.

Table 4.1: Failure patterns of corners tested by Swann (1969)

Corner Reinforcement	Opening Corner			Closing Corner		
	Test no.	Crack pattern	η (%)	Test no.	Crack pattern	η (%)
	3		19	103		81
	4		34	104		77

Experimental and analytical results of moment versus rotation for the two test corners by Swann are shown in Figure 4.3 and Figure 4.4. Rotation is the change in the measured angle between the beam and the column. Each test corner has 3% tensile reinforcement.

The test results for closing corner 103 show a considerable loss in stiffness at a moment of 2.5 kNm, when cracks are likely to have formed. The maximum moment for the test corner is 13.5 kNm, whereas the analysis predicts a maximum moment of 16.5 kNm. In terms of strength, this corner is 81% efficient. After the peak load the test corner continues to deform, indicating that this type of detailing is reasonably ductile. The amount of continuing deformation predicted by the analysis compares quite poorly.

Figure 4.4 shows the results for the same detail, but test specimen 3 was subjected to a load which tended to open the corner. The test corner reached a maximum moment of 2.9 kNm, compared to the predicted maximum moment from the analysis of 15.3 kNm. In terms of strength, this corner is only 19% efficient. This test specimen also shows a higher degree of ductility than the predicted analytical results. Although it is not clear from Figure 4.4, the test corner has undergone some loss in stiffness at about half the maximum moment.
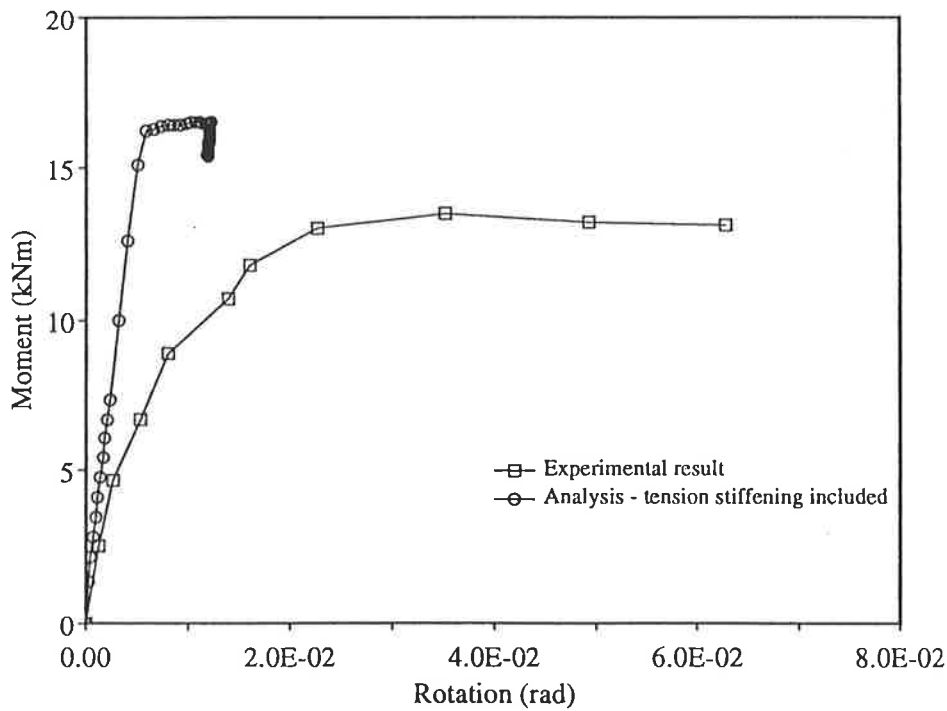
Figure 4.3: Moment versus rotation for test no.103 by Swann (1969)
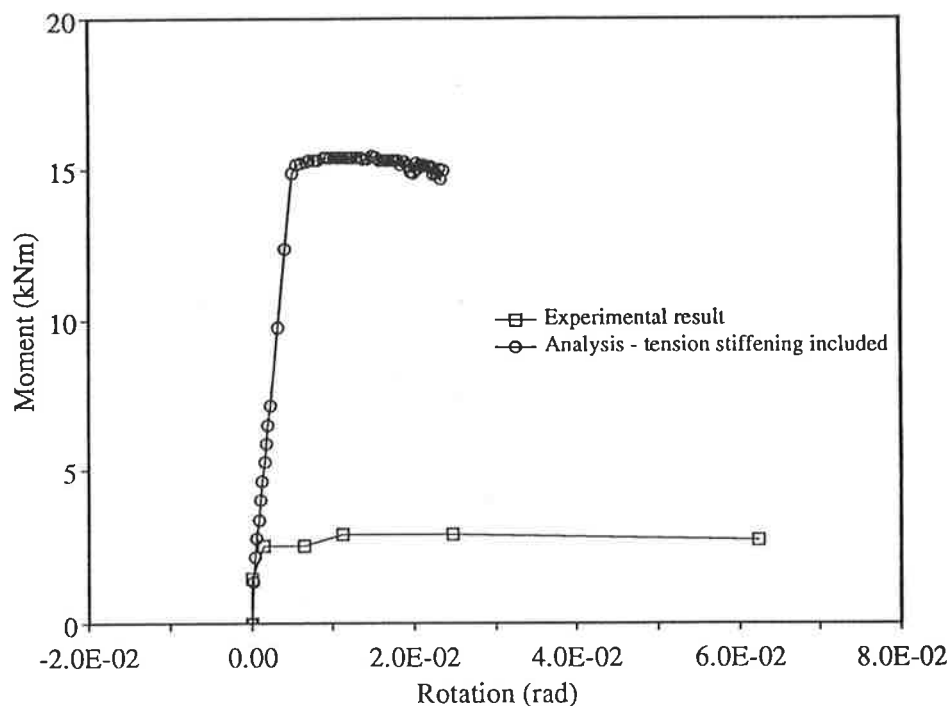
Figure 4.4: Moment versus rotation for test no.3 by Swann (1969)

Swann also showed that strength is affected by placement errors in the reinforcement. A post-failure inspection of one particular test corner revealed that the main reinforcement had sagged to the bottom of the mould during casting. A comparison of the moment at failure in the experiment and the predicted failure moment showed this specimen to have an efficiency of 53%. In a repeat test using the same type of detailing, the efficiency of the corner was calculated to be 81%. It was found that the reinforcement had been well placed in the repeat test.
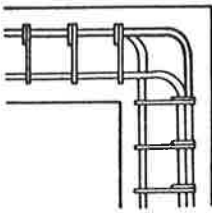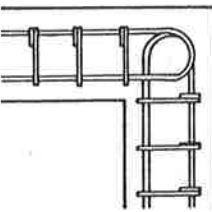
Mayfield *et al.* (1971, 1972) also tested opening and closing corners with different types of reinforcement detailing using a test set-up with the configuration shown in Figure 4.2. Beam and column elements were encased in stirrups and a range of percentages of tensile reinforcement were used for the tests.

Table 4.2 summarises the efficiencies for two types of detail shown. All specimens have 1.0% tensile reinforcement. The results show there is some variability in actual strength. The closing corner tests 2-3 and 2-4 both have the same detail, concrete

strength and physical dimensions, but the efficiencies are 94% and 117% respectively. Similarly, closing corner tests 1-3 and 1-4 have efficiencies of 125% and 137% respectively. It is likely that some variability in strength can be attributed to fabrication and placement of the reinforcement in the corner.

Note that tests 1-3, 1-4 and 2-4 have efficiencies greater than 100%, i.e. the corner itself is stronger than the flexural strength predictions for the beam and column. Concrete within the corners is confined by stirrups, and this effect is taken into account in the concrete compressive stress-strain curve by Kent and Park (1971). While the main reinforcement detailing also confines concrete, its primary purpose is to provide a restraint to crack growth and propagation which appears to influence strength. Restraint provided by the hairpin reinforcement appears to be most effective.

Table 4.2: Efficiencies of corners tested by Mayfield *et al.* (1971)

Corner Reinforcement	Test no.	f_c (MPa)	Main diam. (mm)	reinf. (%)	type of corner	efficiency (%)
	1-1	20.6	12	1.0	opening	19
	1-2	20.6	12	1.0	opening	19
	1-3	20.6	12	1.0	closing	125
	1-4	20.6	12	1.0	closing	137
	2-1	18.6	12	1.0	opening	44
	2-2	18.6	12	1.0	opening	48
	2-3	18.6	12	1.0	closing	94
	2-4	18.6	12	1.0	closing	117

Shown in Figure 4.5 are the crack patterns of four test corners by Mayfield *et al.* The detailing of the corners are similar to those used in tests by Swann (1969) and shown in Table 4.1. Also indicated on the diagrams of crack patterns are the 'load ratios',

which indicate the relative load level when the cracks were first observed. The 'load ratio' is the ratio of the actual moment from the experiment when the cracks were observed to the theoretical maximum moment determined by an analysis.

The crack patterns for test 1-1 show that diagonal splitting cracks formed within the corner at a load ratio of 12. Cracks then spread into both the beam and column and total failure occurred at a load ratio of 19. In test 1-3, flexural type cracks in the beam and column ceased propagating at a load ratio of 83. Across the corner, a splitting crack formed at a load ratio of 124 and appears to have spread rapidly and precipitated failure of the specimen. The maximum load ratio of 125, which corresponds to failure of the specimen, indicates this is an efficient detail.

The second detail shown in Figure 4.5 includes bars in the shape of hairpins. This type of detailing confines the concrete in the corner and resists the growth and spreading of cracks. It is a more efficient detail than the first detail shown. The opening corner failed at a 'load ratio' of 48, whereas the closing corner failed at a 'load ratio' of 117.
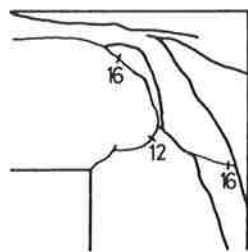
Opening

(a) test 1-1
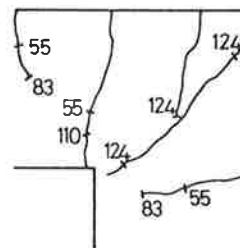
Closing

(b) test 1-3
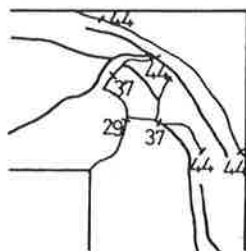
Opening

(c) test 2-2
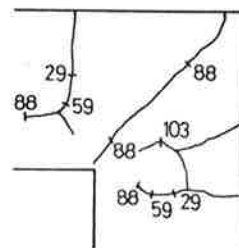
Closing

(d) test 2-4

Figure 4.5: Failure patterns of corners tested by Mayfield *et al.* (1971)

Nilsson (1965, 1968, 1973) tested frames with the configuration shown in Figure 4.6. The loading is symmetric and an opening corner is created at each joint. No axial thrust is present in the columns, but the beam is subjected to a tensile axial thrust. A load P was applied at the base of each column where lateral deflection was also measured.
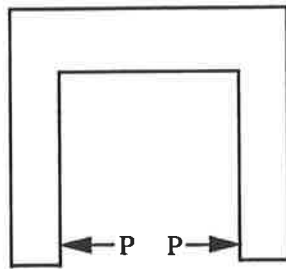
Figure 4.6: Configuration of frames tested by Nilsson

Load versus deflection for frame U22 is shown in Figure 4.7. The percentage of steel in the beam and the columns is 0.89% and 1.15% respectively. Frame failure occurred shortly after the formation of diagonal splitting cracks across each corner and at a load of 11 kN and deflection of 4 mm. The analysis for tension stiffening compares well up to failure of the test specimen. However, the analysis predicts a peak load of 40 kN and continuing deformation after this load.

The results for frame U25, which has hairpin reinforcement, are shown in Figure 4.8. This frame has 0.89% beam tensile steel and 1.15% column tensile steel. Analytical results for this case compare more favourably than for frame U22. Clearly, tension stiffening has a beneficial effect on frame stiffness, but the predicted peak load of 42 kN overestimates the actual failure load of 36 kN by 17%. The improved peak load and ductility for this frame, compared to frame U22, is probably due to the provision of hairpin reinforcement. The discussion of test results obtained by Swann and Mayfield *et al.* in the present study has shown that hairpin reinforcement improves the strength of a corner by confinement and additional restraint to crack growth. This latter effect is also important for ductility requirements.
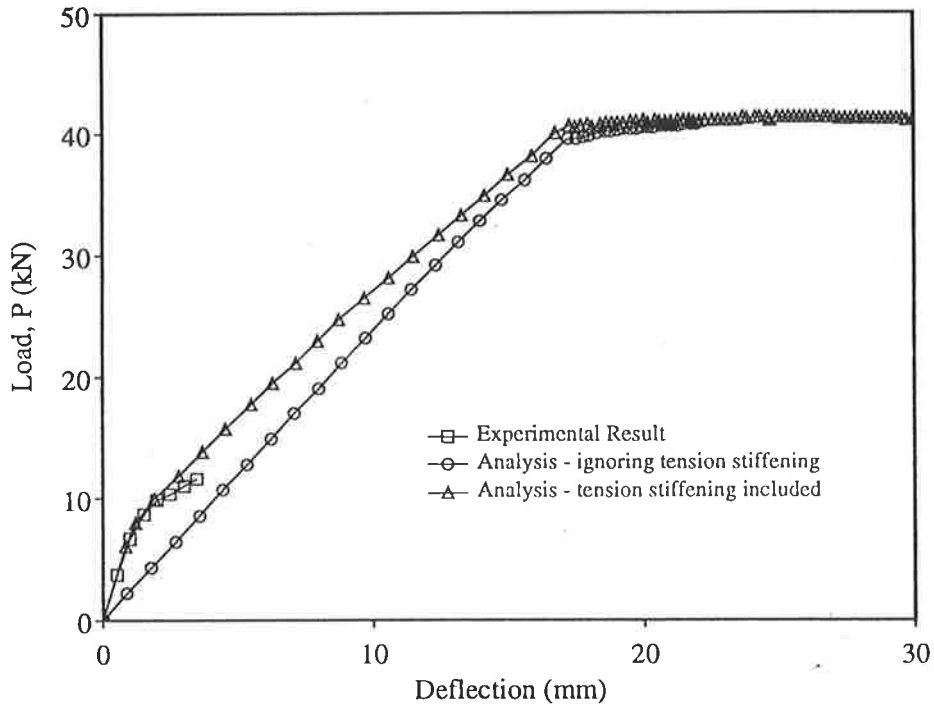
Figure 4.7: Load versus deflection for frame U22 tested by Nilsson (1973)
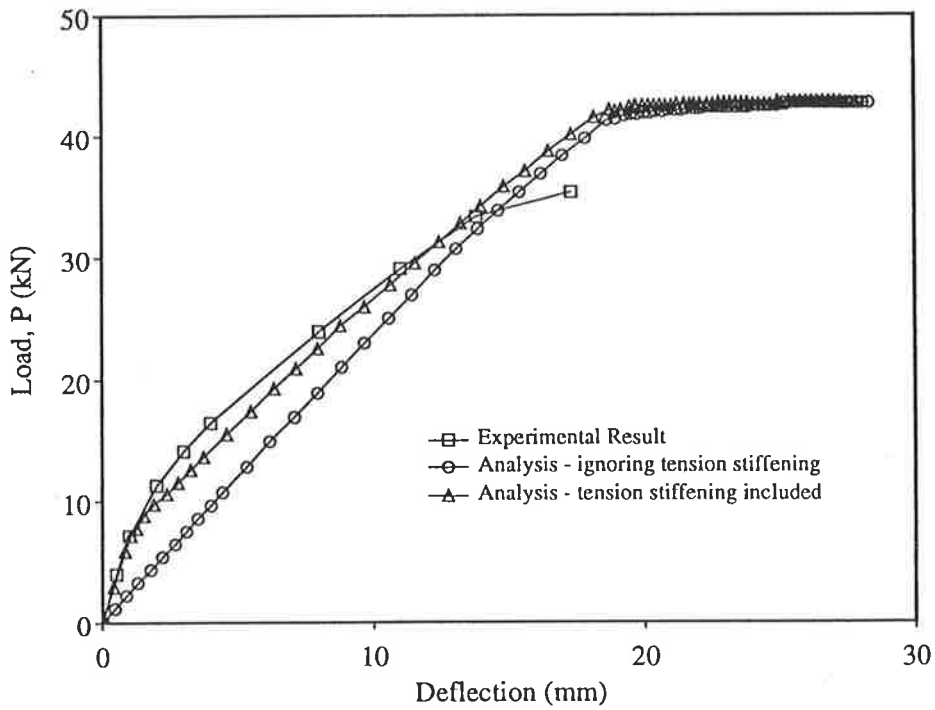
Figure 4.8: Load versus deflection for frame U25 tested by Nilsson (1973)

Finally, Figure 4.9 and Figure 4.10 compare efficiency versus percentage of tensile steel for two types of detail, and include some of the test corner results already discussed in this section. In each case, the percentage of tensile steel is the average value for the beam and column element. Calculations are based on average values because failure generally occurred within the corners, rather than in the beam or column elements.
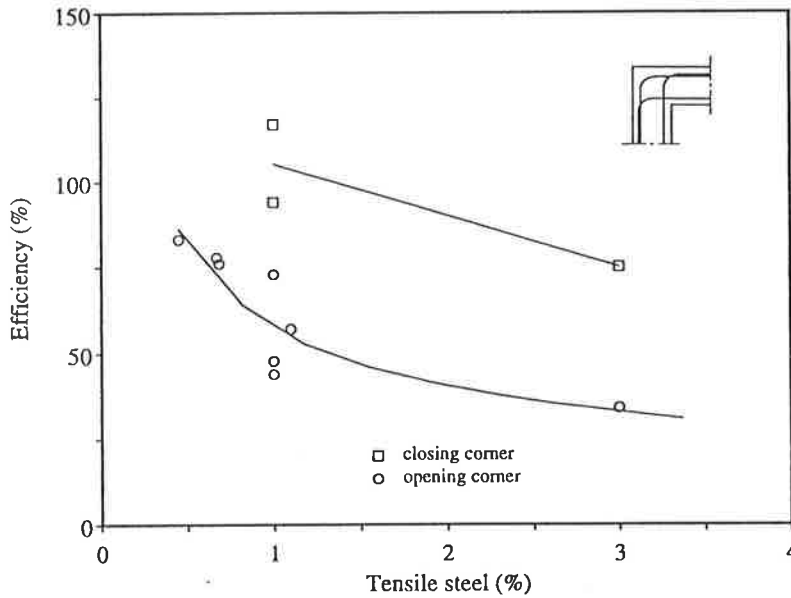
Figure 4.9: Efficiency versus percentage of tensile steel for detail 1
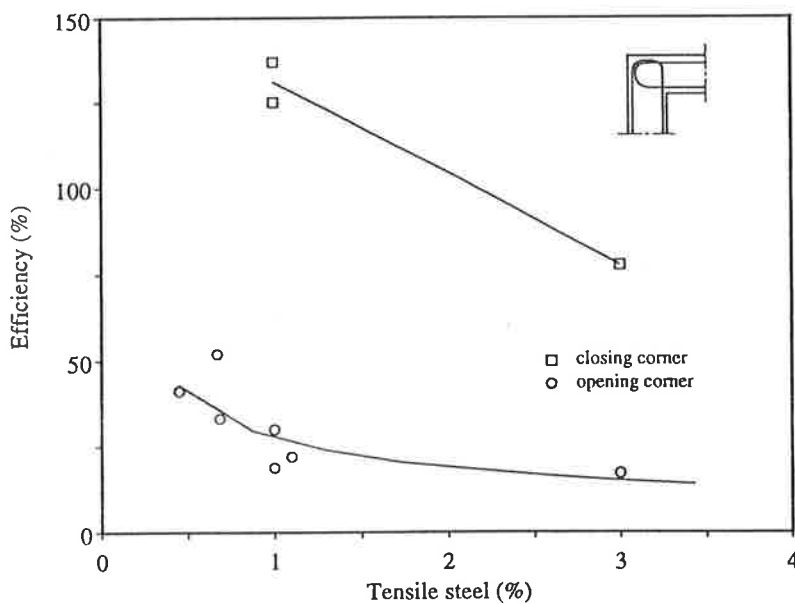
Figure 4.10: Efficiency versus percentage of tensile steel for detail 2

Both graphs in Figures 4.9 and 4.10 show similar trends. In terms of strength, closing corners are more efficient than opening corners, and efficiency improves as the percentage of steel reduces. Somerville and Taylor (1972) noted that highest efficiencies are achieved at very low amounts of steel because tensile strength contributes to overall strength.

In general, the results cannot be related directly to the performance of L-joints within frames because columns are subjected to various levels of axial forces. In all the test cases, a transverse load was applied either to the column or the beam, but the effect of axial loading applied directly to the columns was not included. However, the patterns at failure discussed in this section show the type of deformations which develop within opening and closing corners. Performance is likely to improve for columns in axial compression.

Two types of joint detailing have been examined in this section and in some test cases actual strength has compared poorly with strength predictions. Various alternative corner details have been tested by Swann (1969), Mayfield *et al.* (1971, 1972), Nilsson (1968, 1969a, 1973), and in many cases significant improvements in strength were noted. Most of these types of detail are not used in practice because of difficulties in construction. Notable exceptions are the test corners with haunches and inclined reinforcement tested by Nilsson (1968, 1973). However, the development of the joint model in this chapter is based on those cases where joint detailing and loading conditions may adversely affect strength and stiffness of frames. A study of frames which includes the joint model will be presented in Chapter 6.

4.3.3 Behaviour of T-Joints

T-joints are found in two different locations in a building frame, (see Figure 4.11). The T-joint in the exterior column and the T-joint in the top floor beam both require different construction techniques, and for this reason it is common to specify different reinforcement detailing for each type of joint. Taylor (1974) tested the type of T-joint

found in an exterior column and Nilsson (1973) tested various types of T-joints likely to be used to connect top floor beams to an interior column.
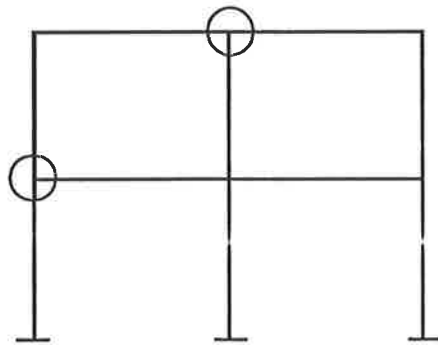
Figure 4.11: Types of T-joints

Taylor tested T-joint specimens with the configuration shown in Figure 4.12. Although four different types of detailing were tested, only the detail shown in Figure 4.12 is examined in the present study. Of the three details not considered here, one detail was designed specifically for a reversed load test and the other two details are not likely to be used in practice. For safety reasons, beams were loaded from the underside, hence beam tensile reinforcement was placed in the bottom face.

In each test, compressive axial loads were applied to the column and at the right hand end of the beam and incremented up to a predetermined level. These load levels were chosen to simulate working load conditions. Lateral restraints were also provided at the top and bottom of each column. Axial loads were then held constant as a transverse loading was applied to the beam and incremented up to collapse.

Two types of failure were observed. All of the specimens with shallow beams, and specimens with deep beams containing lower percentages of steel initially developed flexural cracks in the beams. At later stages of loading, diagonal cracks developed across the beam-column connections. Failure in these cases occurred when the beam steel at the face of the column had yielded. Test specimens with deep beams and steel percentages greater than 2.0% failed in joint shear, i.e. large diagonal cracks formed in

the beam-column connections followed by concrete crushing at the outside face of the columns.
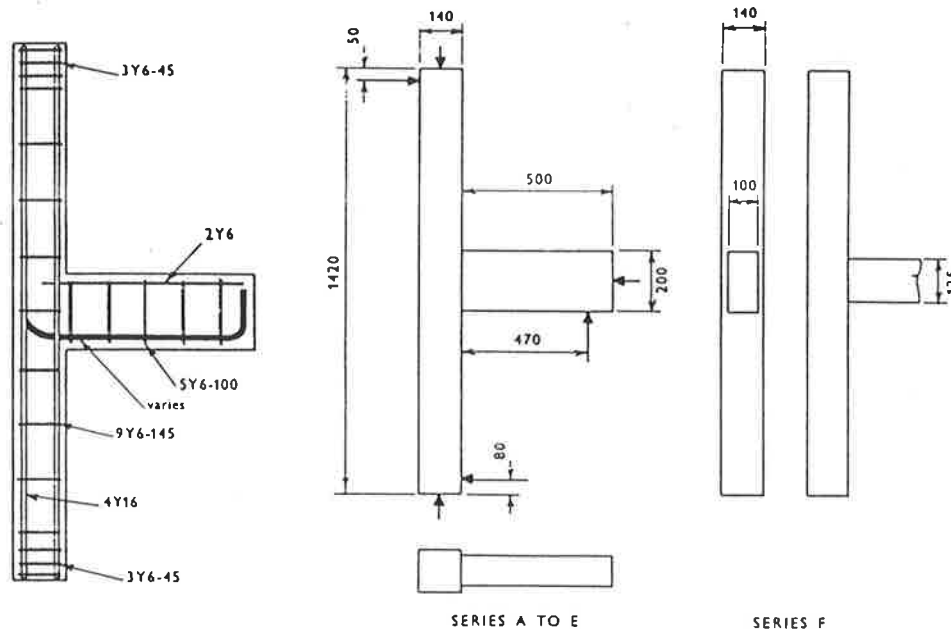
Figure 4.12: Test configuration and detailing used by Taylor (1974)

Plotted in Figure 4.13 is efficiency versus percentage of tensile steel in the beam for two different beam sizes. The calculation for theoretical moment M_{calc} includes beam thrust, and the values for efficiency reported by Taylor (1974) have been used in this study. In all test specimens with shallow beams, i.e. 100 mm by 125 mm, joint efficiency is greater than 100%. The beams within these T-joints failed in flexure. Since axial thrust is taken into account in the strength calculations, the apparent increase in strength is due to other causes. Confinement within the beam-column connections creates multiaxial states of stress and increases in concrete compressive strength from these stresses can be significant, (Kotsovos, 1987).

The specimens with deep beams containing 2.4% tensile beam steel have efficiencies ranging from 50% to 87%. All of these T-joints failed after extensive shear cracking within the joints. The lowest efficiency corresponds to the lowest level of axial thrust in the beam. For the T-joints with the lowest percentages of beam steel, joint efficiency compares most favourably. In these tests, a flexural failure occurred in the beams.
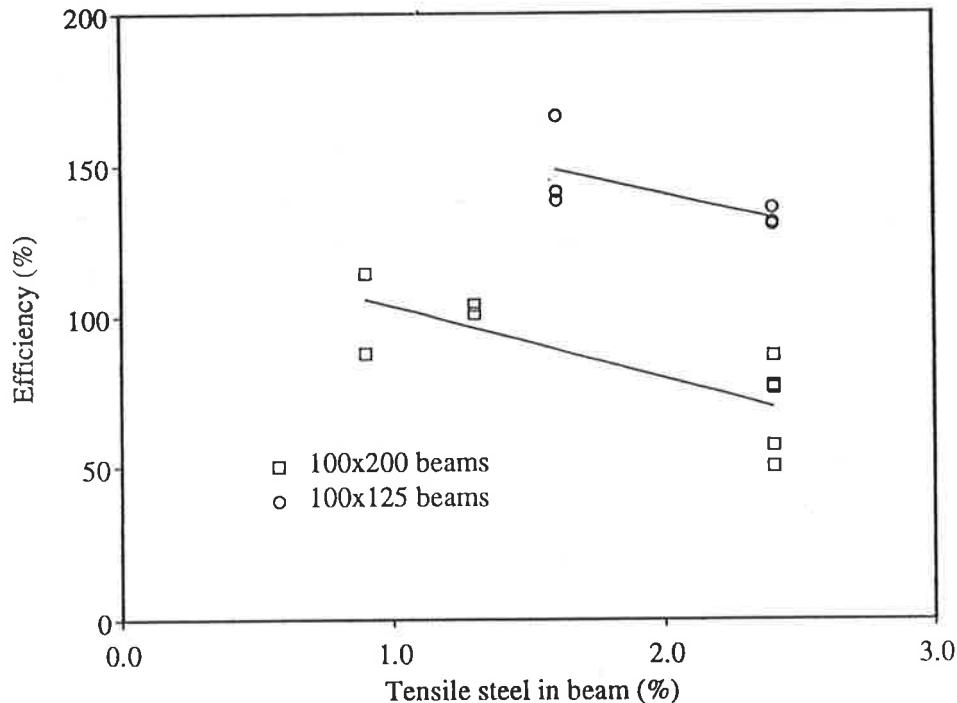
Figure 4.13: Efficiency versus percentage of steel for T-joints tested by Taylor (1974)

Nilsson (1973) tested T-joints with the test set-up shown in Figure 4.14. Plotted in Figure 4.15 is efficiency versus percentage of tensile steel in the column for the two details shown. Detail 1 has column reinforcement splayed outwards into the top floor beam. It is the preferred type of detailing because of the ease of constructability. Detail 2 has bars which extend out of the columns and lap each other in the beams. This is a less common method of detailing. The values of efficiency are those reported by Nilsson (1973) and are based on Equation 4.1. The values for M_{calc} are based on section analyses taken through the columns. The actual ultimate moment from the experiments, M_{test}, is equal to the maximum applied force multiplied by the distance to the centreline of the beams.
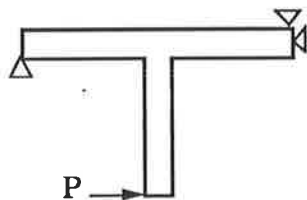
Figure 4.14: Test configuration used by Nilsson (1973)
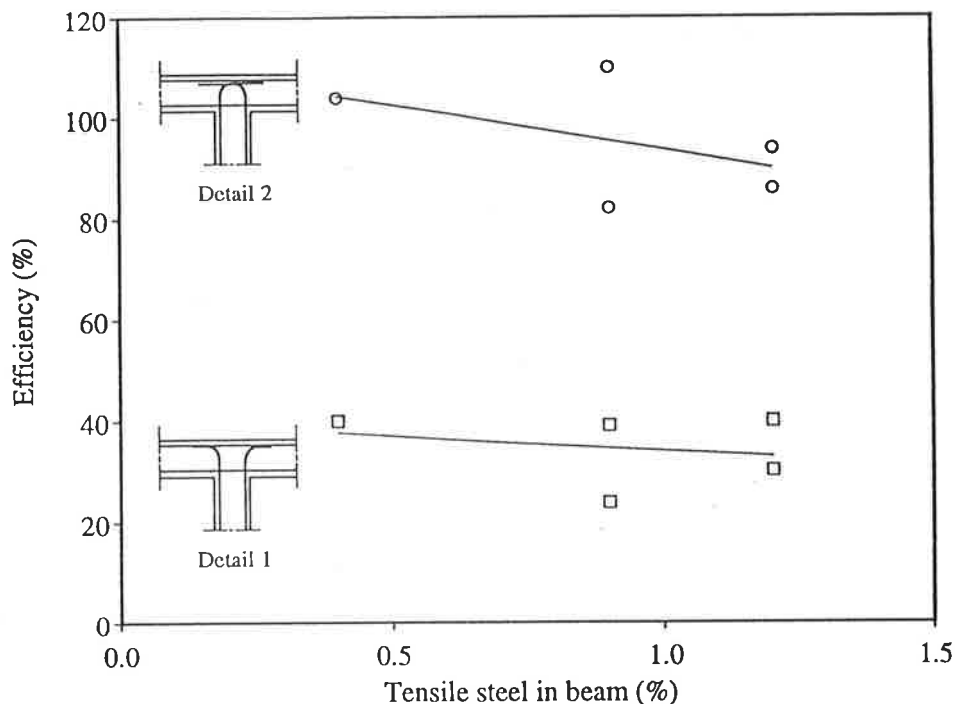
Figure 4.15: Efficiency versus percentage of steel for T-joints tested by

Nilsson (1973)

In all of the T-joints tested by Nilsson a diagonal tension crack formed across the joints, as in Figure 4.16, and failure occurred when the concrete had split from the steel in the outside face of the beams. It is assumed that higher failure loads, hence higher efficiencies, were achieved for detail 2 because the reinforcement detailing in the joints was able to delay the formation of diagonal cracks.
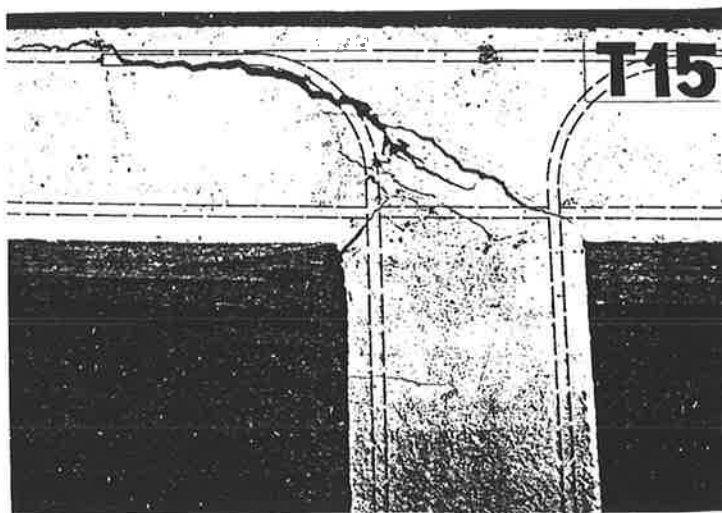
Figure 4.16: Post failure condition of T15 tested by Nilsson (1973)

So far, the influence of joint detailing for T-joints has been described, it is important to note that, similar to L-joints, loading conditions also determine the type of joint deformations. Shown in Figure 4.17a are the direction of moments for the joints tested by Taylor (1974). Diagonal cracking across the joint is due to the combination of M_a and M_b, while in Figure 4.17b, diagonal cracking is due to the moments, M_a and M_c. For these combinations, the moments are of opposite sign. Note this type of cracking pattern also occurs within opening corner L-joints when moments of opposite sign are present.

| (a) | (b) |
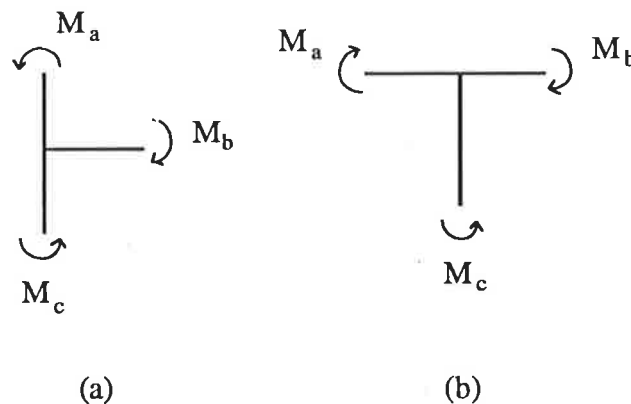
Figure 4.17: Moments acting in T-joints by (a) Taylor (1974); and (b) Nilsson (1973)

4.3.4 Behaviour of X-Joints

Limited test data is available on the behaviour of X-joints under static loading, although Nilsson (1973) tested to failure an X-joint under static loading and reported joint efficiency to be greater than 100%. The performance of X-joints has mainly focussed on tests under cyclic loading, e.g. Meinheit and Jirsa (1981).

X-joints are usually designed with longitudinal reinforcement which is continuous through the beam-column connections and good bond is usually achieved between steel and concrete. Bond can still exist even as beam steel is close to yielding, (Allwood, 1980). Bond deterioration becomes a problem with X-joints subjected to reversed loadings, which contributes to lateral story drift, (Noguchi, 1981). Post-yielding conditions also show that strain hardening of reinforcement can be achieved

(Burnett and Jajoo, 1971). Hence, failure moments can be much higher than moments at yield.

For the present study, the strength and stiffness of X-joints are assumed to be 100% efficient. Hence, additional joint deformations and confinement effects will be ignored for non-linear frame analyses.

4.3.5 Summary of Joint Behaviour

The investigation of isolated test joints in this section has shown that joint performance is mainly influenced by the type of joint detailing and the loading conditions. Three types of joint have been examined, L-, T- and X-joints.

Joint deformations are largely characterised by inclined or diagonal cracks and possible locations can be determined by the sign of the moments in each member entering the connections. These deformations are of most concern in opening L-joints and T-joints. It is assumed the performance of X-joints is not adversely affected by joint deformations. Longitudinal splitting cracks were also observed in some opening L-joints, but the formation of these cracks can be prevented by suitably placed stirrups around the main steel.

The performance of various common types of joint detailing has been investigated and in some cases the detailing appears to be inadequate. Although not classified as a joint detail it is worth considering the performance of joggled splices or lapped splices which are often detailed within column lengths. Tests by Somerville and Taylor (1972) showed that with proper placement, ideal column capacity can be achieved.

The test joints examined in this section were not subjected to column axial loading. It should be noted that the location of hinge forming sections is affected by the presence of axial forces. It is also important to note that an analysis for joint deformations which does not take axial loading into account may produce quite different results to an analysis which considers the influence of axial loading on joint performance.

4.4 Previous Methods of Analysis for Joint Behaviour

4.4.1 Introduction

Most emphasis for the analysis of joint behaviour has been for joints subjected to cyclic or reverse loading because the nature of joint deformations under these conditions is potentially more severe. However, the present discussion of previous methods of analysis is for those cases where static loading is applied. Such methods are applicable to frames subjected to any combination of dead, live and wind loads.

4.4.2 Analytical Methods for Static Loading

Hall (1969a,b) described the block of material where beams and columns meet as the 'joint block'. Using an elastic finite element approach, curves were derived for L-, T- and X- joints which can be used to determine the rigid portion of the joint block. The curves are functions of the cross-sectional dimensions of each column and beam and are useful for determining the effective length of a member.

Rad (1972) also used a linear elastic finite element model and generated EI values for closing and opening corners of frames with the configuration shown in Figure 4.18. Rad noted that confinement under the bearing plate, through which the column axial loads were applied, induces biaxial stresses in the corner. This has a beneficial effect which increases the uniaxial concrete compressive strength. The measurement of the nodal displacements (rotations), θ_L and θ_R, are for the closing corner shown in Figure 4.18. The average curvature, ϕ_{joint}, is given by:

$$\phi_{joint} = \frac{\theta_L - \theta_R}{L} \tag{4.2}$$

The stiffness of the joint is taken to be the average moment for the two nodes where displacement was measured, divided by the average curvature, ϕ_{joint}. The stiffness of

a joint member was found to be approximately five times the cracked stiffness of the beam.

Rad calculated values for all four corners because confinement is provided by the base supports, as well as by the bearing plates through which the vertical loads were applied. These stiffness values were used by Rad in a non-linear plane frame analysis to investigate the behaviour of several test frames. These frames were subjected to non-proportional loading and the experimental and analytical results obtained by Rad are discussed in Chapter 5, Non-Proportional Loading.
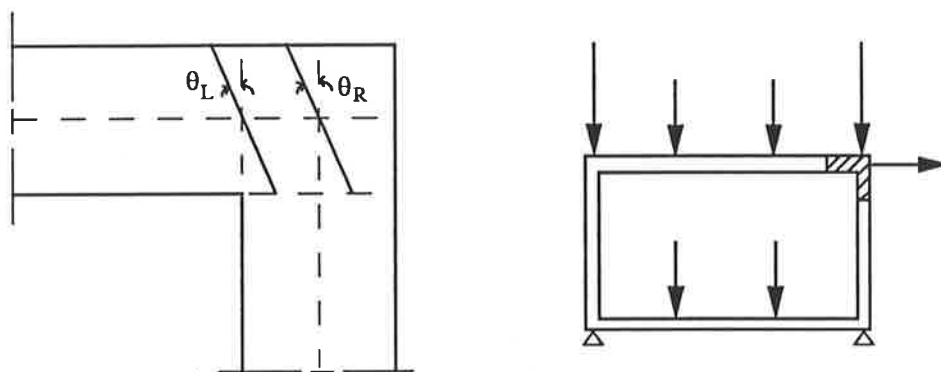
Figure 4.18: Measurement for rotation and moment for closing corner (Rad, 1972)

A common approach in the analysis and design of steel connections is the use of experimental moment-rotation curves, (Attiogbe and Morris, 1991; Bjorhovde *et al.* 1991). Blaauwendraad and de Groot (1983) used experimental moment-rotation curves for reinforced concrete T-joints to predict the strength of braced and unbraced frames. Figure 4.19 shows a bilinear $M - \phi$ plot for an ideal connection and also a typical curve for an imperfect connection. The experimentally derived curves can be linearised or represented by curvilinear expressions and then fed as input into a non-linear structural analysis progam.
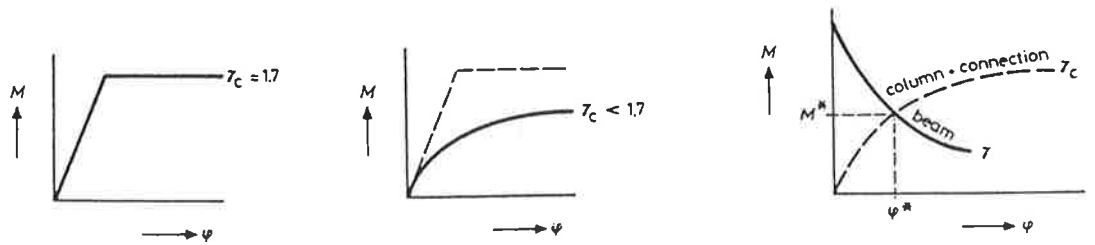
(a) Ideal connection　　(b) Imperfect connection　　(c) M - φ characteristics for

a frame connection

Figure 4.19: Moment-rotation curves by Blaauwendraad and de Groot (1983)

The behaviour of a T-joint in a frame is determined by the M-ϕ characteristics of the beam and the column. Shown in Figure 4.19c is an experimentally derived M - ϕ curve for a column connection and an M-ϕ curve for the beam component which is calculated from a non-linear frame analysis.

Nilsson (1973) derived the following equation to predict the diagonal cracking moment across an L-joint.

$$M_{dc} = 0.53 dbl_{dc}\sqrt{\sigma_c} \qquad\qquad (4.3)$$

This equation is based on the assumption that the tensile stress distribution across the diagonal crack agrees closely with a parabola, where l_{dc} is the length of the crack. The effective depth is given by d and the width of the corner is b. The compressive cube strength for concrete, σ_c, is used in the equation. An equation was also derived for the diagonal cracking moment for a T-joint. Table 4.3 compares results for the theoretical diagonal cracking moment determined by Nilsson and Losberg (1976) and the results from the tests on L-joints.

Table 4.3: Diagonal cracking moments (Nilsson and Losberg, 1976)

Test no.	M_{dc}, in (kNm)		Observed/ calculated
	Calculated	Observed	
U1	46.9	54.9	1.17
U2	31.5	32.8	1.04
U3	46.2	45.7	0.99
U20	9.9	10.0	1.01
U21	12.0	9.7	0.81
U22	10.7	11.9	1.11
U14	12.4	17.2	1.39

The ratio of observed moment to calculated moment varies between 0.81 to 1.39 and suggests that the assumptions in deriving the expression for M_{dc} are very approximate. It is also likely that the diagonal crack length l_{dc} and the distribution of stress varies considerably in each case.

El-Metwally and Chen (1988) modelled a beam-column connection as a concentrated rotational spring with a spring tangent stiffness, K, as shown in Figure 4.20 and given by :

$$K = \frac{K_0}{\left| \frac{1}{1 - \lambda^a} \right|}$$

(4.4)

where K_o is the initial rotational stiffness of the connection and a is a parameter which depends on the amount of energy dissipated. The load factor, λ, is given by $\lambda = M/M_u$ where M is the moment at the connection at the current level of load and M_u is the ultimate moment capacity of the connection.
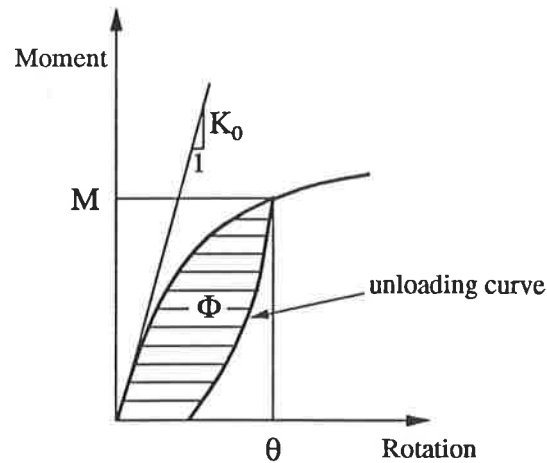
Figure 4.20: Moment-rotation relationship for beam-column connection

The spring stiffness, K, can be implemented into a member stiffness matrix for a non-linear frame analysis. Moment and rotation at any load level is given by the following relationship:

$$M = K\theta \qquad (4.5)$$

To determine the ultimate moment capacity of the connection, M_u, a flexural strength calculation is performed for each member which meets at the connection. Calculations are based on limit analysis theory and assume perfect plastic behaviour of the concrete and steel. The location of flexural hinges can be predicted by a method suggested by Ehsani and Wight (1984).

If the flexural strength of the column element is less than the flexural strength of the beam then a plastic hinge is expected to form in the column. Therefore, the ultimate moment of the connection is equal to the strength of the column. If the flexural strength of the column element is greater than 1.4 times the flexural strength of the beam element, a plastic hinge is expected to form in the beam. The ultimate moment of the connection is then set equal to the flexural strength of the column. If the flexural strength of the column element is between 1.0 and 1.4 times the strength of the beam,

failure is assumed to occur within the joint itself. In this case values for M_u and K_o should be estimated from experimental data using a regression analysis.

This method of locating potential hinges is only approximate because strength of individual members also depends on the level of compressive or tensile axial force. However, it appears to assume that column flexural capacity is more likely to be influenced by a compressive thrust.

Calculation of the initial rotational stiffness, K_o, is based on assumed linear elastic behaviour for the concrete and steel. The parameter K_o is for the member where a flexural hinge is expected to form.

The parameter, a, depends on the amount of energy, Φ, dissipated from the inelastic behaviour of the joint. The magnitude of a varies according to the level of load. The total energy released, Φ, is given by :

$$\Phi = \frac{M_u^2}{K_0} \sum_{n=1}^{\infty} [na(na+2)(\ln \lambda +1)+2] \frac{\lambda^{na+2}}{(na+2)^2} \qquad (4.6)$$

and is the sum of dissipated energy from three sources of material non-linearity. These effects are: (1) deterioration of bond between the steel and concrete; (2) cracks in the concrete; and (3) the inelastic behaviour of the steel and concrete.

The determination of the magnitude of the parameter a for each level of load is a complicated process involving three energy equations to be solved for each effect and at each load level. However, it was suggested for simplicity that a can assumed to be constant and calculated for a predetermined load level. A satisfactory solution can be found by choosing a load level which corresponds to a steel strain. The dissipated energy from each source is then given by the following :

1. Dissipated energy due to bond deterioration, Φ_b :

$$\Phi_b = \sum \frac{d^3 \sigma_s^2}{556,433} \text{ (kgf} - \text{cm)} \tag{4.7}$$

where σ_s = stress in the steel and less than the yield stress, and d = diameter of the bar.

2. Dissipated energy due to cracks in the concrete, Φ_c :

$$\Phi_c = 15.68 \frac{(f_c)^{4/3}}{E_c} \text{x} V \text{(kgf} - \text{cm)} \tag{4.8}$$

where f_c = concrete compressive strength (kgf/cm^2) and E_c = modulus of concrete (kgf/cm^2). The theoretical volume in which cracks are assumed to form is given by $V = byh$. The width of the section is b and the depth of the section is given by y. The term h is the length of a flexural hinge over which the cracks form.

3. Dissipated energy due to material inelasticity, ξ_i :

By choosing the strain level in the steel, ε_0, to be less then the yield strain, ε_y, there is no energy release due to inelastic behaviour of the steel. The energy released due to the inelastic behaviour of the concrete can be found by integrating the stress-strain curve of Soliman and Yu (1967) and shown in Figure 4.21. The integral functions can be found in the paper by El-Metwally and Chen (1988).

The joint model was incorporated in a non-linear frame analysis by El-Metwally and Chen (1989b) who examined two frames tested by Ernst *et al.* (1973). Test frame 2D9H was subjected to sequential loading and the results of this analysis are discussed in Chapter 5 of the present study. The results from five different analyses by El-Metwally and Chen for frame B40 are shown in Figure 4.22. Their study assumed an elasto-plastic relationship for the reinforcing steel, although test results showed strain

hardening of the tensile steel at the top of the right hand column. The tensile capacity of the concrete and shear deformations were also ignored.
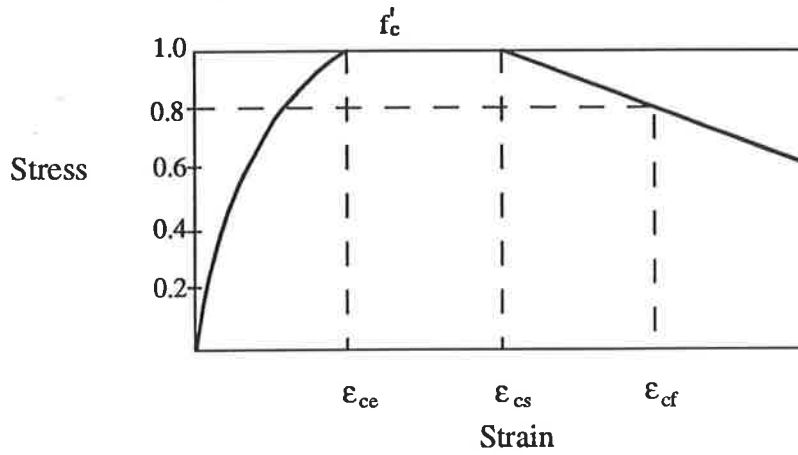
Figure 4.21: Stress-strain curve for concrete confined by rectangular hoops

(Soliman and Yu, 1967)
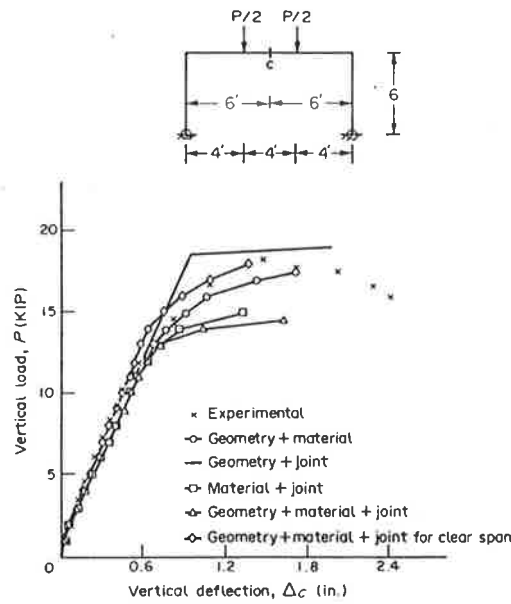
Figure 4.22: Experimental versus analytical results for joint model by

El-Metwally and Chen (1989b)

The plot of load versus deflection for the first analysis, 'geometry + material' effects compare well with the experimental results, although the maximum load is underestimated slightly. When this plot is compared with the results 'geometry + joint' and 'material + joint', the load versus deflection differs considerably for all three, indicating that each non-linear effect has a significant contribution to frame behaviour.

Load versus deflection compares best of all for the fifth analysis, which includes joint modelling for the end of the beam, i.e. the analysis anticipates that a flexural hinge will form first at the end of the beam. From the actual results of the test frame, a hinge formed first at the end of the beam followed by a second hinge at midspan. No hinges formed in the columns of the test frame. Sectional analyses of frame B40 were carried out in the present study and showed that the moment capacities of the column and at midspan of the beam are approximately twice the moment capacity of the end of the beam. The sectional analyses ignored the presence of any axial thrust. This suggests that the joint model used in the fifth analysis has predicted accurately the location of the critical hinge within the joint.

The results of the fifth analysis when compared to the second analysis, 'geometry + material', show that prediction of frame capacity is improved by including the joint model. Under the action of vertical loading, two closing corners are created in the frame. It can be concluded from the fifth analysis by El-Metwally and Chen that the closing corners are more than 100% efficient. Confinement effects are likely to increase with increasing levels of axial thrust in the columns and beam. This in turn improves the strength of the closing corners.

The fourth analysis by El-Metwally and Chen assumes joint deformations occur within the joint and results don't compare well. Peak load is underestimated by 20%. This fourth analysis shows the importance of predicting the hinge forming region at the joints.

Unfortunately, the analyses carried out by El-Metwally and Chen do not predict continuing deflection after peak load. The method of frame analysis is based on a tangent stiffness approach, and only determines the amount of deflection up to the peak load. The method of analysis ignores the effect of tension stiffening and therefore stiffness is likely to be underestimated.

Drysdale and Mirza (1974) also analysed a series of test frames with a similar configuration as frame B40 tested by Ernst *et al*. It was noted that differences between predicted and experimental results were due to the additional effects of joint rotation and diagonal cracking, which had not been taken into account in their method.

Confinement effects were considered in a non-linear finite element method of analysis by van Mier (1987). An element mesh with eight noded plane stress elements was employed, and to model the multiaxial state of stress within closing corners of a portal frame, the compressive strength of the concrete was increased by 50%.

4.4.3   Summary and Conclusions

The methods for modelling joint behaviour described in this section are largely concerned with increases in strength and stiffness which are characteristic of closing L-joints. The method proposed by El-Metwally and Chen is based on constitutive properties. Predictions compare well for frame with closing corners. However, the method may not be suitable for the analysis of frames with T-joints and/or opening L-joints.

The approaches taken by Rad (1972) and Blaauwendraad and de Groot (1983) use load-deformation curves based on experimental results for test joints. However, the approach by Rad is restricted to a particular series of test frames and the curves generated by the latter lack important information.

The multi-directional crack patterns of many of the test joints examined in this chapter suggests that complex states of stress develop as these joints are subjected to

increasing levels of load. Although this type of behaviour can be modelled in a finite element approach, it is not suitable to the analysis of overall frame behaviour. A convenient approach is the use of modified moment-curvature curves such as those described in Chapter 3, Tension Stiffening. The development of these types of curves are often based on experimental results.

4.5 Proposed Model for Joint Behaviour

4.5.1 Introduction

The proposed model for joint behaviour is a global approach which involves modifying ideal moment-curvature-thrust curves. Modified curves can be developed for joints to take into account increases or decreases in strength and stiffness. However, in the present study M-κ-N curves are only developed for two types of joint with common types of detailing: the opening L-joint and the T-joint which connects top floor beams to an interior column. The study of various joint types in this chapter shows these joint types are inefficient under certain loading conditions. Other joint types are assumed to be 100% efficient.

The modified curves will be used in the non-linear method of frame analysis to investigate the influence of joint deformations in frames. The study is described in detail in Chapter 6 and is concerned with situations where joint deformations can potentially reduce frame strength and stiffness.

4.5.2 Joint Segments

For the present study, two segments which enter a joint are designated as 'joint segments'. Each joint segment has a length equal to D, where D is the depth of the member. This is based on the test studies by Swann (1969) and Nilsson (1968, 1973) where joint deformations were generally spread over a distance of D in the beam and a distance of D in the column.

The location of joint segments is found by first performing section analyses to determine the theoretical moment capacities for the beam and column, $M_{u(beam)}$ and $M_{u(col)}$ respectively. Section analyses assume zero axial force. For an L-joint, hinge locations are found by comparing the relative strength of each member entering the joint. This is based on the joint model developed by El-Metwally and Chen.

If the flexural strength of the beam is greater than the flexural strength of the column, as given by Equation 4.9, two segments are placed at the top of the column. On the other hand, two joint segments are inserted in the beam element if the moment capacity of the column is greater than 1.4 times the moment capacity of the beam element. This is given by Equation 4.10.

In some situations, a hinge may also form within the joint itself. This prediction is made if the relative strengths of the connecting members is given by Equation 4.11. Hence, to perform a non-linear analysis for joint deformations, a joint segment is placed at the top of the column and a segment is also placed at the end of the beam
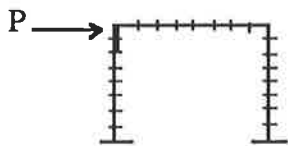
$$M_{u(col)} < M_{u(beam)} \qquad (4.9)$$
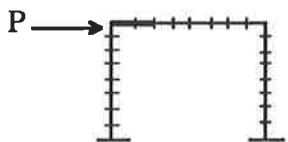
$$M_{u(col)} > 1.4M_{u(beam)} \qquad (4.10)$$
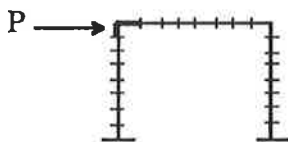
$$M_{u(beam)} \le M_{u(col)} \le 1.4M_{u(beam)} \qquad (4.11)$$

For T-joints, special joint segments are only inserted in the beams. The investigation of T-joints earlier in this chapter showed that regardless of the relative strength of connecting members, joint deformations are largely confined to the beams. Figure 4.23 shows where joint segments are inserted and for the given loading conditions.
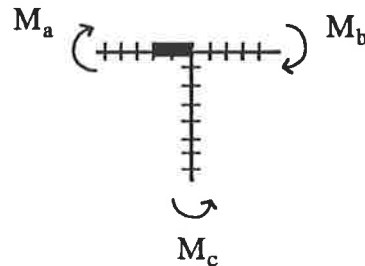
Figure 4.23: Joint segments in a T-joint

4.5.3 Modified M-κ-N Curves

The proposed method involves generating a family of ideal moment-thrust-curvature curves for the joint segments using the sectional analysis procedures of the segmental method of frame analysis. These curves are then modified to take into account losses of strength and stiffness which occur at joints. Note that an analysis for joint deformations also takes tension stiffening into account. The process involved in generating curves for joint modelling is as follows.

A sectional analysis routine generates a family of ten ideal M-κ-N curves, in increments from zero axial thrust up to $0.9N_{uo}$, where N_{uo} is the squash load. Figure 4.24 shows an ideal and a modified moment-curvature curve. The first curve is generated by a section analysis and has three key points. The first key point (M_1, κ_1) is the moment and curvature when the first crack forms and the second key point, (M_2, κ_2), is the moment and curvature at the ultimate moment. The final point on the curve, (M_3, κ_3), is the moment and curvature at the maximum curvature.

Moment and curvature representing the keypoints of the ideal curve are then modified and have corresponding keypoints shown on the modified tri-linear curve.
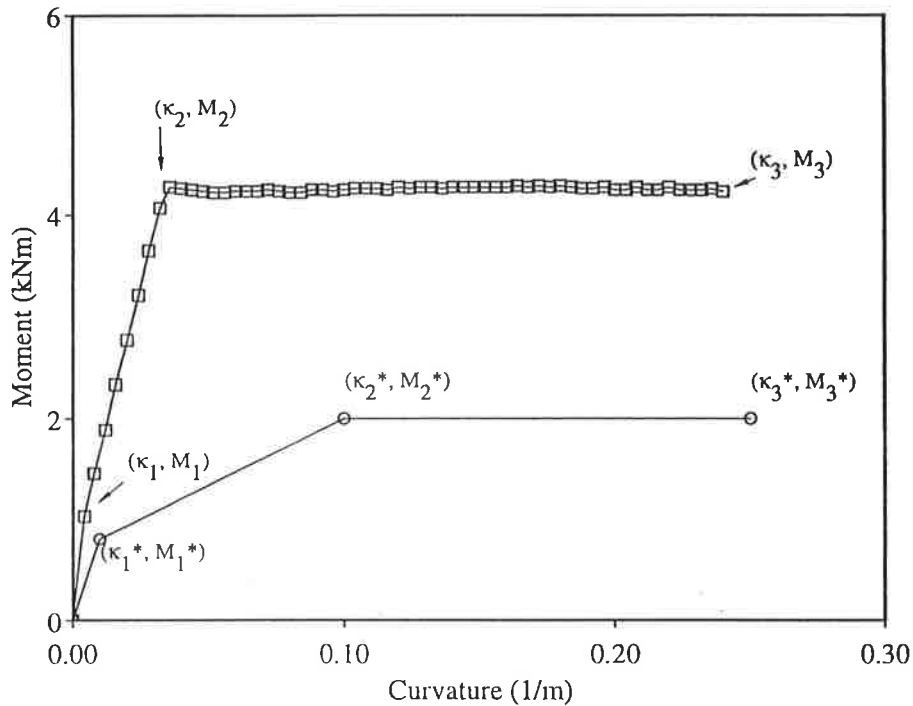
Figure 4.24: Ideal and modified moment-curvature curves

4.5.4   Joint Model for Opening L-Joints

The development of the joint model for opening L-joints is based on a series of sway frames tested by Ferguson and Breen (1966). Eight rectangular frames were tested, and six frames have been chosen for analysis in the present study. Frame L8 was tested under sustained load and was considered unsuitable for analysis. Frame L4 failed prematurely because some elements of the loading frame buckled near the ultimate moment capacity and test results were not published.

Figure 4.25 shows the test set-up, with vertical loads applied to the columns and a horizontal load applied to the top of the left hand column. Loads were applied proportionally up to failure. Table 4.4 summarises frame dimensions and material strengths and Figure 4.26 shows the section details for the beams and columns in the tests.
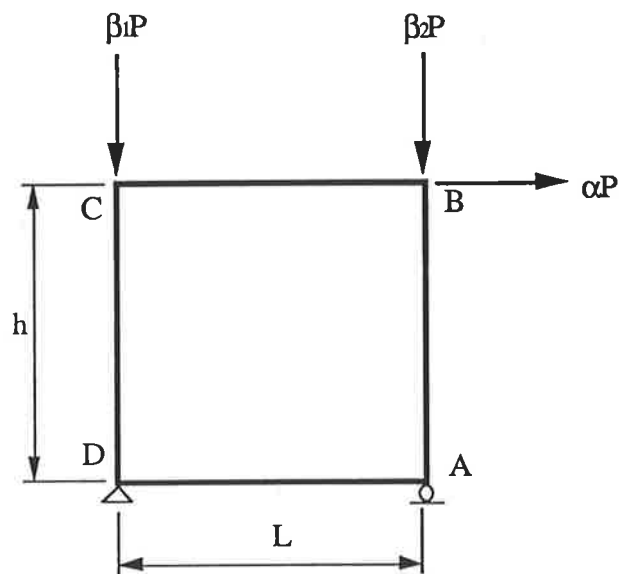
Figure 4.25: Test configuration of frames tested by Ferguson and Breen (1966)

Table 4.4: Frame dimensions and material properties of frames tested by

Ferguson and Breen (1966)

Frame	h (mm)	L (mm)	α	β_1	β_2	f_c (MPa)	f_{sy}(col) (MPa)	f_{sy}(beam) (MPa)
L1	2134	2134	0.02	1.01	0.99	27.4	383	362
L2	2134	2134	0.06	1.01	0.99	28.8	408	359
L3	2113	2134	0.02	1.01	0.99	22.1	389	403
L5	1141	2134	0.12	1.03	0.97	28.0	398	359
L6	1141	2134	0.04	1.02	0.95	25.5	384	359
L7	1097	2134	0.04	1.02	0.98	20.6	393	382
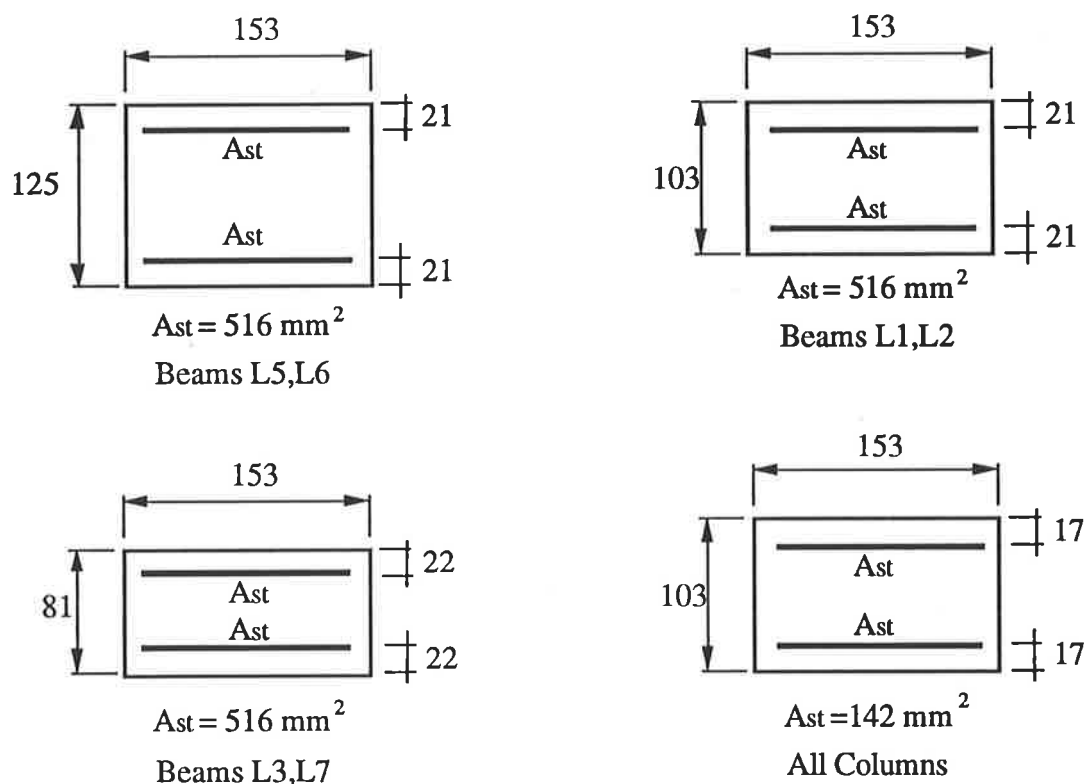
Figure 4.26: Section details of frames tested by Ferguson and Breen (1966)

Two types of failure mode were observed for these test fames. Frames L1, L2 and L3 each failed by concrete crushing on the outside face of the column of corner A which is an opening corner. Failure at other sections within these frames was not reported.

Frame L6 failed when the main reinforcement buckled between the ties in the columns of both corners B and D, and concrete had been completely destroyed. These two corners of frame L6 are closing corners. However, it was not mentioned whether this failure mode is typical of frames L5 and L7. Deformations were not observed in the beams in any of the six test frames analysed here, probably because the beams were heavily reinforced and relatively much stronger than the columns.

In the proposed model for joint behaviour, no modifications are made to the ideal M-κ-N curves for closing corners. Although the closing corners of frame L6 failed prematurely, this type of failure probably could have occurred at any of the four corners. Figure 4.27 shows the type of detailing used in each of the frames tested by

Ferguson and Breen. All columns have 1.1% tensile steel reinforcement and all beams are heavily reinforced with a total area of steel equal to 8% of the gross sectional area. Since the beams are relatively much stronger than the columns, joint segments have been included in the columns only.
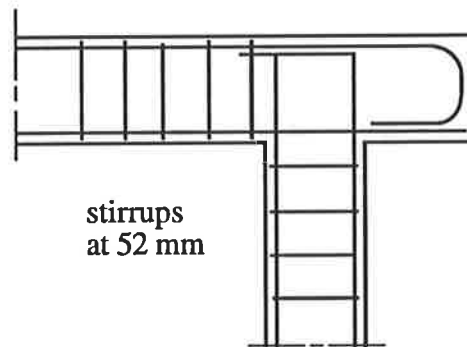
Figure 4.27: Corner detailing for frames (Ferguson and Breen, 1966)

To develop a family of modified M-κ-N curves for the opening L-joint, shown in Figure 4.27, the modified curve corresponding to zero axial thrust is based on the performance of frame U22 tested by Nilsson (1973). This frame has similar joint detailing to the frames tested by Ferguson and Breen. Analytical and experimental results for frame U22 are shown in Figure 4.28. The experimental results show that sudden failure occurred at a load of 11 kN. The line of circles is for an analysis which includes tension stiffening but the effect of joint deformations has been ignored. Load versus deflection compares very well up to the experimental peak load, when the test frame failed suddenly. This brittle type of failure could be attributed to two causes. Firstly, the test was carried out under load control conditions and failure took place when the peak load had been reached. Secondly, the main reinforcement is not well not anchored and therefore as cracks develop within the corner, little or no restraint is provided as the cracks extend well into the beam and column.

The plot showing the line of triangles assumes, in terms of strength, the joint is 30% efficient. This analysis uses a modified M-κ relationship for the segment at the top of the column and the segment at the end of the beam which joins the column. The peak moment of the ideal M-κ relationship is reduced by approximately 70%.
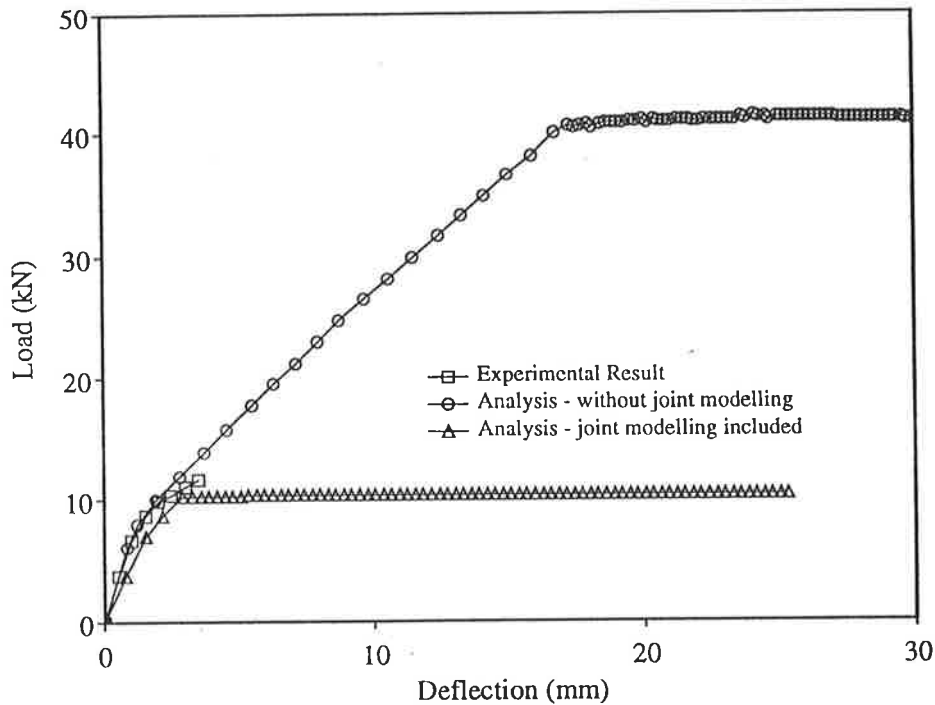
Figure 4.28: Load versus deflection for frame U22 tested by Nilsson (1973)

Figure 4.29 shows families of ideal and modified M-κ-N curves, which have been used to analyse frame L2 of Ferguson and Breen. Note with increasing levels of thrust the ideal moment-curvature curves undergo softening beyond the peak moment. All modified M-κ-N curves in the present study are characterised by horizontal plateaus after the peak moment. It was found that modified curves with post-peak softening portions, similar to the ideal curves, gave poor correlation for predicting load and sway deflection. Moment and curvature at intermediate values of thrust for the modified curves can be obtained by interpolation.

Although the modified M-κ-N curves take into account reductions in flexural stiffness, the joint segments are assumed to be axially rigid. Preliminary checks in the present study showed this to be a reasonable assumption. Tensile axial forces, which may occur in beam elements, are also ignored for the modified curves. It has been shown that large tensile axial forces assist the formation diagonal tension cracking (Mattock, 1969). However, for beam elements, the magnitude of these tensile forces are not likely to be significant.
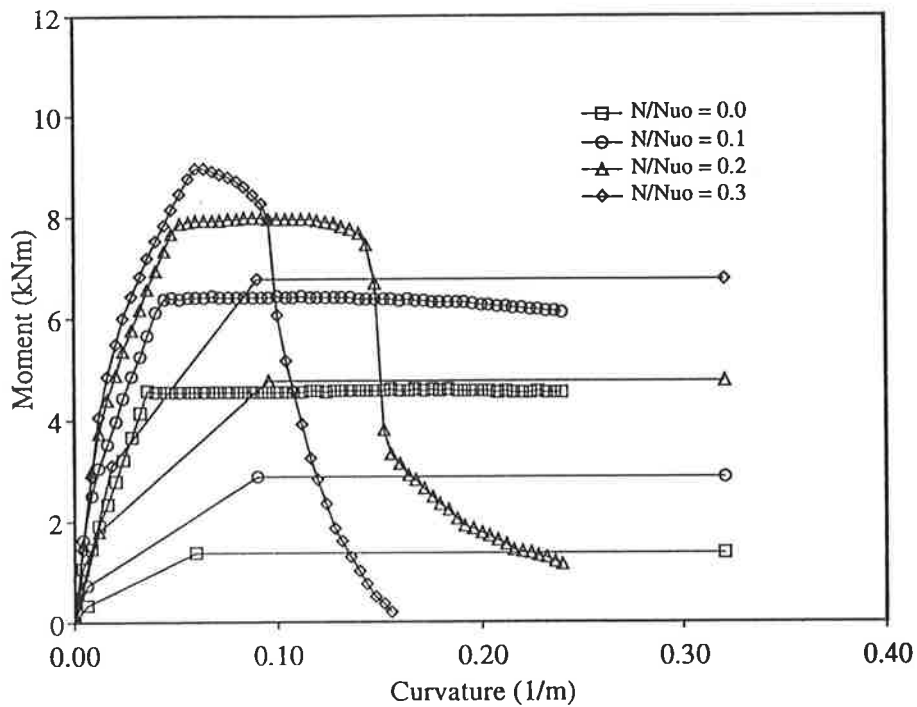
Figure 4.29: Ideal and modified M-κ-N curves for frame L2

Summarised in Table 4.5 is the ratio of modified moment to ideal moment, given by M^*/M, and the ratio of modified curvature to ideal curvature, given by κ^*/κ, for each level of thrust. These ratios of M^*/M and κ^*/κ were used to analyse all six test frames of Ferguson and Breen and in most cases gave reasonable predictions of load and sway deflection.

Table 4.5: Ratios of modified to ideal moment and curvature

N/N_{uo}	M^*/M	κ^*/κ
0.0	0.3	1.5
0.1	0.45	1.5
0.2	0.6	1.5
0.3	0.75	1.5
0.4	0.7	1.5
0.5	0.65	1.5
0.6	0.6	1.5
0.7	0.55	1.5

The experimental and analytical results for load versus deflection for frames L1, L2, L3, L5, L6 and L7 are shown in Figures 4.30a to 4.30f. Two types of analysis have been made for these frames. The first analysis takes tension stiffening into account and the second analysis includes the modified M-κ-N curves for the joint segments. Two joint segments are included at the top of the left hand columns and two joint segments have been included at the bottom of the right hand columns. This corresponds to the two opening corners for these frames.

Stiffness and strength are overestimated for all the analyses which ignore the joint model. Only the analysis for frame L3, with a slight overestimation for strength and stiffness, compares well. Good correlation for this frame has also been achieved previously by others, (Espion, 1986; Gunnin *et al.*, 1977; Wong, 1989). In each of these non-linear analyses, tension stiffening was ignored to obtain a good estimate of stiffness. In addition, the previous analyses also ignored joint deformations. To the author's knowledge, previous investigations of frames L1, L2, L5, L6 and L7 by Ferguson and Breen have not been published.

It is interesting to note that all analyses by the present method which ignore joint deformations actually predict formation of hinges at the top and bottom of both columns as the peak frame load is reached. However, the tests showed that in all cases an insufficient number of hinges had formed. The analyses which include joint modelling predict the formation of hinges in the columns of the opening corners.

Summarised in Table 4.6 are the peak frame loads from each analysis and the experimental failure loads. All analyses take tension stiffening into account. Results show that the analyses which include joint modelling overestimate peak load in three cases. These are 16%, 16% and 12% for frames L1, L6 and L7. The analyses which ignore joint modelling overestimate peak loads of these frames by 44%, 37% and 34%, respectively. Clearly there is an improvement in predicted behaviour by including the joint model in the non-linear frame analyses. Predicted stiffness compares well for frame L7 but the stiffness of frames L1 and L7 is considerably overestimated by the non-linear analysis which includes joint modelling.

The analyses for joint modelling for the other three frames L2, L3 and L5 have underestimated peak load by 7%, 8% and 7% respectively. The best improvement is for frame L2 where the analysis ignoring joint effects overestimated peak load by 33%. Note that stiffness for frames L2, L3 and L5 as determined by the analyses with the joint model compares well with the experimental results. For frame L2, both strength and stiffness are underestimated.

Although the analyses for joint deformations show an overall improvement in predicted behaviour, the correlation for two frames, L1 and L6, is not good. It should be noted that modifications have not been made for any of the beam elements, mainly because no mention was made in the published results of the condition of the beams at failure. A preliminary check showed that modified M-κ-N curves at beam ends within closing corners improved the analytical results for frames L1 and L6.

It was also shown earlier in this chapter that joint performance can be highly variable, depending largely on adequate placement of the joint detailing. To take this into account, comparisons were made with further reductions in strength and stiffness to the modified M-κ-N curves for the columns. This appeared to give better correlation in some cases. However, these further changes to the joint model are not justified.

Note that for all analyses, the joint segment length, which is also the length over which failure is expected to occur, is equal to the depth of the section of the column member. A number of investigators, including Corley (1966), Park *et al.* (1982) and Warner and Yeo (1984), have proposed mathematical formulae to predict this hinge length or contamination length, but the value determined by each formula can vary considerably. It should also be noted that tests on opening joints, such as those by Nilsson, show the extent of the failure region within members entering a joint can be highly variable. It was found in the present study of the frames by Ferguson and Breen that predicted results are sensitive to the length of joint segments. However, a value for the joint segment length equal to the depth of the column member appears to be reasonable.

Table 4.6: Ultimate frame loads for frames tested by Ferguson and Breen (1966)

Frame	Experimental result (kN)	Joint model ignored (kN)	Joint model included (kN)
L1	165	237	192
L2	112	149	104
L3	142	148	130
L5	190	213	176
L6	243	333	281
L7	177	238	199
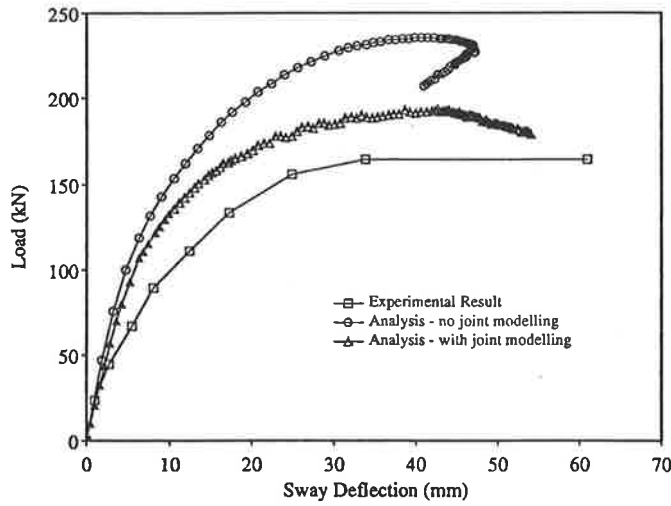
(a) frame L1
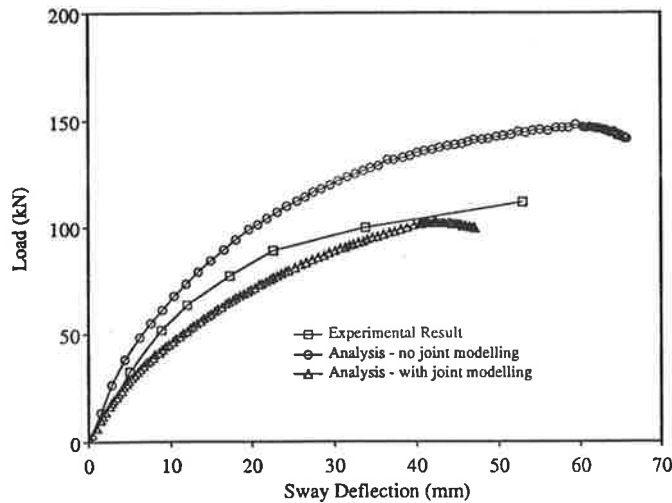
(b) frame L2
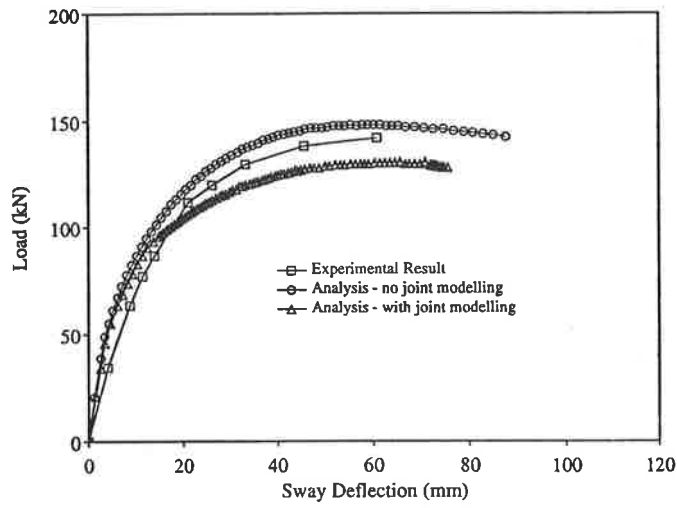
(c) frame L3
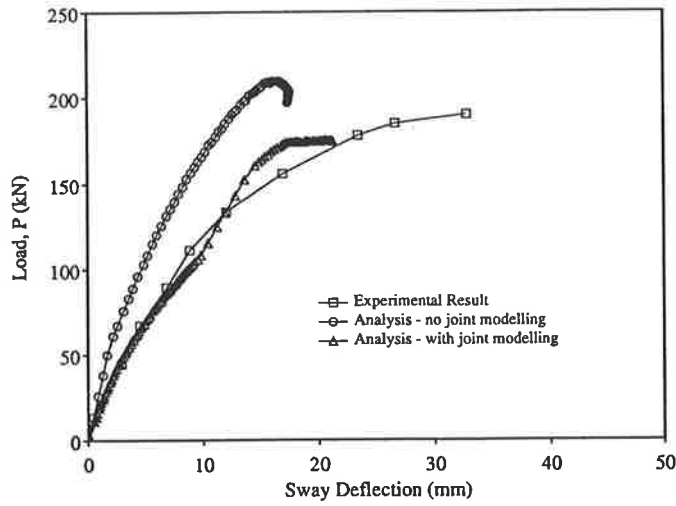
(d) frame L5
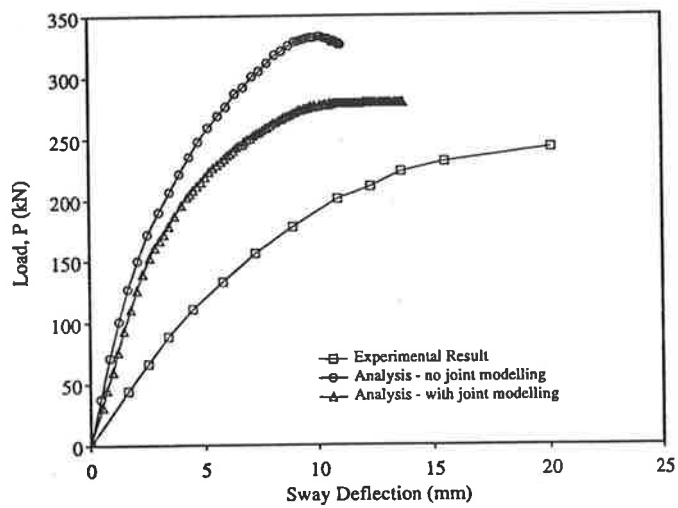
(e) frame L6
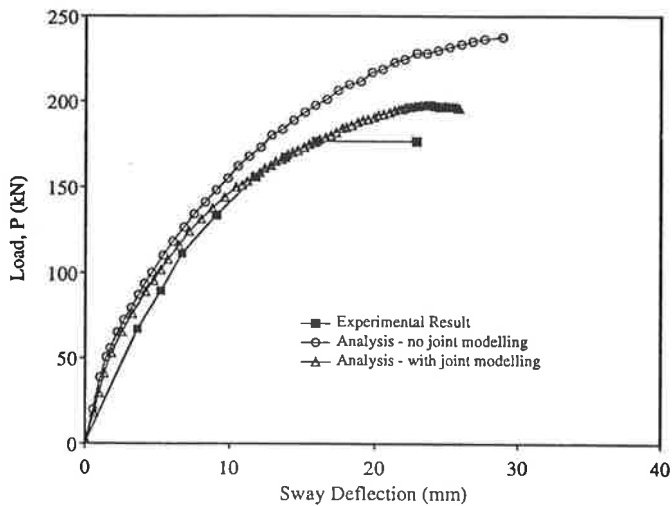
(f) frame L7

Figure 4:30: Load versus deflection for frames tested by Ferguson and Breen (1966)

4.5.5 Joint Model for T-joints

The joint model proposed in this section is based on experimental results for T-joints tested by Nilsson (1973). Test results showed that a common type of detailing can fail prematurely due to the formation of an inclined crack across the beam-column connection. For analysis, joint segments are included in the beams as shown in Figure 4.23. Although cracks initially formed within the joints, they tended to spread to the outer main steel in a beam element, rather than to the columns. In some tests, columns were preloaded with a 2000 kg axial load, but application of this load did not prevent the formation of inclined cracks. There also appeared to be little improvement in strength. These T-joints have not been analysed.

Table 4.7 summarises strength predictions for three frames tested by Nilsson. The values for M_{calc} are the theoretical moment capacities for the beams and columns assuming no axial force. Beam capacities for frames T11 and T25 are 0.71 of the column capacities, whereas the beam capacity for frame T25 is 2.65 times greater than the beam strength. Unlike the opening L-joints, where failure is controlled by the relative member strengths, strength of T-joints are controlled by beam deformations.

Column (4) in Table 4.7 is the predicted maximum moment in the beams, based on modified M-κ relationships. Hence, beam efficiencies are given in column (5).

Table 4.7: Strength predictions for T-joints

Test	(1) M_{calc} beam (kNm)	(2) M_{calc} column (kNm)	(3) $\frac{(1)}{(2)}$ (%)	(4) M_{test} beam (kNm)	(5) $\frac{(4)}{(1)}$ (%)
T11	33.5	47.4	0.71	4.8	14
T15	16.7	23.6	0.71	3.9	23
T25	155	58.6	2.65	9.3	6

Shown in Figure 4.31 is load versus deflection for T15 and T16 tested by Nilsson (1973). Test joint T16 has a higher load capacity because the type of detail delays the formation of inclined cracks. The predicted peak load for the analysis which ignores joint modelling compares well with the actual peak load for this test joint. The analysis overestimates stiffness at 5 kN when cracks within the joint are likely to have formed.

The analysis which ignores joint modelling compares poorly with the experimental results for test joint T15. Note that both T15 and T16 have similar material and section properties. The difference between the two T-joints is the manner in which the column steel is anchored in the beams. The analysis which includes joint modelling assumes the beam is only 23% efficient in terms of strength.

Results for load versus deflection for test joints T25 and T27 are shown in Figure 4.32. The ratio of theoretical beam to column strengths for these T-joints is 2.65 and the difference between these two test joints is the detailing within the beam-column connections. Similar to test T16, the detailing for test T27 greatly improves joint capacity. The analysis which includes joint modelling assumes the beam is only 6% efficient. Predicted strength compares well with the capacity of test T25, but stiffness

is underestimated. This is because curvature has been modified by the same amount as for test T15. The ratio of ideal curvature to modified curvature is 0.02.
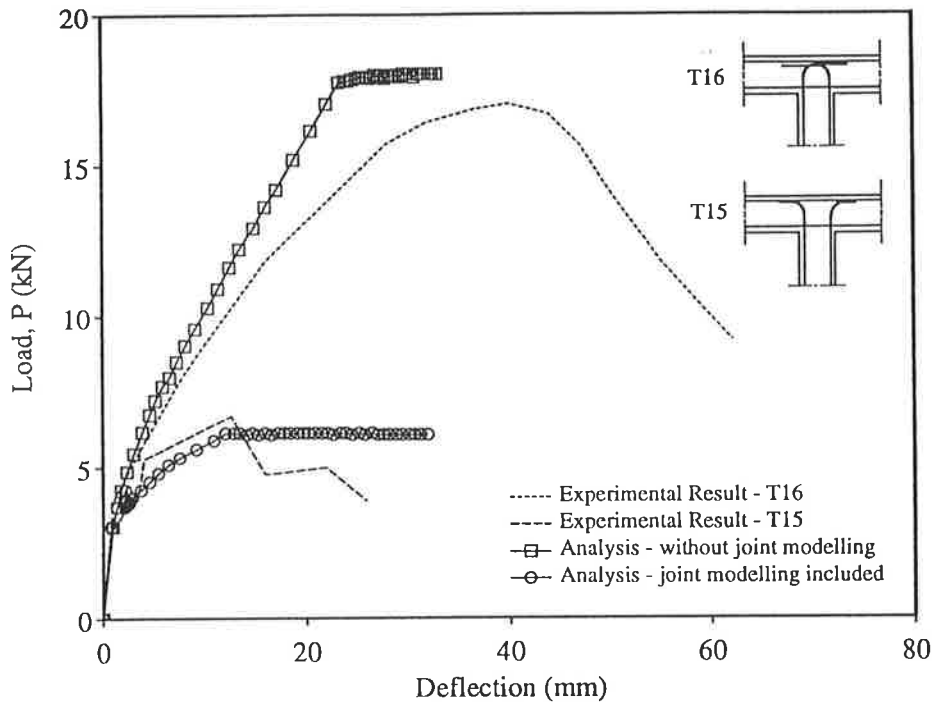
Figure 4.31: Load versus deflection for frames T15 and T16 tested by Nilsson (1973)
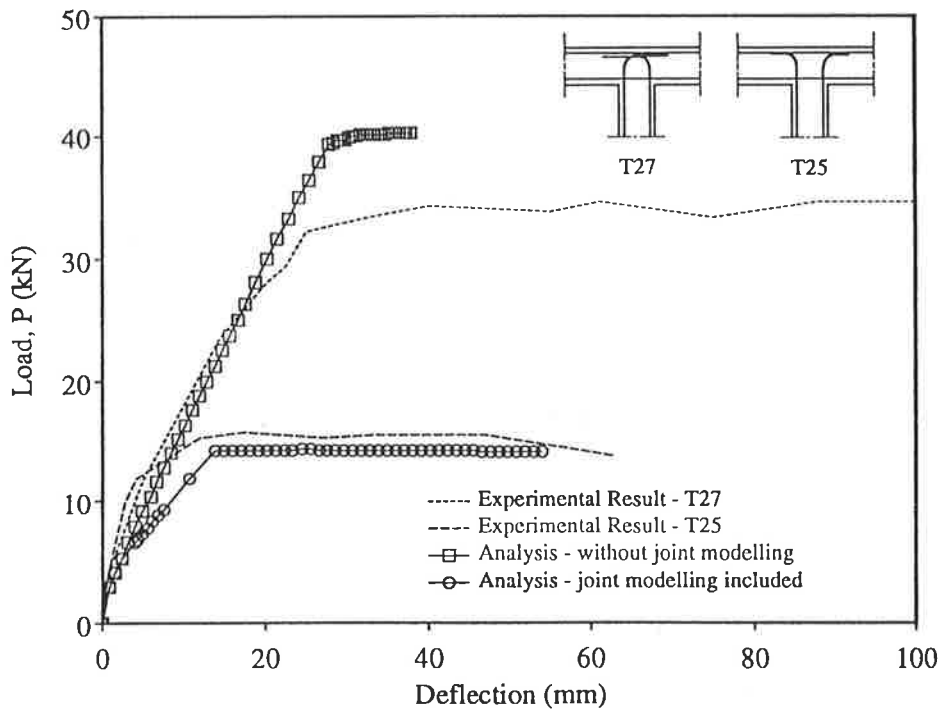
Figure 4.32: Load versus deflection for frames T25 and T27 tested by Nilsson (1973)

4.5.6   Summary of Proposed Joint Model

To develop the proposed joint model, a global approach has been taken, which requires modified M-κ-N relations for joint segments. These are obtained by fitting curves to limited experimental data.

The present study is concerned with situations where strength and stiffness are reduced by joint deformations, the nature of the detailing and the loading conditions. Hence, M-κ-N curves are developed for opening L-joints and T-joints. The proposed model could also be used for joints which are greater than 100% efficient for strength and stiffness. However, the present joint model is concerned with joint deformations which can adversely affect frame behaviour. This will be investigated further in a study of frames in Chapter 6.

The use of modified M-κ-N relations can be used to develop M-N strength interaction diagrams. Figure 4.33 shows an ideal and a modified strength interaction diagram. The relationship between the two curves, M^*/M (modified moment to ideal moment) at different levels of thrust, is similar in principle to the strength reduction factor, ϕ, defined by the Australian Standard AS 3600.
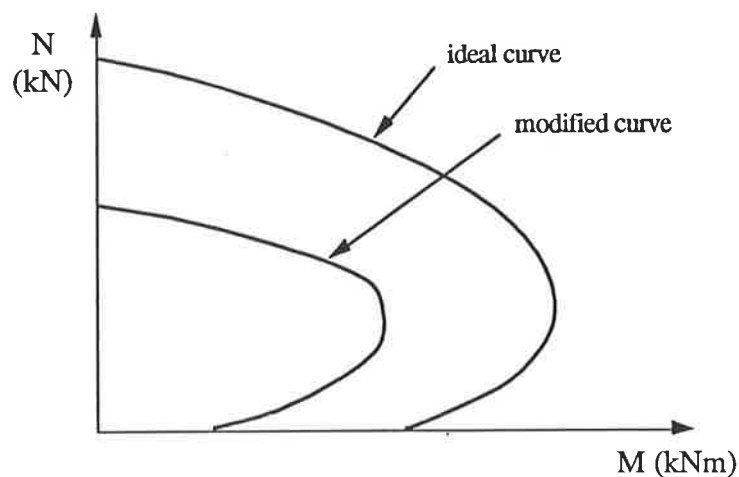
Figure 4.33: Strength interaction diagrams

4.6 Analysis of Frames with Closing Corners

4.6.1 Introduction

This section investigates the non-linear behaviour of various test frames with closing L-joints. These types of frames have been tested by a number of investigators, including, (Blomeier, 1968; Breen, 1962; Ernst *et al.*, 1973; Furlong, 1963). In all cases, vertical load patterns were incremented proportionally. Unless noted otherwise, analytical predictions include tension stiffening effects.

4.6.2 Frames Tested by Furlong (1963)

Furlong (1963) tested seven rectangular frames which were also reported by Furlong and Ferguson (1966). Frames F2, F3, F4, F6 were chosen for the present analysis. Frame F7 was subjected to a sustained load for a period of 102 days, and is not suitable for analysis in the present study. Testing of frame F5 was complicated by a leaking pump in the test equipment and load-deflection data were not published.

In the present study, each frame is analysed as a half structure due to symmetry in the load patterns, frame dimensions and sectional properties. This is shown in Figure 4.34 along with the section details. Beams and columns in all frames are 152 mm wide and 102 mm deep in section. All columns have 1.1% steel in each face and all beams are heavily reinforced with 4.1% steel in each face.

Frames F2 and F4 have been examined in non-linear frame analyses by Wong (1989) and Gunnin *et al.* (1977). In both studies, tension stiffening and joint behaviour were not taken into account. To take into account lateral deflections within the columns, Wong (1989) compared two and four elements per column, but there was only a minor difference in results between the two cases. Hence, it was decided for the present study to include only two elements per column for frame analyses.
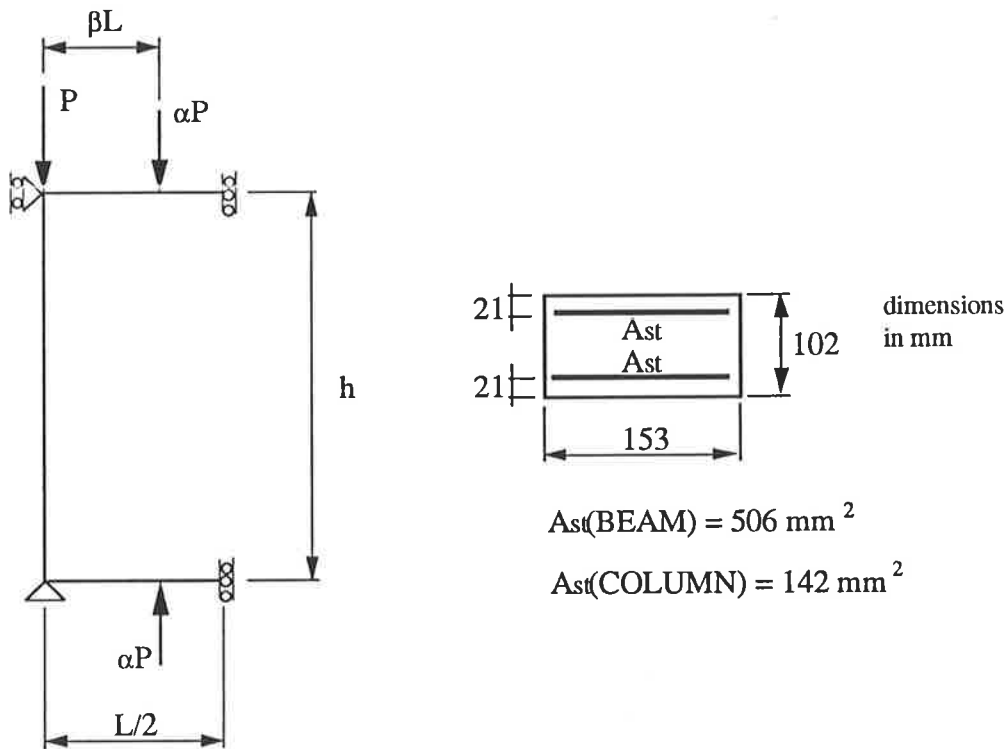
Figure 4.34: Test configuration and section details of frames tested by Furlong (1963)

Table 4.8 lists the physical properties for each frame examined. The average compressive strength of the concrete from a cylinder test is f_c and each frame was tested on the eighth day after casting. The reinforcing bars in each test have a modulus of 2×10^5 MPa with an average yield strength which is given by f_{sy}. In each frame analysed, the concrete compressive strength in each member is assumed to be $0.95 f_c$ and a corresponding strain of 0.002. Concrete modulus is assumed to be $5000 \sqrt{f_c}$ and a maximum compressive strain of 0.006 is assumed. Tension stiffening is also taken into account.

Table 4.8: Frame details and material properties of frames tested by Furlong (1963)

Frame	h (mm)	L (mm)	βL (mm)	α	f_c (MPa)	f_{sy} (MPa)
F2	2134	3150	1067	0.0256	29.7	379
F3	2134	3150	1067	0.0814	23.0	394
F4	2134	1727	457	0.15	22.3	372
F6	1626	3759	1219	0.0555	24.5	350

Figures 4.35 to 4.38 show experimental and analytical results for load versus deflection at column mid-height. The most noticeable aspect is the inconsistency between experimental and analytical results. Stiffness for frame F2 compares well up to the actual peak load, but the strength of this frame is overestimated by about 20%. On the other hand, stiffness for frames F3 and F4 is underestimated, although the predicted strengths compare well. Finally, frame F6 has reasonably good agreement for stiffness and failure load.
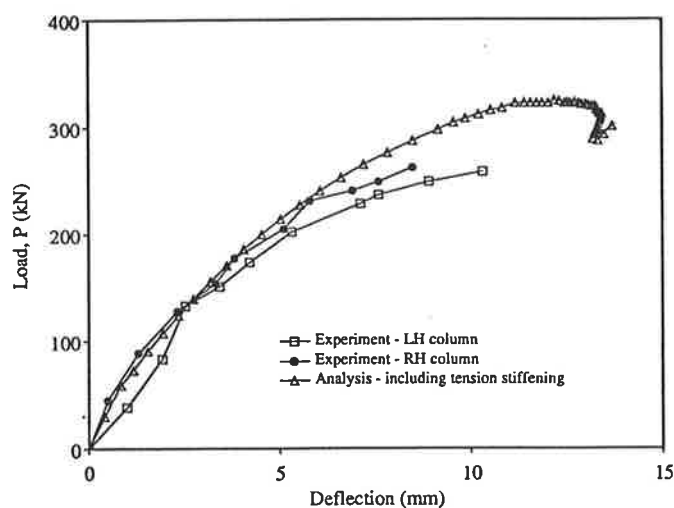
Figure 4.35: Load versus deflection for frame F2 tested by Furlong (1963)
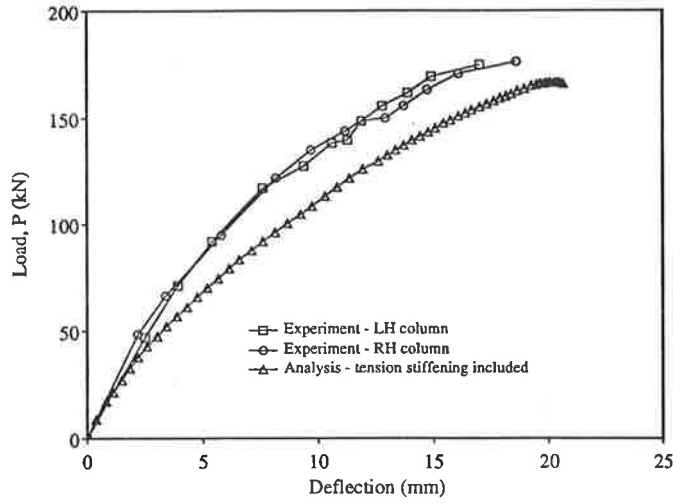
Figure 4.36: Load versus deflection for frame F3 tested by Furlong (1963)
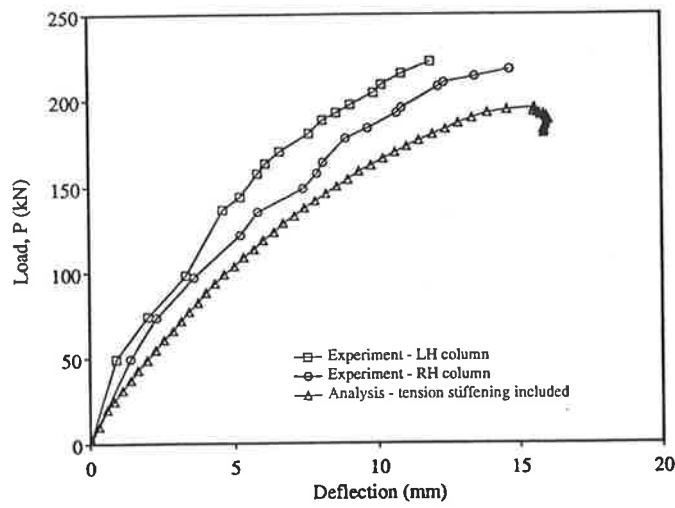
Figure 4.37: Load versus deflection for frame F4 tested by Furlong (1963)
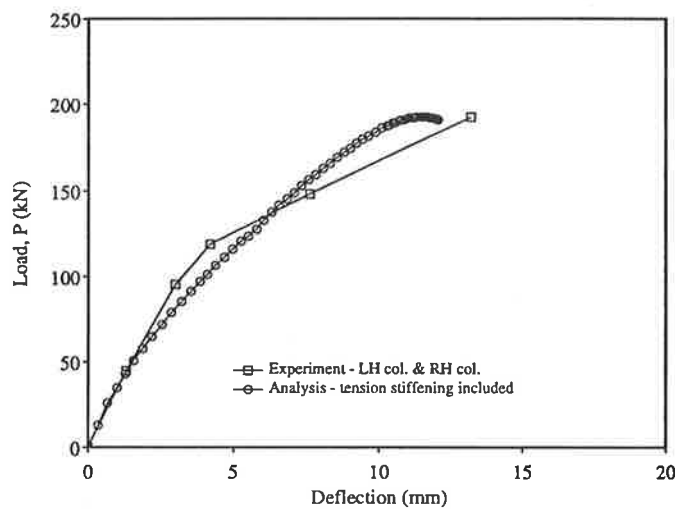
Figure 4.38: Load versus deflection for frame F6 tested by Furlong (1963)

In each frame, failure was initiated by crushing of the concrete on the inside face at approximately mid-height of one of the columns. The measured compressive strain at failure varied from 0.002 for frame F2 to 0.0038 for frame F6. In frames F4 and F6, a second failure then occurred at approximately mid-height in the other column. There was no second failure in frame F3, but in frame F2 a second failure occurred when the concrete crushed at the top of the left hand column where a maximum compressive strain of 0.008 was recorded. It is worth noting that the beams were relatively much stiffer than the columns and there was no incidence of failure occurring in a beam element. The tests were also performed under load control conditions, and it can be expected that higher strains would have been recorded if deformation control testing had been used.

Load and deflection was measured at mid-height for both columns within the test frames. Although columns for each test are theoretically identical, there is a noticeable difference in experimental results for frames F2 and F4. Wong (1989) pointed out that differences in lateral deflection in each column of a test frame was possibly due to the difficulty in applying a symmetrical load pattern. Other factors may have also affected test results.

In the present study, and in the investigations by Wong (1989) and Gunnin *et al.* (1977) the influence of the beam stubs and lateral restraint were ignored, i.e. it has been assumed that vertical movement and rotation are free from any restraint. However, it is possible that the stub and roller abutting the lateral load cell, as in Figure 4.39, may influence stiffness. The short stub, which is an extension of the beam, allows for adequate anchorage of the steel in the corner. Load is applied vertically through a load cell, and there is also some confinement here. It is has been noted in Chapter 3 that strength and stiffness are influenced by load transfer through plates and internal supports.

Stiffness and strength may also be affected by placement errors in the reinforcing steel. Although cover to steel can vary along the length of the member, this is not likely to be a problem in a laboratory test situation where it is usual to monitor construction.

However, it is often difficult to achieve perfect fabrication of steel and placement within joints, even in a carefully monitored situation. It is likely that joint detailing also influenced the stiffness of the frame either by improving or reducing stiffness.
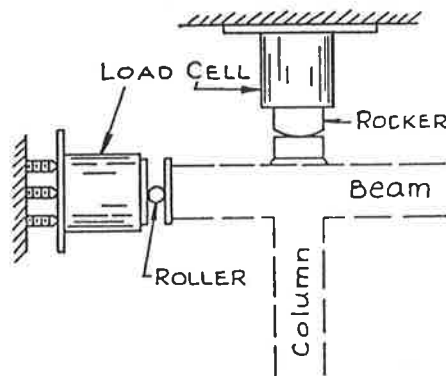
Figure 4.39: Load cell and column restraint for frames tested by Furlong (1963)

4.6.3 Frames Tested by Ernst, Smith, Riveland and Pierce (1973)

A second series of frames, tested by Ernst *et al.* (1973), was chosen for analysis. Twelve portal frames were tested under proportional loading. A further three frames were tested under non-proportional loading, and the results of these frames will be discussed in Chapter 5. All twelve frames with proportional loading were analysed, but only the results of four frames are reported here. The results are representative and show the different type of prediction of frame response to loading. Each frame was subjected to vertical loads which were applied at third points on the beam element, as shown in Figure 4.40. The physical properties are summarised in Table 4.9. The mean compressive strength of the concrete from a cylinder test is given by f_c, and for each frame analysis, the compressive strength of concrete in each member is assumed to be $0.95f_c$ with a corresponding strain of 0.002. Concrete modulus is assumed to be $5000\sqrt{f_c}$ and a maximum compressive strain of 0.006 is assumed. Tension stiffening is also taken into account.
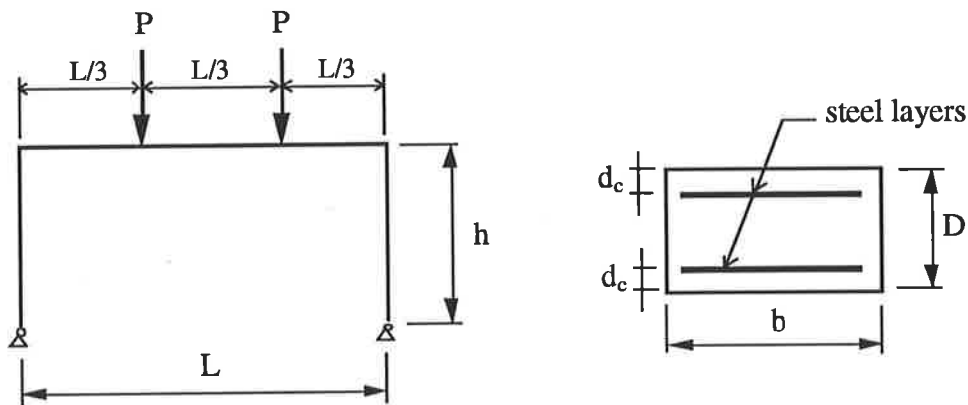
Figure 4.40: Test configuration and section parameters for frames tested

by Ernst *et al.* (1973)

Details of the different types of main reinforcement for the frame elements are given in Table 4.10. Note that f_y is the yield stress for the bar which corresponds to a strain of ε_y. The strain at initial strain-hardening of the steel is ε_{sh}. The slope of the tensile stress-strain curve at the initiation of strain-hardening is E_{sh} and f_{ult} is the ultimate tensile strength of the bar. For bars designated Type II to Type VIII, the terms are shown on a stress-strain diagram in Figure 4.41.

Type I bar, a #3 deformed bar, is not characterised by a stress-strain curve with a yield plateau followed by strain-hardening, and is assumed to be characterised by the top curve in Figure 4.42, which is taken from Park and Paulay (1975). In each test frame by Ernst *et al.*, a number of types of bar were used for main reinforcement and are summarised in Table 4.10. Different grades of steel were used in each face of the beam and column elements and this has been taken into account in each frame analysis.

Table 4.9: Frame, section and material properties of frames tested by
Ernst *et al.* (1973)

Frame	Span	Height	Beam			Column			Concrete
	L	h	b	D	d_c	b	D	d_c	f_c
	(mm)	(mm)	(mm)	(mm)	(mm)	(mm)	(mm)	(mm)	(MPa)
A40	3658	1830	114	203	38	114	203	38	29.1
B40	3658	1830	114	203	38	114	203	38	29.1
2D12	3658	1830	152	229	38	152	152	25	40.8
2D12S	3658	1830	152	229	38	152	152	25	43.2
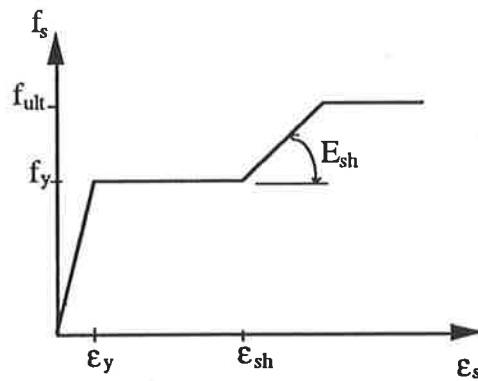
Figure 4.41: Linearised curve for reinforcing steel used by Ernst *et al.* (1973)
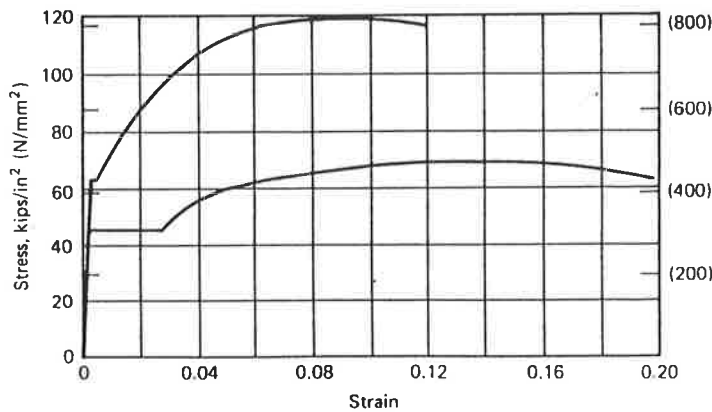
Figure 4.42: Stress-strain relationship for Type I bar (Park and Paulay, 1975)

Table 4.10: Stress-strain data for reinforcing bars used by Ernst *et al.* (1973)

Type	Diam (mm)	f_y (MPa)	f_{ult} (MPa)	E_{sh} (MPa)	ε_y	ε_{sh}
I	9.5	472	837	–	–	–
II	13	348	538	5583	0.00171	0.0140
III	13	396	675	5927	0.00203	0.0082
IV	13	455	702	9649	0.00218	0.0092
V	16	353	527	5927	0.00185	0.0150
VI	16	425	700	11580	0.00234	0.0068
VII	19	359	590	5720	0.00184	0.0145
VIII	19	441	791	15300	0.00225	0.0043

Table 4.11: Member reinforcing details (Ernst *et al.*, 1973)

Frame	Beam						Column					
	Top face			Bottom face			Outside face			Inside face		
	Typ	no.	diam	Typ	no.	diam	Typ	no.	diam	Typ	no.	diam
A40	V	2	16	V	2	16	V	2	16	V	2	16
B40	II	2	13	VII	2	19	V	2	16	VII	2	19
2D12	IV	2	13	IV	2	9.5	I	3	13	IV	2	13
2D12S	IV	2	13	IV	2	9.5	I	3	13	IV	2	13

Figures 4.43 to 4.45 compare the experimental and analytical results for each frame. Also shown in each figure is a diagram showing gauge locations where strain in the reinforcing steel was measured in the tests. In each case, the reinforcing steel was strained in tension. Locations 1 and 5 refer to the steel in the outside face at the top of the column. Locations 2 and 4 refer to steel in the top face at the ends of the beams and location 3 refers to steel in the bottom face at midspan of the beam. Noted on the graphs are Y1,Y2,...Y5 which indicate when the reinforcing steel at locations 1, 2,...5 had reached their yield strength. Similarly, SH1, SH2,...SH5 indicate the onset of strain hardening.
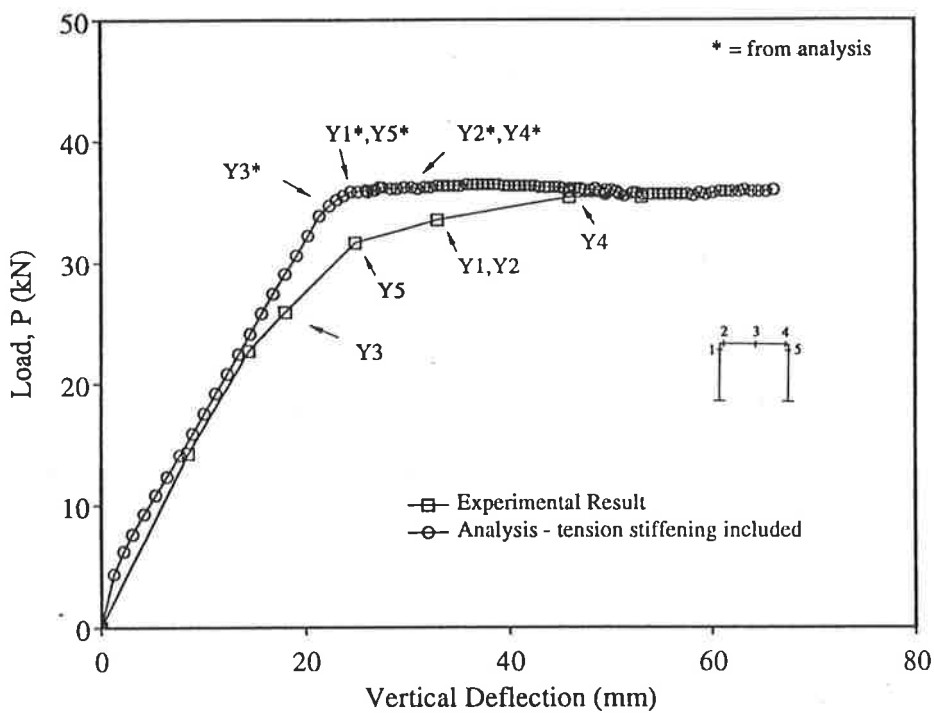
Figure 4.43: Load versus deflection for frame A40 tested by Ernst *et al.* (1973)
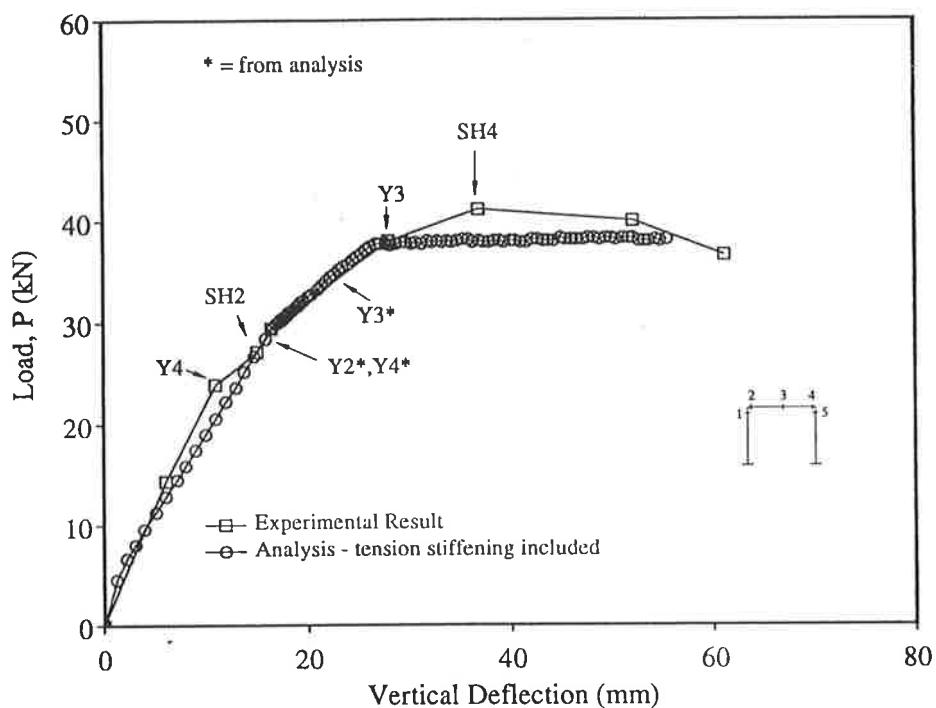
Figure 4.44: Load versus deflection for frame B40 tested by Ernst *et al.* (1973)
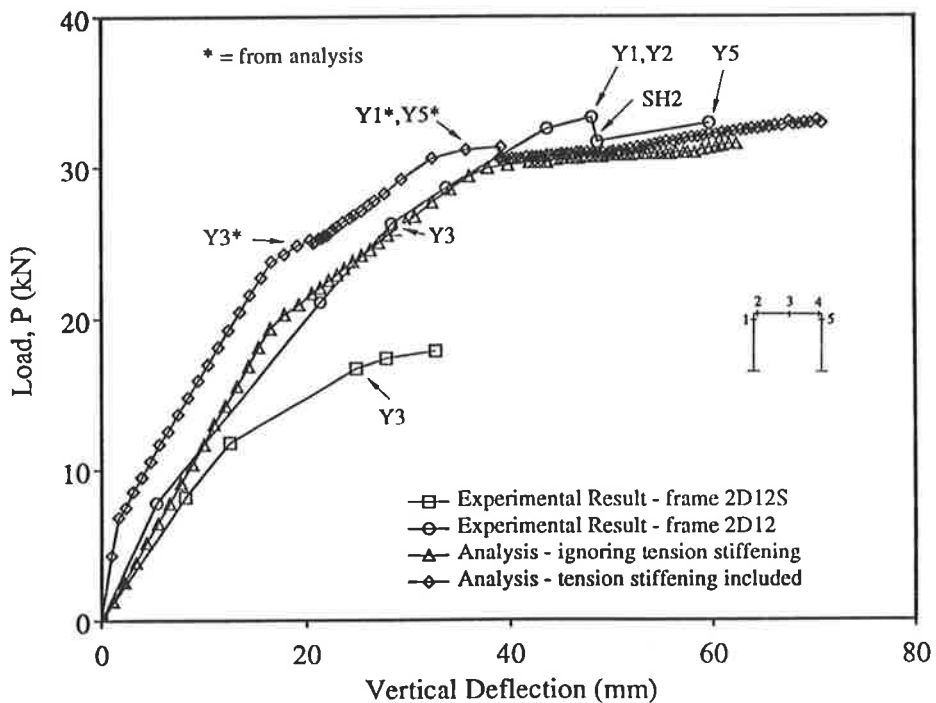
Figure 4.45: Load versus deflection for frames 2D12 and 2D12S

tested by Ernst *et al.* (1973)

Experimental results and analytical predictions for frame A40 are shown in Figure 4.43. Peak load is predicted accurately, but stiffness only compares well up to 22 kN. At this load level, additional joint deformations may have occurred which have not been predicted. Note the sequence of yielding of the tensile steel at each location compares well with the actual results.

Results for frame B40 are shown in Figure 4.44. Analytical results, which include tension stiffening, compare well up to the load when the steel yielded in the middle of the beam. Peak load is underestimated by approximately 8%. This strength increase may be due to strain hardening, which has not been predicted. Note that yielding of the beam steel was first observed at the strain gauge location 4. Although this frame is assumed to be symmetrical, yielding was not observed at the other end of the beam at location 2.

Figure 4.45 compares results from test frame 2D12. Also shown are the results for frame 2D12S. These two frames have the same dimensions, section details, main reinforcement and similar concrete strengths. However, frame 2D12 has reinforcement which is continuous and anchored at the knee, whereas frame 2D12S has reinforcement detailing which is not continuous and not anchored. The test results for frame 2D12S show a brittle failure at approximately half the maximum load of frame 2D12. A loss in stiffness is also evident from the commencement of loading. Although the joint detailing for frame 2D12S is inadequate, it is interesting to note that failure took place soon after the tensile steel had yielded at midspan of the beam. The brittle type failure most likely corresponds to severe cracking within the corners. As no reinforcement was placed in the corners, restraint against cracking is not possible.

Although the peak load for frame 2D12 is underestimated by only 5%, the analysis for tension stiffening effects, has overestimated stiffness. By ignoring tension stiffening effects, load and deflection compare more favourably. It is possible the value for concrete tensile strength, which can be highly variable, is much less than the assumed value for this analysis. It is also likely the actual stiffness for the closing corners is

much less than predicted. This is worth noting because joint stiffness has a large influence on the overall frame stiffness.

4.6.4 Summary of Frames with Closing Corners

In this section, several frames with closing L-shaped corners have been analysed. Tension stiffening was taken into account, but joint modelling was ignored, and generally analytical and experimental results compared well. Some variability in results was observed which can be attributed to several causes. Most notably, performance is affected by the quality of detailing. Confinement provided by detailing within the corners and also under loading plates may be responsible for increases in strength and stiffness.

4.7 Summary and Conclusions

Tests for various X-, T- and X- joints have shown that joint performance depends largely on the type of detailing and the loading conditions. In some cases, strength and stiffness can be adversely affected, while in other cases there are noticeable improvements.

The condition of joints at various stages of loading up to failure suggests that complex states of stress develop, and to accurately predict these deformations requires a finite element type of analysis. For the present study, a simplified global approach for modelling joint behaviour has been adopted which uses modified M-κ-N relations to describe behaviour at joints. This method of treating joint behaviour is similar to a smeared approach for modelling tension stiffening and described in the previous chapter. It has suitable application in the segmental method of frame analysis because it uses the existing section analysis procedures.

Modified M-κ-N relations have been developed for opening L-joints and T-joints but as experimental data is limited, comparisons with test frames have not been made. A number of theoretical frames with these joint types will be investigated in Chapter 6.

A study of various frames with closing L-joints showed that modifications to these types of joints are not necessary. Tests for X-joints and T-joints connecting external columns also showed these joint types are efficient.

Test joints and frames subjected to proportional loading were chosen for analysis to isolate the effect of joint deformations. In the following chapter, frames will be investigated for sequential loading and the influence of joint deformations in the first and second loading systems will be taken into account.

Chapter 5

Non-proportional Loading

5.1 Introduction

An assumption of the simplified linear elastic methods of analysis of most design codes and standards, such as AS 3600, is that load patterns are applied to the structure simultaneously and proportionally. However, in many real situations load patterns are applied in sequence, or in a non-proportional manner. Because of the highly non-linear, and inelastic response of reinforced concrete, the assumption that load patterns can be superimposed needs to be investigated.

In the present study, the effects of two sequences of applied load on frame behaviour are considered. The first loading pattern consists of a set of external loads which are increased progressively to a predetermined level and then held constant. A second separate loading pattern is then incremented until the strength of the structure is reached.

The analysis for non-proportional loading developed in this chapter uses the segmental method of frame analysis proposed by Wong (1989). To check the accuracy of the proposed method, analytical results have been compared with results for non-proportional loading of actual test frames.

5.2 Proposed Method of Analysis for Non-proportional Loading

5.2.1 Introduction

Two load systems are considered, and denoted as I and II. Analysis under the first load system is made by simulating a load control test. Initially, the second load system also simulates load control, but as the peak frame load is approached frame analysis switches to deformation control. This allows conditions at collapse and in the post collapse (softening range) to be handled without numerical instabilities.

At the commencement of deformation control, a "key segment" is located which has the maximum absolute increment of curvature from the application of the second load system. This curvature is scaled so that it equals a predetermined target curvature. A set of curvatures in all segments corresponding to the curvatures under load system I and the scaled increment of curvatures under load system II are applied to the structure.

5.2.2 Notation

$EA(lsys, m)$ = axial stiffness for member m under load system $lsys$;

$EI(lsys,i,n)$ = flexural stiffness in the n-th segment at convergence of the i-th step under load system $lsys$;

$EI_{old}(lsys,i,n)$ = stored flexural stiffness;

$EI_{trial}(lsys,i,n)$ = flexural stiffness in the n-th segment from a sectional analysis;

$EI_1(n)$ = flexural stiffness for the n-th segment at the end of the application of load system 1;

istep = a typical computational step;

key_2 = key segment under load system 2;

lsys = 1 or 2; refers to an analysis under load system 1 or 2;

$M(lsys,i,n)$ = moment in the n-th segment at convergence of the i-th step under load system *lsys* ;

$M_e(lsys,i,n)$ = moment in the n-th segment from a linear elastic analysis in the i-th step under load system *lsys*;

$M_{trial}(lsys,i,n)$ = moment in the n-th segment from a sectional analysis in the i-th step under load system *lsys* ;

$M_1(n)$ = moment in the n-th segment at the end of application of load system 1;

ncycle = number of iterative cycles for convergence of a computational step;

nstep = final load step for analysis under *lsys*;

pkstep = final analytical step under load control for load system 2;

$Q_{comb}(i)$ = the set of combined loads at convergence of the i-th step under load system 2, equal to the sum of Q_{1max} and $Q_2(i)$;

$Q_1(i)$ = the set of applied loads for load system 1 which creates the set of curvatures $\kappa(1,i,n)$ and other deformations;

$Q_2(i)$ = the set of external loads for the second load pattern when applied with Q_{1max} creates the set of curvatures $\kappa(2,i,n)$;

Q_{1max} = load system 1; a set of predetermined loads which are applied to the structure and then held constant while load system 2 is applied;

Q_{2max} = set of peak loads for load system 2;

$SF(i)$ = scale factor for Q_{2max} corresponding to convergence of the i-th step;

$SF_{trial}(i)$ = trial value for scale factor for second load system Q_{2max} ;

$\Delta_{lsys,i}$ = set of global deformations at the i-th step for load system *lsys*;

Δ_{1max} = set of global deformations at the end of load system 1;

ΔQ_2 = increment in load for load system 2;

$\Delta \kappa_{key2}$ = increment in target curvature for load system 2;

$\kappa(lsys,i,n)$ = curvature in the n-th segment at convergence of the i-th step under load system $lsys$;

$\kappa_e(lsys,i,n)$ = curvature in the n-th segment from a linear elastic analysis at the i-th step under load system $lsys$;

$\kappa_{key2}(2,i)$ = target curvature at the i-th step under load system 2;

$\kappa_{trial}(2,i,n)$ = trial curvature in the n-th segment required for a sectional analysis at the i-th step under load system 2;

$\kappa_1(n)$ = curvature in the n-th segment at the end of application of load system 1;

5.2.3 Analysis Under Load System No.1

Application of the first load system involves subjecting the structure to increasing levels of a proportional load pattern, $Q_1(1),...Q_1(ISTEP),...Q_1(NSTEP)$. At the final load step, $NSTEP$, the predetermined set of loads, Q_{1max}, is applied to the structure and held constant.

For the commencement of the first step, flexural and axial stiffnesses are set to values corresponding to gross sectional values. The trial flexural stiffnesses, $EI_{trial}(1,1,n)$, are given by $EI_{gross}(n)$. These nominal gross sectional values are updated with sectional analyses for all segments throughout the structure.

Procedures required for a typical computational step are as follows :

1. Assemble the global stiffness matrix $[K_{1,ISTEP}]$ from element matrices $[k_{1,ISTEP}]$ and transformation matrices $[T]$ with most recent global displacements, $\Delta_{1,ISTEP}$. For the start of the first step, the undeformed nodal geometry is used.

$$[K_{1,ISTEP}] = [T]^T[k_{1,ISTEP}][T] \tag{5.1}$$

2. Form the nodal load matrices $\{Q_{1,ISTEP}\}$ and $\{Q_{1,out\text{-}bal,ISTEP}\}$. The matrix $\{Q_{1,ISTEP}\}$ is assembled from the set of applied loads, $Q_1(ISTEP)$. Expressions for fixed end moments and shears due to loads applied within the elements are given in Appendix C. The matrix $\{Q_{1,out\text{-}bal,ISTEP}\}$ comprises the out-of-balance nodal loads corresponding to the changes in structural geometry during the load step.

3. Obtain the set of global element deformations $\{\Delta_{1,ISTEP}\}$ by solving the following matrix equation:

$$\{Q_{1,ISTEP}\} + \{Q_{1,out\text{-}bal,ISTEP}\} = [K_{1,ISTEP}]\{\Delta_{1,ISTEP}\} \tag{5.2}$$

4. Calculate the displacements $\{\delta_{1,ISTEP}\}$ at the ends of elements and in the local member reference system. Terms comprising the transformation matrix, $[T]$, are based on the most recent global nodal displacements $\{\Delta_{1,ISTEP}\}$ obtained by Equation 5.2.

$$\{\delta_{1,ISTEP}\} = [T]\{\Delta_{1,ISTEP}\} \tag{5.3}$$

5. Using standard procedures, obtain the forces $\{q_{1,ISTEP}\}$ at the ends of elements and in the local member reference system.

$$\{q_{1,ISTEP}\} = [k_{1,ISTEP}]\{\delta_{1,ISTEP}\} \tag{5.4}$$

6. Based on the local element forces and displacements obtained from steps 4 and 5, obtain moments and curvatures, $M_e(1,ISTEP,n)$ and $\kappa_e(1,ISTEP,n)$, within all segments. Calculations are based on the most recent values for segmental stiffnesses $EI_{trial}(1,ISTEP,n)$.

$$\kappa_e(1,ISTEP,n) = \frac{M_e(1,ISTEP,n)}{EI_{trial}(1,ISTEP,n)} \qquad (5.5)$$

7. Store the previous stiffnesses before segmental stiffnesses are updated :

$$EI_{old}(1,ISTEP,n) = EI_{trial}(1,ISTEP,n) \qquad (5.6)$$

8. Sectional analyses of all segments are carried out to determine trial segmental moments $M_{trial}(1,ISTEP,n)$ from the set of curvatures, $\kappa_e(1,ISTEP,n)$. Updated flexural stiffnesses are obtained :

$$EI_{trial}(1,ISTEP,n) = \frac{M_{trial}(1,ISTEP,n)}{\kappa_e(1,ISTEP,n)} \qquad (5.7)$$

Axial stiffnesses $EA(1,m)$ in all elements are also updated from the sectional analyses.

9. Calculate the out-of-balance nodal forces $\{Q_{1,out\text{-}bal,ISTEP}\}$. These forces correspond to the difference in the deformed state at the beginning of the iterative cycle and nodal deformations at the end of the cycle.

10. Check for convergence for all segmental stiffnesses

$$\frac{EI_{trial}(1,ISTEP,n) - EI_{old}(1,ISTEP,n)}{EI_{old}(1,ISTEP,n)} \leq \varepsilon \qquad (5.8)$$

If convergence is not achieved a further iterative cycle commences and steps 1 to 10 are repeated. At least two iterative cycles are required and the stiffnesses for the commencement of a new cycle are set to the most recent values obtained from sectional analyses. When convergence is achieved between successive cycles of the computational step *ISTEP*, the moment, curvature and stiffness in segment *n* are :

$$M(1, ISTEP,n) = M_{trial}(1, ISTEP,n) \qquad (5.9)$$

$$\kappa(1, ISTEP,n) = \kappa_e(1, ISTEP,n) \qquad (5.10)$$

$$EI(1, ISTEP,n) = EI_{trial}(1, ISTEP,n) \qquad (5.11)$$

In the final computational step, *NSTEP*, under the first load system, the applied loads are set to the predetermined values of Q_{1max}. This is given by:

$$Q_1(NSTEP) = Q_{1max} \qquad (5.12)$$

At convergence of this final step, moment, curvature and stiffness in segment *n* are :

$$M_1(n) = M_{trial}(1, NSTEP,n) \qquad (5.13)$$

$$\kappa_1(n) = \kappa_e(1, NSTEP,n) \qquad (5.14)$$

$$EI_1(n) = EI_{trial}(1, NSTEP,n) \qquad (5.15)$$

An analysis which includes geometric non-linearities must take into account the global nodal displacements $\{\Delta_{1,NSTEP}\}$ corresponding to the set of loads Q_{1max}. Hence, for subsequent analytical steps, under the second load system, these structural deformations are given by:

$$\{\Delta_{1max}\} = \{\Delta_{1,NSTEP}\} \qquad (5.16)$$

Note also that the set of out-of-balance nodal loads at this final step are required for analysis under the second load system. These are given by:

$$\{Q_{1,out-bal,max}\} = \{Q_{1,out-bal,NSTEP}\} \qquad (5.17)$$

5.2.4   Analysis Under Load System No.2

5.2.4.1   Analysis for Load Control

Analysis for combined loading involves applying increments ΔQ_2 of the second load pattern with the set of constant loads Q_{1max} until the peak structural load Q_{2max} is reached. To ensure good convergence, the increment size for ΔQ_2 should not be too large. For the commencement of the first step, the trial stiffnesses $EI_{trial}(2,1,n)$ are set equal to the values $EI_1(n)$ at convergence of *NSTEP* of the analysis for the first load system.

Analysis up to *PKSTEP* simulates a load control test set-up and procedures for a typical step are as follows:

1. Assemble the global stiffness matrix, $[K_{2,ISTEP}]$. The element stiffness matrices, $[k_{2,ISTEP}]$, for all elements are based on the updated secant stiffnesses EI and EA. The transformation matrices, $[T]$, for all elements are based on the most recent global nodal displacements. For the commencement of the first step, the displacements $\{\Delta_{1max}\}$ are used.

2. Form the nodal load matrix, $\{Q_{2,ISTEP}\}$, from the applied loads Q_{1max} and $Q_2(ISTEP)$ and also the nodal load matrix due to the out-of-balance loads. The set of loads comprising the second load system is given by:

$$Q_2(ISTEP) = Q_2(ISTEP\text{-}1) + \Delta Q_2 \qquad (5.18)$$

For the first step $Q_2(1)$ is set equal to ΔQ_2.

3. Obtain the displacements $\{\Delta_{2,ISTEP}\}$ by performing a linear elastic analysis.

$$\{Q_{2,ISTEP}\} + \{Q_{2,out\text{-}bal,ISTEP}\} = [K_{2,ISTEP}]\{\Delta_{2,ISTEP}\} \qquad (5.19)$$

4. Displacements $\{\delta_{2,ISTEP}\}$ at the ends of elements and in the local member reference system are found. The terms comprising the transformation matrix, $[T]$, are based on the most recent global nodal displacements due to the first and second load systems, i.e. $\{\Delta_{2,ISTEP}\}$. Note the transformation matrices are also updated with these global displacements.

$$\{\delta_{2,ISTEP}\} = [T]\{\Delta_{2,ISTEP}\} \qquad (5.20)$$

5. Forces $\{q_{2,ISTEP}\}$ at the ends of elements and in the local member reference system are found.

$$\{q_{2,ISTEP}\} = [k_{2,ISTEP}]\{\delta_{2,ISTEP}\} \qquad (5.21)$$

6. From the end forces $\{q_{2,ISTEP}\}$ and end displacements $\{\delta_{2,ISTEP}\}$ perform a segmental method of analysis to determine moments, $M_e(2,ISTEP,n)$ and curvatures, $\kappa_e(2,ISTEP,n)$ in all segments. This is shown in Figure 5.1.

7. Store previous stiffnesses before calculating updated values.

$$EI_{old}(2, ISTEP,n) = EI_{trial}(2, ISTEP,n) \qquad (5.22)$$

8. Sectional analyses are performed to determine segmental moments and curvatures. A new set of trial stiffnesses is found :

$$EI_{trial}(2,ISTEP,n) = \frac{M_{trial}(2,ISTEP,n)}{\kappa_e(2,ISTEP,n)} \qquad (5.23)$$

9. Calculate the out-of-balance nodal forces $\{Q_{2,out-bal,ISTEP}\}$. These forces correspond to the difference in the deformed state at the beginning of the iterative cycle and nodal deformations at the end of the cycle.

10. Check convergence in all segments by comparing the updated trial stiffnesses with previous values for stiffness.

$$\frac{EI_{trial}(2,ISTEP,n) - EI_{old}(2,ISTEP,n)}{EI_{old}(2,ISTEP,n)} \le \varepsilon \qquad (5.24)$$

If convergence does not occur for all segments then a further iterative cycle commences. At convergence of *ISTEP*, the moment, curvature and stiffness in segment n are :

$$M(2, ISTEP,n) = M_{trial}(2, ISTEP,n) \qquad (5.25)$$

$$\kappa(2, ISTEP,n) = \kappa_e(2, ISTEP,n) \qquad (5.26)$$

$$EI(2, ISTEP,n) = EI_{trial}(2, ISTEP,n) \qquad (5.27)$$

To avoid non-convergence problems, analysis switches from load control to deformation control just before the peak frame load is reached. The final step under load control is given by *PKSTEP*.

5.2.4.2   Analysis for Deformation Control

The structure is analysed for combined loading under deformation control in which increments in target curvature, $\Delta\kappa_{key2}$, are imposed upon a "key segment". The key segment has the maximum absolute curvature due to the second load system. Stiffness

values for the commencement of this analysis, $EI_{trial}(2, PKSTEP + 1, n)$, are set equal to the values, $EI(2, PKSTEP, n)$, at convergence of the previous step.

At the commencement of each load step, an estimate is made for the proportion of the second load system, so that combined loads, $SF_{trial}(ISTEP) \times Q_2(PKSTEP)$ and Q_{1max} are applied to the structure. Initially, the estimated loads for structural analysis is the set of loads $Q_2(PKSTEP)$. This means the value for $SF_{trial}(ISTEP)$ is set equal to 1.0 for $ISTEP = PKSTEP+1$.

For the commencement of subsequent load steps in the analysis under load system 2, the new stiffnesses are set equal to the values from the end of the previous step. Typical steps required for convergence under deformation control for the second load system are as follows (also summarised in Figure 5.3):

1. Assemble the global stiffness matrix, $[K_{2,ISTEP}]$. The element stiffness matrices, $[k_{2,ISTEP}]$, for all elements are based on the updated secant stiffnesses EI and EA. The transformation matrices, $[T]$, for all elements are based on the most recent global nodal displacements.

2. Set the value for the trial scale factor equal to the scale factor at convergence of the previous step.

$$SF_{trial}(ISTEP) = SF(ISTEP-1) \qquad (5.28)$$

For the commencement of computational step $PKSTEP+1$, the trial scale factor, $SF_{trial}(1+PKSTEP)$, is set equal to 1.0.

3. Form the nodal load matrix $\{Q_{2,ISTEP}\}$ from the applied loads Q_{1max} and $SF_{trial}(ISTEP) \times Q_2(PKSTEP)$. The nodal load matrix from the out-of-balance nodal loads is also formed and given by:

$$Q_{1,out\text{-}bal,max} + SF_{trial}(ISTEP)\text{x}[Q_{2,out\text{-}bal,ISTEP} - Q_{1,out\text{-}bal,max}]$$

4. From the following linear elastic analysis obtain the displacements, $\Delta_{2,ISTEP}$.

$$\{Q_{2,ISTEP}\} + \{Q_{2,out\text{-}bal,ISTEP}\} = [K_{2,ISTEP}]\{\Delta_{2,ISTEP}\} \qquad (5.29)$$

5. Displacements $\{\delta_{2,ISTEP}\}$ at the ends of elements and in the local member reference system are found. The terms comprising the transformation matrix, $[T]$, are based on the global deformations $\{\Delta_{1max}\}$ from the end of load system 1 and the most recent global nodal displacements due to the second load system. These are given by $\Delta_{1max} + SF_{trial}(ISTEP)\text{x}[\Delta_{2,ISTEP} - \Delta_{1max}]$.

$$\{\delta_{2,ISTEP}\} = [T]\{\Delta_{2,ISTEP}\} \qquad (5.30)$$

6. Forces $\{q_{2,ISTEP}\}$ at the ends of elements and in the local member reference system are found as follows:

$$\{q_{2,ISTEP}\} = [k_{2,ISTEP}]\{\delta_{2,ISTEP}\} \qquad (5.31)$$

7. From the end forces $\{q_{2,ISTEP}\}$ and end displacements $\{\delta_{2,ISTEP}\}$ perform a segmental method of analysis to determine moments, $M_e(2, ISTEP, n)$ and curvatures, $\kappa_e(2, ISTEP, n)$ in all segments.

8. A search is carried out to locate the key segment, $n=key_2$, which has the maximum absolute curvature from the application of the second load pattern, i.e.

$$\text{Max} |\kappa_e(2, ISTEP,n) - \kappa_1(n)|$$

$$= |\kappa_e(2, ISTEP,key_2) - \kappa_1(key_2)| \qquad (5.32)$$

8. Curvature $\kappa(2, ISTEP-1,key_2)$ in the key segment at the end of the previous step is incremented by the target increment in curvature, $\Delta\kappa_{key_2}$. This is given by the following:

If $\kappa_e(2, ISTEP,key_2) > 0$, the target curvature is given by :

$$\kappa_{key_2}(2, ISTEP) = \kappa(2, ISTEP-1,key_2) + \Delta\kappa_{key_2}$$

If $\kappa_e(2, ISTEP,key_2) < 0$, the target curvature is given by :

$$\kappa_{key_2}(2, ISTEP) = \kappa(2, ISTEP-1,key_2) - \Delta\kappa_{key_2}$$

10. A new value for the scale factor $SF_{trial}(ISTEP)$ is calculated :

$$SF_{trial}(ISTEP) = \frac{\kappa_{key_2}(2,ISTEP) - \kappa_1(key_2)}{\kappa_e(2,ISTEP,key_2) - \kappa_1(key_2)} \qquad (5.33)$$

11. Trial curvatures are determined for all segments.

$$\kappa_{trial}(2,ISTEP,n)$$

$$\qquad (5.34)$$

$$= \kappa_1(n) + SF_{trial}(ISTEP) \times [\kappa_e(2,ISTEP,n) - \kappa_1(n)]$$

The trial curvature in the key segment, $\kappa_{trial}(2, ISTEP,key_2)$, will always equal the target curvature, $\kappa_{key_2}(2, ISTEP)$. Figure 5.2 shows trial curvature in the softening region.

12. Store the previous stiffnesses prior to calculating updated values.

$$EI_{old}(2, ISTEP,n) = EI_{trial}(2, ISTEP,n) \qquad (5.35)$$

13. Sectional analyses are performed to determine trial segmental moments and curvatures. A new set of trial stiffnesses is found :

$$EI_{trial}(2,ISTEP,n) = \frac{M_{trial}(2,ISTEP,n)}{\kappa_{trial}(2,ISTEP,n)} \qquad (5.36)$$

14. Calculate the out-of-balance nodal loads $\{Q_{2,out\text{-}bal,ISTEP}\}$ due to the first and second load systems.

15. Check convergence in all segments by comparing the updated trial stiffnesses with the stiffnesses used at the start of the cycle.

$$\frac{EI_{trial}(2,ISTEP,n) - EI_{old}(2,ISTEP,n)}{EI_{old}(2,ISTEP,n)} \le \varepsilon \qquad (5.37)$$

At convergence of *ISTEP* for the analysis under combined loading, the moment, curvature and secant stiffness in segment *n* are :

$$M(2, ISTEP,n) = M_1(n) + SF(ISTEP) \times [M_e(2, ISTEP,n) - M_1(n)] \qquad (5.38)$$

$$\kappa(2, ISTEP,n) = \kappa_1(n) + SF(ISTEP) \times [\kappa_e(2, ISTEP,n) - \kappa_1(n)] \qquad (5.39)$$

$$EI(2, ISTEP,n) = EI_{trial}(2, ISTEP,n) \qquad (5.40)$$

Note that the scale factor at convergence, *SF(ISTEP)*, is given by the most recent value for trial scale factor, $SF_{trial}(ISTEP)$. The corresponding applied loads for the computational step *ISTEP* greater than *PKSTEP* are :

$$Q_{comb}(ISTEP) = Q_{1max} + Q_2(ISTEP) \qquad (5.41)$$

where

$$Q_2(ISTEP) = SF(ISTEP) \times Q_2(PKSTEP) \qquad (5.42)$$
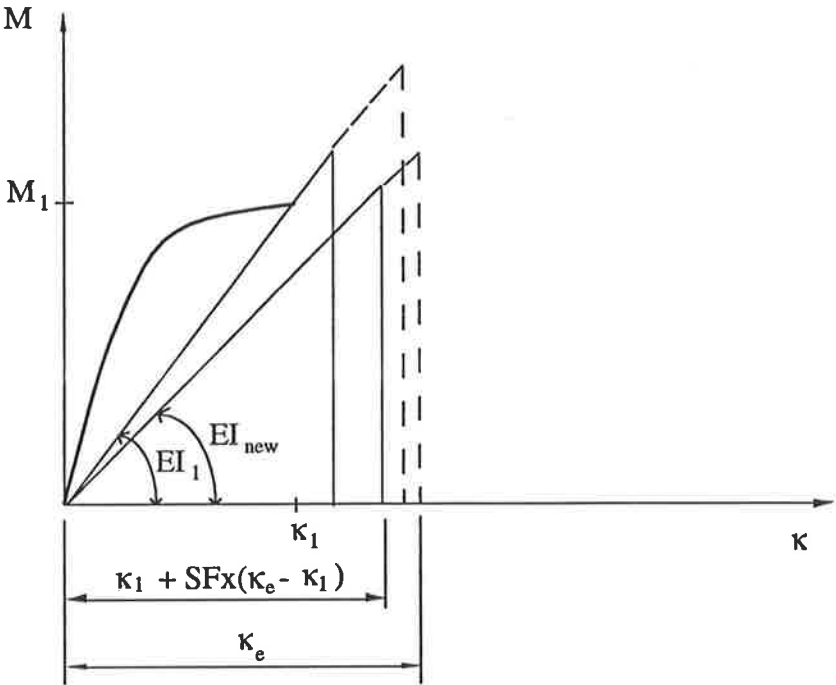
Figure 5.1: Moment and curvature for a typical segment
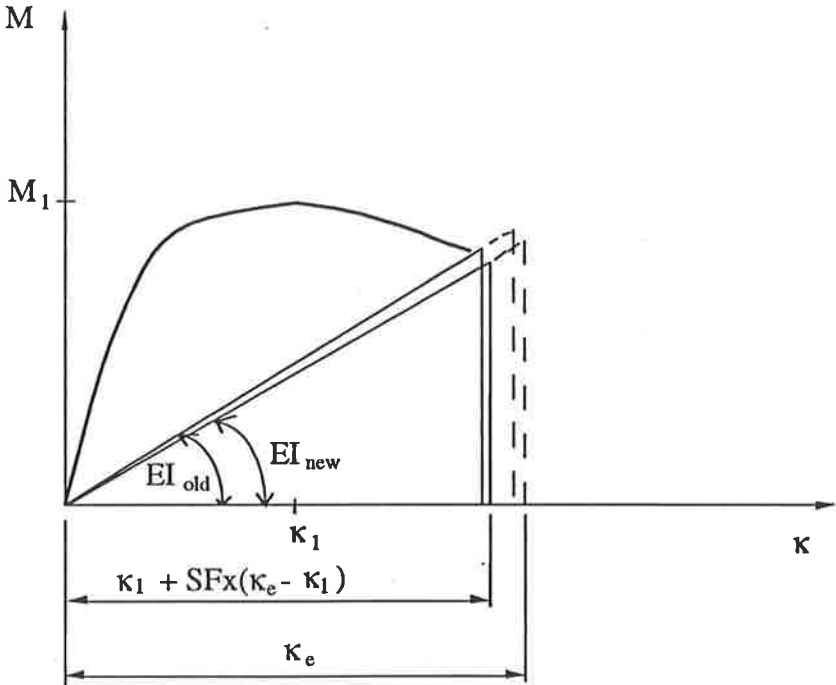
Figure 5.2: Analysis for softening

ISTEP = PKSTEP+1

SF(1+PKSTEP) = 1.0

Commence Step ISTEP

Set curvature of key segment to
$\kappa_{key2} = \kappa(ISTEP-1) + \Delta\kappa_{key2}$

Set EI(n)=EIold(n)

Set ICYCLE=0

ICYCLE = ICYCLE + 1

Apply Q1max + SF(ISTEP) x Q2max:
perform a frame analysis and obtain values for $\kappa_e(n)$

Calculate scaling factor:
$$SF(ISTEP) = \frac{\kappa_{key2} - \kappa_1(key_2)}{\kappa_e(key_2) - \kappa_1(key_2)}$$

Segmental Method of Analysis -
obtain trial curvatures for all segments:
$\kappa_{trial}(n) = \kappa_1(n) + SF(ISTEP) x [\kappa_e(key_2) - \kappa_1(n)]$

EIold(n)=EI(n)

Section Analyses: to obtain updated stiffnesses
$EI_{trial}(n) = M_{trial}(n) / \kappa_{trial}(n)$ and $EA(m) = N(m) / \epsilon$

Yes / Check convergence :
Is [EItrial(n) - EIold(n)]/EIold(n) < tolerance ? / No

ISTEP = ISTEP + 1

SF(ISTEP) = SF(ISTEP-1)

Figure 5.3: Steps for analysis under deformation control

5.2.4.3   Local Unloading Effects

It has been noted earlier, (Birnstiel and Iffland, 1980; De Donato and Maier, 1972), that the order of application of vertical and horizontal load patterns influences the response of inelastic structures. It is not unusual for a segment to unload during the application of the first load system and then reload with an internal moment of opposite sign during the second load system. To take into account inelastic response, it is necessary to define secant stiffness when complete unloading occurs.

Figure 5.4 shows the moment, M_1, and curvature, κ_1, at the end of the first load system. At the point of complete unloading, where curvature becomes zero, primary cracks are assumed to have closed completely and the secant flexural stiffness is reset to the gross sectional value assuming an uncracked section. As loading of the structure continues, cracks may develop in the opposite face.
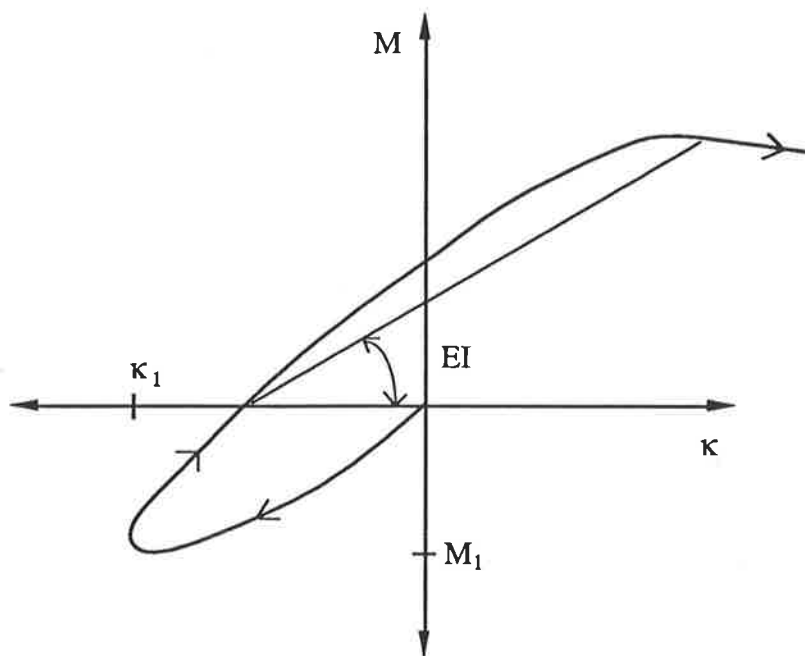
Figure 5.4: Secant stiffness for reversed loading

De Donato and Maier (1972) used pre-generated moment-rotation curves for non-proportional loading, which are similar in shape to the moment-curvature curve in Figure 5.4. This type of curve could be considered to form the first cycle of a hysteresis loop. A structure undergoing one or more cycle of loading requires additional storage requirements during analysis, i.e. keypoints defining points of unloading and reloading need to be stored.

5.3   Comparisons with Results for Test Frames

5.3.1   Introduction

To check the validity of the proposed method of analysis, predicted results were compared with experimental results for several frames. Tension stiffening was included and two types of analysis were made for these frames. Firstly, load systems were applied in the same manner as in the tests. This involved incrementing a system of vertical loads up to a predetermined level which were then held constant. A pattern of horizontal loads was then incremented up to failure. This is more usual than incrementing horizontal loads followed by a set of vertical loads, because of the difficulty involved in subjecting a structure solely to a set of horizontal loads. Note also that actual conditions are simulated, i.e. dead loads (or live loads) are placed on the structure followed by a system lateral loads which may, for example, represent wind loading.

The second type of analysis is for proportional loading. In this case, the vertical loads and horizontal loads were applied simultaneously. The ratio in which these loads were applied was based on the predetermined magnitude for the vertical loads and the peak values for the horizontal loads, H_{max}.

In all frames analysed, geometric non-linearities were taken into account by updating the nodal geometry of the frames as increasing levels of load were applied. A preliminary check showed there was very little influence on secondary moments by

including additional nodes within the length of columns. For clarity, results shown here are only for secondary effects due to lateral movement at the ends of columns.

5.3.2 Frames tested by Ernst, Smith, Riveland and Pierce (1973)

Details for two frames tested by Ernst *et al.* (1973) are shown in Figure 5.5. Concrete properties for these frames are as follows: average compressive strength, f_{cm} = 28.8 MPa, f_{cmax} = 27.6 MPa, i.e. $0.95f_{cm}$ and E_c = 26830 MPa. Note that a factor of 0.95 has been used to convert concrete cylinder strength to strength within a structural member. This value has been chosen because the frames were cast horizontally. Concrete modulus is based on a value of $5000\sqrt{f_{cm}}$. Two different grades of steel were used for these frames; details which have been summarised in Chapter 4 in the investigation of frames tested by Ernst *et al.* under proportional loading.

Two types of non-linear analysis were made in the present study for the frames tested by Ernst *et al.* One analysis is for non-proportional loading and the other for proportional loading. In both cases, tension stiffening and full geometric effects are taken into account, but neither analysis includes the proposed joint model. Under non-proportional loading, the vertical loads create closing corners within both L-joints. With application of the horizontal load, unloading occurs at the right L-joint, but the opening moments which develop are very small in magnitude. In the other L-joint, the left joint, closing moments develop under both load systems. A preliminary check showed there was only a minor influence on stiffness by including the joint model.

Shown in Figure 5.6 are results for frame 2D9H. For the non-proportional loading analysis the vertical beam loads, P, were incremented up to 24.9 kN and then held constant while the horizontal load, H, was incremented into the post-peak region. The predicted peak value for H_{max} is 12.1 kN compared to the experimental peak load of 13.0 kN. Hence for the proportional loading analysis the horizontal load and vertical loads were applied in this ratio, i.e. H/P = 2.08. This analysis also predicts a peak horizontal load of 12.1 kN. The apparent difference in the two sets of analytical

results is shown by the predicted stiffness. The non-proportional loading analysis provides the best estimate for stiffness.
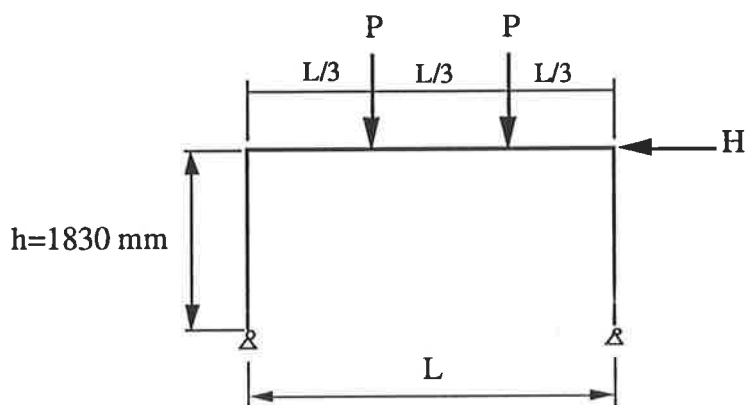
Frame 2D9H   : L = 2743 mm

Frame 2D12H : L = 3658 mm
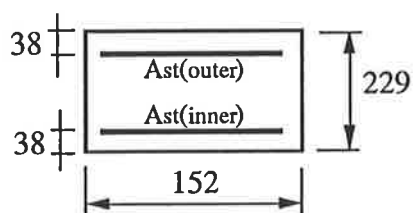
Beams

$A_{st}(outer) = 266$ mm^2 , Type IV steel

$A_{st}(inner) = 71$ mm^2 , Type IV steel
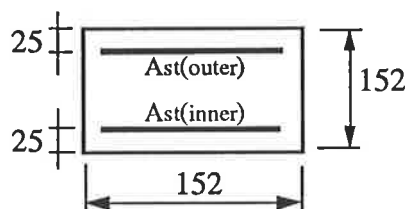
Columns

$A_{st}(outer) = 400$ mm^2 , Type I steel

$A_{st}(inner) = 133$ mm^2 , Type IV steel

Figure 5.5: Section details and configuration for frames tested by Ernst *et al.* (1973)

Also shown in Figure 5.6 are results for three separate analyses by El-Metwally and Chen (1989b). However, no mention was made whether the analyses are for proportional or non-proportional loading. Results for 'geometry+material' take into account geometric non-linearities but ignore tension stiffening. The joints are assumed to be fully rigid and results for this analysis provide the most accurate predictions.

The analysis for 'geometry+material+joint' assumes that additional joint deformations occur within the joint. This analysis slightly overestimates peak frame load. The analysis for 'geometry+material+joint for clear span' assumes a flexural hinge occurs within the beam element at the joint. Results for this analysis compare poorly. It is interesting to note the actual test results showed a hinge formed first in the column at the joint. Unfortunately, a non-linear analysis with joint modelling for the columns at the joints was not carried out by El-Metwally and Chen.
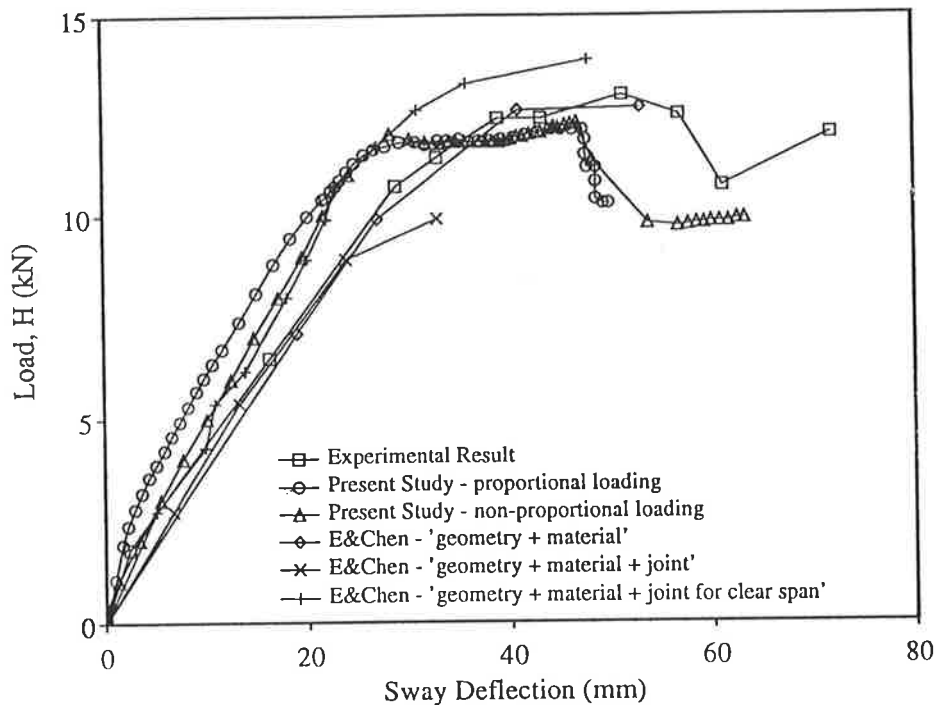
Figure 5.6: Horizontal load versus sway deflection for frame 2D9H tested by Ernst *et al.* (1973)

Shown in Figure 5.7 are analytical and experimental results for frame 2D12H. This frame has the same reinforcing details, concrete properties and section details as frame 2D9H. The important difference is that frame 2D12H has a clear beam span, L, of 3.658 m (or 9 feet) whereas frame 2D9H has a beam span, L, of 2.743 m (or 6 feet).

The vertical loads for test frame 2D12H were held constant at a value of 17.5 kN. For the non-proportional loading analysis, beam loads were incremented up to this same load level. This analysis predicts a maximum frame load under horizontal loading of

12.5 kN which is 10% less than the test peak load of 13.7 kN. Note also stiffness is underestimated. The analysis for proportional loading assumes the horizontal and vertical loads are applied in the ratio 17.5 to 12.5, or $H = 1.3P$. The predicted stiffness and ultimate load of 13.4 kN compare very well with the experimental results.

In general, results for load and stiffness for both frames 2D9H and 2D12H by non-proportional loading are more conservative than the proportional loading results. However, both methods of analysis appear to be satisfactory.
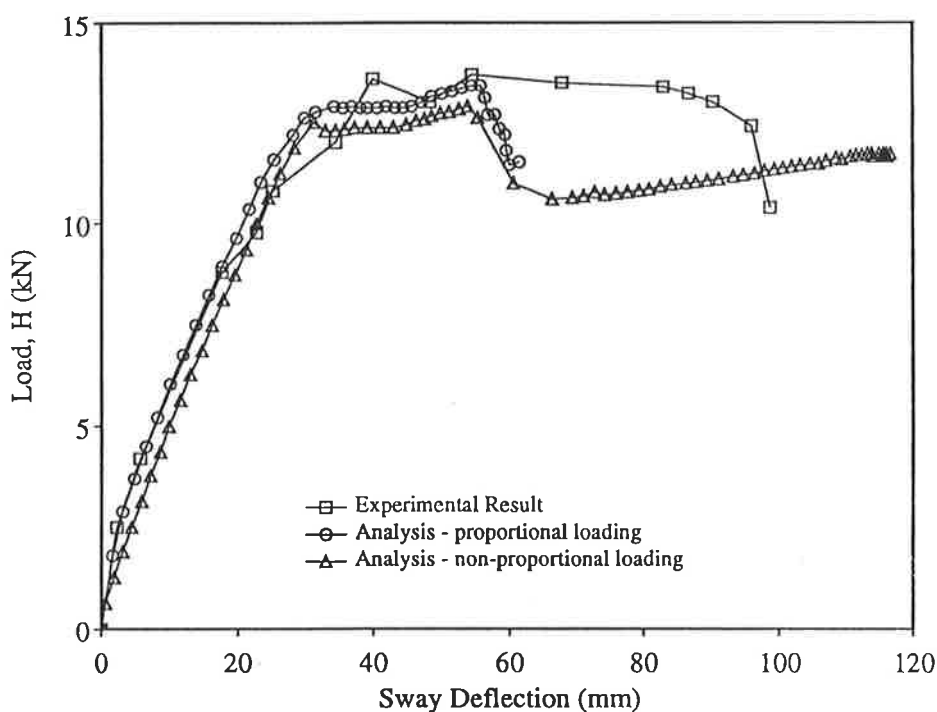
Figure 5.7: Horizontal load versus deflection for frame 2D12H tested by

Ernst *et al.* (1973)

5.3.3 Frames tested by Rad (1972)

Five frames were tested under short term sequential loading by Rad (1972), also discussed by Rad and Furlong (1980). However, only the performance of frame A3, with the configuration shown in Figure 5.8, is investigated in the present study. All test frames were subjected to vertical loads which were held constant, followed by increments of horizontal loading up to collapse. The results for load and deflection for

frames other than A3 showed significant lateral deflection from the application of the vertical loads. While some lateral movement at the tops of columns due to vertical loading can be expected, it was also noted by Rad that member misalignment had occurred after casting. Such construction errors are common in practice.

It was also noted by Rad that some error in the alignment of the column loads had occurred. A misalignment of ± 0.1 degrees in these frames can induce a horizontal force component of 1 kN. It was verified in the present study that this amount of error influences frame stiffness, but has no affect on overall strength. Note that errors in member or load alignment can in some cases be beneficial.

Frame details for frame A3 are shown in Figure 5.8. Concrete properties for this horizontally cast frame are as follows: average compressive strength, $f_{cm} = 30.8$ MPa, $f_{cmax} = 29.3$ MPa, i.e. $0.95 f_{cm}$ and $E_c = 27750$ MPa. Steel in the columns has a higher yield strength than steel placed in the beams.

Frame A3 was subjected to vertical loads before the horizontal load was applied. Column loads were $P_L = 304$ kN and $P_R = 258$ kN, and the load $Q = 8.5$ kN was applied at third points on the beams. The maximum horizontal load for the test frame was $H_{max} = 11.2$ kN.

Analytical and experimental results for load versus deflection for frame A3 are shown in Figure 5.9. The analyses in the present study are for non-proportional and proportional loading and include tension stiffening but ignore joint modelling. A preliminary check, under non-proportional loading, showed that one of the two opening corners which developed under the first load system unloaded during the second load system and developed into a closing corner. However, at the other opening corner, at the bottom of the right hand column, moment and curvature increase monotonically during both the first and second load systems. Although joint modelling hasn't been included it may have improved the prediction for stiffness during the second load system of non-proportional loading.

Analytical predictions for the frames by Rad show good correlation was achieved by ignoring joint modelling. It can be concluded the type of corner detailing in these frames was more efficient than the detailing used in the frames by Ferguson and Breen, which are also the basis for the joint model for opening L-joints. Unfortunately, the joint detailing used in the test frames by Rad was not published.

Both analyses in the present study accurately predict the peak horizontal load, but the proportional loading analysis overestimates stiffness. This was also observed in the analyses for the frames by Ernst *et al.* Shown in Figure 5.9 are the predicted results by Rad (1972), which are also reported by Gunnin *et al.* (1977). The analysis 'without stiffened joints' compares poorly with the experimental results. The other two analyses include the joint model discussed in Chapter 4. The model by Rad assumes that a small portion of the beam and column at each joint has a higher strength and five times higher stiffness due to confinement under the loading plates and the base supports. Results show an improvement in overall strength and stiffness. However, the analytical predictions for non-proportional loading in the present study, which ignores joint deformations, compares most favourably.

The remaining frames by Rad were examined in the present study. In all cases, there was little difference in the predicted horizontal peak load, H_{max}, for the proportional loading and non-proportional loading analyses and the experimental peak load. The proportional loading results tended to overestimate frame stiffness.

Figure 5.10 shows frame A3 with potential hinge forming regions marked A to I. Results for moment and curvature from the non-proportional analysis are shown in Figures 5.11 to 5.14. The vertical load pattern was incremented up to a load level corresponding to an estimated column axial load of 75% of the squash load. Actual frame failure corresponds to the formation of hinges in segment C in the top beam and segment I in the bottom beam. The analytical results show that moment and curvature in segments C and I increase monotonically until the peak frame load is reached, although failure in these segments does not occur.
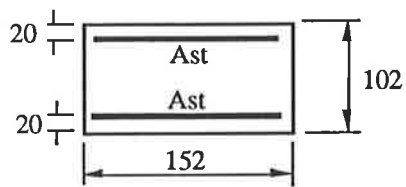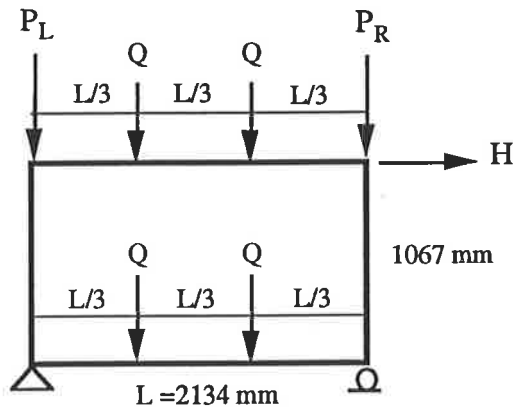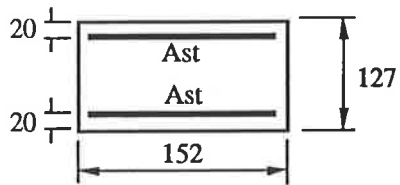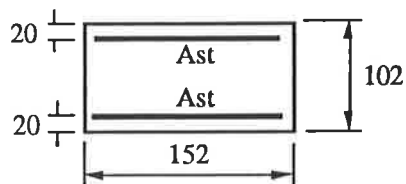
Figure 5.8: Configuration for frame A3 tested by Rad (1972)
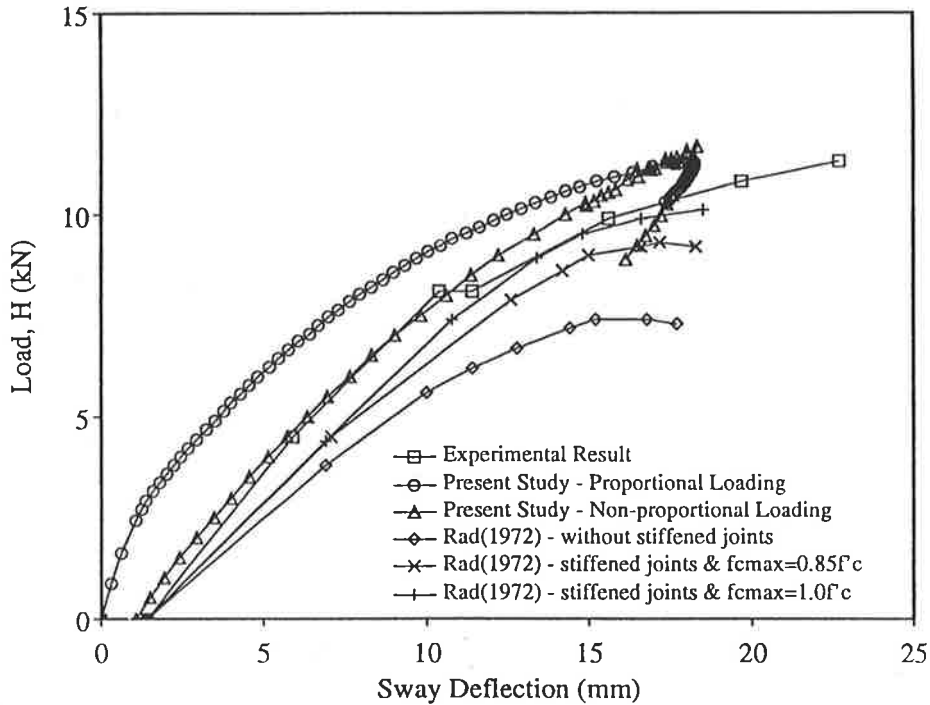
Figure 5.9: Horizontal load versus deflection for frame A3 tested by Rad (1972)

The moment-curvature plots for segment A (left end of the top beam) and segment H (left end of the bottom beam) show that cracks form at a corresponding moment of about 1.0 kNm, and when the first load system is finally incremented there is a considerable loss in stiffness. Elastic unloading takes place during application of the second load system, which is evident by moment and curvature passing through the origin. At this point, cracks are assumed to have closed and as loading continues, the shape of the M-κ curve indicates that cracks form in the opposite face.

Under the vertical load pattern, both columns are bent in double curvature but response to horizontal loading for the left column is quite different to that for the right column . Segments D and E of the left column actually undergo inelastic unloading and with further increments of the horizontal load moment and curvature actually change sign. The magnitude of moment and curvature in the right column continue to increase monotonically with the second load system, and segment F eventually undergoes softening.
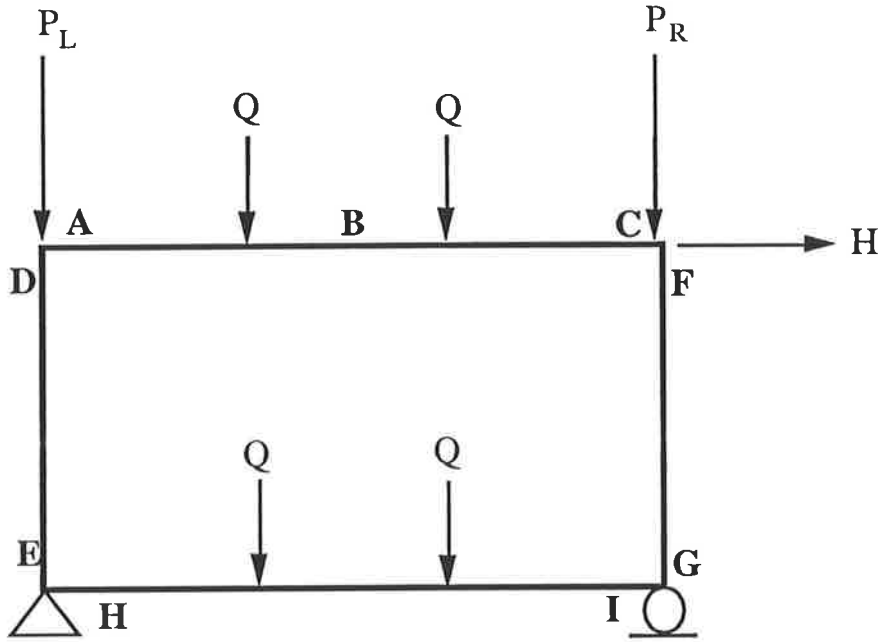
Figure 5.10: Potential hinge forming regions for frame A3
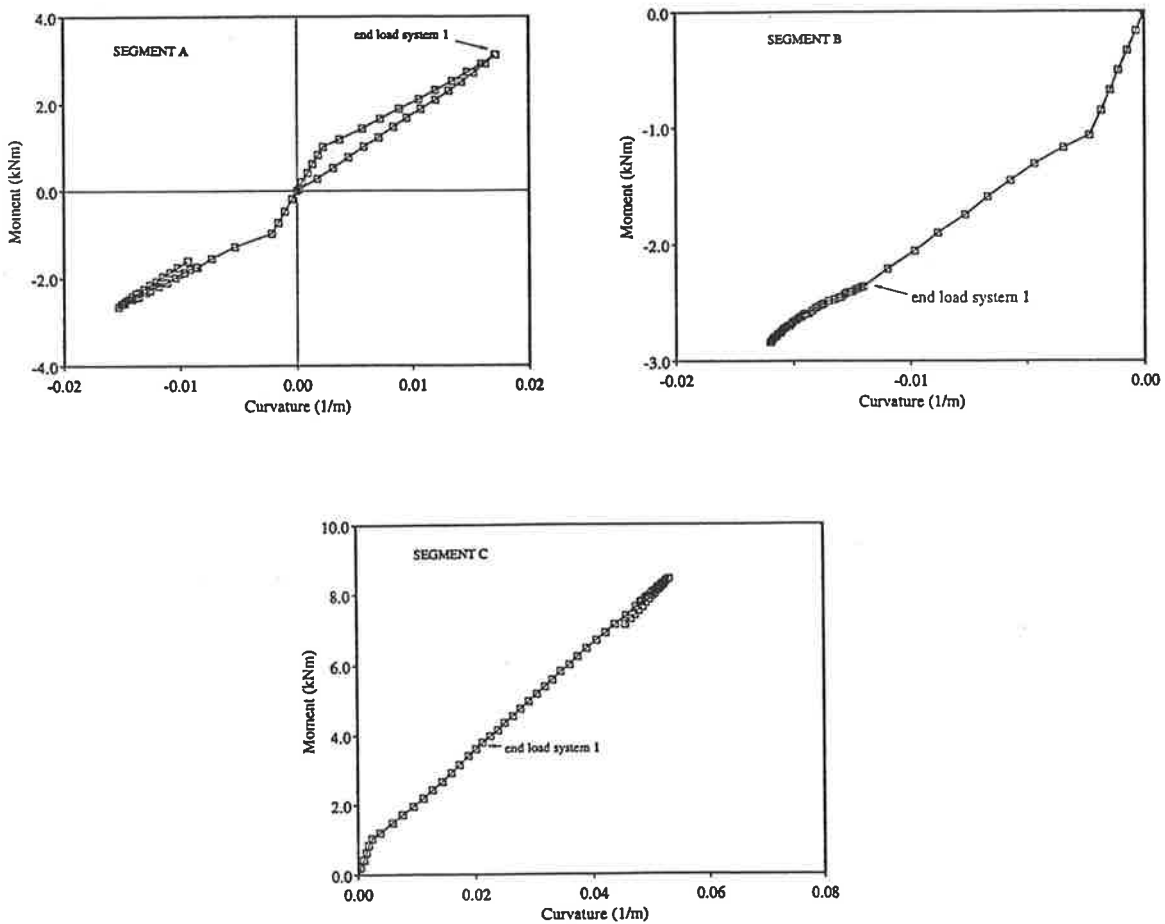
Figure 5.11: Moment curvature relations for top beam of frame A3
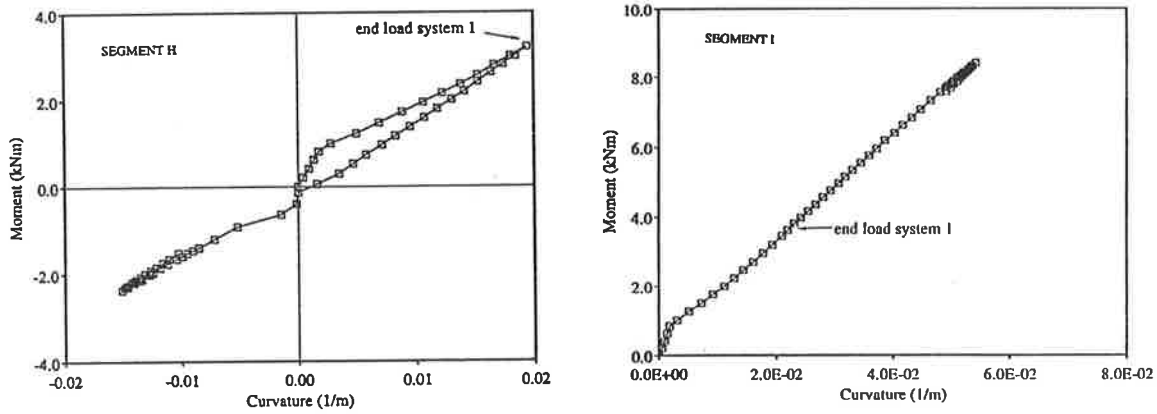
Figure 5.12: Moment curvature relations for bottom beam of frame A3
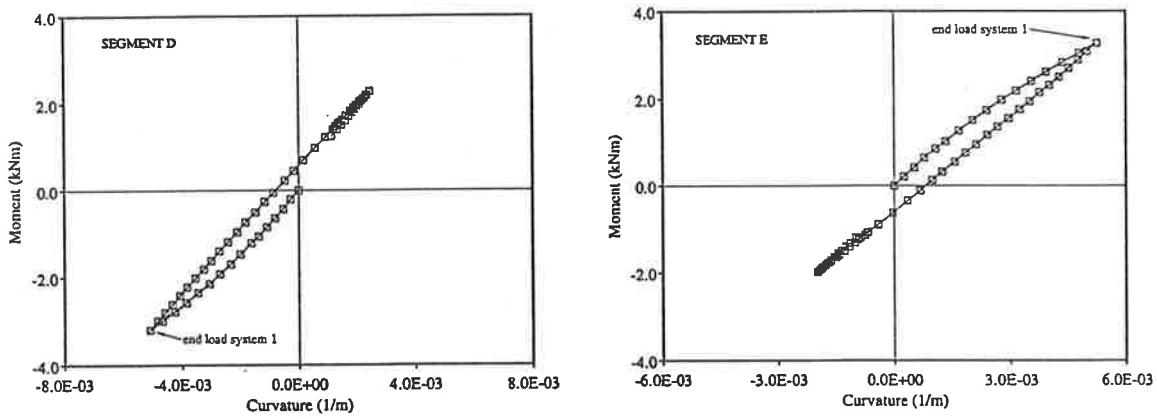
Figure 5.13: Moment curvature relations for left column of frame A3
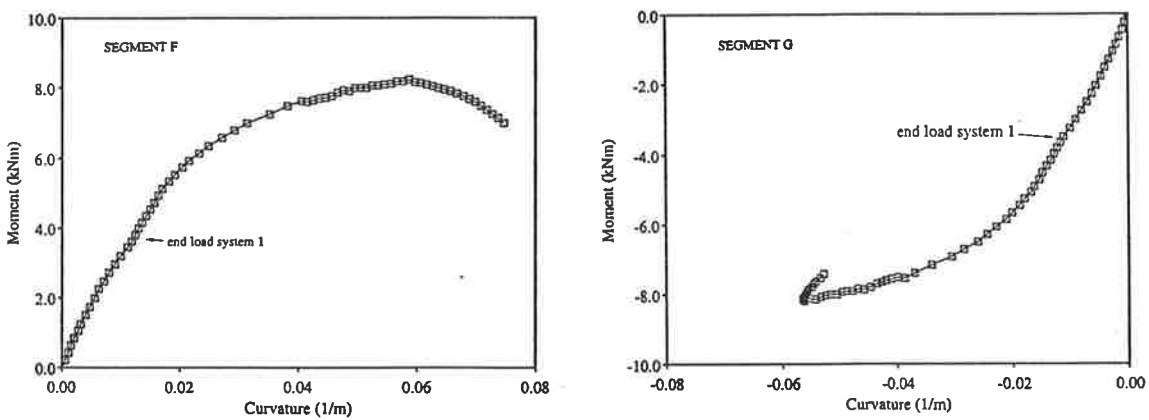
Figure 5.14: Moment curvature relations for right column of frame A3

5.3.4 Frames tested by Ford (1977)

Frame FC-7 tested by Ford has been chosen for analysis and frame details are shown in Figure 5.15. Concrete properties for this frame are as follows: average compressive strength, f_{cm} = 42.2 MPa, f_{cmax} = 40 MPa, i.e. $0.95f_{cm}$ and E_c = 32480 MPa. A number of different grades of steel were used for this frame and the yield strengths are summarised in Table 5.1. The Young's modulus for all types of reinforcing steel is assumed to be 2×10^5 MPa and the stress-strain relationships are elasto-plastic.

The first load system comprised the vertical loads, P, $\alpha_1 P$, $\alpha_2 P$ and Q, where α_1=1.23, α_2=0.77, and Q/P = 0.011. These loads were incremented proportionally up to the values of 476 kN, 587 kN, 369 kN and 5.1 kN respectively and held constant as a horizontal load was applied to the top of the column. The test frame reached a maximum horizontal load, H_{max}, of 17 kN, followed by noticeable softening after the peak load.

Table 5.1: Section details for frame FC-7

Member	b (mm)	D (mm)	d_{st} (mm)	A_{st} (mm^2)	f_{sy} (MPa)
Beams 1-3,8-10	152	102	21	142	395
Column 4	152	102	19	142	441
Column 5	152	127	19	142	507
Column 6	152	102	19	142	445
Column 7	152	81	17	84	494

Results for load and deflection for frame FC-7 are shown in Figure 5.16, and joint modelling for the T-joints has been ignored for the analyses in the present study. The discussion of T-joints in Chapter 4 showed that joint deformations depend on the direction of the moments acting in each element at the connection. Such deformations

can be expected when the sign of the column moment is the opposite sign to either of the beam moments. A check for the segmental moments at T-joints under the first and second load systems showed that joint deformations are not expected to occur. Hence, joint modelling was not carried out for the present analysis of frame FC-7.
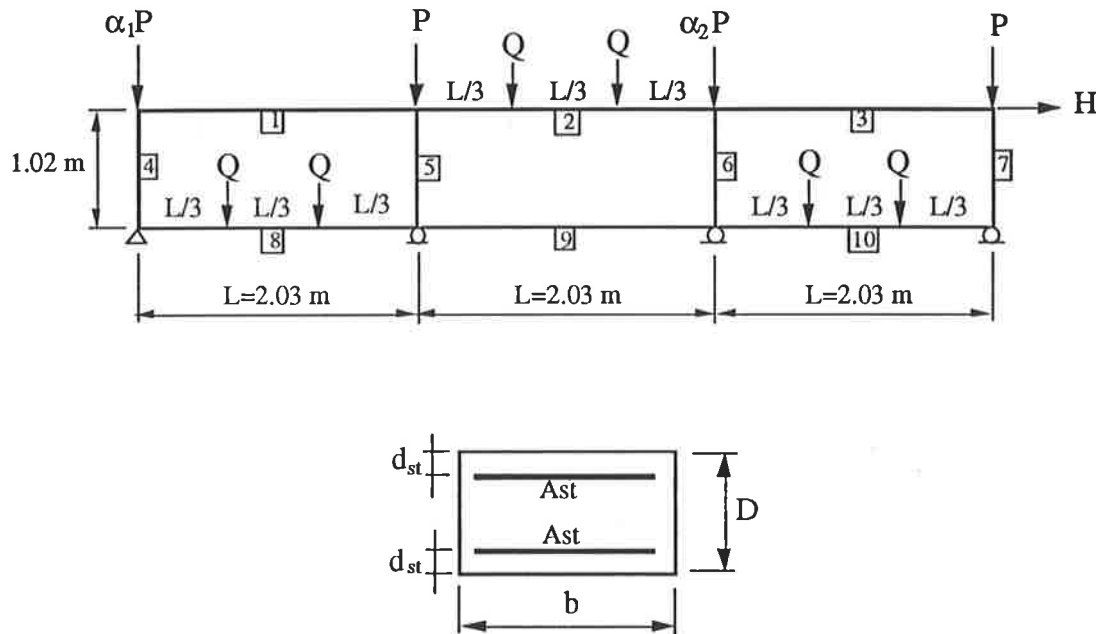
Figure 5.15: Configuration for frame FC-7 tested by Ford (1977)

The results for proportional loading give the best estimate for the maximum frame load, although frame stiffness is overestimated. Vertical and horizontal loads were applied in ratios given by the peak loads for the test specimen. The non-proportional loading analysis with f_{cmax} equal to $0.95f_{cm}$ gives a more conservative estimate for load and deflection. The peak load of 14 kN is 21 % less than the experimental peak load. This analysis also gives a better estimate for stiffness. There appears to be very little difference in results when f_{cmax} equals $1.15f_{cm}$.

It is possible joint performance is improved by confinement due to the applied loading and support conditions. These aspects were considered in the analyses by Ford (1977). Ford proposed a modified stress-strain curve for concrete in compression, as shown in Figure 5.17. This curve is based on the well known curve proposed earlier by Hognestad (1951).

The maximum compressive stress f_c'' at all sections, except within the joints, is taken as $0.95f_c'$ for horizontally cast columns, where f_c' is the characteristic cylinder strength. The corresponding softening portion of the modified curve, with a slope index of $m = 20$, is based on curve fitting to experimental results. The ultimate strain ε_u includes a term in brackets which takes into account confinement by reinforcing hoops or stirrups. The second term in the expression for ultimate strain, $0.02b/z$, depends on the width of the confined concrete, b, and the distance between the point of maximum moment and zero moment which is given by z. The equation for ε_u is similar to an equation proposed by Corley (1966).

For concrete within the joints, the uniaxial strength is artificially increased by assuming the value for f_c'' is equal to $1.15f_c'$. The corresponding slope index, m, has a value of 5, (Ford, Chang and Breen, 1981b).
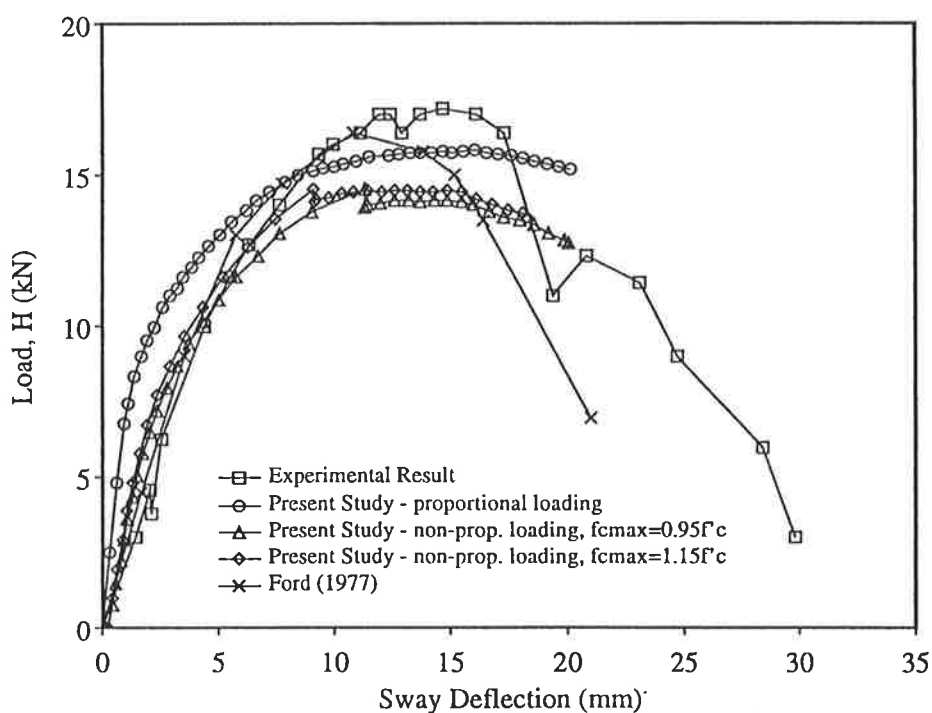
Figure 5.16: Horizontal load versus deflection for frame FC-7 tested by Ford (1977)
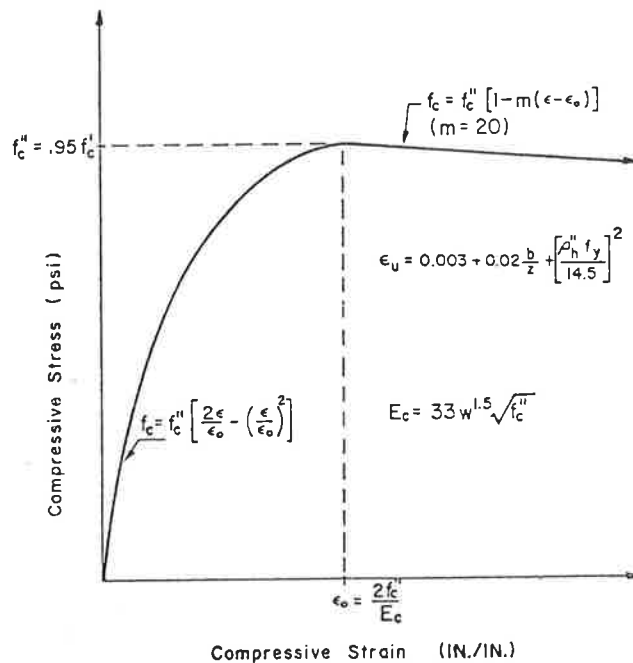
Figure 5.17: Modified concrete compressive stress-strain curve,

(Ford, 1977; Ford, Chang and Breen, 1981a)

Shown in Figure 5.16 are the analytical predictions by Ford, also reported in Ford *et al.* (1981c). Results from this analysis compare favourably with the experimental results. Remaining test frames were also analysed by Ford and good correlation was achieved. In each case, the concrete properties within the joints were adjusted to reflect the improvement in strength and stiffness from confinement. Note also that special spring supports were included in the analyses to account for increases in stiffness when the specimens made contact with the base safety frames. Neither of these effects were modelled in the present study, hence analytical results for some of these frames underestimated strength and stiffness considerably. Results for frame FC-7 gave the best predictions by the present method of analysis for non-proportional loading.

5.3.5 Summary of Analytical Predictions

Several test frames have been analysed for proportional and non-proportional loading. Good correlation has been achieved and results indicate, that by assuming proportional loading, strength and stiffness may be only overestimated slightly. Predictions by other investigators have also been discussed. It is interesting to note that in each case

increases in strength and stiffness at joints had been taken into account by various means. Such improvements in behaviour have been ignored in the present study, although these effects can be treated in future studies by modifying the proposed joint model of Chapter 4.

The test comparisons showed only minor differences between proportional and non-proportional loading. This may not always be the case, and to investigate the situation further a number of theoretical frames are analysed by both methods in the following section.

5.4   Frame Behaviour Under Non-proportional Loading

5.4.1   Introduction

Analytical results for three frames for proportional and non-proportional loading are presented in this section. The frames are two single-storey and one multi-storey. Several other frames had been analysed, but comparisons for strength and stiffness were very similar and of little interest for discussion.

In each case, the first load system in the non-proportional loading analysis comprises a set of vertical loads with a magnitude equal to the maximum vertical load under proportional loading. It has been noted previously, (Mo, 1986), that moment redistribution and ultimate load are influenced by the loading history of the structure. It can also be appreciated that as the magnitude of the first load system reduces, frame strength and stiffness is governed by the second load system. Hence, comparisons between proportional and non-proportional loading become less significant.

Concrete parameters for the three selected frames are: $f_{cm} = 28.6$ MPa, $f_{cmax} = 27.2$ MPa, $E_c = 26740$ MPa and $\gamma_1 = 2.08$. Reinforcing steel has a yield strength, f_{sy}, equal to 460 MPa and a yield strain, ε_{sy}, of 0.0023. Beam and column members are 300

mm by 300 mm in section and the total area of steel for all members is 2% of the gross sectional area. This steel is distributed equally to two layers and the cover to the centre of the bars is 40 mm in each face.

5.4.2 Single-storey Frames

Load configurations for frame A and frame B are shown in Figure 5.18. The amount of horizontal load for proportional loading analyses is $0.1wL$ and $0.05wL$ respectively, where w is the vertical uniformly distributed load to be applied to the beam. The maximum vertical and horizontal loads for frame A are $w_{max} = 50$ kN/m and $H_{max} = 30$ kN respectively. Analysis for frame B under proportional loading also predicts a maximum vertical load of $w_{max} = 50$ kN/m, but for horizontal loading, H_{max} is equal to 15 kN.

For the non-proportional loading analysis for frame A, the beam loading was incremented up to 50 kN/m and held constant as the horizontal load, H, was incremented up to a peak value, H_{max}, of 30 kN. This is the same value for peak load as determined by the proportional loading analysis.

Horizontal load versus sway deflection for frame A are shown in Figure 5.19. Noted on the plot for proportional loading are the load steps at which flexural hinges occur. This analysis predicts the formation of four hinges for the frame, i.e. a full plastic collapse mechanism occurs. The locations for potential hinge forming regions for frame A and frame B are also shown in Figure 5.20.

It is also useful to compare the bending moment in each segment and axial force in each member at various stages of loading. Shown in Figure 5.21a are these moments and member axial forces at the peak load under proportional loading. Figure 5.21b shows two sets of moments and axial forces for non-proportional loading: one at the end of the first load system and the other, with values in brackets, at the peak load for the second load system. Note that compressive axial forces are acting in all members and the moment diagram is plotted on the tension face.
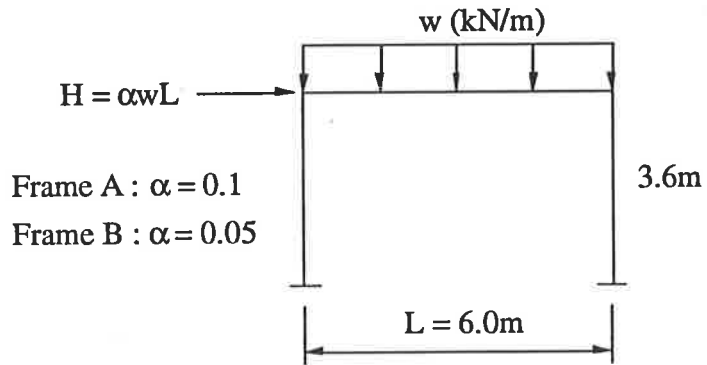
(a) Proportional Loading
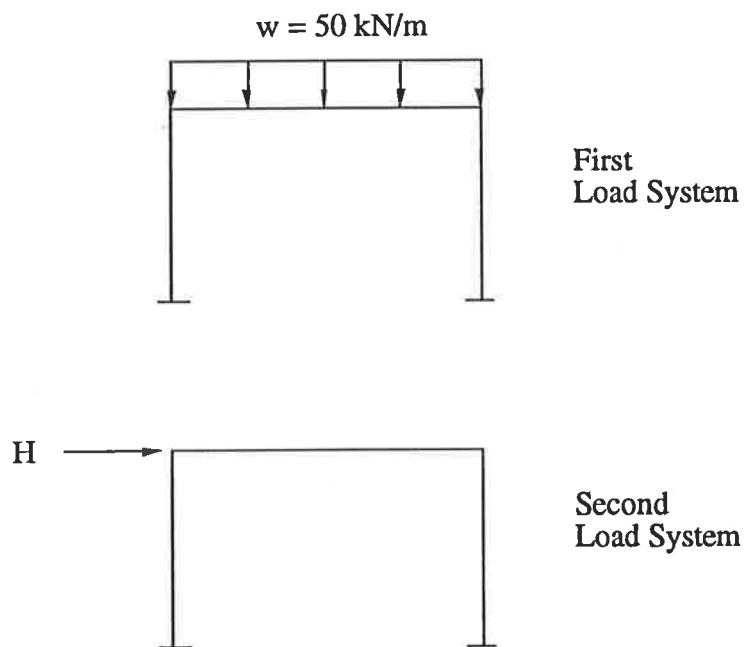
(b) Non-proportional Loading

Figure 5.18: Portal frame
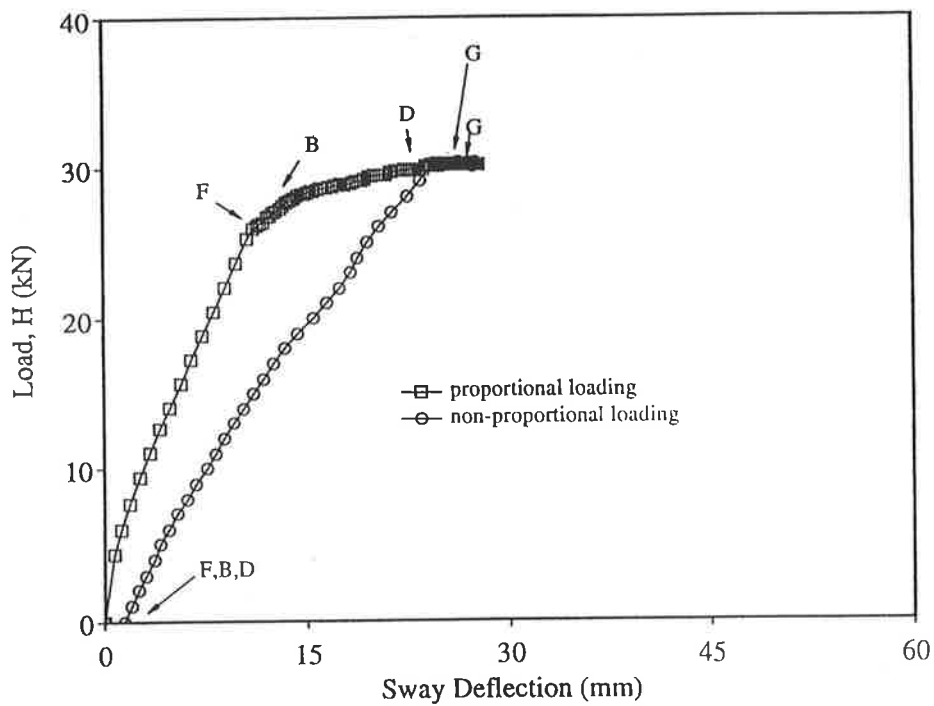
Figure 5.19: Load versus deflection for frame A
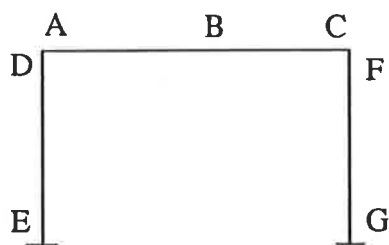
Figure 5.20: Potential hinge forming regions

97   100

113   113

150   150

67

105

150   150

4   112

Moments and axial forces at peak load

(a) Proportional Loading

99 (95)   99 (101)

112   112
(112)   (113)

52 (67)

150   (148)   (149)   150

102 (102)

(15)   60   (112)   60

Compressive
Axial force

Compressive
Axial force

in brackets -
Moments and axial forces
at peak value for second
load system

Moments and axial forces
at end of first load system
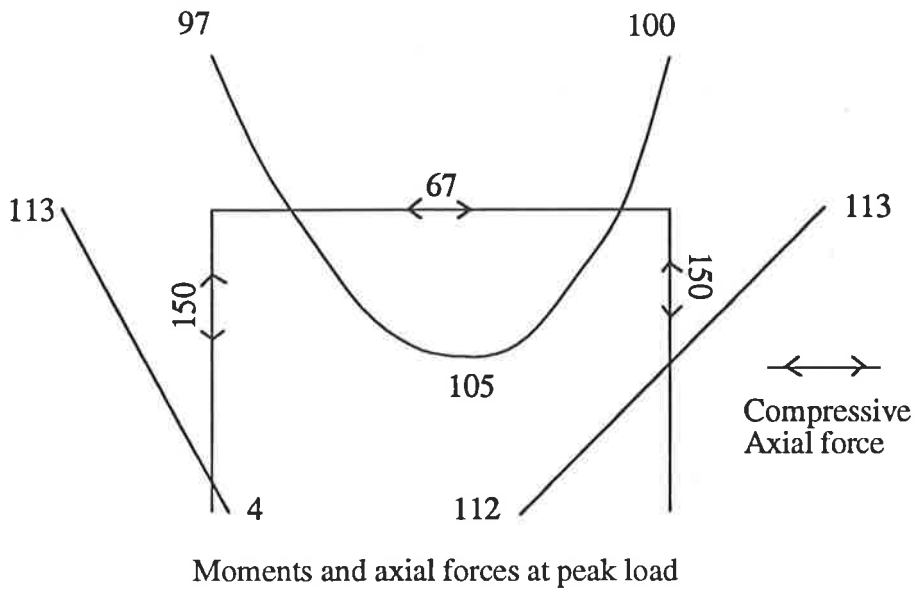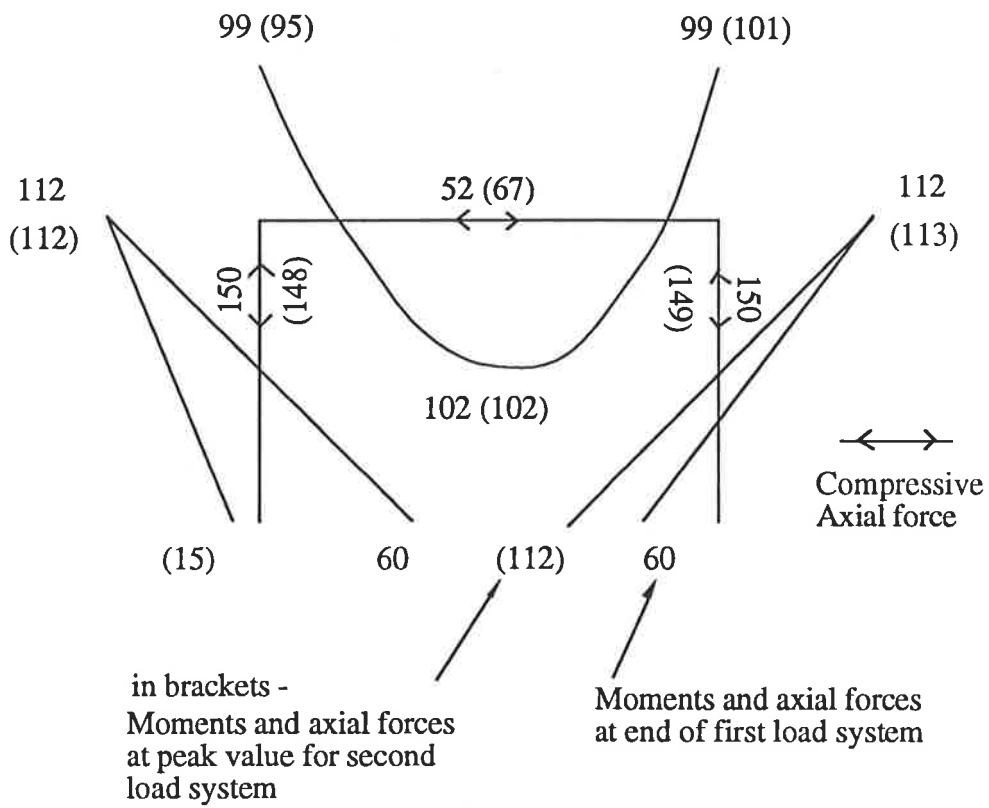
Non-proportional Loading

Figure 5.21: Bending moment and axial forces for frame A

The analysis for non-proportional loading predicts the formation of hinges in segments B, D and F at the completion of the first load system, i.e. with the beam loading fully incremented to 50 kN/m. Note that the distribution of moments for proportional loading and non-proportional loading are very similar.

At the end of the first load system for non-proportional loading, maximum moment has just been reached in segments B, D and F, and corresponds to the formation of flexural hinges. Of particular interest is the predicted behaviour in segment E and G at the base of each column under non-proportional loading.

At the end of the first load system, the moments in segments E and G are both equal to 60 kNm, and as expected the bending moment and axial force diagrams are symmetrical. With application of the second load pattern, segment E unloads. On the other hand, moment and curvature for segment G continue to increase monotically. The maximum moment for this segment is reached as the peak frame load, H_{max}, reaches 30 kN. At this point, a full plastic collapse mechanism has formed with a set of four hinges. A similar collapse mechanism develops under proportional loading.
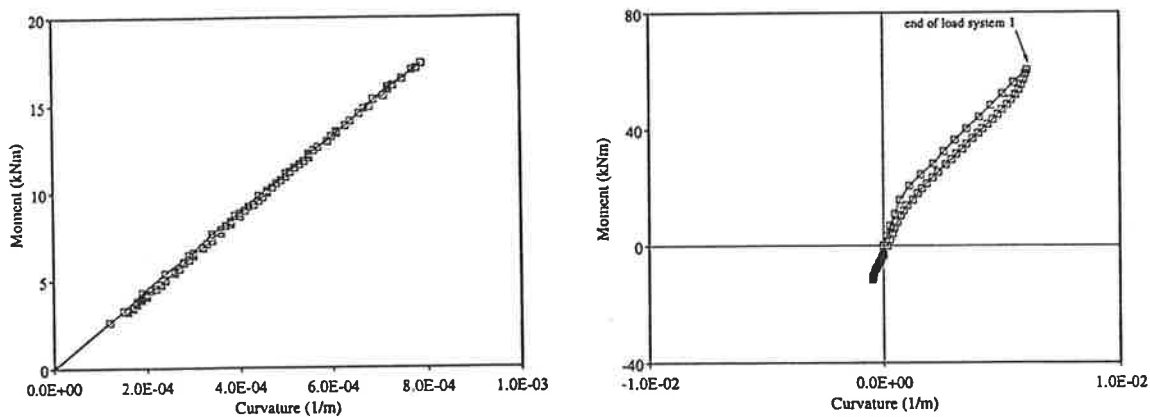
(a) proportional loading   (b) non-proportional loading

Figure 5.22: Moment and curvature for segment E of frame A

The major difference in segmental behaviour for these two analyses is shown by the plot of moment and curvature for segment E in Figure 5.22. Under proportional loading, this segment reaches a peak moment of 17.5 kNm, but as the first hinge forms in segment F at a load, *H*, of 26 kN, unloading takes place in segment E. This segment also unloads during non-proportional loading, but at the end of the first load system the segmental moment is 60 kNm. For both analyses, the unloading for segment E appears to be elastic.

It is interesting to note that as the peak frame load is reached for non-proportional and proportional loading the set of axial forces and moments in the key hinge forming regions are very similar. The overall difference is the distribution of moments in the left column.

Although there is no noticeable difference in the peak load for proportional and non-proportional loading, there is a difference in the predicted stiffnesses. The proportional loading analysis gives a higher estimate for stiffness. In neither case is softening evident after the peak load.

Shown in Figure 5.23 is load versus deflection for frame B. This frame has the same properties as frame A, but has a lower ratio of horizontal to vertical load. The maximum loads under proportional loading for frame B are 50 kN/m for the beam load and 15 kN for the horizontal load. Under non-proportional loading, the peak horizontal load is 30 kN. This represents a 100% improvement in frame capacity. Note also the analysis for proportional loading overestimates stiffness considerably.

It should be noted that the first load system with a beam load, *w*, equal to 50 kN/m is actually the maximum value for vertical load this structure can sustain. It is most unlikely a real structure would be subjected to this level of vertical load before application of a second loading system. However, this theoretical example illustrates a case where both strength and stiffness are influenced by the application of non-proportional loading.
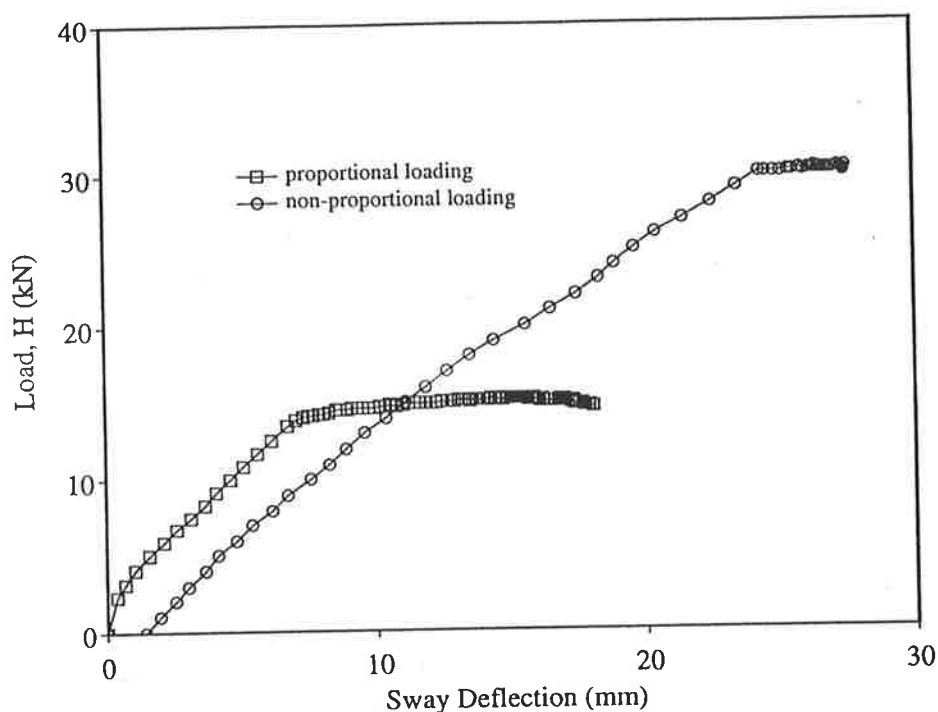
Figure 5.23: Load versus deflection for frame B

5.4.3 Multi-storey Frame

Both frames A and B were subjected to relatively low axial forces in the columns. Frame C with nine storeys, as shown in Figure 5.24, has columns in the lower storeys which are subjected to much higher axial loads.

Under proportional loading, the maximum vertical load, w_{max}, is 24.7 kN/m and the maximum horizontal load, H_{max}, is 3.7 kN. Load versus deflection for this analysis is shown in Figure 5.25. For non-proportional loading, the vertical load, w, was incremented up to 24.7 kN/m. These loads were held constant as the horizontal load at each floor level was incremented up to a maximum value of H equal to 3.6 kN. There is no noticeable difference in strength for each analysis, although analysis for proportional loading predicts a higher stiffness.
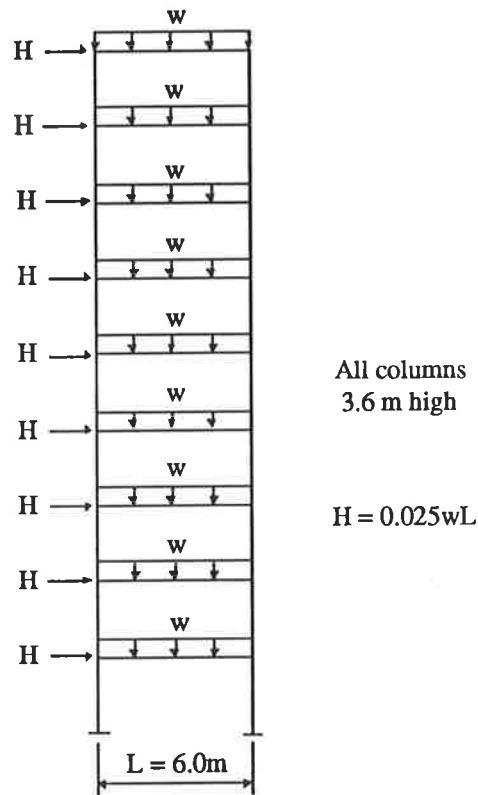
Figure 5.24: Frame C
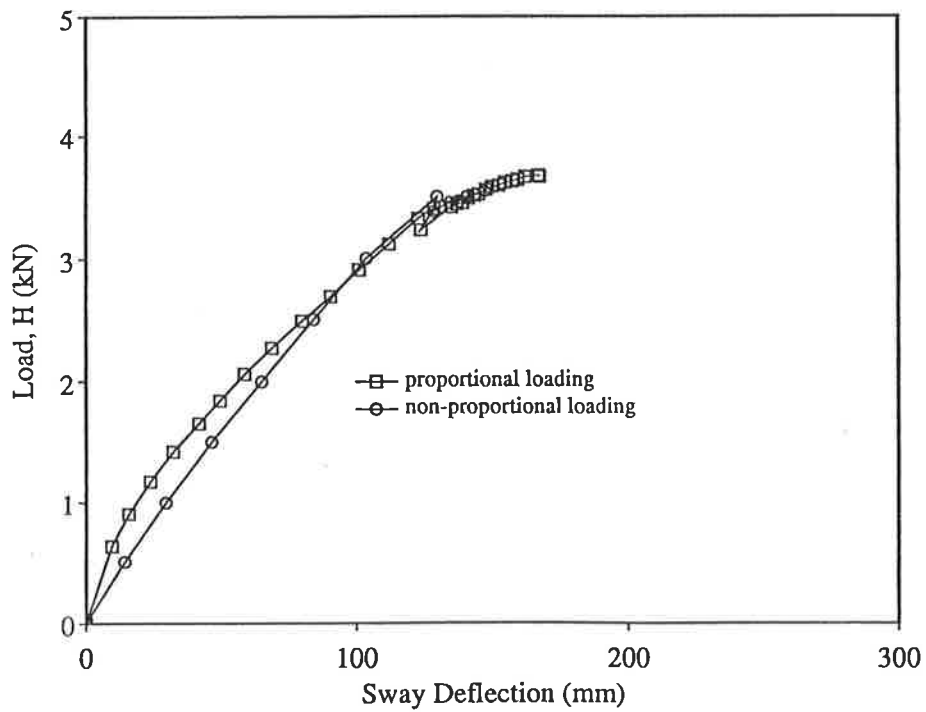
Figure 5.25: Load versus deflection for frame C

5.5 Summary and Conclusions

A method of analysis for sequential non-proportional loading of a reinforced concrete frame structure has been developed for the purposes of investigating this effect. The method allows for post-peak behaviour under the second load system by incrementing deformations to the structure. Reversal of loading during the second load system is also allowed for.

Good correlation was achieved between analytical predictions and results for experimental frames subjected to sequential loading. Comparisons were also made between analytical predictions for non-proportional loading and analyses with equivalent systems of proportional loads. In each case, predicted strengths were similar, although non-proportional loading tended to give more conservative estimates for stiffness.

Several theoretical frames were compared for proportional loading and for non-proportional loading. The first load system under non-proportional loading was incremented up to a maximum value for vertical load and the second load system incremented horizontal load up to a maximum. Results suggest the assumption of proportional loading is reasonable.

Chapter 6

Investigation of the Accuracy of the Simplified Methods of Analysis/Design of Slender Columns

6.1 Introduction

The Australian Standard AS 3600 allows for three levels of sophistication for the analysis and design of reinforced concrete structures. In order of increasing accuracy, these approaches are defined here as the bottom-tier, middle-tier and top-tier methods.

The bottom-tier method when applied to slender columns is referred to as the moment magnifier method. It is an approximate method of analysis and is the most popular because of its simplified procedures.

The middle-tier approach requires a second order elastic analysis which takes into consideration geometric non-linearities. This type of analysis is more complicated than a first order analysis, but its increasing popularity can be attributed to increasing availability of second order analysis computer programs.

Finally, AS 3600 recommends that all relevant material and geometric non-linearities be taken into account in a rigorous structural analysis. For the present study, this type of analysis is referred as a top-tier approach. Although the analysis and design of a structure by a top-tier approach is not usually carried out in practice, the development of a rigorous method of analysis assists in the evaluation of the accuracy and adequacy of the middle-tier and bottom-tier methods.

Both the moment magnifier method and the second order elastic method are described in this chapter, as well as the bottom-tier 'model column method'. This latter method is the basis of the column analysis/design procedures for columns in non-sway frames mentioned in the draft European code, EN 1992 Eurocode EC2. The results of previous investigations of the moment magnifier method and the middle-tier method are also summarised in this chapter.

In the study of frames described in this chapter, the peak loads of a wide range of sway frames were predicted by the bottom-tier moment magnifier and middle-tier methods. Comparisons were made with predictions obtained by the accurate segmental method of frame analysis incorporating the non-linear models developed in Chapters 3, 4, and 5. This accurate method of analysis is referred in this chapter as a top-tier approach.

Frames chosen for analysis cover a range of practical design examples and various non-linear effects are investigated. Full geometric non-linear effects were taken into account in all frames analysed.

For discussion purposes the frames are categorised into a number of series. In Series I, the influence of two types of material non-linearity on the behaviour of several

single storey frames is investigated. These effects are tension stiffening and joint flexibility and are included in the top-tier non-linear method of analysis. Ultimate strength predictions are also made by the simplified bottom-tier and middle-tier methods of AS 3600. All safety coefficients and capacity reduction factors are removed from the calculations. Material properties are based on average values and not characteristic values.

The study in Series II includes three five-storey frames which are subjected to beam loading and lateral loading applied at each floor level. In this series, two types of analysis are made for the bottom, middle and top-tier accurate methods. Firstly, ultimate strength predictions are made and, secondly, comparisons are made with design strength predictions, whereby all safety coefficients are included, and material properties are based on characteristic values. Series III investigates the effect of chequerboard loading by comparing proportional and non-proportional loading in top-tier non-linear analyses. Finally, Series IV involves ultimate and design strength predictions for a ten storey frame.

Following the study of frames is a study of several isolated pin-ended columns. Analytical predictions by the moment magnifier and the model column method methods are compared with those obtained by top-tier analyses.

6.2 The Moment Magnifier Method

6.2.1 The Effective Length Concept

Analysis and design by the moment magnifier method involves a linear elastic frame analysis with assumed stiffness values, EI and EA, for each member. Load patterns are assumed to be applied to the structure simultaneously and proportionally, to obtain first order forces and moments. To account for the increase in bending moments in a compression member due to lateral displacements, the first order moments are

increased by one of two moment magnifiers. These two moment magnifiers are described in Sections 6.2.2 and 6.2.3.

Before calculating the column moment magnifiers, the column under consideration is isolated and reduced to a standard equivalent pin-ended column with equal end eccentricities. This involves determining an effective length, L_e, which is equal to kL_u. The effective length factor, k, is obtained from the Jackson-Moreland charts and L_u is the unsupported length of the column. Evaluation of the effective length factor takes into account the relative rotational stiffnesses of the connecting members at each end of the column. However, the calculation for the end restraints is based on geometric properties and does not take into consideration the percentage of steel of the connecting beams and columns.

Breen *et al.* (1972) showed that *EI* values based on gross-sectional values are accurate only for a limited number of cases. An earlier study by Pagay *et al.* (1970) found that beam stiffness can have a great effect on column strength. Beams with low percentages of reinforcement tend to be more flexible than beams with higher amounts of reinforcement. A further analytical study by Okamura *et al.* (1970) showed that the reduced stiffness of cracked beams also affects the strength of columns.

6.2.2 Moment Magnifier for a Braced Column

From the linear elastic analysis the design moments at the ends of each column are M_1* and M_2*, where M_2* is greater than M_1*. The design axial force is given by $N*$. The moment M_2* is then magnified by the braced moment magnifier, δ_b. There is no magnification of the design axial force. The value of δ_b depends on the ratios of M_2*/M_1* and $N*/N_c$, where N_c is the elastic critical buckling load, given by the following equation:

$$N_c = \frac{\pi^2}{L_e^2} \frac{(200 d\phi M_{ub})}{1+\beta_d} \qquad (6.1)$$

In Equation 6.1, the equivalent stiffness EI is evaluated as M_{ub}/κ_{ub}, which corresponds to the balanced point on the strength interaction diagram. Although iterative procedures, such as those by Chang (1967) and van den Beukel (1977), can be used to determine the critical buckling load a single representative value for EI is recommended by AS 3600. This value, which is chosen for convenience, is based on the studies of Menn (1974), and MacGregor *et al.* (1975), and Oelhafen (1974).

By taking the neutral axis depth equal to $0.6d$ and the maximum compressive strain in the outer concrete fibre equal to 0.003, the value of EI is expressed by $200dM_{ub}$. The term, L_e, is the effective length of the column. Also included in Equation 6.1 is the design strength reduction factor ϕ and creep factor β_d. The relationship between ϕ and the design strength interaction curve is shown in Figure 6.1.
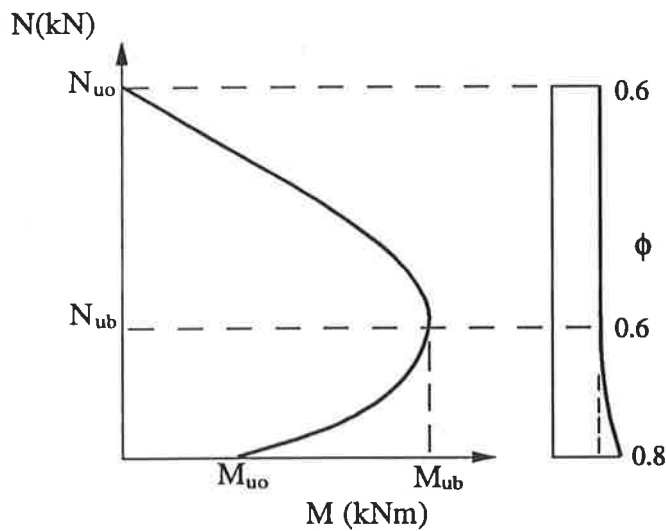
Figure 6.1: Strength reduction factor, ϕ

Second order moments due to geometric effects are taken into account by the determination of the braced moment magnifier, which is given by:

$$\delta_b = \frac{k_m}{1 - \dfrac{N^*}{N_c}}$$

(6.2)

where $k_m = 0.6 - 0.4\ M_1^*/M_2^*$. If the value of δ_b by Equation 6.2 is less then unity, the maximum moment occurs at the end of the column and no magnification is needed. In this case, δ_b equals 1.0. A minimum value of 0.4 applies to k_m and accounts for unwinding under high axial loads. This may occur in columns bent in double curvature, where $0.5 < M_1^* / M_2^* < 1.0$. Tests of reinforced concrete columns bent in double curvature by MacGregor and Barter (1966) and Martin and Olivieri (1966) showed that columns under high axial loads tended to unwind rather suddenly with columns approaching the instability mode. The drastic change from double to single curvature is referred to as unwrapping or unwinding.

The moment magnifier method by AS 3600 is similar in principle to the approach given by the American concrete standard ACI 318-83. However, in the determination of the elastic critical buckling load and the effective length factor k for columns by the latter, it is recommended for short term loading the stiffness EI be evaluated by Equation 6.3, which is derived from the study by MacGregor *et al.* (1970).

$$\frac{E_c I_g}{5} + E_s I_{se} \tag{6.3}$$

where $E_s I_{se}$ is the contribution of the reinforcing steel to flexural stiffness. An alternative expression which gives more conservative results is the following:

$$\frac{E_c I_g}{2.5} \tag{6.4}$$

6.2.3   Moment Magnifier for an Unbraced Column

To check the failure of a structure in the sidesway mode, the effect of all columns within each storey is taken into account in the calculation of an unbraced moment magnifier.

This 'sway' moment magnifier is given by:

$$\delta_s = \frac{1}{1 - \frac{\Sigma N^*}{\Sigma N_c}}$$

(6.5)

Based on the findings of MacGregor and Hage (1977), if the value of δ_s exceeds 1.5, an instability failure mode may occur and the moment magnifier method should not be used for column analysis.

6.2.4 Overall Frame Stability

Simplified calculations can be made to check the critical loads of tall frames. Based on the second order analyses by Rosenblueth (1965) and Stevens (1967), the following approximate expression for the critical load on the *i*-th storey in a sway frame was suggested by MacGregor and Hage (1977):

$$P_c = \frac{K_{1i} h_i}{\gamma} = \frac{H_i}{\gamma} \frac{h_i}{\Delta_{1i}}$$

(6.6)

In these expressions, h_i is the height of the *i*-th storey, γ is a factor which varies from 1.0 for stiff columns and flexible beams to 1.22 for flexible columns and stiff beams. In general, γ approaches 1.0 in the lower storey of a tall building. The lateral stiffness of the *i*-th storey is $K_{1i} = H_i/\Delta_i$, where H_i is the horizontal load above the *i*-th storey and Δ_i is the first order lateral deflection within the height h_i.

6.3 The Model Column Method

The draft publication, EN 1992 Eurocode 2: Design of Concrete Structures, describes the model column method for the analysis/design of columns in braced frames. This is a first order approach and, like the moment magnifier method, involves the effective length concept to isolate a column member from a frame. However, the method uses a

direct calculation of the second order moment by performing an equivalent strength calculation to determine column capacity.

The "model column" is represented by a cantilever column, as in Figure 6.2, with a total eccentricity due to three effects. These are a first order eccentricity, e_e, a second order lateral deflection, e_2, and an eccentricity, e_a, due to misalignment of columns during construction.
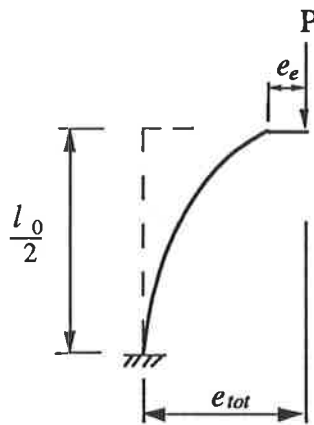
Figure 6.2: Model column

The total eccentricity, e_{tot}, is given by:

$$e_{tot} = e_a + e_e + e_2 \tag{6.7}$$

It has been shown by MacGregor (1979) that column eccentricity due to out-of-plumb columns can be significant. The previous Australian Standard for concrete structures, AS 1480-1982, allowed for this effect, but unfortunately, no provision is made in the current standard, AS 3600, for such an additional eccentricity. This effect is ignored in the present study as it does not affect the comparisons being made.

The term, e_e, given by Equation 6.8 is the initial eccentricity in the model column and is calculated from the end eccentricities in the real column.

$$e_e = 0.6e_{0_2} + 0.4e_{0_1} \geq 0.4e_{0_2} \tag{6.8}$$

In this expression, e_{0_1} and e_{0_2} are the eccentricities at the ends of the column, where $\left|e_{0_2}\right| \geq \left|e_{0_1}\right|$. Calculation of the eccentricity, e_e, is similar to the evaluation of the coefficient, k_m, in the moment magnifier method, i.e. first order end eccentricities are replaced with an equivalent eccentricity of constant magnitude along the length of the column.

Second order column deflections are derived from a parabolic distribution for deflection along the model column length. The maximum deflection, e_2, which occurs at the base of the column is given by the following :

$$e_2 = K_1 \frac{l_0^2}{10} \frac{1}{r} \tag{6.9}$$

where l_0 is the column effective length and $1/r$ is the curvature from equilibrium based on a strength calculation. This value for curvature is determined from the assumed strain distribution at failure for the given level of axial compression under consideration.

The reduction factor K_1 is given by either Equation 6.10 or 6.11, and depends on the column slenderness ratio, λ.

$$K_1 = (\lambda / 20) - 0.75, \ \ 15 \leq \lambda \leq 35 \tag{6.10}$$

$$K_1 = 1, \ \lambda \geq 35 \tag{6.11}$$

In the simplified model column method, curvature can be evaluated from the following expression:

$$\frac{1}{r} = \frac{2K_2 \varepsilon_{yd}}{0.9d} \tag{6.12}$$

In this expression, ε_{yd} is the design yield strain of the steel reinforcement, d is the effective depth, and K_2 is given by the following:

$$K_2 = \frac{N_{ud} - N_{Sd}}{N_{ud} - N_{bal}} \leq 1.0 \qquad (6.13)$$

where, N_{ud} is the design axial load capacity, N_{Sd} is the design axial force, and N_{bal} is the axial load at the balanced moment capacity. The term, K_2, takes into account the decrease in curvature with increasing axial force in a section. In lieu of Equation 6.12, a conservative estimate for K_2 is 1.0.

A column is considered to be slender if the slenderness ratio of the column, λ, is greater than 25 or $\sqrt{\upsilon_u}$, whichever is the greater. In the second expression, the longitudinal force coefficient for the column element, υ_u, is given by the following:

$$\nu_u = N_{Sd} / (A_c f_{cd}) \qquad (6.14)$$

This expression is the ratio of the design axial force to the contribution of the unfactored area of concrete in the calculation for the column squash load. Second order effects can be ignored in isolated slender columns in non-sway frame structures if the slenderness ratio is less than the critical slenderness ratio and given by Equation 6.15.

$$\lambda_{crit} = 25(2 - e_{0_1} / e_{0_2}) \qquad (6.15)$$

A column is assumed to be stable if the following conditions are satisfied:

$$N_{Rd} \geq N_{Sd} \qquad (6.16)$$

and

$$M_{Rd} \geq N_{Rd} e_{tot} \qquad (6.17)$$

where N_{Rd} and M_{Rd} are the axial force and moment from the strength interaction curve and N_{Sd} is the first order axial force in the model column.

6.4 The Middle-Tier Method

According to AS 3600 analysis of frames by the middle-tier method can be carried out if the relative displacement at the ends of compression members is less then $L_u/250$ under the design loads for strength. Based on the findings of MacGregor and Hage (1977), an instability failure may occur if the calculated relative displacement is greater than this ratio.

Material non-linear effects are taken into account by using EI values which are representative of the deflections at the factored design loads. Based on the recommendations by MacGregor and Hage (1977), the stiffness of beam members is assumed to be $0.4E_cI_g$ and for columns, $0.8E_cI_g$, where E_c is the Young's modulus for concrete and I_g is the second moment of area. Calculation for axial stiffness is given by E_cA.

Since the column procedures of AS 3600 are similar in application to its American counterpart, ACI 318-83, it is of interest to compare calculation of stiffnesses. Based on the studies by MacGregor, Oelhafen and Hage (1975) and Oelhafen (1974), the ACI concrete code, ACI 318-83 recommends EI values to be taken as $0.5E_cI_g$ for beams and $E_cI_g(0.2+1.2\rho_tE_s/E_c)$ for columns. In the evaluation of column stiffness, the percentage of reinforcement is taken into account by the term ρ_t. The stiffness terms recommended by AS 3600 and ACI 318-83 are not representative of all cases, but are intended to provide a margin of safety for column design.

In a second order elastic analysis, geometric non-linear effects due to the lateral displacement of joints must be taken into account. For convenience, second order elastic methods of analysis for geometric effects can be categorised as either direct or iterative methods.

The direct determination of second order moments, shears and deflections can be found by using a method proposed by Fey (1966) and Parme (1966). Based on these same approaches, Wood *et al.* (1976a, b) proposed an iterative second order method which is intended to provide a more accurate solution. The following steps are required:

(1) Perform a first order frame analysis to determine the first order lateral deflections Δ_{1i} in each storey, (see Figure 6.3).

(2) Obtain an estimate of the total storey drift, Δ_{2i}, which includes second order effects. The total storey drift is given by the following expression:

$$\Delta_{2i} = \frac{\Delta_{1i}}{1 - \dfrac{\Sigma P_i \Delta_{1i}}{H_i h_i}}$$

(6.18)

where ΣP_i = sum of the axial forces in the column at the i-th storey

h_i = height of the i-th storey

H_i = shear in the i-th storey

(3) Obtain the additional storey shears due to the vertical loads, as shown in Figure 6.3. The sway force at each floor level is the sum of the storey shears from the columns above and below the floor.

(4) Perform a first order analysis by adding the sway forces to the applied vertical and lateral loads to obtain the total moment, shears and displacements. Further iterative cycles may be required to obtain a converged solution for Δ_{2i}.
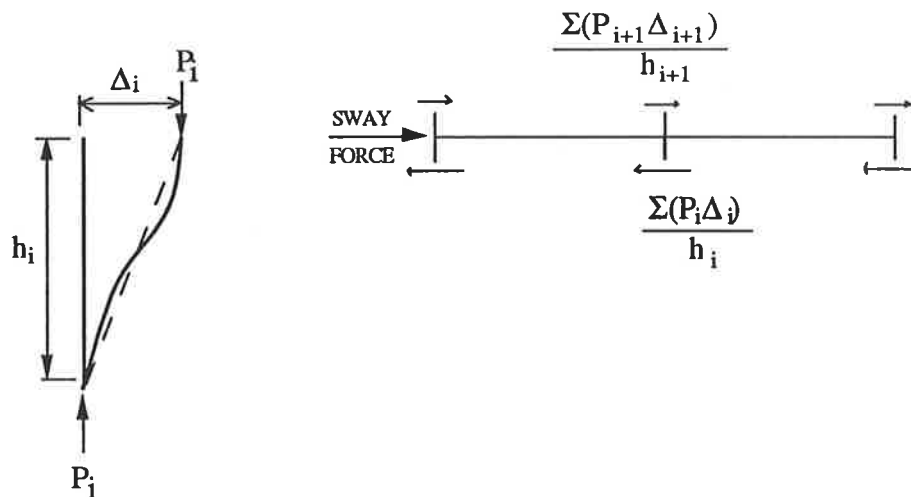
Figure 6.3: Calculation of storey shear, (MacGregor and Hage, 1977)

MacGregor and Hage found that the methods by Fey, Parme and Wood *et al.* gave accurate results provided the columns developed material failures. A stability index was proposed which determines if a second order analysis is appropriate. The stability index, Q, is given by the following formula:

$$Q = \frac{\Sigma P \Delta_1}{Hh} \qquad (6.19)$$

When $Q < 0.0475$, second order effects can be ignored and the structure can be treated as a braced frame. For Q between 0.0475 and 0.2, a second order analysis can be performed. Frames with $Q > 0.2$ are likely to fail by instability and a second order elastic analysis is not likely to yield accurate results.

The methods described so far ignore the influence of axial compression on flexural stiffness. For structures with very slender members, this effect can be significant. Lai and MacGregor (1983) proposed a method in which two types of non-linear geometric effects are take into account. Firstly, the second order effect of lateral loading on columns in sway frames and secondly, the interactive effect of axial load on flexural behaviour and flexural forces on axial stiffness. A frame is decomposed into a fully braced non-sway frame and a sway frame with the final force resultants obtained by

superposition, (Lai, MacGregor and Hellesland, 1983). Axial forces in the members of the non-sway frame and the sway frame are equal to the set of axial forces of the original frame and at the current state of loading. The traditional stability functions are used in a first order elastic analysis and are updated as loads are applied to the structure.

Fraser (1983) also considered the influence of axial compression on flexural stiffness in a second order analysis. In this approach, the determination of effective length factors takes into account the reduced stiffness of restraining members due to axial forces.

6.5   Previous Investigations of the Bottom and Middle-Tier Methods

6.5.1   Investigations of Isolated Pin-ended Columns

Smith and Bridge (1984) checked the accuracy of the moment magnifier method by modelling isolated pin-ended columns with eccentric loading. It was found that Equation 6.2 is accurate for columns with a slenderness ratio $L/r < 40$; at higher slenderness ratios the method becomes increasingly conservative. Bridge and Pham (1987) checked the reliability of the moment magnifier method for isolated pin-ended columns and found it gave a consistent margin of safety, particularly for long beam-columns.

6.5.2   Investigations of Columns in Slender Frames

Wong (1989) carried out a comprehensive study of the moment magnifier method and the middle-tier method by investigating columns within frames. Results for the moment magnifier method were also published in Wong, Yeo and Warner (1990) and the middle-tier method was also reported in Wong and Warner (1990).

In the study by Wong (1989), braced and unbraced portal frames and several multi-storey frames were examined. To limit the number of variables, all beams and columns were assumed to be 300 mm by 300 mm in section. In the series of portal frames, the following parameters were varied:

type of loading : four different loading patterns were used, (see Figure 6.4)

column reinforcement : 2 and 4 per cent of the gross sectional area

beam reinforcement : 0.5, 1, 2, 3, 4 and 5 per cent of the gross sectional area

column height : 3m, 6m and 9m, with corresponding slenderness ratios l_e/r (based on AS 3600) of 48, 88 and 127
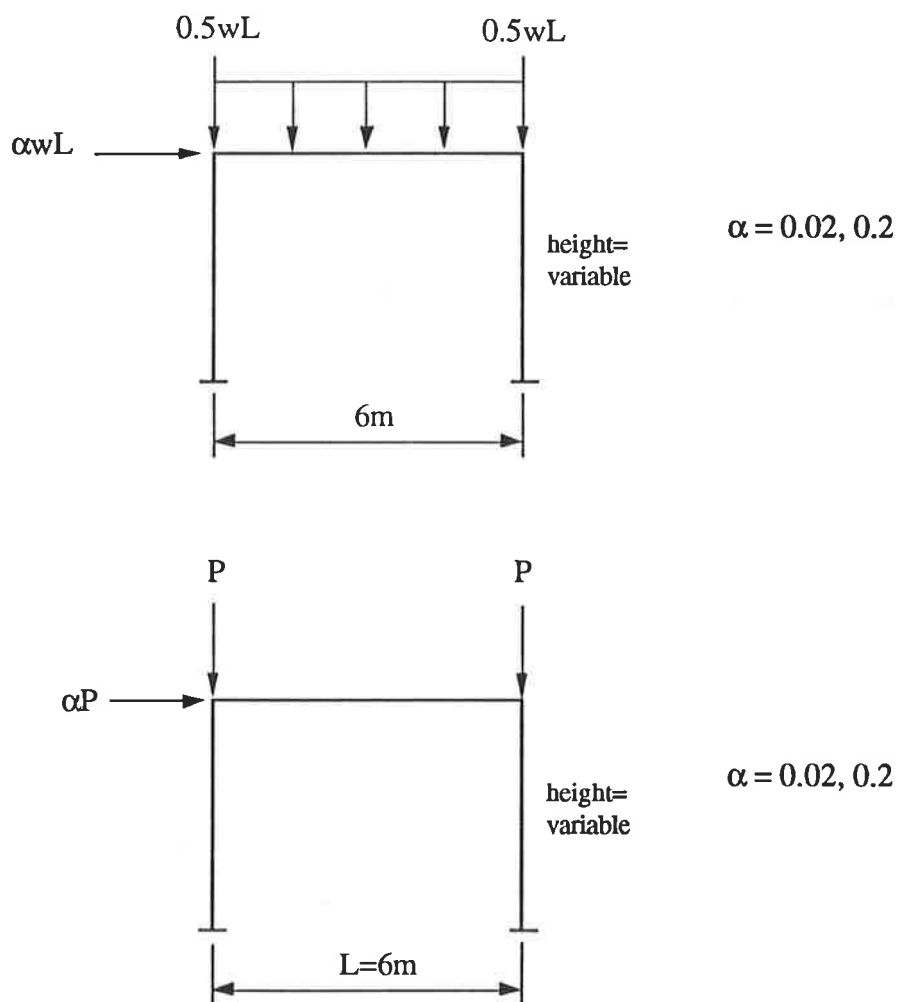
Figure 6.4: Configuration of unbraced portal frames analysed by Wong (1989)

A wide range of values for beam reinforcement was used in the study by Wong to allow the influence of beam reinforcement on column strength to be investigated. An earlier study by Pagay *et al.* (1970) showed that beam reinforcement has a significant effect on column strength.

To compare analytical results between the top, middle and bottom-tier methods, two types of strength prediction were made. These approaches were termed ultimate strength and design strength predictions. In the ultimate strength prediction, material properties were based on average (not characteristic) values. For concrete, the average compressive strength, f_{cm}, was 35 MPa, with a peak strength, $f_{cmax} = 0.85f_{cm}$. The average yield stress for steel was $f_{sy} = 460$ MPa. All strength capacity reduction factors were removed. For the moment magnifier method, there was no upper limit for the unbraced storey magnifier, δ_s, and for the middle-tier approach, second order analyses were performed without any limitation on the relative displacements of compression members.

For design strength predictions, material properties were based on characteristic values. The characteristic strength for concrete, f'_c, was assumed to be 30 MPa and the yield strength of the reinforcement was assumed to be 400 MPa. To check the design strength of frames by the bottom-tier and middle-tier methods, the strength reduction factor, ϕ, was included in each analysis. For the moment magnifier method, an upper limit of δ_s equal to 1.5 was imposed. AS 3600 restricts a second order elastic analysis to frames where the relative displacement of the ends of compression members is $L_u/250$. Unfortunately, the design strength predictions by Wong appear to have been made assuming no limit to the relative displacements.

To enable comparisons between the top-tier method and the two simplified methods for design strength prediction, a global strength reduction factor was applied to the load determined by the top-tier method. This was deemed to be more appropriate than applying the factor to the section strength because ultimate frame load does not necessarily occur when the ultimate strength of a single cross section is first reached.

The global strength reduction factor was assumed to be equal to the strength reduction factor, ϕ, at the critical section governing the design strength of the bottom-tier or middle-tier methods. Even for the simplest of frames this is a crude approach, which does not take into account the degree of indeterminacy, (Warner, 1993).

Analytical results for all unbraced frames are summarised in the four histograms in Figures 6.5 and 6.6. Plotted along the horizontal axis is the ratio of ultimate load predicted by the middle-tier or bottom-tier method to the ultimate load determined by the top-tier method. A ratio greater than 1.0 indicates the simplified method is unconservative. The vertical axis, labelled frequency, is the number of times each ratio occurred.
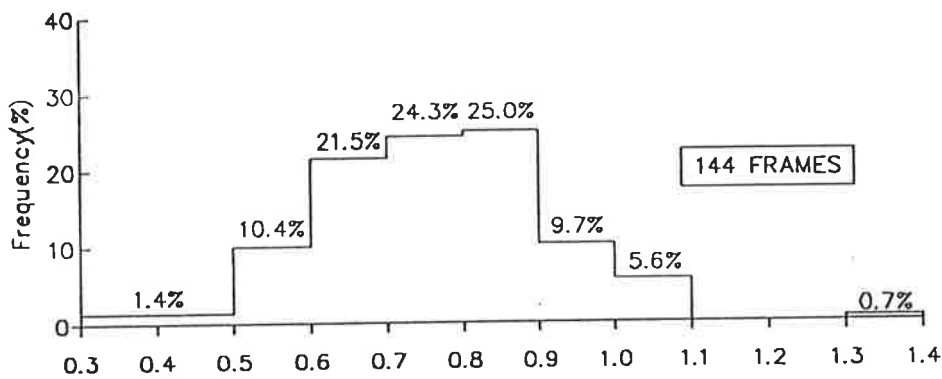
(a) ultimate strength
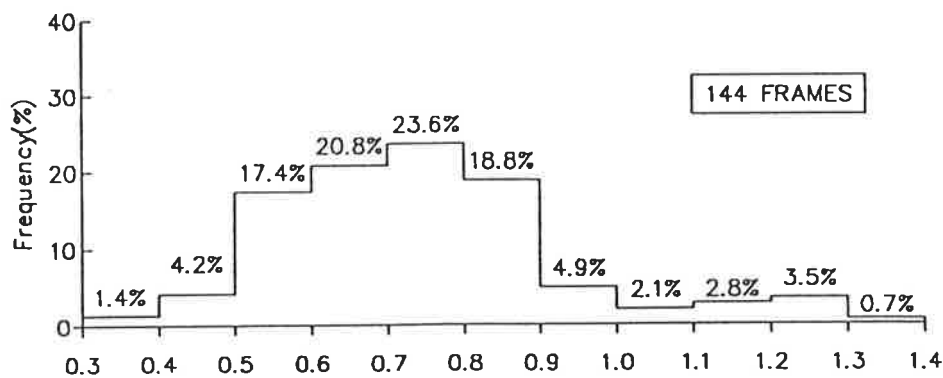
(a) design strength

Figure 6.5: Histograms for bottom-tier method
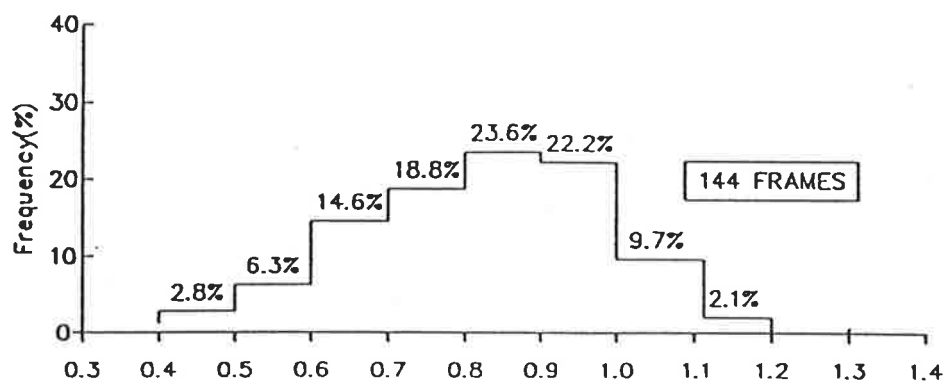
(a) ultimate strength
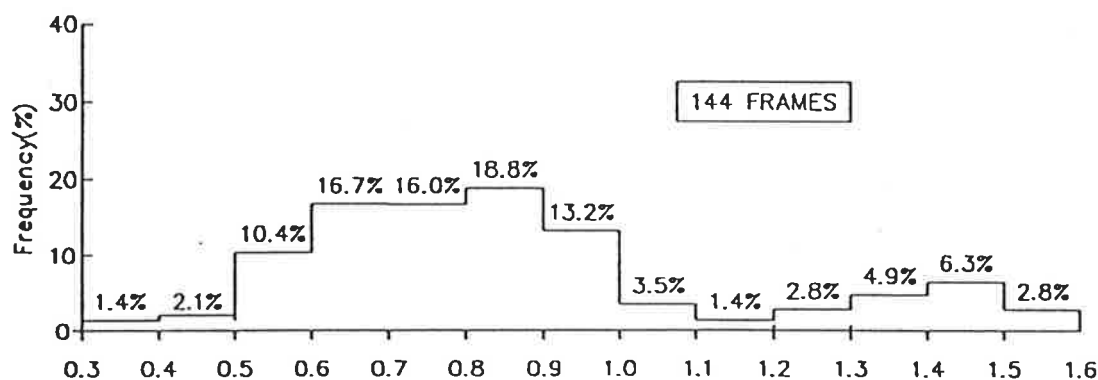
(b) design strength

Figure 6.6: Histograms for middle-tier method

Figure 6.5a shows that 6.3% or 9 of the 144 frames yielded unconservative results for prediction of ultimate strength by the bottom-tier method. All nine frames had no beam loading and were subjected to horizontal loads of 0.02P, where P is the column axial load. It is possible the mode of failure in each case was a stability failure. Of the 144 frames analysed, bottom-tier beam failure occurred in 55 frames, and 89 frames were limited by bottom-tier column failure.

Comparisons of bottom-tier design strength predictions for the unbraced frames are shown in Figure 6.5b. The results show that 38 frames were eliminated because the

storey moment magnifier was greater than 1.5. In these cases, a bottom-tier method of design and analysis is unsuitable and a rigorous method of analysis is required. However, the comparison ratios of the remaining 106 frames, show that the bottom-tier method is conservative. The frames with very conservative comparison ratios, e.g. ratios which are less than 0.5, have bottom-tier beam failures as limiting criteria for peak load.

To a carry out a second order elastic analysis, computer program NEWTONR was developed by Wong. The method involves augmenting the standard first order linear elastic stiffness matrix with a geometric matrix proposed by Jennings (1968). This latter matrix takes into account changes in nodal positions of a structure under load, but not the displacements which can develop within the length of columns. Material effects are taken into consideration with constant values of EA and the modified flexural stiffness values for beam and columns of $0.4E_cI_g$ and $0.8E_cI_g$ respectively.

Comparison ratios for ultimate strength prediction for the middle-tier method are shown in Figure 6.6a. A total of 17 (or 11.8%) frames out of the set of 144 frames produced unconservative results. The bottom-tier method also predicted unconservative results for these frames. In all cases, the column axial loads and lateral loads are likely to induce significant second order effects. Middle-tier beam failure occurred in 83 frames and column failure occurred in 61 frames. This varies considerably from the bottom-tier predictions of 55 frames with beam failure and 89 frames with column failures corresponding to the peak loads on the structures. One reason is that both approaches assume different values for beam and column flexural stiffness.

The results for design strength by the middle-tier method are summarised in Figure 6.6b and show that 31 (or 21.7%) of the 144 frames analysed give unconservative results. In addition, 30 of these frames have horizontal and column axial loading but no beam loading. Unfortunately, no mention was made that the method should only be used if the relative end displacement of the columns is less than $L_u/250$. Four of these frames are re-examined in the present study to determine whether middle-tier

analyses are appropriate. The properties of the frames are summarised in Table 6.1 and each frame is subjected to column axial loading, P, and horizontal loading, $0.02P$.

Table 6.1: Portal frames analysed by middle-tier method

| | Frame height | l_e/r | Reinforcement | | P_{mid}/P_{top} | $L_u/250$ (mm) | Sway Deflection (mm) |
			Beam (%BH)	Column (%BH)			
FRAME1	3m	48	5.0	2.0	1.28	12	10
FRAME2	9m	127	3.0	2.0	1.31	36	100
FRAME3	3m	48	4.0	4.0	1.28	12	13
FRAME4	6m	88	3.0	4.0	1.23	24	68

For all four frames summarised in Table 6.1, the peak load predicted by middle-tier analyses is greater than the peak load predicted by top-tier analyses, i.e. the comparison ratios P_{mid}/P_{top} are greater than 1.0. This indicates the middle-tier results are unconservative. However, for FRAME2, FRAME3 and FRAME4 the column lateral displacement from middle-tier analyses is greater than the recommended limit of $L_u/250$. Note that FRAME1 has a column sway deflection of 10 mm at the peak load which is just less than the allowable limit of 12 mm. AS 3600 also recommends the simplified methods should only be used if the column slenderness ratio is less than 120; FRAME2 has a slenderness ratio of 127.

The middle-tier analytical results suggest a stability failure may have occurred in these frames. It is interesting to note that top-tier analytical results predicted frame instability in all four frames. It can be concluded from these results that an upper limit of $L_u/250$ for column displacements is a reasonable estimate for predicting an instability failure in a middle-tier analysis.

A series of braced frames was also examined in the study by Wong (1989). Predictions of ultimate and design strength for middle-tier and bottom-tier methods were made and in all cases the comparison ratios were conservative, i.e. the failure loads predicted by the simplified methods were lower than the peak loads determined by the top-tier method of analysis.

6.5.3   Conclusions

Previous investigations for the accuracy and adequacy of the simplified methods have been made for isolated pin-ended columns and for columns in braced and unbraced frames. In the study of frames by Wong (1989), the moment magnifier method and the second order elastic method gave satisfactory results. Results in some cases were overconservative, i.e. 30% to 50% of the top-tier predicted results. Unconservative strength predictions were made for a number of frames, but in these cases the allowable limits of $\delta_s = 1.5$ for the storey moment magnifier and $L_u/250$ for the second order method were exceeded. Hence, these two simplified approaches appear to be satisfactory.

Two three-storey two-bay frames with 300 mm by 300 mm beam and column sections were also analysed by Wong. Although the dimensions for the beam sections appear to be unrealistic for multi-storey frames, both the moment magnifier method and the middle-tier method gave conservative results for the two frames analysed.

In the frames study by Wong, non-linear behaviour due to concrete compressive and steel stress-strain relationships and geometric effects were taken into account. However, tension stiffening and the influence of joint deformations on frame strength were ignored. The effect of these non-linearities on frame strength are investigated in the following section. Columns within multi-storey frames and multi-bay frames are also examined in Section 6.6.

6.6 Present Investigation of Slender Columns in Sway Frames

6.6.1 Introduction

Frames chosen for analysis are divided into a number of series to investigate various non-linear effects. The frames are described in Sections 6.6.3 to 6.6.6.

6.6.2 Analytical Models

To investigate frame behaviour and strength predictions by the moment magnifier and middle-tier approaches, two types of strength prediction made. These are: (1) ultimate strength; and (2) design strength predictions.

Ultimate strength predictions are based on average values for material properties and all safety coefficients and strength reduction factors are ignored. This allows second order predictions to be compared directly with results from a rigorous method of analysis.

Construction of the strength interaction diagram is based on a ϕ factor set equal to 1.0. To determine frame capacity by either the middle-tier or moment magnifier methods, each individual beam and column member is checked for its capacity. Frame capacity corresponds to the lowest value of peak load in a member. This approach differs to ultimate frame load determined by a top-tier analysis, where strength in one or more sections may have been reached before the ultimate frame load is reached.

Design strength predictions are made in order to investigate the effect of safety coefficients and design values for material properties. Similar to the study by Wong (1989), a global strength reduction factor is applied to the peak load determined by the top-tier method. This value is assumed, for convenience, to be equal to the strength

reduction factor, ϕ, at the critical section governing the design strength of the bottom-tier or middle-tier methods.

The code recommended limits of δ_s equal to 1.5 for the moment magnifier method and $L_u/250$ for the middle-tier method only apply to design strength calculations. No limit applies where ultimate strength calculations are made.

Where a member is subjected to bending and axial tension, a simplified strength interaction diagram is constructed, as in Figure 6.7. A straight line is drawn between the ultimate strength in bending, M_{uo}, and the ultimate strength in tension without bending, for an axially loaded cross-section, N_{uot}. The value of N_{uot} assumes the concrete to have no tensile capacity.
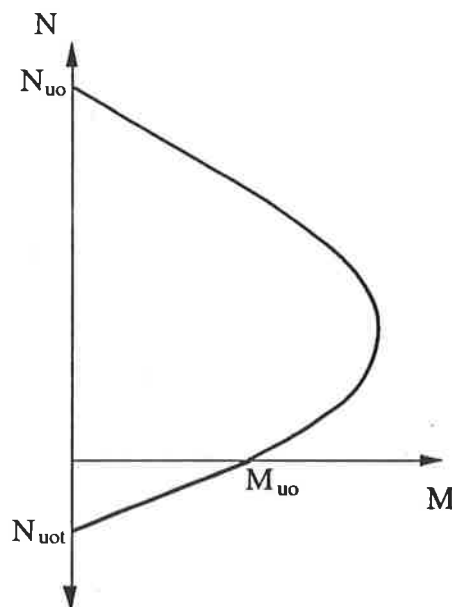
Figure 6.7: Strength interaction diagram for a member in tension

All frames analysed in this section are unbraced against sidesway. Beam and column elements have reinforcement which is 2.0% of the gross sectional area and, for convenience, the reinforcing steel is assumed to be distributed equally to two layers.

Various non-linear effects are taken into account in each rigorous method of analysis. The following analytical models are used to describe increasing levels of material non-linearity:

- Model I : tension stiffening is ignored
- Model II : tension stiffening effects are included
- Model III : tension stiffening and joint modelling are included

In all cases, full geometric effects are allowed for, and is done so by inserting a sufficient number of nodes in the column members. This takes into account lateral movement at the column ends and also within the length of the columns. Second order effects are not usually a problem in beams. Hence, they are represented by single elements.

Material properties for ultimate strength are given by the following:

Concrete

- average compressive strength : $f_{cm} = 37$ MPa;
- peak strength in a member : $f_{cmax} = 0.85 f_{cm}$;
- elastic modulus : $E_c = 5000 \sqrt{f_{cm}}$, f_{cm} and E_c in MPa

Steel

- average yield stress : $f_{sy} = 460$ MPa;
- elastic modulus : $E_s = 200{,}000$ MPa

Material properties for design strength are:

Concrete

- characteristic strength : $f'_c = 32$ MPa;
- peak strength in a member : $f_{cmax} = 0.85 f'_c$;

- elastic modulus : $E_c = 5000\sqrt{f'_c}$, f'_c and E_c in MPa

Steel

- design yield stress : $f_{sy} = 400$ MPa;
- elastic modulus : $E_s = 200,000$ MPa

6.6.3   Series I Frames

6.6.3.1   Introduction

Frame capacities by ultimate strength predictions are calculated for several single storey frames. Strength predictions are also made by top-tier models I, II and III.

Frames are either single bay or have five bays and all column sections are 400 mm by 400 mm. To investigate the influence of tension stiffening and joint flexibility on frame behaviour, two types of beam section have been chosen. Beams which are relatively stronger and stiffer are 400 mm by 800 mm deep. The other type of beam, which is 400 mm by 400 mm deep, is more flexible.

Although it is usual to ignore tension stiffening in ultimate strength predictions, a previous study by Okamura *et al.* (1970) showed that cracked beam stiffness has an influence on column strength. Top-tier model I ignores tension stiffening and top-tier model II includes the tension stiffening model developed in Chapter 3 .

Frames in Series I are also analysed for joint deformations by including in the non-linear frame analysis the joint model for T-joints and L-joints which has been developed in Chapter 4. This analysis is top-tier model III. The study of test corners and test frames in Chapter 4 showed that the performance of L-joints and T-joints can be adversely affected by certain loading conditions.

6.6.3.2   Configuration of Frames

Frames 1A1 and 1A2, which have columns with fixed bases, are shown in Figure 6.8. Columns in frame 1A1 have a slenderness ratio of 44, and frame 1A2 with shallow beams has columns with a slenderness ratio of 51. Frames 1A1 and 1A2 are analysed for joint deformations because opening corners are created under the given loading conditions. An opening corner is created at the left hand L-joint and a closing corner is created at the right hand L-joint. Beam loading has not been included because application of beam loading reduces the magnitude of opening corner moments. At higher ratios of vertical load to horizontal load, the moments in the left hand L-joints actually change sign and closing corner moments are created.

All members of frames in Series I have percentages of steel, p, of 1.1%, where $p = A_{st}/bd$. Note in this expression the effective depth d has been used. From the study of beam sections in Chapter 3, it can be expected tension stiffening to be significant at this percentage of tensile reinforcement.

All of the five-bay frames, 1B1, 1B2, 1C1 and 1C2, have pinned feet. Frames 1B1 and 1C1 have identical structural properties and all columns have a slenderness ratio of 66. Frames 1B2 and 1C2, with shallow beams, have external columns with a slenderness ratio of 75 and internal columns with a slenderness ratio of 68.

Frames 1B1 and 1B2, shown in Figure 6.9, are also analysed for joint deformations. These frames are subjected to column axial loading and lateral loading which create opening corners in the left hand L-joints. An inspection of the moments in each member entering the T-joints showed that joint deformations can also be expected to occur within these joints.

Shown in Figure 6.10 are frames 1C1 and 1C2, which are subjected to beam loading. These frames are not analysed by top-tier model III because joint deformations do not develop under the given loading pattern. Application of the beam loading tends to

close the angle between each beam and column element of the L-joints and T-joints, thus preventing the formation of inclined cracks.
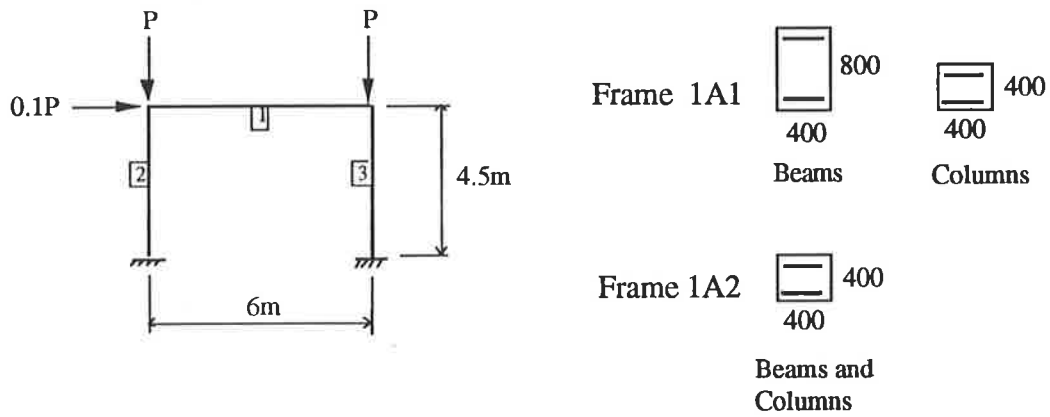
Figure 6.8: Configuration of single bay portal frames, 1A1 and 1A2
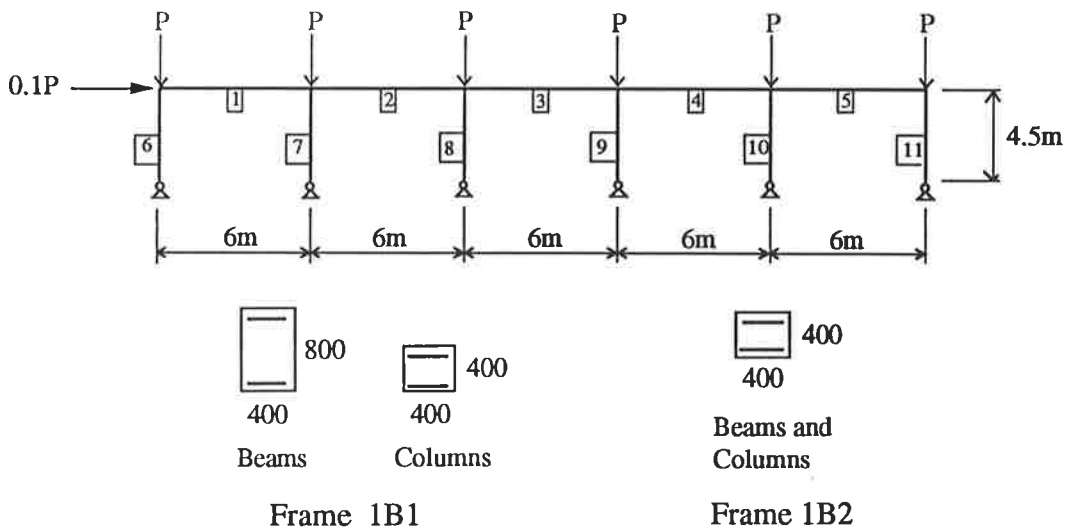
Figure 6.9: Configuration of multi-bay frames 1B1 and 1B2
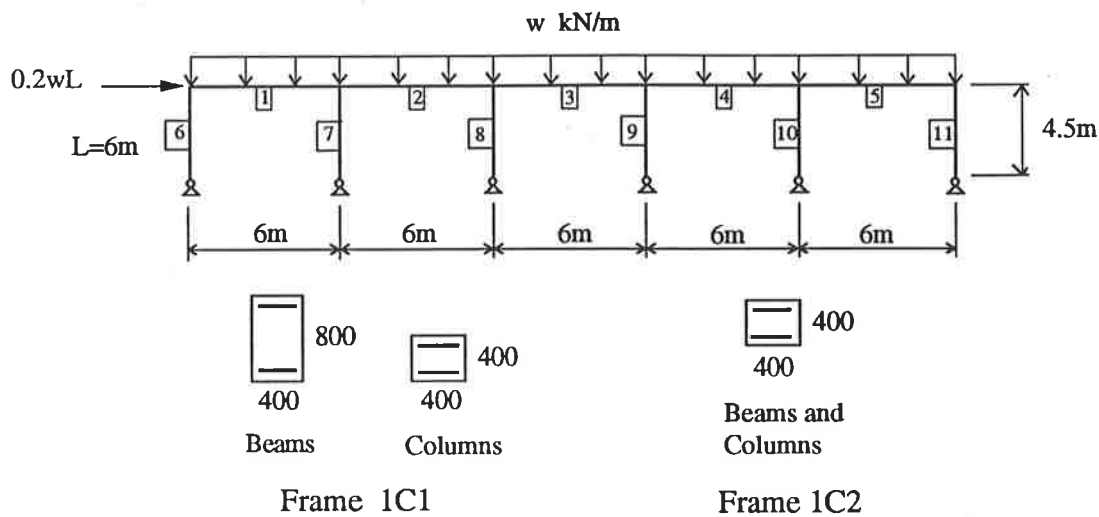
Figure 6.10: Configuration of multi-bay frames 1C1 and 1C2

6.6.3.3 Analytical Results for Series I Frames

As shown in Table 6.2, the top-tier model II analysis predicts a peak load of 3163 kN for frame 1A1. This analysis includes the influence of tension stiffening, but ignores additional joint deformations. Top-tier model I which ignores the effect of tension stiffening, predicts a peak frame load of 3125 kN. This analysis underestimates the peak load of model II by only 1.0%.

Shown in Figure 6.11 is load versus deflection of frame 1A1 for analyses by top-tier model II and model III. At the peak load of model II, material strength has been reached in a segment at the bottom of column 3. With increasing deformation, a softening hinge forms in this critical section. Frame instability failure occurs, corresponding to the formation of an insufficient number of hinges. This frame also has limited ductility.

Table 6.2: Comparison ratio of P_{ult} for each analysis to P_{ult} by top-tier (model II) for frames 1A1 and 1A2

Method of Analysis	Frame 1A1		Frame 1A2	
	P_{ult} (kN)	ratio	P_{ult} (kN)	ratio
Top-tier (model I)	3125	0.99	2597	0.99
Top-tier (model II)	3163	1.0	2618	1.0
Top-tier (model III)	2904	0.92	2176	0.83
Middle-tier	3024	0.96	2504	0.96
Moment magnifier	2738	0.87	2374	0.9
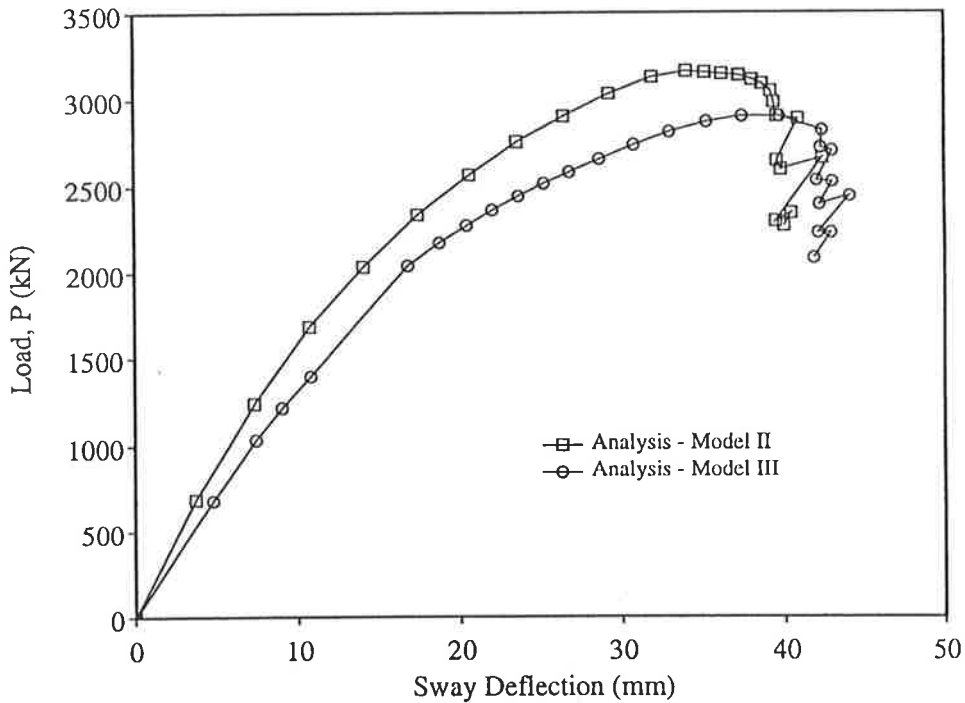
Figure 6.11: Load versus deflection for frame 1A1

Top-tier model III analysis includes joint modelling for the left hand L-joint where an opening corner is created. A sectional analysis for the beam element and a separate calculation for a section through the column element showed that beam strength is greater than 1.4 times the strength of the column. Note also that beam depth is twice

the column thickness. Based on the joint model by El-Metwally and Chen (1988), and discussed in Chapter 4, a hinge is expected to form at the top of the column. Hence, analysis for joint deformations by the proposed joint model in the present study includes two segments at the top of column 2, where joint deformations are expected to occur. This analysis predicts a peak load of 2904 kN, but frame capacity is only reduced by 8% due to joint deformations.

Table 6.2 shows that the peak load predicted by the moment magnifier method is 2738 kN and the critical section occurs within column 3. The middle-tier analysis predicts a peak load of 3024 kN, which is an underestimation of the peak load of top-tier model II by 4%. The middle-tier analysis also predicts the critical section to occur at the base of column 3.
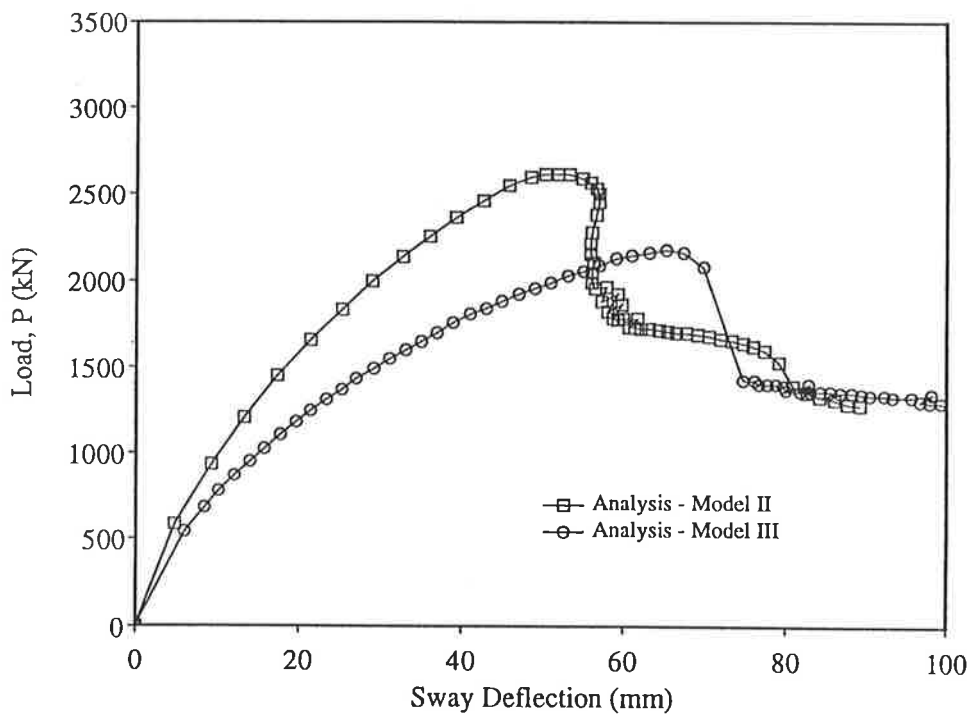
Figure 6.12: Load versus deflection for Frame 1A2

Table 6.2 shows that by ignoring tension stiffening (i.e. model I), the peak frame load for frame 1A2 is underestimated by only 1%. Figure 6.12 shows that for top-tier model II the frame undergoes load softening after the peak load of 2618 kN. The peak load also corresponds to the formation of softening hinges at three locations: the left hand of the beam and at the bases of column 2 and column 3.

The top-tier analysis for joint deformations is given by model III. Under the given loading configuration, an opening corner is created at the top of column 2. Since the beam and column elements have the same section properties, hence the same flexural strength, a joint segment is inserted at the left hand end of the beam element and a joint segment is included at the top of column 2. A considerable reduction in stiffness due to joint deformations is evident. The maximum load for this analysis is 2176 kN and frame capacity is also reduced by 17% due to joint deformations.

It is interesting to note that in this analysis overall frame behaviour is controlled by the load-deformation response of the segment at the top of column 2, which enters the opening corner. This is in contrast to the top-tier analyses by model I and model II, where the critical sections are at the base of column 3.

The predicted peak frame load by the moment magnifier method is 2374 kN, which is 10% less than the peak value determined by the top-tier model II analysis. The critical section by the moment magnifier method is within column 3. The middle-tier analysis underestimates frame capacity by 4%, and although frame instability has occurred, the middle-tier analysis provides an accurate prediction of the frame peak load.

Table 6.3: Comparison ratio of P_{ult} for each analysis to P_{ult} by top-tier (model II) for frames 1B1 and 1B2

Method of Analysis	Frame 1B1		Frame 1B2	
	P_{ult} (kN)	ratio	P_{ult} (kN)	ratio
Top-tier (model I)	2860	0.98	2088	0.98
Top-tier (model II)	2932	1.0	2153	1.0
Top-tier (model III)	2890	0.99	1465	0.68
Middle-tier	2883	0.98	2184	1.01
Moment magnifier	2567	0.88	2320	1.08
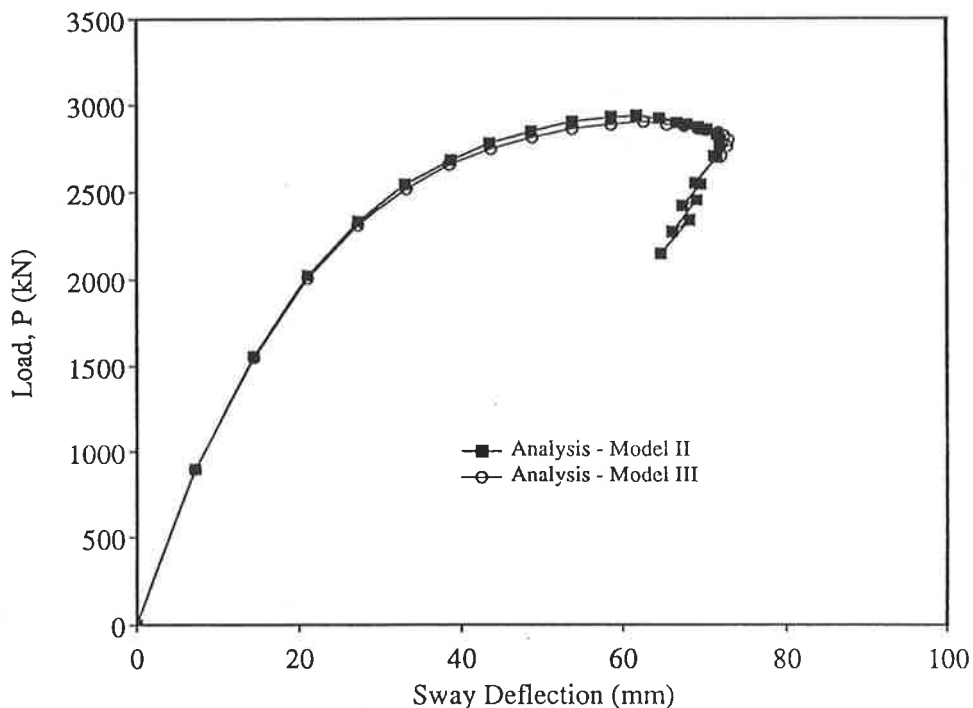
Figure 6.13: Load versus deflection for frame 1B1

Analytical results for frame 1B1 are shown in Table 6.3. The non-linear analysis ignoring tension stiffening predicts a peak load of 2860 kN, compared to a peak frame load of 2932 kN as predicted by the analysis including tension stiffening effects. The difference here is only 2%. Just prior to the peak load of model II, a softening hinge forms at the top of column 7. Hinges also form shortly after at the tops of columns 8, 9 and 10. Failure within the beams does not occur. One likely reason is that the beams are 800 mm deep and relatively much stronger than the columns which are 400 mm deep. Note also that the columns are subjected to significant axial loading, whereas the beams act primarily as flexural elements.

Shown in Figure 6.13 is load versus deflection for analyses by top-tier model II and model III. Analysis by the latter takes into account joint deformations and has predicted a peak load of 2890 kN. Frame capacity is only reduced by 1.0% and there appears to be no noticeable loss of stiffness under increasing load. The study of T-joints in Chapter 4 showed that, regardless of relative member sizes, joint deformations are largely confined to the beam element. Joint segments have been

inserted in the beam elements of frame 1B1 for the model III analysis, but the beams appear to have sufficient residual strength and stiffness so that frame performance is not adversely affected by joint deformations.

The moment magnifier method predicts a peak load of 2567 kN and the critical section occurs in column 7. Frame capacity is underestimated by 12%.

The peak load of 2883 kN for frame 1B1 by the middle-tier analysis is only a 2% underestimation of the value predicted by the top-tier model II analysis. The critical section also occurs at the top of column 7.
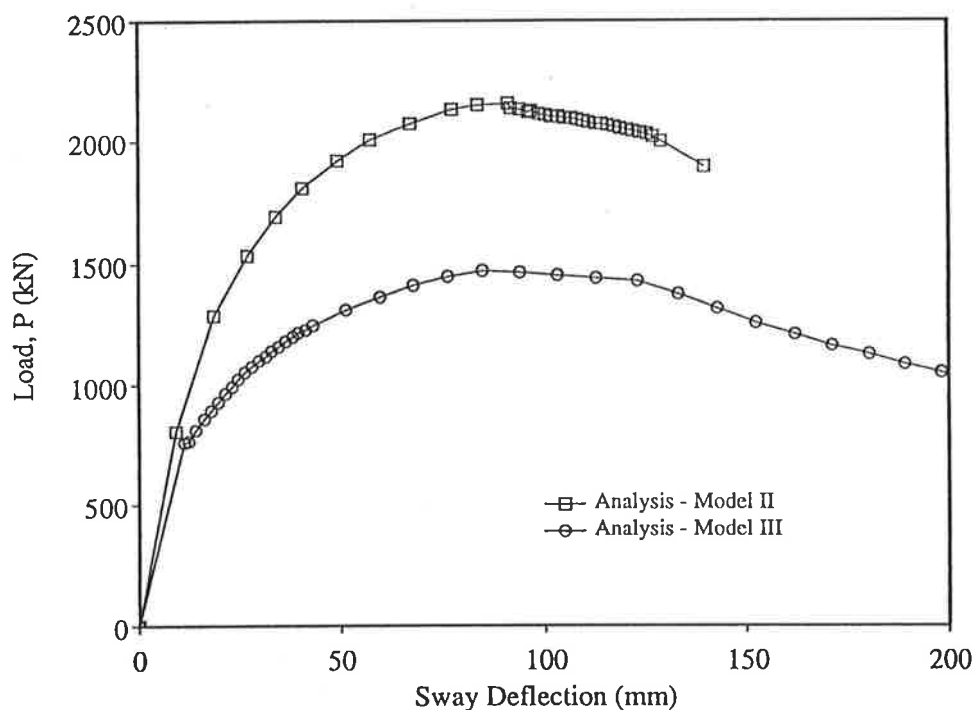
Figure 6.14: Load versus deflection for frame 1B2

Analytical results for frame 1B2 are also summarised in Table 6.3. Top-tier analytical model I, which ignores tension stiffening effects, only underestimates frame capacity of top-tier model II by 2%. Analysis by model II showed that, although significant deformations occur in the beam elements, frame failure corresponds to the formation of an insufficient number of hinges.

Figure 6.14 shows load versus deflection for frame 1B2. Unlike frame 1B1, the effect of joint deformations on frame behaviour is noticeable here. A gradual loss in frame stiffness can be observed with increasing load and the overall strength of the frame is reduced from 2153 kN to 1465 kN, i.e. a reduction of 32%. Note that frame 1B2 has beams which are 400 mm deep, compared to frame 1B1 with 800 mm deep beams. It is apparent the effect of inefficient T-joints on frame behaviour is most severe with relatively shallow beams.

The moment magnifier method overestimates peak load by 8% and the critical section occurs within column 7. In contrast, the middle-tier analysis shows a very good estimate of peak load of 2184 kN, which is within 1% of the top-tier model II prediction of 2153 kN. The critical section by the middle-tier analysis occurs within beam 1, which is also the location of the first formed hinge by the top-tier analysis.

The middle-tier analysis also predicts column capacities of all internal columns which are within 3% of the capacity of the critical section. This compares well with the top-tier analytical results, which showed hinges had formed at the top of columns 7 and 8.

Table 6.4: Comparison ratio of w_{ult} for each analysis to w_{ult} by top-tier (model II) for frames 1C1 and 1C2

Method of Analysis	Frame 1C1		Frame 1C2	
	w_{ult} (kN/m)	ratio	w_{ult} (kN/m)	ratio
Top-tier (model I)	303	0.98	104	0.98
Top-tier (model II)	308	1.0	106	1.0
Middle-tier	191	0.62	63	0.6
Moment magnifier	200	0.65	61	0.58

Table 6.4 summarises the analytical results for frames 1C1 and 1C2, which are single-storey five-bay frames. Top-tier model III analyses for joint deformations were not

performed because under the given loading configuration opening corners are not created in the L-joints, and the moments in the beam elements entering the T-joints also tend to close these joints. In both frames 1C1 and 1C2, the analyses which ignore tension stiffening only underestimate the frame peak loads by top-tier model II by 2%.

The load versus deflection results for frame 1C1 are shown in Figure 6.15. This frame displays a catastrophic failure after the peak frame load of 308 kN/m. Two column sections have failed: at the top of column 6 and the top of column 11. Frame failure is sudden, and there is no obvious failure of the beams.

The moment magnifier method predicts the critical section to occur within column 11, and the corresponding peak load of 200 kN/m underestimates the peak load by top-tier model II analysis by 35%.

The middle-tier analysis predicts an ultimate frame load of 191 kN/m corresponding to a critical section in column 11. This is a conservative estimate for peak load and is 62% of the top-tier model II prediction of ultimate load. Lateral displacement of columns is 28 mm at the peak load which is considerably less than the deflection at peak load of 90 mm predicted by the top-tier model II analysis. It is worth noting that, while this analysis gives a conservative prediction of frame strength, the predicted capacities in remaining members are more than 40% higher than the capacity of the critical section. This point illustrates the importance of choosing the critical section as the basis for determining frame capacity.

Top-tier model II analysis for frame 1C2 (Figure 6.16) shows that a series of beam hinges form as loading increases up to the peak load of 106 kN/m. Failure within the columns is not predicted. Although the analysis was not carried out into the collapse region, results showed that after the peak load all columns had undergone unloading of moment and curvature.

The moment magnifier method predicts the critical section to occur in beam 1. The failure load for this element is 61 kN/m which is 58% of the top-tier model II

prediction for frame strength. The predicted capacity by the bottom-tier method for beam 4 is 66 kN/m. Figure 6.16 shows that a hinge forms in beam 1 at a load of 75 kN/m followed shortly by a second hinge in beam 4. Predicted column capacities are considerably higher than the capacity of the critical section. These predictions appear to be reasonable.

The middle-tier analysis also predicts a conservative estimate of peak load. The value of 63 kN/m is 60% of the top-tier model II value. Middle-tier results also show that the critical section occurs within beam 1 and the predicted capacity for beam 4 is 67 kN/m. This suggests that the middle-tier method has provided a reliable prediction for frame capacity and column analysis.
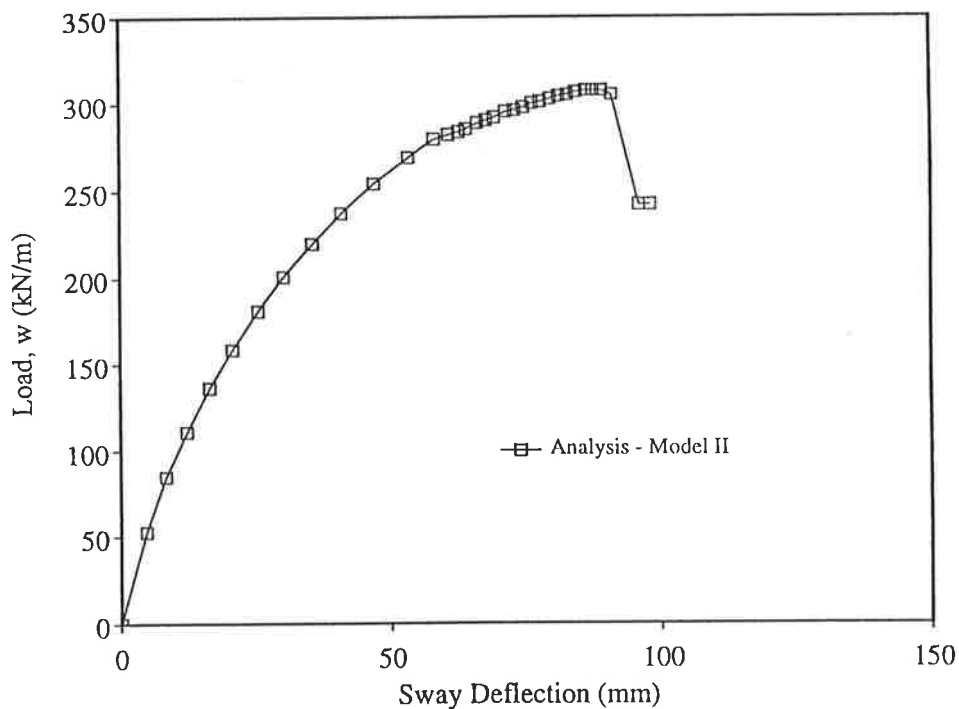
Figure 6.15: Load versus deflection for frame 1C1
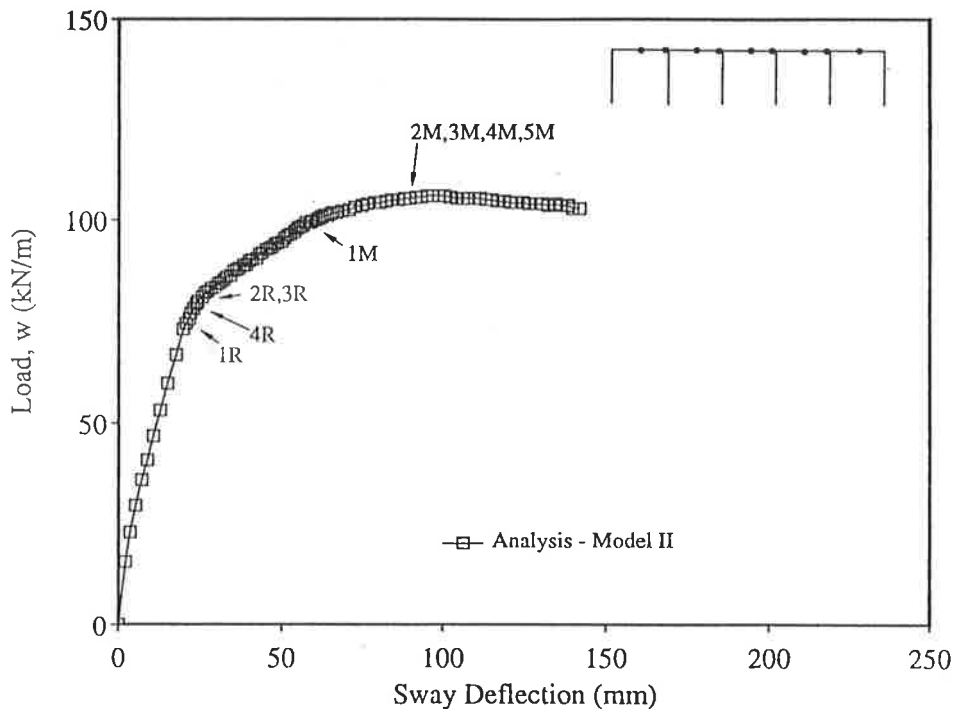
Figure 6.16: Load versus deflection for frame 1C2

6.6.3.4   Summary and Conclusions

Beams and columns within frames in Series I contained relatively low percentages of steel, hence the effect of tension stiffening on stiffness was beneficial. It was aslo shown in this section that frame strength was increased by 1-2% due to tension stiffening effects. It had been shown in an earlier study by Okamura *et al.* (1970) that cracked beam stiffness affects the strength of adjoining column members.

Usually, tension stiffening is ignored in strength calculations, which is reasonable for simple beams. It is also a reasonable assumption for frames with high percentages of steel, e.g. where members have greater than about 2.5-3.0% tensile steel.

The influence of joint deformations on frame performance was also investigated in Series I. It was shown that both strength and stiffness can be adversely affected by the behaviour of T-joints and L-joints of single-storey frames. This occurred in frames with columns and beams of similar section reinforcing details and section size. Frames with deeper beams, e.g. where beam depth is twice the column thickness, have additional beam stiffness to resist lateral loading.

Frame 1A1, with an 800 mm deep beam, had a 8% strength reduction due to joint deformations in the opening L-joint. This compares with a 17% strength reduction in frame 1A2 due to joint deformations. This frame has a 400 mm deep beam.

Multi-bay frame 1B1, with 800 mm deep beams, was analysed for deformations in the T-joints. Capacity reduction for this frame was only 1%, and results for load versus deflection showed a very minor loss in stiffness due to joint flexibility. However, frame 1B2, with 400 mm deep beams, was severely affected by joint deformations. Strength was reduced by 32% and the gradual reduction in stiffness became noticeable at about half the peak frame load.

Of the six frames analysed in Series I, slightly unconservative results by the simplified methods only occurred for frame 1B2. The comparison ratio by the middle-tier and moment magnifier methods, by ultimate strength predictions, were 1.01 and 1.08 respectively. However, the top-tier model II analysis, which included tension stiffening but ignored joint modelling, showed this frame failed by instability.

Unfortunately, neither simplified approach can determine a stability failure. The code restriction that the unbraced moment magnifier δ_s must be less than 1.5 and the column sway deflection in a second order elastic analysis must be less than $L_u/250$ only apply if design strength predictions are made. However, the ultimate strength calculations by the two simplified methods predicted significant second order moments. Taking into account the code recommended limits just mentioned, it is very likely that design strength calculations would have indicated stability failures.

6.6.4 Series II Frames

6.6.4.1 Introduction

In this series, three five-storey frames are analysed and both ultimate strength and design strength predictions are made. Each frame is also analysed by top-tier model II, which includes tension stiffening, but ignores the effect of joint deformations. Although the frames analysed in Series I showed that by ignoring tension stiffening effects frame capacity is only understimated by 1.0 to 2.0%, all top-tier analyses in Series II include tension stiffening to allow more accurate predictions of overall frame performance to be made.

A preliminary check of the frames in this series showed that joint deformations are not likely to occur within the L-joints and the top floor T-joints. The loading conditions imposed on each frame tend to close the beam elements of these joint types, thus preventing the formation of any inclined cracks.

6.6.4.2 Configuration of Frames

All frames have uniform beam and column sizes throughout. Beam sizes differ with each frame type, but columns within all storeys of each frame are 400 mm by 400 mm in section. Beams and columns have reinforcing steel which is 2.0% of the gross-sectional areas, and steel is distributed equally between two layers. The cover to reinforcing layers is 50 mm for all sections, except for the 300 mm deep beams of frame 2C which have cover of 40 mm. Such uniformity throughout a structure is not usually encountered in practice, but has been done for the present study to restrict the number of variables which may influence frame behaviour.

Frame 2A, and shown in Figure 6.17, has beams spanning 8 metres. All columns are 4 metres in height and slenderness ratios are reasonably uniform. Columns within the first storey have l_e/r ratios between 40 and 42, while columns within the second to

fifth storeys have l_e/r ratios in the range 36 to 41. This frame has a relatively low ratio of lateral load to vertical beam load.

Frame 2B, and shown in Figure 6.18, has relatively stiffer beams than frames 2A and 2C and also a relatively higher ratio of lateral load to beam load. Columns within the first storey are 6 metres in height and have l_e/r ratios between 60 and 61. Columns within the second to fifth storeys are relatively stocky with l_e/r ratios in the range 25 to 29.

Structural geometry and section sizes for frame 2C are shown in Figure 6.19. This frame has the same beam spans and column heights as frame 2B. However, the beams of frame 2C are more flexible and have a relatively lower flexural strength. This frame is subjected to a relatively low ratio of lateral to vertical loading. Columns within the first storey of frame 2C are the most slender of all columns analysed in this series, with slenderness ratios between 65 and 71. Columns in the second to fifth storeys are not so slender, with l_e/r ratios in the range 32 to 46.
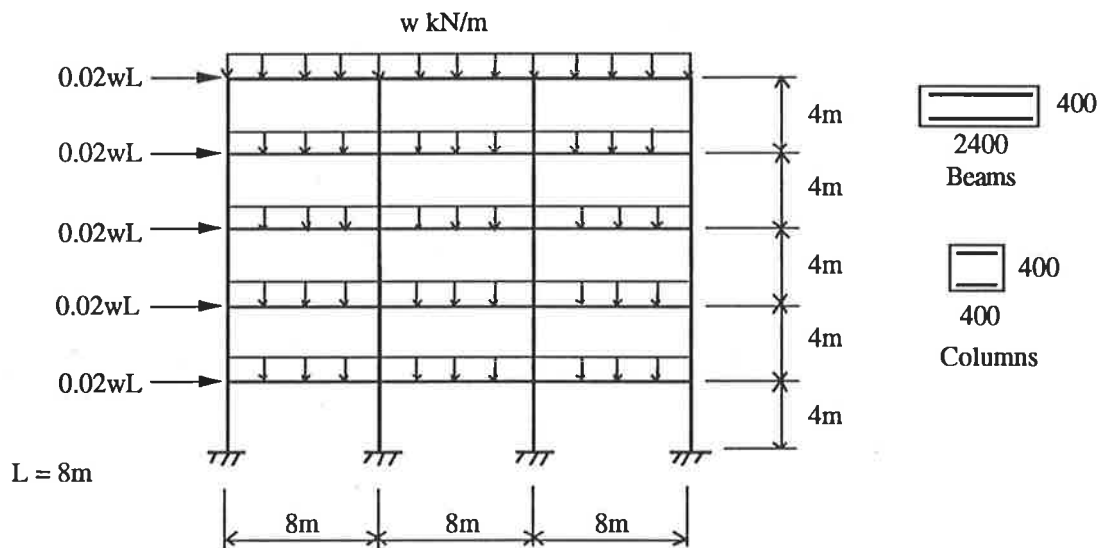
Figure 6.17: Configuration of frame 2A
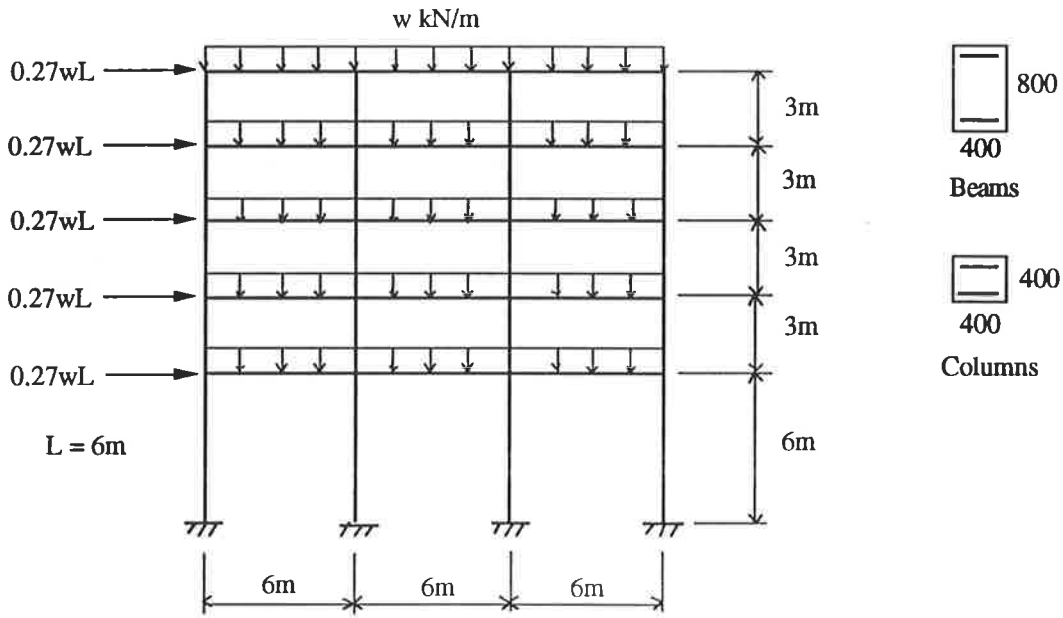
Figure 6.18: Configuration of frame 2B
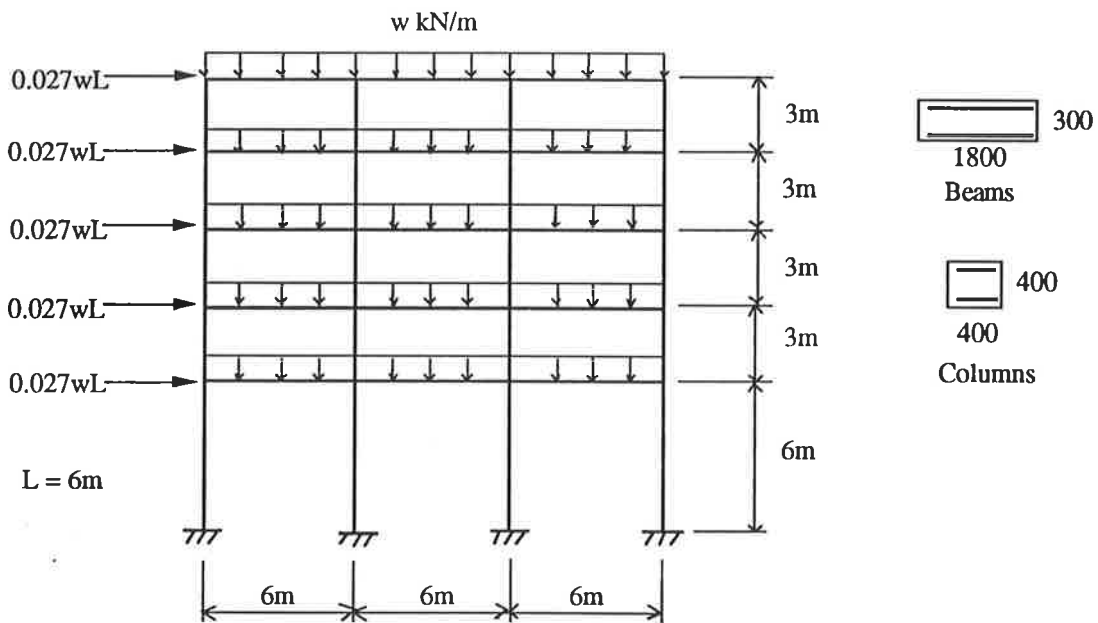
Figure 6.19: Configuration of frame 2C
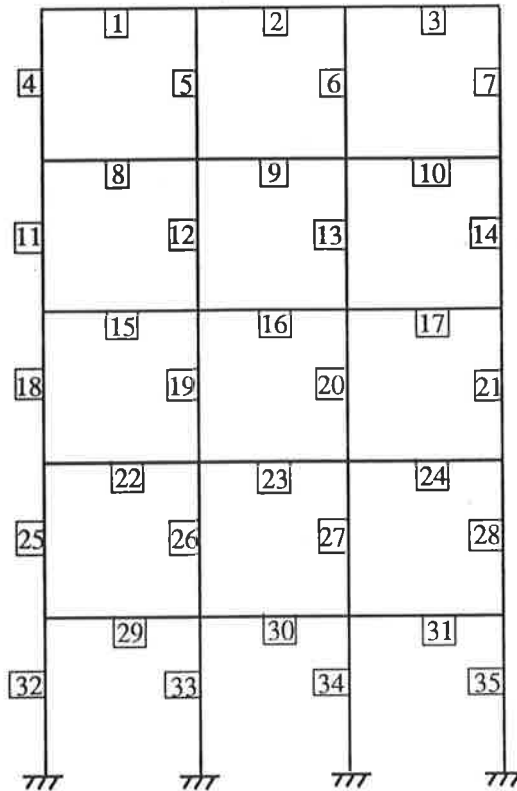
Figure 6.20: Member numbering for five storey frames

6.6.4.3 Analytical Results by Ultimate Strength Predictions

Results for peak frame loads by ultimate strength predictions for each method are shown in Table 6.5. The peak load for frame 2A by top-tier model II is 147 kN/m. The plot of load versus deflection (Figure 6.21) for this analysis also shows that frame failure is catastrophic. Prior to the peak load, hinges have formed at the top and bottom of the first storey internal columns 33 and 34. However, these columns are subjected to significant axial forces and at the peak load of 147 kN/m the axial force in column 33 is approximately $0.98N_{uo}$.

The middle-tier analysis predicts the critical section to occur within column 7. This column fails by primary tension and frame capacity corresponds to a load of 97 kN/m or 0.6 of the peak load predicted by top-tier model II. Column 4 fails at a frame load of 103 kN/m. Similar to the top-tier model II predictions, the middle-tier analysis also

predicts member capacity of column 33 to be reached at 147 kN/m. However, frame capacity by this simplified approach must be taken as the lowest value for any member.

It is interesting to note that the top-tier analysis chooses the key segment at the top of column 7. Although significant deformation occurs within this column, and also within column 4, frame failure by the top-tier analysis is due to the heavy axial loading of columns 33 and 34. These columns have limited ductility which contributes to the instability failure of this frame.

The bottom-tier moment magnifier method also predicts the critical section to occur within column 7, and frame strength is assumed to be reached at a load of 120 kN/m, or 0.82 of the top-tier predicted maximum load. This method also predicts columns 33 and 34 to reach capacity loads of 137 and 143 kN/m respectively.

Table 6.5: Ratio of w_{ult} for each analysis to w_{ult} by top-tier (model II) for Series II frames

Method of Analysis	Frame 2A		Frame 2B		Frame 2C	
	w_{ult} (kN/m)	ratio	w_{ult} (kN/m)	ratio	w_{ult} (kN/m)	ratio
Top-tier (model II)	147	1.0	61	1.0	177	1.0
Middle-tier	97	0.66	48	0.79	118	0.67
Moment magnifier	120	0.82	44	0.72	129	0.73
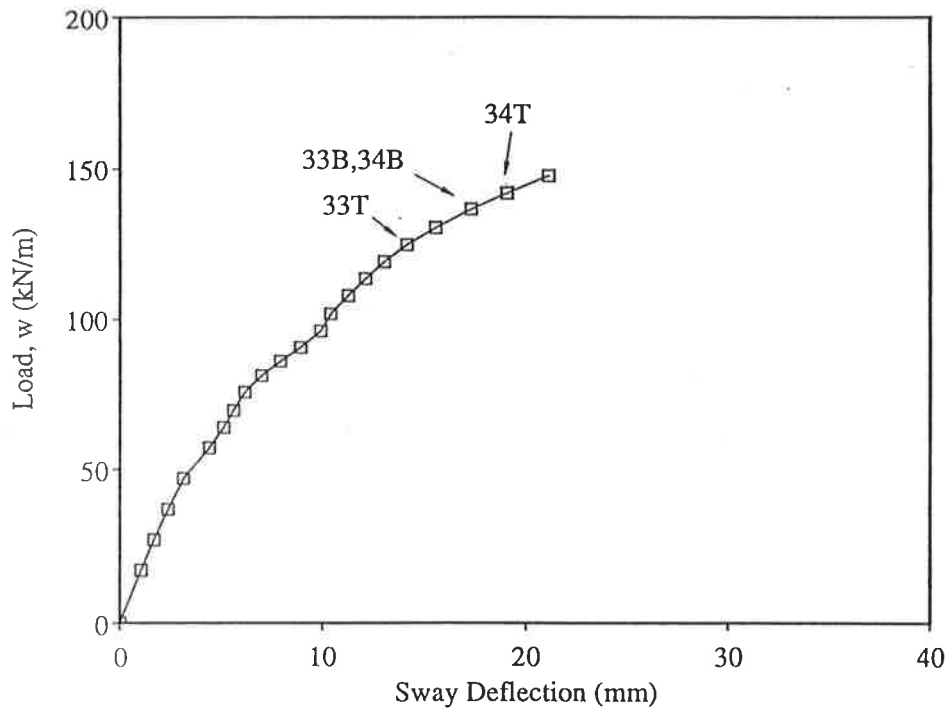
Figure 6.21: Load versus deflection for frame 2A

The load versus deflection results for frame 2B by top-tier model II are shown in Figure 6.22. Hinges form in several first storey columns before the peak frame load of 61 kN/m is reached. However, unlike frame 2A, columns within frame 2B are not subjected to significant axial forces. Note that frame 2B is also subjected to a higher ratio of lateral load to vertical load, which tends to increase the level of moment and reduce the amount of compressive axial force within the first storey columns.

The middle-tier analysis predicts a frame peak load of 48 kN/m corresponding to a critical section at the base of column 32. This value is 79% of the top-tier value of 61 kN/m. Hence, the middle-tier results appear to be satisfactory.

Based on a braced moment magnifier of 1.0, the moment magnifier method predicts the capacity of column 32 to be 55 kN/m. However, frame capacity by this approach is determined by the unbraced moment magnifier for column 32 and the predicted peak load is 44 kN/m. The value for δ_s is 1.19.
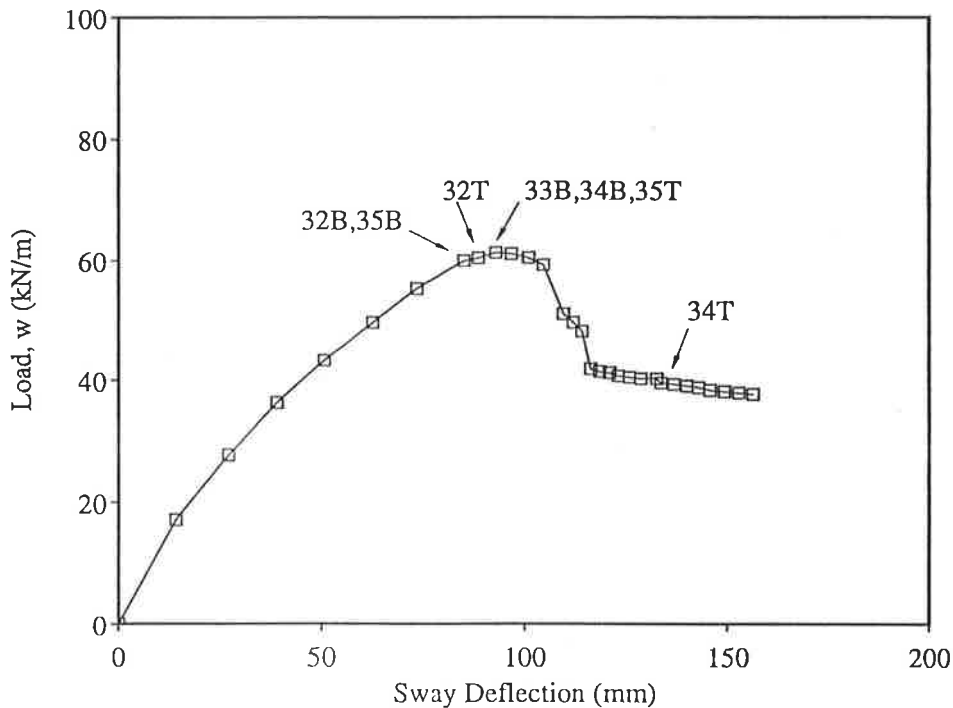
Figure 6.22: Load versus deflection for frame 2B

The results of load versus deflection for frame 2C are shown in Figure 6.23. Failure of this frame is catastrophic and, similar to frame 2A, the first floor internal columns are subjected to very high axial forces. Compared to frame 2B, both frame 2A and frame 2C have relatively low lateral load to vertical load ratios.

The middle-tier analysis predicts a peak frame load for frame 2C of 118 kN/m and the corresponding critical section is within column 7. This analysis also predicts the capacities of columns 33 and 34 to be 177 kN/m and 180 kN/m respectively. The ultimate frame load for this frame by the top-tier analysis is 177 kN/m.

The moment magnifier method also predicts the critical section to occur within column 7. Predicted frame capacity is 129 kN/m which is 73% of the top-tier maximum frame load of 177 kN/m. The unbraced moment magnifier, δ_s, for this column is 1.04. It is noted that values for δ_s for the columns within the first storey are all greater than 3.0.
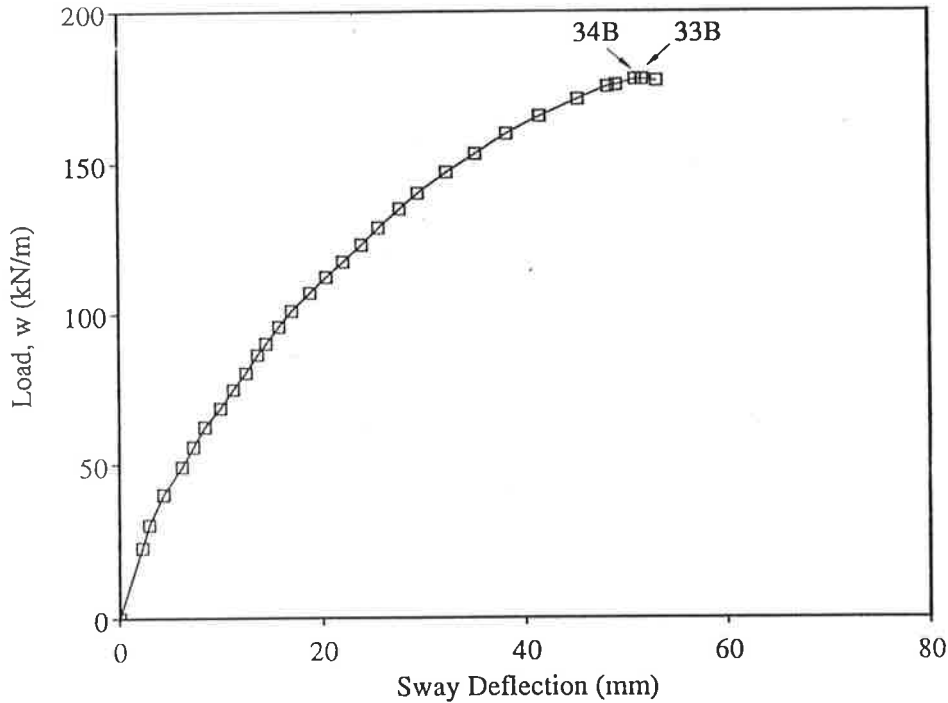
Figure 6.23: Load versus deflection for frame 2C

6.6.4.4   Analytical Results for Design Strength Predictions

Design strength calculations for frames 2A, 2B and 2C have been made by the middle-tier and moment magnifier methods and results for each frame are summarised in Tables 6.6, 6.7 and 6.8, respectively. Material properties used in the top, middle and bottom-tier methods are based on characteristic values. Member capacity by the simplified methods corresponds to the intersection of the M-N loading curve and the design strength M-N interaction curve. Frame capacity, w_{des}, is then taken to be the lowest value of all member capacities.

To determine design strength by the top-tier model II analysis, a strength reduction factor must be applied to the peak load. However, its value is difficult to determine because one or more hinges may form before the peak load is reached. For the present study, the 'global strength reduction factor' applied to the peak load by the top-tier

analysis is that value corresponding to the critical section by the given simplified method.

Summarised in Tables 6.6, 6.7 and 6.8 are the design strength loads, w_{des}, determined by each simplified method and the values of ϕ are the corresponding strength reduction factors for the critical sections. The comparison ratio is then given by the ratio of the value for w_{des} to the value of ϕ multiplied by the top-tier peak load.

Table 6.6: Design strength predictions for frame 2A

Method of analysis	w_{des} (kN/m)	ϕ	Comparison ratio
Middle-tier	63	0.78	0.65
Moment magnifier	75	0.77	0.79

The moment magnifier method predicts a design strength of 75 kN/m for frame 2A, (Table 6.6), which corresponds to a critical section within column 7. The comparison ratio of 0.79 indicates that the top-tier design strength is 95 kN/m. Calculation of the storey moment magnifier, δ_s, for this column is 1.06, which is less than the allowable limit of 1.5. Furthermore, the moment magnifier method also gives a conservative estimate of frame capacity, hence it is a satisfactory approach.

The middle-tier analysis also determines the critical section to occur within column 7, but this analysis gives a more conservative estimate of the maximum design load for this frame. The comparison ratio of 0.65 corresponds to a top-tier peak load of 97 kN/m. In both the moment magnifier and the second order middle-tier analyses, the factor, ϕ, indicates that column 7 fails by primary tension. All columns within this frame are 4 m high and the displacement calculation, $L_u/250$, for these columns is 16 mm. The maximum relative displacement for any column by the middle-tier analysis is

2 mm. This is less than the recommended allowable limit of 16 mm. This approach also gives a conservative estimate for frame strength and the method can be considered satisfactory.

Table 6.7: Design strength predictions for frame 2B

Method of analysis	w_{des} (kN/m)	ϕ	Comparison ratio
Middle-tier	31	0.77	0.74
Moment magnifier	20	0.7	0.53

Table 6.7 summarises the design strength predictions for frame 2B. The moment magnifier method predicts the critical section to occur within column 33 in the first storey. The design strength is 20 kN/m and the storey moment magnifier, δ_s, is 1.26. The global strength reduction factor, ϕ, equals 0.7 and when applied to the top-tier peak load, yields a corresponding design strength of 38 kN/m. Hence, the comparison ratio is 0.53.

The middle-tier analytical results also show that overall frame performance is controlled by the member capacities of the first-storey external columns 32 and 35. The comparison ratio for this analysis is 0.74 and suggests the analysis is conservative. The permissible limit, $L_u/250$, is 24 mm for the first storey columns and 12 mm for the columns in the second to fifth storeys. The maximum relative displacement of any column is 27 mm, which occurs in column 32. Although the middle-tier analysis prediction for strength is conservative, AS 3600 suggests a column stability failure may occur and a rigorous method of analysis should be used. Obviously, the permissible limit, $L_u/250$, for a second order analysis is on the conservative side.

Table 6.8: Design strength predictions for frame 2C

Method of analysis	w_{des} (kN/m)	ϕ	Comparison ratio
Middle-tier	76	0.77	0.64
Moment magnifier	72	0.68	0.69

Results for frame 2C are summarised in Table 6.8. The moment magnifier method predicts the design strength member capacity for column 33 is 72 kN/m. The strength reduction factor, ϕ, is 0.68. The value for the unbraced moment magnifier, δ_s, for this column is 2.95, which is greater than the permissible value of 1.5. AS 3600 states that above this value a column stability failure may occur and a rigorous method of analysis should be performed to predict column capacity. However, the comparison ratio, 0.69, for this frame analysis is conservative, i.e. less than unity. Although a column stability failure cannot be determined by a design strength prediction, the results for frame 2C suggest that the maximum value for moment magnifier of 1.5 is conservative.

The allowable limit of $L_u/250$ for the columns of frame 2C are 24 mm for the first storey columns and 12 mm for the columns in the second to fifth storeys. The middle-tier results show that relative column displacements are 2 mm for column 4, within the fifth storey, and 10 mm for column 32 in the bottom storey. These values are acceptable and, as suggested by AS 3600, a second order linear elastic analysis can be used. The critical columns by this analysis are columns 4 and 7, and design strength capacities are 76 kN/m and 80 kN/m respectively. The comparison ratio of 0.64 suggests this analysis is conservative.

6.6.4.5 Summary and Conclusions

The ultimate strength analyses of frames 2A, 2B and 2C by top-tier model II show that frames 2A and 2C are characterised by a sudden catastrophic failure, whereas frame

2B softens markedly after the peak frame load. In making these comparisons, it is interesting to note the ratio of horizontal load to vertical load for each frame. Frames 2A and 2C have relatively low ratios, and frame 2B has a much higher ratio. Moments caused by the horizontal loading tend to act in the opposite direction to the moments corresponding to the vertical load pattern. The horizontal loads also tend to reduce the level of compressive axial load in the bottom storey columns.

The catastrophic failure of frames 2A and 2C corresponds to high column axial loads combined with small moments in the bottom storey columns. The bottom storey columns of frame 2B were subjected to a lower level of axial load. At the peak frame load, the axial compressive thrust in column 32 was approximately $0.3N_{uo}$. External columns in the top floor of all frames were also heavily loaded. However, these columns tended to carry relatively high moments and low column axial loads, and when failure occurred this was characterised by a primary tension type failure.

Failure type for all three frames is a partial collapse mechanism because a full set of hinges had not developed by the final collapse.

There is some inconsistency in the use of the code recommended limits for stability by the simplified methods. The values of δ_s for the critical sections for frames 2A, 2B, 2C are 1.06, 1.26, 2.95 respectively. For these frames, AS 3600 recommends the moment magnifier method should not be used to analyse frame 2C because δ_s is greater than 1.5. On the other hand, only the value of $L_u/250$ for frame 2B by the middle-tier method is exceeded. Hence, AS 3600 suggests the middle-tier method should not be used to analyse frame 2B.

It is interesting to note that the comparison ratio for design strength was more conservative than the comparison ratio for ultimate strength for each frame analysed. A global strength reduction factor was taken for top-tier design strength predictions and its value was assumed to lie between the values of 0.6 and 0.8.

6.6.5 Series III Frames

6.6.5.1 Introduction

In the design and analysis of structures subjected to sequential loading, e.g. combinations of dead + live load or dead + wind load, it is common practice in the calculation for strength to assume linear elastic behaviour and that load systems can be superimposed. In this section, non-linear analytical predictions are performed and the adequacy of this approach is investigated.

6.6.5.2 Analytical Results

Two frames have been chosen for analysis which have identical structural geometries, material and sectional properties as frames 2B and 2C from Series II. For Series III, these two frames are named frame 3B and frame 3C. The frames are analysed for sequential loading by applying a uniform load pattern to all beams which may simulate dead load. This first load system is held constant followed by a second load system which is incremented until the strength of the structure is reached. The second load system comprises a checkerboard beam load pattern, which could simulate live load, and a set of lateral loads applied at each floor level which simulates wind loading. Analyses for sequential loading are made with the non-proportional method of analysis developed in Chapter 5. Results are compared with proportional load analyses with equivalent systems of loads.

As already mentioned, these frames have been analysed in Series II, but under different loading conditions. Figure 6.24 shows the load patterns for analysis by non-proportional loading. The first load system, w_{1n}, is incremented up to a predetermined magnitude, given by w_{1n}^*. Since the value of w_{1n}^* for each non-proportional loading analysis must be predetermined, two separate analyses were made to determine the ultimate values, $w_{1n}(max)$, under this load pattern. The peak load for frame 3B, with all beam spans loaded, is 198 kN/m. The corresponding peak load,

$w_{1n}(\text{max})$, for frame 3C with all beam spans loaded, is 209 kN/m. The predetermined magnitudes of load system 1, w_{1n}^*, for frames 3B and 3C are given in Table 6.9 and are approximately 25% of the ultimate load of $w_{1n}(\text{max})$ for each frame.

When the first load system is fully incremented to w_{1n}^* it is held constant and the second load system is applied. The vertical load pattern, w_{2n}, is applied to alternate spans and the horizontal load pattern, H_n, given by $\alpha_n w_{2n} L$, is applied at each floor level. The peak frame load for non-proportional loading corresponds to $w_{2n}(\text{max})$ and $H_n(\text{max})$ from the second load system. These values are summarised in Table 6.9.

For the proportional loading analyses for frames 3B and 3C, three loading patterns are applied to the structures. Shown in Figure 6.25 are two load patterns, w_{1p} and w_{2p}, applied to the beams and a system of lateral loads, H_p, given by, $\alpha_p w_{1p} L$, applied at each floor level. The relative proportions in which these loads are incremented is determined from the magnitude of w_{1n}^* and the peak values, $w_{2n}(\text{max})$ and $H_n(\text{max})$, for load system 2 from the non-proportional loading analyses.

The ratio, $w_{1p}{:}w_{2p}$, in which the vertical loads are applied for proportional loading analyses is in the same ratio as $w_{1n}^*{:}w_{2n}(\text{max})$. The magnitudes for w_{1n}^* and $w_{2n}(\text{max})$ for frame 3B are 40 kN/m and 20 kN/m respectively, therefore the vertical load patterns for the proportional loading are given by $w_{2p} = 0.5 w_{1p}$. From the non-proportional loading analysis for frame 3C, the vertical loads at frame capacity are: $w_{1n}^* = 50$ kN/m and $w_{2n}(\text{max}) = 156$ kN/m. Hence, the relationship between the vertical loads for the proportional loading analysis is given by $w_{2p} = 3.12 w_{1p}$.

The relative proportion between the horizontal loads and the vertical loads for proportional loading are based on the magnitude of loads at the peak frame loads from the non-proportional loading analyses. The following equation is used to calculate the factor, α_p.

$$\alpha_p = \frac{H_n(\text{max})}{w_{1n}^* L} \tag{6.20}$$

In this expression, L is the beam span. For frames 3B and 3C, all beam spans are 6m. From the non-proportional loading analysis of frame 3B, the magnitude of $w_{1n}*$ is 40 kN/m and for $H_n(max)$ the value is 96 kN. Hence, for proportional loading analysis α_p is 0.4. For frame 3C, the factor α_p for the proportional loading analysis is equal to 0.17. This is based on magnitudes of 50 kN/m and 50 kN for $w_{1n}*$ and $H_n(max)$ respectively.
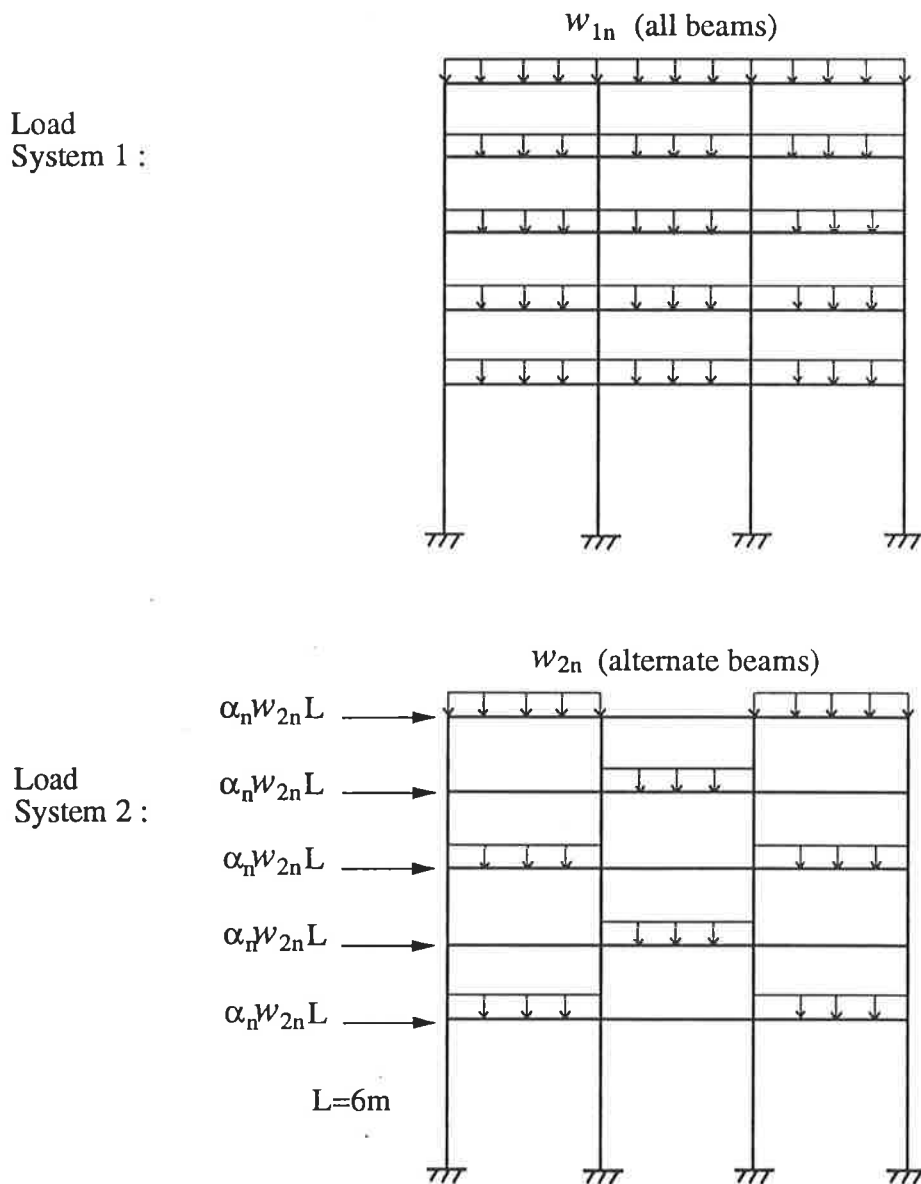
Figure 6.24: Loading configuration for non-proportional loading

Table 6.10 summarises the peak loads for the proportional loading analyses for frames 3B and 3C. By comparing values of $w_{1p}(\text{max})$ and $H_p(\text{max})$ with corresponding values for w_{1n}^* and $H_n(\text{max})$ in Table 6.9, there is very little difference in frame capacity for the analyses for non-proportional loading and proportional loading. The non-proportional loading analyses showed that member capacity had not been reached in any member. It should be noted that w_{1n}^* for both non-proportional loading analyses are 25% of the maximum possible values for w_{1n}. It was shown in Chapter 5 that frame capacity depends on the amount of load applied by the first load system to the structure. With higher values of w_{1n}^*, it can be expected the deformed structure may influence the amount of load applied by the second load system.
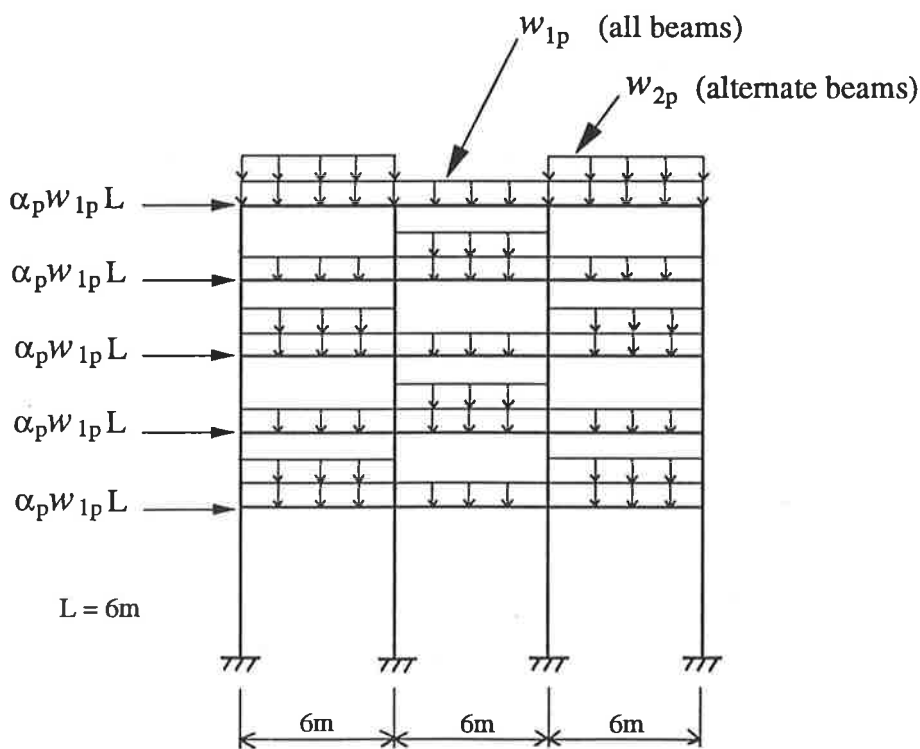
Figure 6.25: Loading configuration for proportional loading

Table 6.9: Peak loads for non-proportional loading

	w_{1n}* (kN/m)	w_{2n}(max) (kN/m)	α_n	H_n(max) (kN)
Frame 3B	40	20	0.8	96
Frame 3C	50	156	0.053	50

Table 6.10: Peak loads under proportional loading

	w_{1p}(max) (kN/m)	w_{2p}(max) (kN/m)	α_p	H_p(max) (kN)
Frame 3B	39	59	0.4	95
Frame 3C	49	205	0.17	49

6.6.5.3 Summary and Conclusions

The difference in the predicted peak frame load for non-proportional and proportional loading for the two frames considered is minor. Results suggest that sequential load systems can be replaced by an equivalent set of proportional loads. However, this study does not cover all possible cases and there may be situations where this is not a reasonable assumption. A more comprehensive study is recommended for further investigations.

6.6.6   Series IV Frame

6.6.6.1   Introduction

In this section, ultimate strength and design strength analyses are made to predict the capacity of a ten storey frame. This frame has the same beam and column properties as frame 2C which has been shown in Figure 6.19. Frame 4 has a uniform loading pattern, w (kN/m), on all beam spans and a lateral load, $0.027wL$, applied to each storey. Columns within the first storey are 6 m high and columns within the second to tenth storeys are 3 m high. For discussion purposes, the first storey columns are numbered 67 to 70 and the columns within the tenth storey are numbered 4 to 7.

6.6.6.2   Analytical Results by Ultimate Strength Predictions

Analytical results for the top-tier model II, middle-tier and the bottom-tier moment magnifier methods are summarised in Table 6.11. The top-tier analysis predicts a peak frame load of 92 kN/m. Frame failure is catastrophic (Figure 6.26) and occurs shortly after the strengths of the first storey interior columns 68 and 69 are reached. These columns carry high axial loads, approximately $0.85N_{uo}$ at failure, and consequently have poor ductility. Hinges have not formed in any of the remaining columns or beams.

The middle-tier analysis also predicts frame strength is controlled by the capacity of columns 68 and 69. The peak load of 88 kN/m corresponds to the member capacity for both these columns.

The moment magnifier method gives the most conservative estimate for frame capacity. The peak load of 58 kN/m corresponds to the critical section occurring within column 70 in the first storey. Note that the capacity of columns 68 and 69 is 59 kN/m. The unbraced moment magnifier δ_s for column 70 is 2.4, indicating the development of significant second order moments.

Table 6.11: Ratio of w_{ult} for each analysis to w_{ult} by top-tier (model II) for frame 4

Method of Analysis	w_{ult} (kN/m)	Comparison ratio
Top-tier (model II)	92	1.0
Middle-tier	88	0.96
Moment magnifier	58	0.63
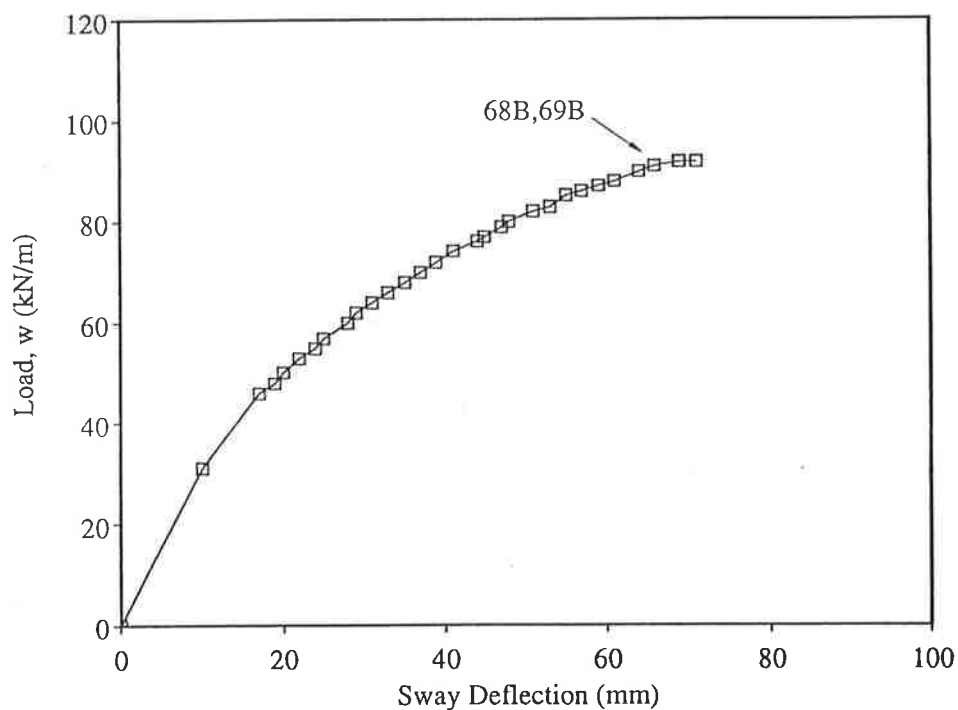
Figure 6.26: Load versus deflection for frame 4

6.6.6.3 Analytical Results by Design Strength Predictions

Design strength predictions for frame 4 have been made for the moment magnifier and middle-tier methods. These results are summarised in Table 6.12. The moment magnifier analysis gives a design strength load of 39 kN/m for frame 4 and the critical

section is within column 70. Both columns 68 and 69 are also highly loaded and have calculated capacities of 42 kN/m. The value of the moment magnifier, δ_s, for column 70 is 3.83. This is much greater than the allowable limit of 1.5 for design purposes, although the strength comparison ratio of 0.72 indicates this analysis is conservative.

The middle-tier method is slightly unconservative, with a comparison ratio of 1.02. This method predicts the critical section is within column 7 with a capacity of 65 kN/m, while the capacity of columns 68 and 69 is 69 kN/m. The value of $L_u/250$ for all first storey columns is 24 mm and the maximum relative displacement for columns within this storey is 21 mm. This value for displacement is less than the allowable limit and is in contrast to the condition applying to the moment magnifier method where the value of δ_s is much greater than the limit of 1.5.

Table 6.12: Design strength predictions for frame 4

Method of Analysis	w_{des} (kN/m)	ϕ	Comparison ratio
Middle-tier	65	0.78	1.02
Moment magnifier	39	0.66	0.72

6.6.6.4   Summary and Conclusions

The ultimate strength and design strength predictions by the two simplified approaches have yielded quite different results. The moment magnifier method is more conservative, with comparison ratios of 0.63 and 0.72 for ultimate and design strengths respectively, in contrast to the middle-tier results of 0.96 and 1.02. The moment magnifier method also indicates that a stability failure has occurred, whereas the magnitude of column sway deflections by the middle-tier method show that a stability failure does not occur.

6.7 Present Investigation of the Simplified Methods for Isolated Pin-ended Columns

In Section 6.6, columns within unbraced frames were investigated. In all cases, the unbraced moment magnifier was the governing criterion for determining strength by the bottom-tier approach of AS 3600. In this section, the ultimate strength of isolated pin-ended columns is determined by the braced moment magnifier method, the model column method and top-tier model II. The columns have equal end eccentricities as shown in Figure 6.27.

$$f_{cm} = 37 \text{ MPa}$$
$$f_{cmax} = 0.85 f_{cm} = 32 \text{ MPa}$$

$$Ast = 1600 \text{ mm}^2$$
$$cover = 50 \text{ mm}$$
$$f_{sy} = 460 \text{ MPa}$$
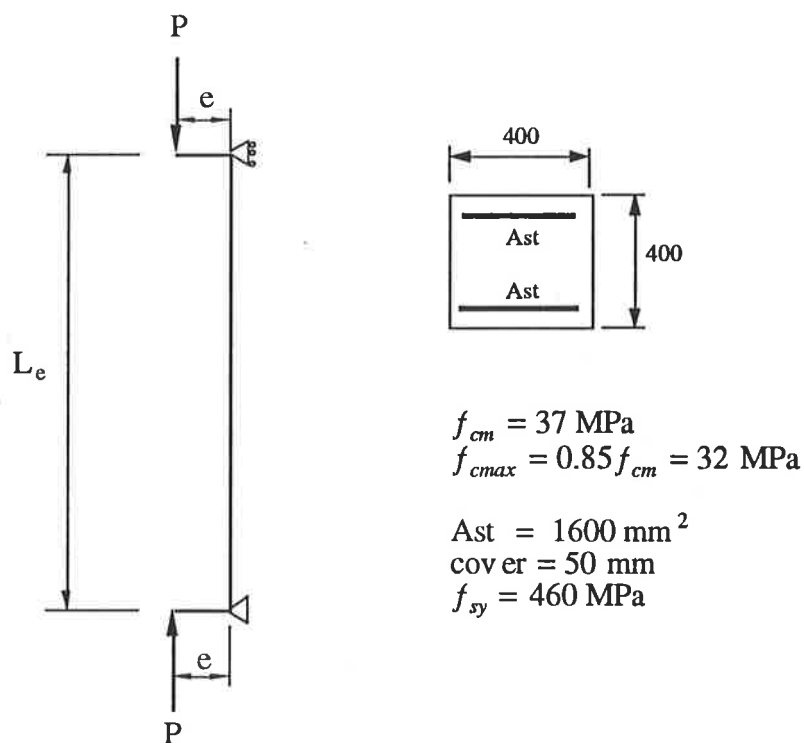
Figure 6.27: Pin-ended column

Table 6.13: Top-tier model II results for columns with $l_e/r = 25$

column	eccentricity	Top-tier results	
	e	M_{ult}	N_{ult}
	(mm)	(kNm)	(kN)
A1	40	223	4796
A2	120	391	3008
A3	200	447	2095

Shown in Table 6.13 are the results obtained by the top-tier model II for three columns, A1, A2 and A3, with increasing values for eccentricity. Each column is relatively stocky with a slenderness ratio of 25. Top-tier model II predicts a material failure in each column which is shown by the intersection of the M-N loading lines and the solid line representing the strength interaction curve in Figure 6.28.

Loading lines are also plotted in Figure 6.28 for the results obtained by the braced moment magnifier. Ultimate moment and thrust are found from the intersection of each line and the strength interaction curve, and the value of δ_b for columns A1, A2 and A3 are 1.16, 1.1 and 1.06 respectively. Ultimate moment and thrust by the model column method, which are found by iteration, are shown by the three single circles.

In all cases, ultimate moment and thrust by these simplified methods are only 1 to 3% higher than the results by top-tier model II. Second order moments in these columns are not significant, although for column A1 the moment magnifier predicts a 16% contribution due to second order effects
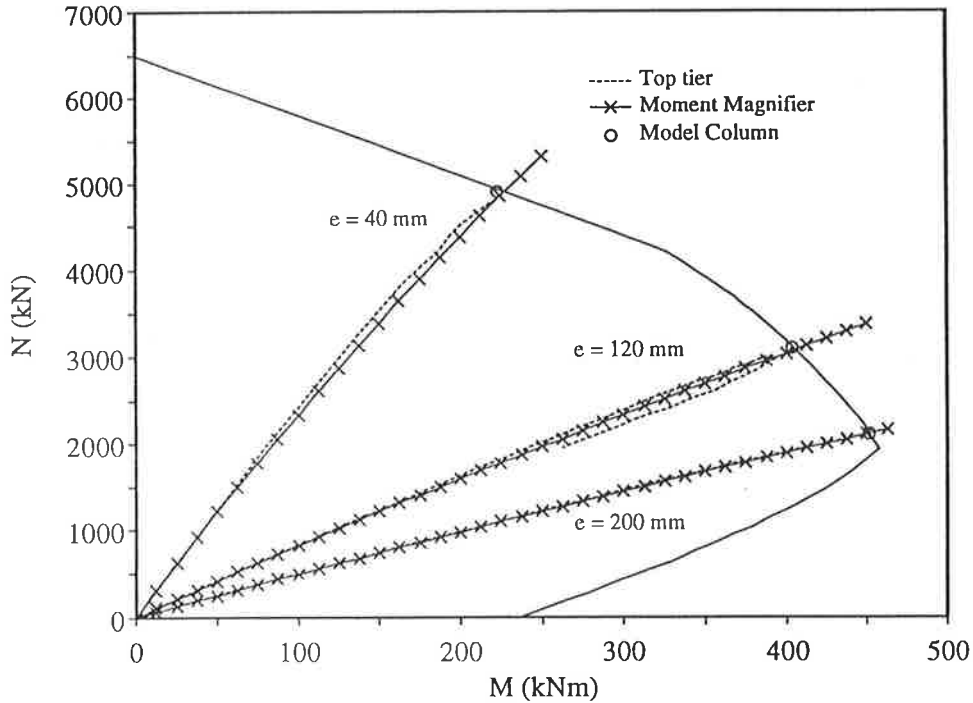
Figure 6.28: Results for columns A1, A2 and A3

A study of slender columns with slenderness ratios of 75 was also made. Results for these columns B1, B2 and B3, with eccentricities of 40 mm, 120 mm and 200 mm respectively, are shown in Figures 6.29 to 6.31.

Results for column B1, which has an eccentricity of 40mm, are shown in Figure 6.29. The top-tier model II predicts a peak thrust of 3394 kN at a moment of 332 kNm. A column stability failure occurs and is followed by significant softening, i.e. moment and thrust decrease in value after the peak load.

The moment magnifier method predicts an ultimate moment and thrust of 419 kNm and 2840 kN respectively. The braced moment magnifier value of 3.98 is very high, but this method cannot determine if a stability failure has occurred. For unbraced frames, the sway moment magnifier has a limiting value of δ_s equal to 1.5. Above this value a stability failure may occur. Peak moment by the braced moment magnifier is 26% higher than the value determined by top-tier model II.

The line of triangles represents calculations for predicted strength by the model column method. However, this does not represent a loading line and has only been plotted to reflect the iterative nature of the model column method. The only point which is of interest occurs at the intersection of the strength interaction curve where ultimate moment and thrust are 405 kN and 3102 kN respectively. Peak moment in this case is 22% higher than the top-tier value for peak moment. Similar to the moment magnifier method, this method has predicted a column material failure, whereas the top-tier method has predicted a stability failure.
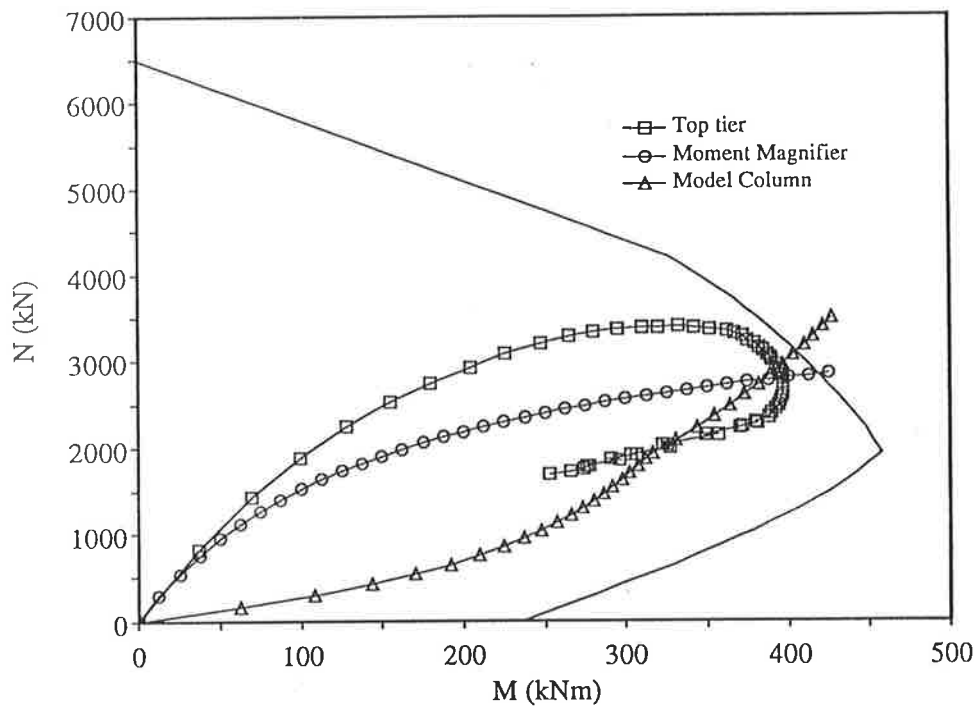
Figure 6.29: Results for column B1

Results for column B2, which has an eccentricity of 120 mm, are shown in Figure 6.30. Top-tier model II has predicted a peak moment of 447 kNm and peak thrust of 1891 kN. A material failure has occurred at column mid-height and this is followed by softening. The braced moment magnifier, δ_b, has a value of 1.98. However, the moment magnifier method predicts a failure moment of 456 kNm which is only 2% higher than the predicted top-tier value. The peak thrust value of 1925 kN is also 2% higher than the top-tier value at failure. Hence, results by the moment magnifier method are satisfactory.

The model column method results also compare very well. The ultimate moment is 446 kNm and the corresponding thrust value of 1754 kN is only 7% less than the top-tier value of 1925 kN.
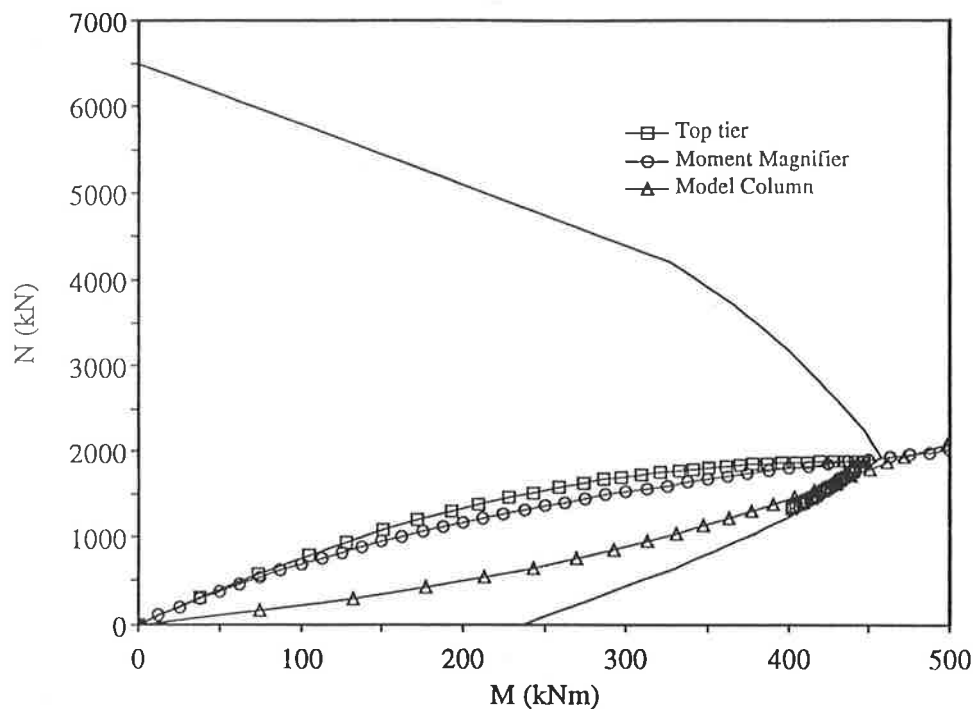
Figure 6.30: Results for column B2

Column B3, with an eccentricity of 200 mm, is characterised by a primary compression failure as shown in Figure 6.31. At failure, the predicted top-tier ultimate moment is 392 kNm. The corresponding thrust value of 1285 kN is equal to $0.2N_{uo}$, where N_{uo} is the squash load value of 6500 kN. Softening after the peak load has also occurred.

The braced moment magnifier value is 1.53 and the ultimate moment and thrust values are both only 5% higher than the predicted top-tier values. Similar to column A2, results for column A3 by the moment magnifier method are satisfactory.

The model column method predicts an ultimate moment and thrust which are 0.9 and 0.64 of the corresponding top-tier values. Results by this simplified approach are conservative, yet satisfactory.
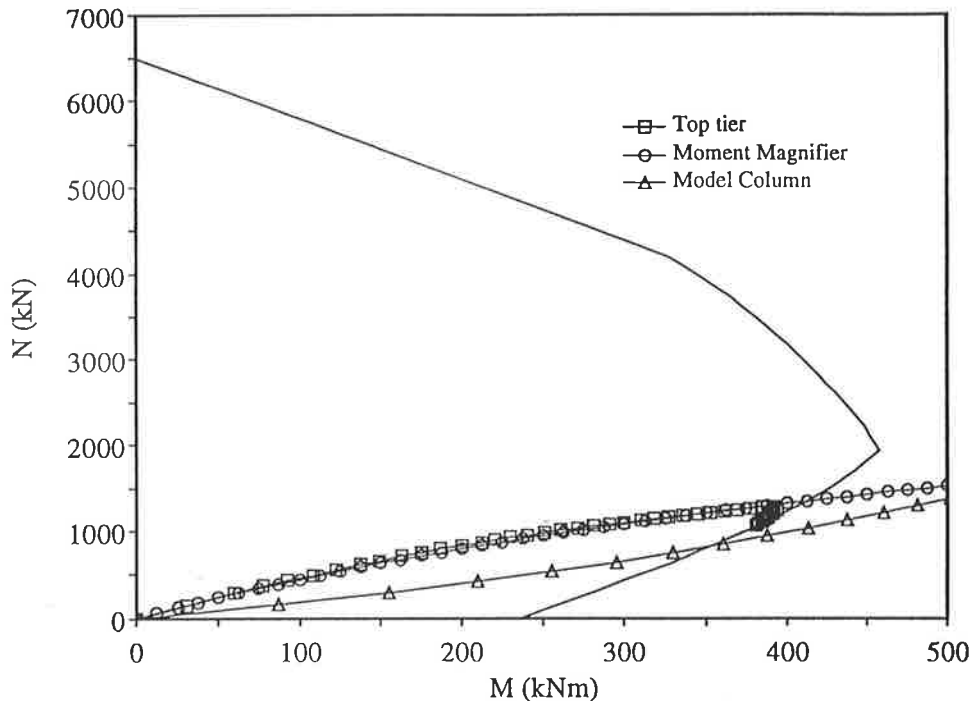
Figure 6.31: Results for column B3

6.8 Summary and Conclusions

In this chapter, four series of unbraced slender frames have been analysed for various non-linear effects. The non-linear method of frame analysis has been used to investigate the influence of tension stiffening and joint deformations on frame performance in Series I. The adequacy of representing sequential loads by a system of proportional loads has been investigated in Series III. Ultimate and design strength predictions were made by top-tier, middle-tier and bottom-tier methods of analysis in Series I, II and IV. Finally, several pin-ended columns were analysed by the top-tier, moment magnifier and model column methods. From the results of the study in this chapter, a number of conclusions have been drawn.

1. Tension stiffening effects can be ignored in the calculation for strength. Non-linear analytical results of two portal frames and six single-storey five-bay frames showed that by ignoring the effects of tension stiffening ultimate frame load is underestimated by only 1.0 to 2.0%. Previous studies have tended to ignore tension stiffening in strength calculations.

2. Joint deformations within opening L-joints of portal frames reduce frame stiffness and strength. Reductions in strength and stiffness are greater for frames with relatively shallow beams, i.e. where the beam depth equals column thickness.

3. Deformations within top floor T-joints of single storey frames are not likely to have an adverse effect on frame strength and stiffness, if the beam depth is twice the column thickness. However, strength can be reduced by 30% and stiffness also reduced significantly if beams and columns at T-joints are the same size.

4. Analytical results by the top-tier method showed that frame stability failure occurred in most frames. Furthermore, hinge formation in the single storey-frames was controlled by the presence of inefficient joints. Failure in the multi-storey frames occurred in the bottom-storey columns, which were subjected to the highest levels of axial loading, corresponding to primary compression or stability failures. External columns in the top-storeys were also heavily loaded and tended to be characterised by primary tension failure, i.e. material failure below the balanced condition.

5. For most frames, the middle-tier and moment magnifier methods accurately predicted the critical sections within frames. Generally this occurred within bottom-storey and top-storey external columns of the multi-storey frames and columns on the windward face of the single-storey sway frames.

6. A previous study by Wong (1989) showed that design strength predictions by the middle-tier method were unconservative for a number of sway frames. Further investigation of these frames in the present study showed that column sway deflections were greater than the allowable limit of $L_u/250$. Under this condition, the use of the middle-tier method is not recommended by AS 3600. Results by the top-tier non-linear method of analysis also suggested that stability failures may have occurred in some cases. Hence, the middle-tier method can be used safely if column deflections are less than a value of $L_u/250$.

7. Ultimate strength predictions by the moment magnifier and middle-tier methods were found to be satisfactory for all but one case. Strength was overestimated by 8% and 1% respectively, for a single-storey five-bay frame with relatively shallow beams. Top-tier results indicated a stability failure.

8. Design strength comparison ratios were less than unity for all cases, except for the ten storey frame. However, the middle-tier method overestimated frame capacity by only 2 %. Both the moment magnifier and middle tier methods can be considered to provide satisfactory predictions for design strength.

9. Comparisons were made for three unbraced five-storey frames and one unbraced ten-storey frame. Comparisons of ultimate and design strength predictions by top, middle and bottom methods for each frame analysed showed that design strength predictions tended to be more conservative than ultimate strength predictions. However, large differences in frame capacity were observed when comparing the middle-tier and moment magnifier methods. For example, ultimate strength capacity of frame 2A (five storeys) by the moment magnifier method was 24% higher than the middle-tier result. On the other hand, ultimate strength capacity of frame 4 (ten storeys) by the middle-tier method was 52 % higher than the moment magnifier result.

10. The allowable limits suggested by AS 3600 of $L_u/250$ for design strength by the middle-tier method and δ_s for design strength by the unbraced moment

magnifier method appear to be satisfactory. If these values are exceeded, it is suggested a stability failure may occur and a rigorous method of analysis should be used. However, in some cases, these limiting values may be conservative.

11. An inconsistency exists with the bottom-tier magnifier method in the calculation of the parameter k for the effective length and for the stiffness EI for the elastic critical buckling load. The effective length is based on gross-sectional values for beam and column stiffnesses, but the critical buckling load is calculated from a column stiffness value for the balanced condition. Although conservative results have been achieved for strength predictions by the bottom-tier moment magnifier method in the present study, there is no rationale for the assumed values of stiffness. A previous study by Wong (1989) showed that the amount of beam reinforcement influences frame strength. It should also be mentioned that column strength is influenced by the level of axial thrust.

12. An over-simplified approach in the calculation of member stiffnesses is also adopted by the middle-tier method. Reduced stiffness values of $0.4EI$ for beam elements and $0.8EI$ for column elements are assumed to represent conditions at the ultimate state. These values also ignore the presence of reinforcing steel. No reduction in axial stiffnesses are made, and gross-sectional values for EA are assumed for all sections throughout the structure.

13. A study of pin-ended columns showed that the moment magnifier method and the model column method gave satisfactory results for columns with slenderness ratios of 25 and 75. Although AS 3600 does not place a limit on the magnitude for the braced moment magnifier, an upper limit of δ_b equal to 1.5 would be satisfactory, to guard against stability failure.

Chapter 7

Conclusions and Recommendations

7.1 Conclusions

A study of the non-linear behaviour of reinforced concrete frames has been described in this thesis. Following a discussion of an existing non-linear method of analysis, which included comparisons with test data, improvements to the method were proposed. An investigation of the performance of various multi-storey and single storey frames was carried out and comparisons with predictions by code recommended simplified elastic methods of design/analysis were also made. The following major points summarise the work undertaken:

1. Refinements have been made to a non-linear method of frame analysis developed by Wong (1989). These include provisions for sequential, non-proportional loading and short-term material non-linearities due to tension stiffening and joint deformations. Each effect was modelled by considering

286

compatibility with existing analytic procedures. Hence, good accuracy and computational efficiency were achieved.

2. A study of simple test beams showed that tension stiffening has a beneficial effect on flexural stiffness for beams with low percentages of tensile steel. With increasing amounts of steel, the contribution of tensile concrete to overall stiffness reduces. Tension stiffening is most significant in the loading region up to the formation of primary cracks and diminishes gradually as the yield moment is reached. For deflection calculations, tension stiffening effects can be ignored for beams with greater than 3% tensile reinforcing steel. The study of frames in Chapter 6 showed the increase in frame strength due to tension stiffening is only between 1% to 2%.

3. In the study of test beams for tension stiffening, strength and stiffness were underestimated in several cases. This was attributed to additional, beneficial effects due to confinement under load plattens and at internal supports of two-span continuous beams, neither which had been taken into account. Recommendations for modelling these effects are mentioned in Section 7.2.

4. The study of beam-column connections in Chapter 4 showed that joint deformations, characterised by inclined and longitudinal cracking, are potentially more severe in two types of joints: opening L-joints and top floor T-joints. Joint deformations are also influenced by the relative size and strength of the beams and columns entering the joint. The behaviour of the joint depends very much on the detailing of the reinforcement in the region, and in particular whether or not well-anchored steel is located correctly to carry the internal tensile forces.

5. Joint deformations in opening L-joints and T-joints are most likely to occur in single-storey frames with a high ratio of lateral load to vertical load. The application of vertical beam loading tends to reduce the severity of joint deformations. Frames with relatively shallow beams have greater reductions in

strength and stiffness than frames with relatively deep beams, e.g. where beam depth is twice the column thickness.

6. The assumption that a system of vertical loads followed by horizontal loads can be replaced by an equivalent system of proportional loads appears to be reasonable for multi-storey frames.

7. The code restrictions that $\delta_s \leq 1.5$ for the unbraced moment magnifier and relative end displacements of column members for the middle-tier method must not be greater than $L_u/250$ provide an adequate safeguard against stability failure for design strength. In some cases, the restriction placed on the use of the moment magnifier method was conservative.

8. In most cases, the simplified methods accurately predicted critical sections within frames at ultimate strength. In all but one frame, these occurred within column members. The most critically loaded columns in the multi-storey frames tended to be in the top storey and the bottom storey.

9. Top-tier results for ultimate strength generally showed, other than for the portal frames, the formation of an insufficient number of hinges at ultimate load. An instability failure was evident in a number of these frames.

10. Ultimate strength predictions by the moment magnifier and middle tier methods for all frames analysed gave satisfactory results. However, neither approach can predict stability failure.

11. Design strength predictions for three five-storey frames and one ten-storey by the simplified methods were satisfactory. In these cases, comparison ratios were less than 1.0, although the middle tier method comparison ratio for the ten storey frame was 1.02. However, two of the frames analysed by the moment magnifier method showed $\delta_s > 1.5$ and one frame analysed by the middle tier

method showed relative end displacements $> L_u/250$. In these cases AS 3600 recommends the simplified approaches should not be used.

12. Comparisons for design strength between the moment magnifier and middle tier methods varied considerably. Although these strength predictions were satisfactory, the simplified methods do not adequately take into account the influence of material and geometric non-linear effects. In particular, neither method considers the amount of reinforcement in the calculation of stiffness.

13. Analytical results for six pin-ended isolated columns showed that both the moment magnifier method of AS 3600 and the model column method of the draft Eurocode gave reasonably accurate predictions for strength. These columns had slenderness ratios of 25 and 75.

7.2 Recommendations for Further Research

To study further the non-linear behaviour of reinforced concrete frames, the following recommendations are made:

- Development of a suitable model for the influence of confinement due to method of loading and support conditions on strength and stiffness. A global approach can be made by adjusting the ideal M-κ curves for beam elements.

- Limited information is available for the behaviour of beam-column connections under varying levels of axial load. Further testing needs to be carried out, particularly for connections which are inefficient under zero axial loading.

- Carry out a study of slab-column connections and develop a suitable model for predicting behaviour in frames.

- A numerical model for creep and shrinkage effects can be included in the method of frame analysis to allow for investigation of long-term behaviour in frames.

Appendix A

Derivation of the Geometric Stiffness Matrix for a Beam Element
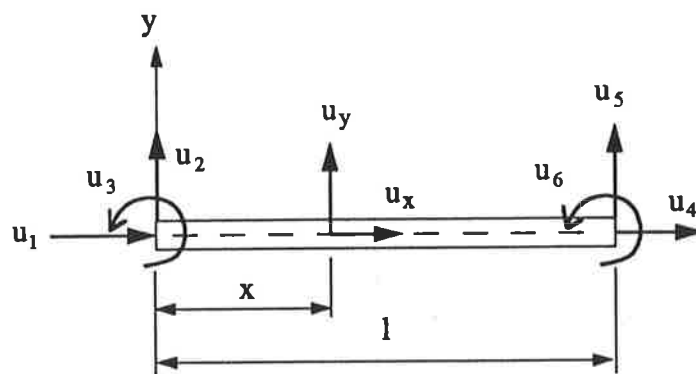
Figure A.1: Beam element with six d.o.f.

Shown in Figure A.1 is a two dimensional beam element in a local coordinate system (Przemieniecki, 1985). The element has six degrees of freedom, with transverse displacements and rotations only.

The displacement functions for this element are given by the following:

$$
\begin{bmatrix} u_x \\ u_y \end{bmatrix} = \begin{bmatrix} 1-\xi & 6(\xi-\xi^2)\eta & (-1+4\xi-3\xi^2)l\eta & \xi & 6(-\xi+\xi^2)\eta & (2\xi-3\xi^2)l\eta \\ 0 & 1-3\xi^2+2\xi^3 & (\xi-2\xi^2+\xi^3)l & 0 & 3\xi^2-2\xi^3 & (-\xi^2+\xi^3)l \end{bmatrix} \begin{bmatrix} u_1 \\ u_2 \\ u_3 \\ u_4 \\ u_5 \\ u_6 \end{bmatrix}
$$

$$(A.1)$$

where $u_1,....,u_6$ are the end displacements as shown in Figure A.1. The non-dimensional parameters are given by:

$$
\xi = \frac{x}{l} \quad \eta = \frac{y}{l}
$$

$$(A.2)$$

The normal strain ε_{xx} at a distance x given by:

$$
\varepsilon_{xx} = \frac{\partial u_0}{\partial x} - \frac{\partial^2 u_y}{\partial x^2} y + \frac{1}{2}\left(\frac{\partial u_y}{\partial x}\right)^2
$$

$$(A.3)$$

where y is measured from the neutral axis of the beam and u_0 denotes the x displacement at $y = 0$. In the calculation of the strain energy U_i, shearing strains are neglected and only the normal strains are considered.

$$U_i = \frac{E}{2}\int_v \varepsilon_{xx}^2 \, dV$$

$$= \frac{E}{2}\int_v \left[\frac{\partial u_0}{\partial x} - \frac{\partial^2 u_y}{\partial x^2} y + \frac{1}{2}\left(\frac{\partial u_y}{\partial x}\right)^2 \right]^2 dV$$

$$= \frac{E}{2}\int_{x=0}^{l}\int_A \left(\frac{\partial u_0}{\partial x}\right)^2 + \left(\frac{\partial^2 u_y}{\partial x^2}\right)^2 y^2 + \frac{1}{4}\left(\frac{\partial u_y}{\partial x}\right)^4 - 2\frac{\partial u_0}{\partial x}\frac{\partial^2 u_y}{\partial x^2}y$$

$$-\frac{\partial^2 u_y}{\partial x^2}\left(\frac{\partial u_y}{\partial x}\right)^2 y + \frac{\partial u_0}{\partial x}\left(\frac{\partial u_y}{\partial x}\right)^2 dx \, dA$$

The higher-order term $\frac{1}{4}(\partial u_y / \partial x)^4$ can be neglected in this expression. Integrating over the cross-sectional area A and noting that since y is measured from the neutral axis, all integrals of the form $\int y dA$ must vanish, hence

$$U_i = \frac{EA}{2}\int_0^l \left(\frac{\partial u_0}{\partial x}\right)^2 dx + \frac{EI}{2}\int_0^l \left(\frac{\partial^2 u_y}{\partial x^2}\right) dx + \frac{EA}{2}\int_0^l \frac{\partial u_0}{\partial x}\left(\frac{\partial u_y}{\partial x}\right)^2 dx \qquad \text{(A.4)}$$

where I is the moment inertia of the cross section. The first two integrals in Equation A.4 are contributions from the linear strain energy and the third integral is the contribution from the non-linear strain component. The following expressions are obtained from Equation A.1:

$$\frac{\partial u_0}{\partial x} = \frac{1}{l}(-u_1 + u_4) \qquad \text{(A.5)}$$

$$\frac{\partial u_y}{\partial x} = \frac{1}{l}\left[6(-\xi + \xi^2)u_2 + (1 - 4\xi + 3\xi^2)lu_3 + 6(\xi - \xi^2)u_5 + (-2\xi + 3\xi^2)lu_6\right] \quad (A.6)$$

$$\frac{\partial^2 u_y}{\partial x^2} = \frac{1}{l^2}\left[6(-1 + 2\xi)u_2 + 2(-2 + 3\xi)lu_3 + 6(1 - 2\xi)u_5 + 2(-1 + 3\xi)lu_6\right] \quad (A.7)$$

Substituting Equations A.5, A.6 and A.7 into A.4 gives the following:

$$U_i = \frac{EA}{2l}(u_1^2 - 2u_1u_4 + u_4^2)$$

$$+\frac{2EI}{l^3}(3u_2^2 + l^2u_3^2 + 3u_5^2 + l^2u_6^2 + 3lu_2u_3 - 6u_2u_5 + 3lu_2u_6$$

$$-3lu_3u_5 + l^2u_3u_6 - 3lu_5u_6)$$

$$+\frac{EA}{l^2}(u_4 - u_1)(\frac{3}{5}u_2^2 + \frac{1}{15}l^2u_3^2 + \frac{3}{5}u_5^2 + \frac{1}{15}l^2u_6^2$$

$$+\frac{1}{10}lu_2u_3 - \frac{6}{5}u_2u_5 + \frac{1}{10}lu_2u_6 - \frac{1}{10}lu_3u_5 - \frac{1}{30}l^2u_3u_6 - \frac{1}{10}lu_5u_6) \quad (A.8)$$

Equation A.9 is obtained by noting the elemental axial force is constant.

$$F = \frac{EA}{l}(u_4 - u_1) \approx \text{constant} \quad (A.9)$$

By applying Castigliano's theroem (part I) to the strain energy expression of Equation A.8, the following element force-displacement equation is obtained.

$$
\begin{bmatrix} S_1 \\ S_2 \\ S_3 \\ S_4 \\ S_5 \\ S_6 \end{bmatrix}
=
\begin{bmatrix}
\dfrac{EA}{L} & 0 & 0 & -\dfrac{EA}{L} & 0 & 0 \\[2mm]
 & \dfrac{12EI}{L^3} & \dfrac{6EI}{L^2} & 0 & -\dfrac{12EI}{L^3} & \dfrac{6EI}{L^2} \\[2mm]
 & & \dfrac{4EI}{L} & 0 & -\dfrac{6EI}{L^2} & \dfrac{2EI}{L} \\[2mm]
 & & & \dfrac{EA}{L} & 0 & 0 \\[2mm]
 & \text{SYMMETRIC} & & & \dfrac{12EI}{L^3} & -\dfrac{6EI}{L^2} \\[2mm]
 & & & & & \dfrac{4EI}{L}
\end{bmatrix}
\begin{bmatrix} u_1 \\ u_2 \\ u_3 \\ u_4 \\ u_5 \\ u_6 \end{bmatrix}
$$

$$
+\,F
\begin{bmatrix}
0 & 0 & 0 & 0 & 0 & 0 \\[2mm]
 & \dfrac{6}{5L} & \dfrac{1}{10} & 0 & -\dfrac{6}{5L} & \dfrac{1}{10} \\[2mm]
 & & \dfrac{2L}{15} & 0 & -\dfrac{1}{10} & -\dfrac{L}{30} \\[2mm]
 & & & 0 & 0 & 0 \\[2mm]
 & \text{SYMM-} & & & \dfrac{6}{5L} & -\dfrac{1}{10} \\[1mm]
 & \text{ETRIC} & & & & \dfrac{2L}{15}
\end{bmatrix}
\begin{bmatrix} u_1 \\ u_2 \\ u_3 \\ u_4 \\ u_5 \\ u_6 \end{bmatrix}
\qquad (A.10)
$$

This last equation can be written as:

$$
\mathbf{S} = (\mathbf{k_e} + \mathbf{k_g})\mathbf{u} \qquad\qquad (A.11)
$$

where $\mathbf{k_e}$ is the first order linear elastic matrix, and $\mathbf{k_g}$ is the geometrical stiffness matrix. The force and displacement vectors are given by $\mathbf{S}$ and $\mathbf{u}$ respectively.

Appendix B

Derivation of the Stiffness Matrix for a Segmented Element

An element of length L is divided into *nseg* segments as shown in Figure B.1. Variations in flexural stiffness within the element are derived from the moment and curvature at mid-length of the segments. Forces and displacements at mid-segment are assumed to be average values for the segment.

The following forces and displacements are shown in Figure B.1 :

V_o, V_{end} = shear forces at the left end and right end;

M_o, M_{end} = bending moments at the left end and right end;

Δ_{yo}, Δ_{yend} = transverse displacements at the left end and right end;

θ_i = change in rotation and measured at mid-point of segment i ;

Θ_o, Θ_{end} = rotations at the left end and right end.

296
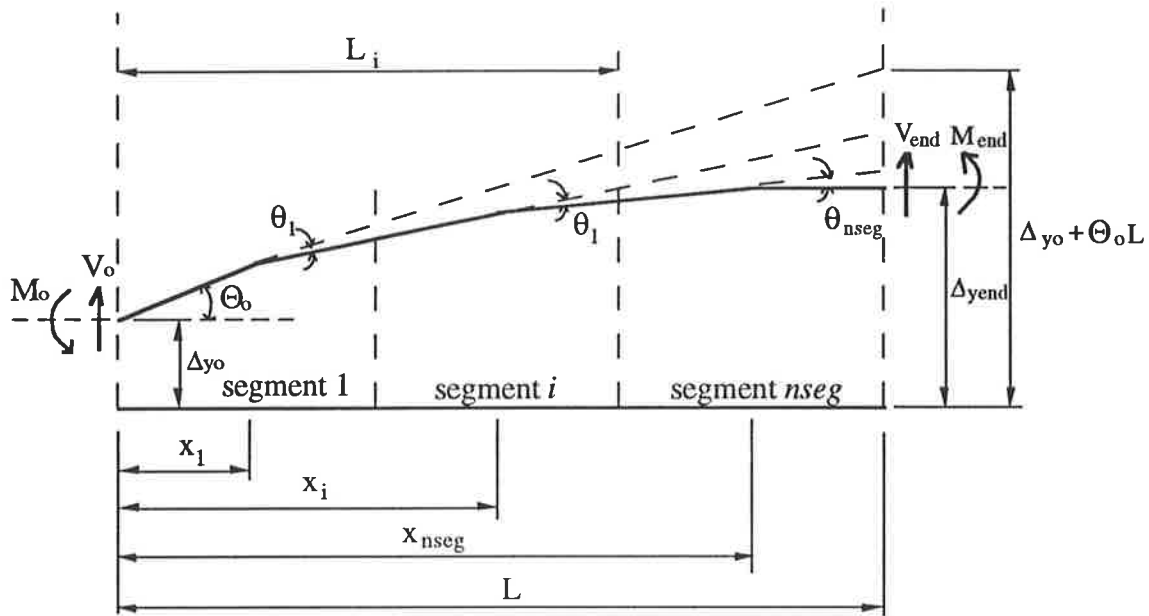
Figure B.1: Typical Segmented Element

It can be shown that the change in rotation θ_i is related to the sum of the moments, $M_o - V_o x_i$, at mid-point of segment i and the stiffness term S_i by the following expression :

$$\theta_i = \frac{M_o - V_o x_i}{S_i} \qquad (B.1)$$

where

$S_i = EI_i/L_i$; and

l_i = length of segment i

From Figure B.1, the slope and displacement at the right end of a typical segment i are:

$$\Theta_i = \Theta_o - \theta_1 - \theta_2 - ... - \theta_i \qquad (B.2)$$

$$\Delta_i = \Delta_{yo} + \Theta_o L_i - \theta_1 (L_i - x_1) - \theta_2 (L_i - x_2) - ... - \theta_i (L_i - x_i) \qquad (B.3)$$

In Equation B.3 the distance from the left end of the element to the end of the segment i is given by L_i. By assuming small rotational changes, the term $\tan \theta_j$ is replaced by

θ_j in Equation B.3. Hence it can be shown the deformations at the right hand end of the element are :

$$\Theta_{end} = \Theta_o - \theta_1 - \theta_2 - ... - \theta_i - ... - \theta_n \tag{B.4}$$

$$\Delta_{yend} = \Delta_{yo} + \Theta_o L - \theta_1 (L - x_1) - ... - \theta_i (L - x_i) - ... - \theta_n (L - x_n) \tag{B.5}$$

Substituting Equation B.1 into Equations B.4 and B.5 yields the following expressions:

$$\Theta_{end} = \Theta_o - M_o \sum_{i=1}^{nseg} \frac{1}{S_i} + V_o \sum_{i=1}^{nseg} \frac{x_i}{S_i} \tag{B.6}$$

$$\frac{\Delta_{yend} - \Delta_{yo}}{L} = \Theta_o - M_o \sum_{i=1}^{nseg} \frac{1}{S_i} + \frac{M_o}{L} \sum_{i=1}^{nseg} \frac{x_i}{S_i} + V_o \sum_{i=1}^{nseg} \frac{x_i}{S_i} - \frac{V_o}{L} \sum_{i=1}^{nseg} \frac{x_i^2}{S_i} \tag{B.7}$$

Let $C_1 = \sum_{i=1}^{nseg} \frac{1}{S_i}$, $C_2 = \sum_{i=1}^{nseg} \frac{x_i}{S_i}$ and $C_3 = \sum_{i=1}^{nseg} \frac{x_i^2}{S_i}$.

Combining Equations B.6 and B.7 gives :

$$\Theta_{end} - \Theta_0 = -M_o C_1 + V_o C_2 \tag{B.8}$$

$$\frac{\Delta_{yend} - \Delta_{yo}}{L} - \Theta_o = -M_o C_1 + \frac{M_o}{L} C_2 + V_o C_2 - \frac{V_o}{L} C_3 \tag{B.9}$$

Solving Equations B.8 and B.9 gives the following expressions for moment and shear force at the left end of the element:

$$M_o = \frac{1}{C_1 C_3 - C_2^2} [C_2 \Delta_{yo} + C_3 \Theta_o + C_2 \Delta_{yend} + (C_2 L - C_3) \Theta_{end}] \tag{B.10}$$

$$V_o = \frac{1}{C_1 C_3 - C_2^2} [C_1 \Delta_{yo} + C_2 \Theta_o + C_1 \Delta_{yend} + (C_1 L - C_2) \Theta_{end}] \tag{B.11}$$

From equilibrium M_{end} and V_{end} are obtained from the following :

$$V_o + V_{end} = 0 \tag{B.12}$$

$$M_o + M_{end} - V_o L = 0 \tag{B.13}$$

The axial stiffness, $S(m)$, is assumed to be constant for the element and combining this and Equations B.10, B.11, B.12 and B.13 gives the element stiffness matrix shown below :

$$
\begin{vmatrix}
P_o \\
V_o \\
M_o \\
P_{end} \\
V_{end} \\
M_{end}
\end{vmatrix}
= [K] \times
\begin{vmatrix}
\Delta_{xo} \\
\Delta_{yo} \\
\Theta_o \\
\Delta_{xend} \\
\Delta_{yend} \\
\Theta_{end}
\end{vmatrix}
\tag{B.14}
$$

where $[K]$ is the segmented elemental stiffness matrix shown below :

$$
\begin{vmatrix}
S(m) & 0 & 0 & -S(m) & 0 & 0 \\
& S_{22} & S_{23} & 0 & -S_{22} & LS_{22}-S_{23} \\
& & S_{33} & 0 & -S_{23} & LS_{23}-S_{33} \\
& SYM\text{-} & & S(m) & 0 & 0 \\
& METRIC & & & S_{22} & S_{23}-LS_{22} \\
& & & & & L^2S_{22}-2LS_{23}+S_{33}
\end{vmatrix}
\tag{B.15}
$$

where $S_{22} = \dfrac{C_1}{C_1 C_3 - C_2^2}$, $S_{33} = \dfrac{C_3}{C_1 C_3 - C_2^2}$, $S_{23} = \dfrac{C_2}{C_1 C_3 - C_2^2}$

For the same values for flexural stiffness, *EI*, in all segments, Equation B.15 reduces to the standard first-order linear elastic stiffness matrix.

Appendix C

Derivation of Fixed End Moments for a Segmented Element

The calculation for fixed end moments and shears for a segmented element take into account contributions from tranverse loads applied within the element. These fixed end moments are shown in Figure C.1.

The variation in moment and stiffness along the element is plotted on the horizontal axis. By using the moment area method and taking a tangent which passes through point A and point B, the following expressions are given:

$$\left[\text{Moment of } \frac{M}{EI} \text{ diagram about A} \right]_A^B = 0 \qquad\qquad \text{(C.1)}$$

$$\left[\text{Moment of } \frac{M}{EI} \text{ diagram about B} \right]_A^B = 0 \qquad\qquad \text{(C.2)}$$
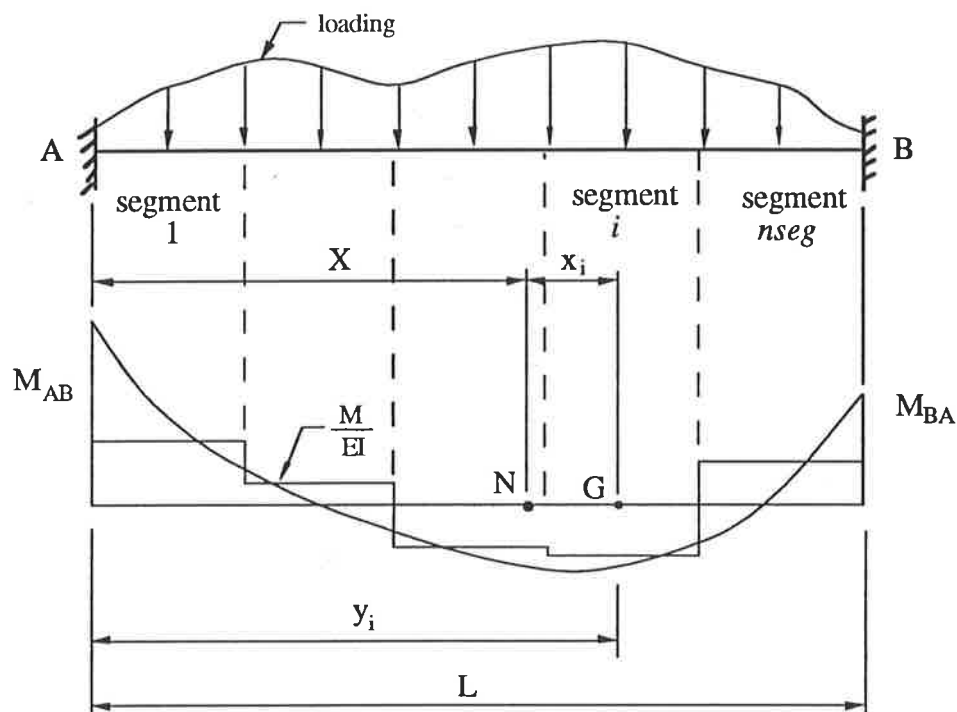
Figure C.1: Fixed end moments for segmented element

The bending moment, M_{xi}, at mid-length of segment i, given by point G, is found by summing two bending moments. The contribution from the bending moment given by M_{ppi} assumes the element is acting simply supported. The bending moment resulting from the end moments M_{AB} and M_{BA} is given by the following expression:

$$M_{fi} = M_{AB} - \frac{(X + x_i)}{L}\left[M_{AB} + M_{BA}\right] \tag{C.3}$$

The total moment at G is the sum of M_{ppi} and M_{fi} and given by:

$$M_{xi} = M_{ppi} + M_{AB} - \frac{(X + x_i)}{L}\left[M_{AB} + M_{BA}\right] \tag{C.4}$$

Combining Equations C.3 and C.4 with Equations C.1 and C.2 gives the following two expressions:

$$\sum_{i=1}^{nseg}\left\{\left[M_{ppi}+M_{AB}-\frac{(X+x_i)}{L}(M_{AB}+M_{BA})\right]\frac{X+x_i}{EI_i}\right\}=0 \tag{C.5}$$

$$\sum_{i=1}^{nseg}\left\{\left[M_{ppi}+M_{AB}-\frac{(X+x_i)}{L}(M_{AB}+M_{BA})\right]\frac{L-X-x_i}{EI_i}\right\}=0 \tag{C.6}$$

By choosing point N as the centroid for the $1/EI$ diagram the distance X is given by:

$$X=\frac{\displaystyle\sum_{i=1}^{nseg}(y_i\ /\ EI_i)}{\displaystyle\sum_{i=1}^{nseg}(1\ /\ EI_i)} \tag{C.7}$$

and

$$\sum_{i=1}^{nseg}\frac{x_i}{EI_i}=0 \tag{C.8}$$

Let $P=\sum_{i=1}^{nseg}\frac{1}{EI_i},R=\sum_{i=1}^{nseg}\frac{x_i^2}{EI_i},S=\sum_{i=1}^{nseg}\frac{M_{ppi}}{EI_i},T=\sum_{i=1}^{nseg}\frac{M_{ppi}x_i}{EI_i}$

Equations C.5 and C.6 become:

$$XS+T+\frac{M_{AB}}{L}\left[X(L-X)P-R\right]-\frac{M_{BA}}{L}\left[X^2P+R\right]=0 \tag{C.9}$$

$$[L-X]S-T+\frac{M_{AB}}{L}\left[(L-X)^2P+R\right]-\frac{M_{BA}}{L}\left[X(L-X)P-R\right]=0 \tag{C.10}$$

By solving Equations C.9 and C.10 simultaneously, the fixed end moments M_{AB} and M_{BA} are given by:

$$M_{AB}=\left[\frac{XT}{R}-\frac{S}{P}\right] \tag{C.11}$$

$$M_{BA}=\left[\frac{(L-X)T}{R}+\frac{S}{P}\right] \tag{C.12}$$

Appendix D

Tension Stiffening in Beams Tested by Clark and Spiers

Table D.1: Concrete parameters for beams tested by Clark and Spiers (1978)

Beam			Concrete Properties					
Name	Width (mm)	Depth (mm)	f_c (MPa)	f_{cmax} (MPa)	f_{tmax} (MPa)	E_c (MPa)	γ_l	γ_t
1	203	410	27.3	25.9	2.83	26120	2.02	8.5
1R	202	412	28.1	26.7	2.89	26500	1.99	7.1
2	203	408	26.8	25.5	2.80	25250	1.98	19.2
2R	204	408	32.5	30.9	3.18	28500	1.85	19.6
3	204	407	31.1	29.5	3.09	27910	1.89	27.6
4	204	409	22.9	21.7	2.52	23900	2.20	33.5
5	203	204	23.3	22.1	2.55	24140	2.18	10.7
6	203	306	20.7	19.6	2.35	22750	2.32	22.1
6R	203	308	27.6	26.2	2.85	26270	2.00	22.5
7R	204	511	23.3	22.1	2.55	24140	2.18	30.3

Table D.2: Reinforcing details for beams tested by Clark and Spiers (1978)

Beam			Top Steel				Bottom Steel				
Name	Width (mm)	Depth (mm)	No. of bars	Diam (mm)	Area (mm²)	Depth (mm)	No. of bars	Diam (mm)	Area (mm²)	Depth (mm)	Amt. (%)
1	203	410	2	16	402	37	3	25	1472	380	1.91
1R	202	412	2	16	402	35	3	25	1472	368	1.99
2	203	408	2	8	101	20	3	20	943	363	1.28
2R	204	408	2	8	101	24	3	20	943	367	1.26
3	204	407	2	8	101	33	3	16	603	373	0.79
4	204	409	2	8	101	35	3	12	339	379	0.44
5	203	204	2	12	226	26	3	16	603	167	1.78
6	203	306	2	8	101	30	3	16	603	268	1.11
6R	203	308	2	8	101	30	3	16	603	273	1.09
7R	204	511	2	8	101	32	3	16	603	473	0.63
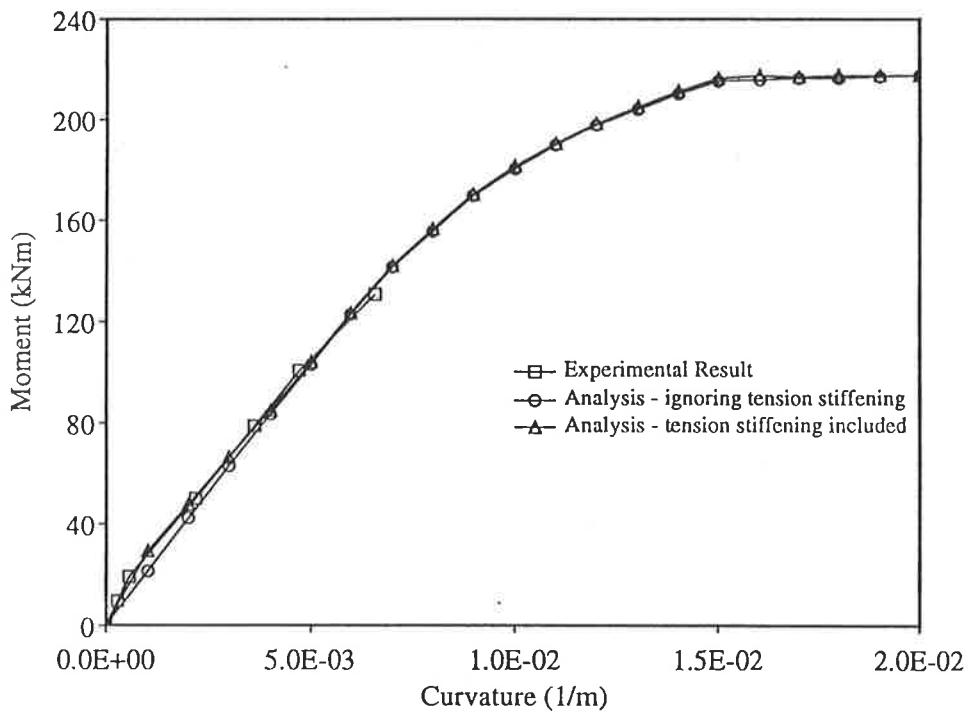
Figure D.1: Moment versus curvature for beam 1
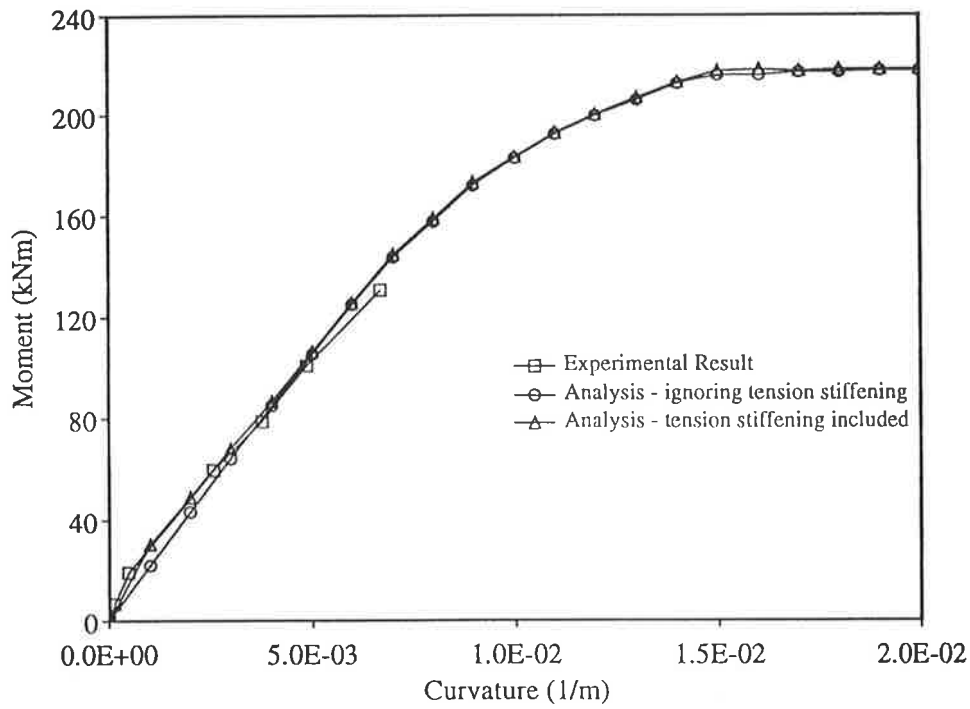
Figure D.2: Moment versus curvature for beam 1R
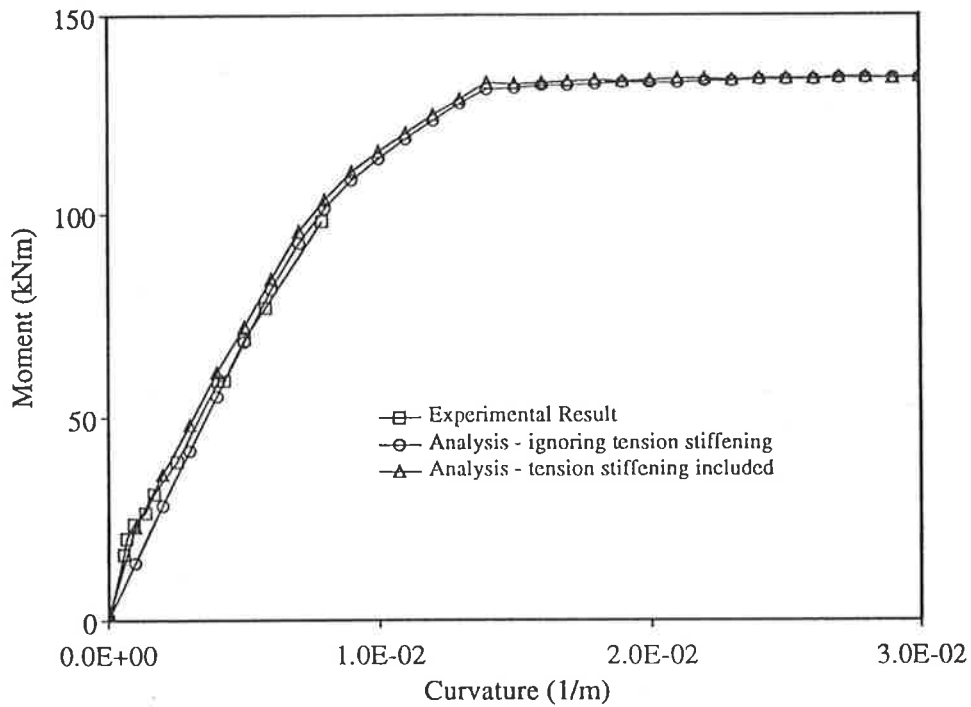
Figure D.3: Moment versus curvature for beam 2
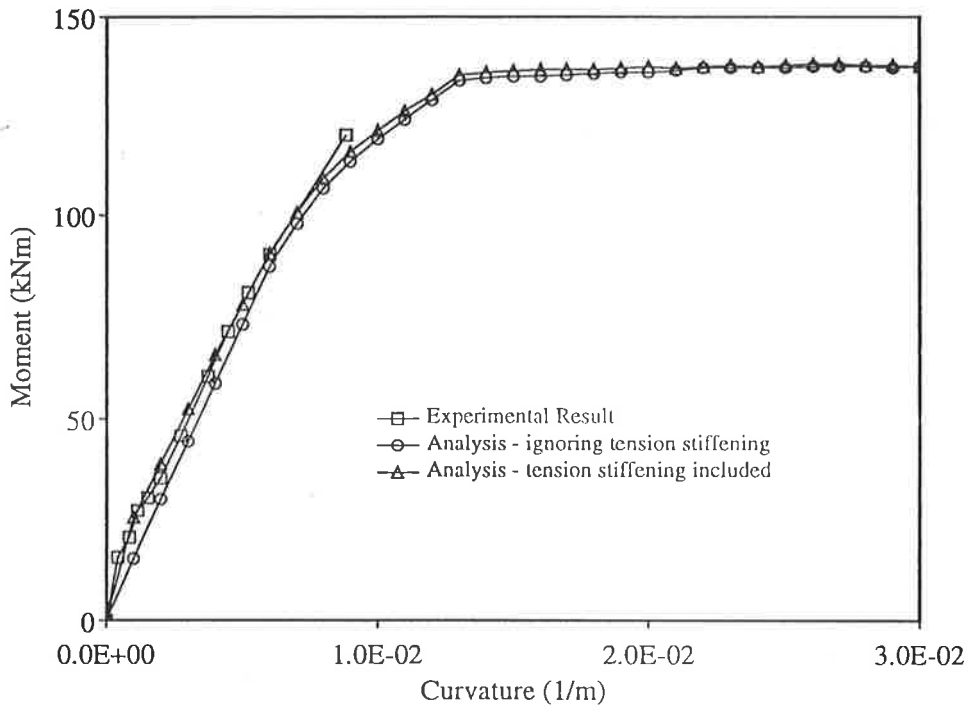
Figure D.4: Moment versus curvature for beam 2R
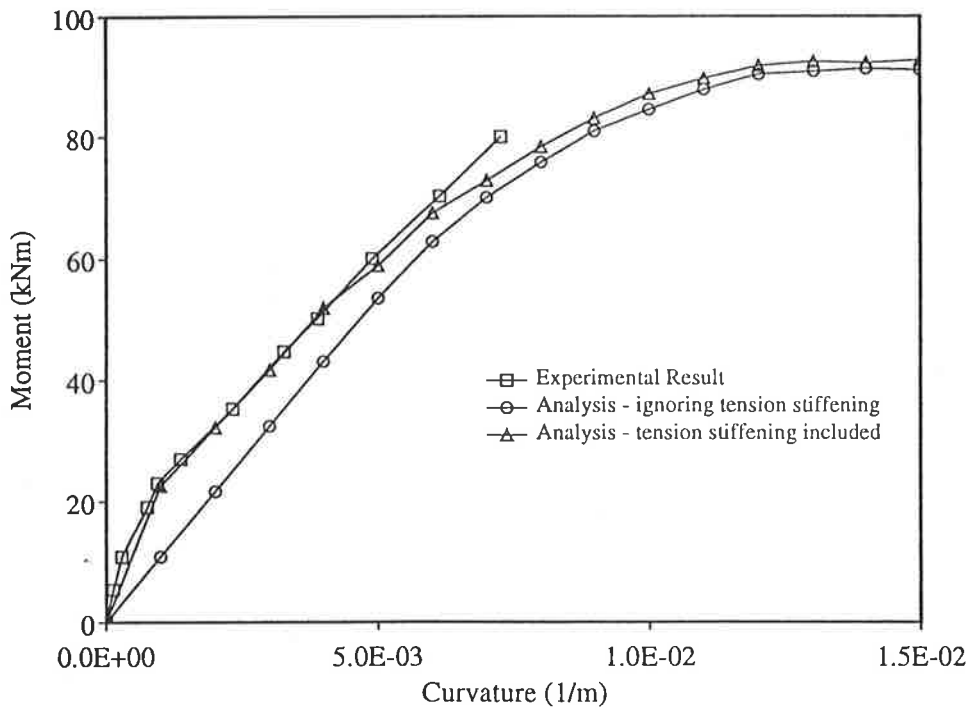
Figure D.5: Moment versus curvature for beam 3
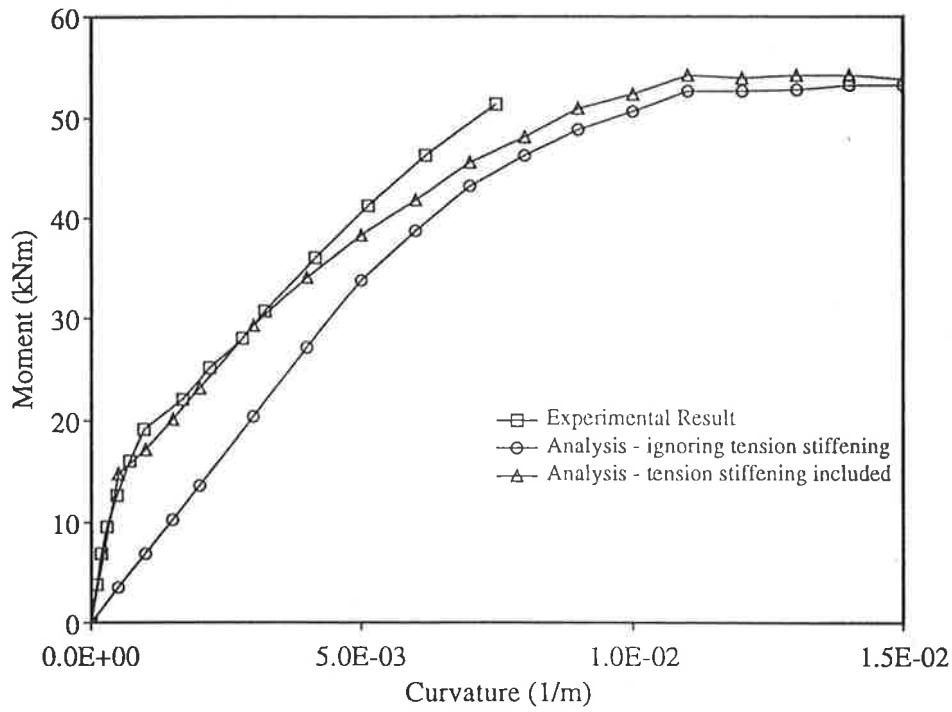
Figure D.6: Moment versus curvature for beam 4
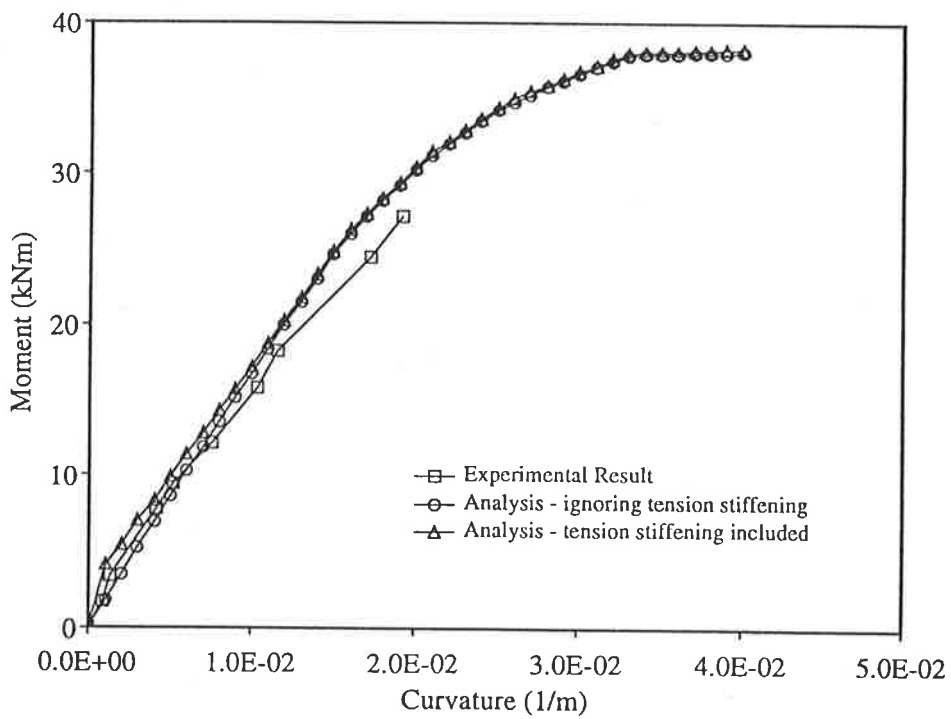
Figure D.7: Moment versus curvature for beam 5
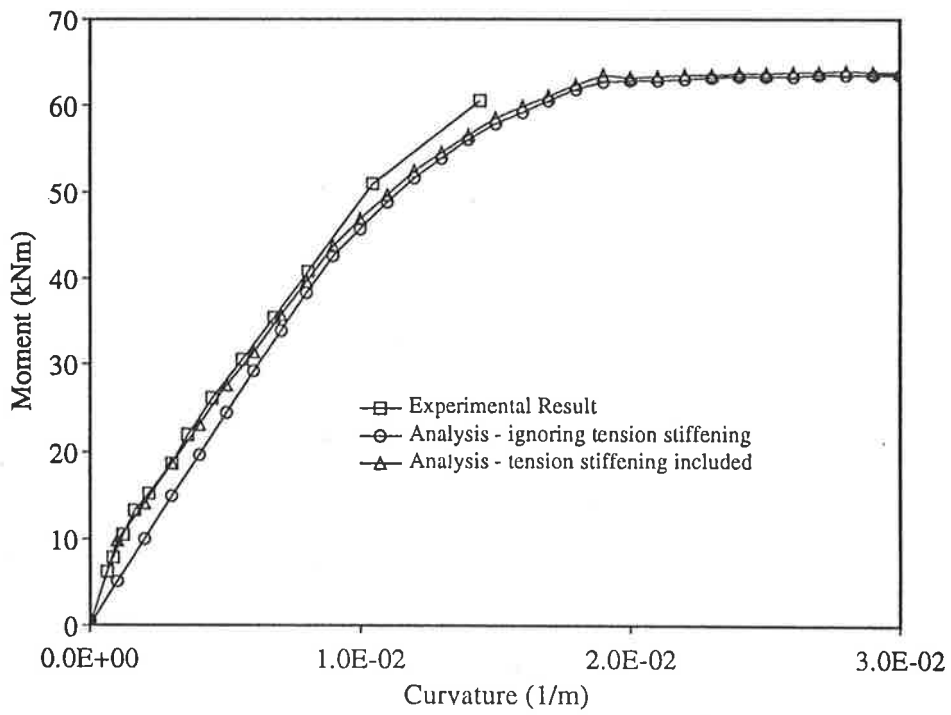
Figure D.8: Moment versus curvature for beam 6
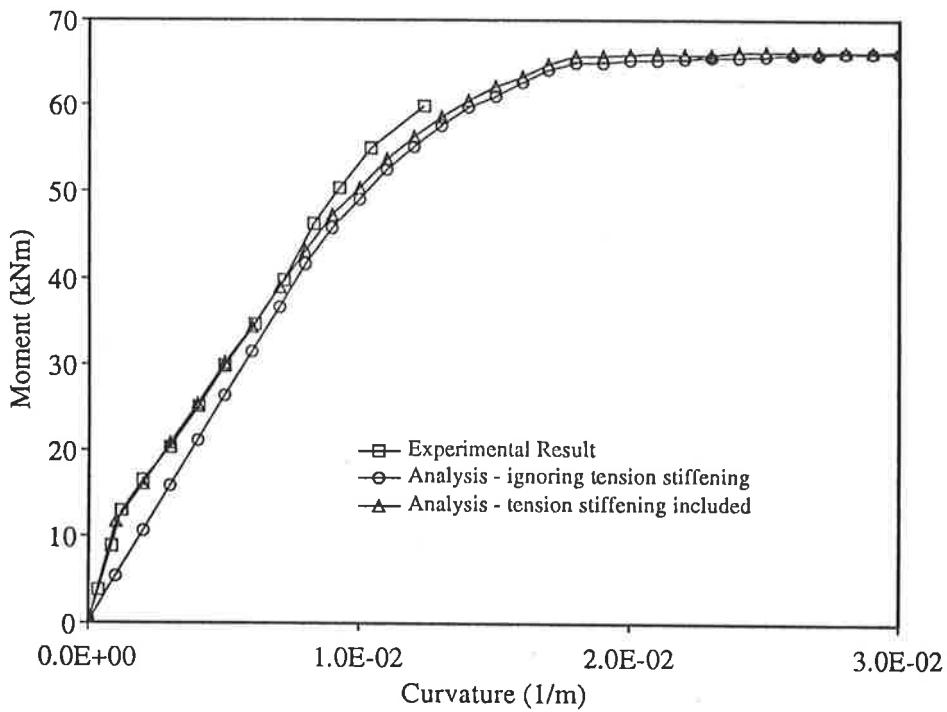
Figure D.9: Moment versus curvature for beam 6R
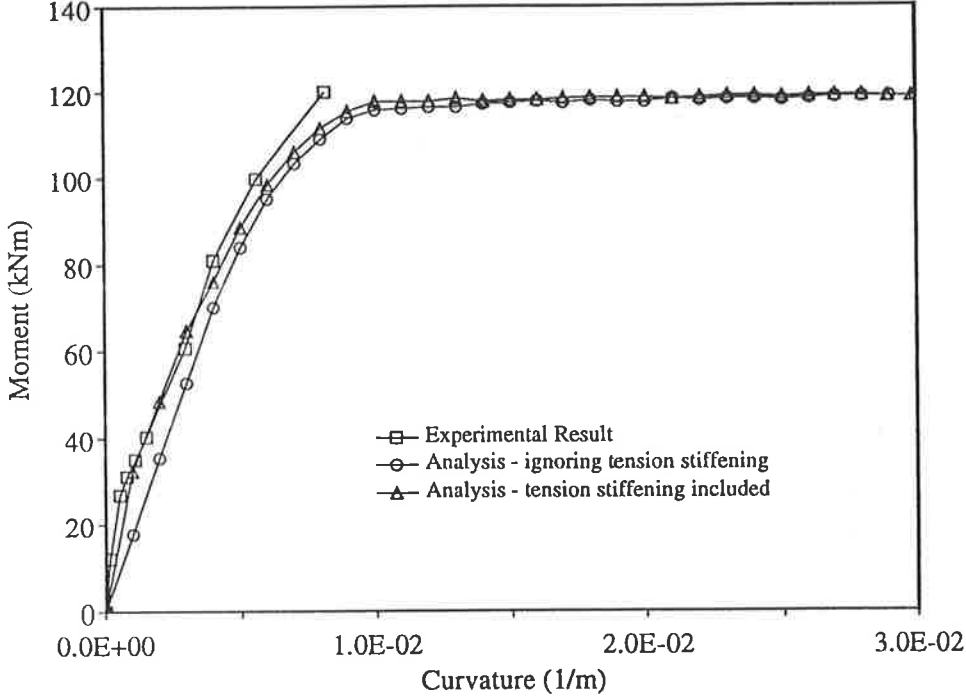
Figure D.10: Moment versus curvature for beam 7R

Bibliography

[1]   Aas-Jakobsen, K. and Grenacher, M.(1974), "Analysis of Slender Reinforced Concrete Frames," *IABSE, Publications*, Vol.34-I, Zürich, pp.1-17.

[2]   ACI Committee 209(1982), "Prediction of Creep, Shrinkage and Temperature Effects in Concrete Structures," *American Concrete Institute*, Detroit, 92 pp.

[3]   ACI Committee 224(1986), "Cracking of Concrete Members in Direct Tension," *ACI Journal*, Vol.83, no.1, Jan-Feb, pp.3 -13.

[4]   ACI Committee 318(1983), "Building Code Requirements for Reinforced Concrete (ACI 318-83)," *American Concrete Institute*, Detroit, 111 pp.

[5]   Aguado, A., Murcia, J. and Mari, A.(1981), "Nonlinear Analysis of Concrete Structures by the Imposed Deformations Method. Comparison with Experimental Results," *IABSE, Reports of the Working Commission*, BD 33, Delft, pp.255-262.

[6]   Ahmad, A. and Warner, R.F.(1984), "Ductility Requirements for Continuous Reinforced Concrete Structures," *Research Report no.R62*, Dept. of Civil Engineering, University of Adelaide, January, 23 pp.

[7]   Aldstedt, E. and Bergan, P.G.(1974), "Large Deformation and Stability Analysis of Reinforced Concrete Frames Considering Material Nonlinearities," *IABSE, Reports of the Working Commission*, BD 16, Quebec, pp.61-69.

[8]   Allwood, R.J.(1980), "Reinforcement Stresses in a Reinforced Concrete Beam-Column Connection," *Magazine of Concrete Research*, Vol.32, no.112, September, pp.143-146.

[9]   Alwis, W.A.M.(1990), "Trilinear Moment-Curvature Relationship for Reinforced Concrete Beams," *ACI Structural Journal*, Vol.87, no.3, May-June, pp.276-283.

[10]   Al-Zaid, R.Z., Al-Shaikh, A.H. and Abu-Hussein, M.M.(1991), "Effect of Loading Type on the Effective Moment of Inertia of Reinforced Concrete Beams," *ACI Structural Journal*, Vol.88, no.2, March-April, pp.184-190.

[11]   Argyris, J.H.(1966), "Continua and Discontinua, " *Proceedings, Conference on Matrix Methods in Structural Mechanics*, Wright-Patterson Air Force Base, Ohio, Oct. 26-28, 1965, AFFDL TR 66-80, pp.11-189.

[12]   AS1480-1982 (1982), *SAA Concrete Structures Code*, Standards Association of Australia, 104 pp.

[13]   AS3600-1988 (1988), *SAA Concrete Structures Code*, Standards Association of Australia, 108 pp.

[14]   Attiogbe, E. and Morris, G.(1991), "Moment-Rotation Functions for Steel Connections," *Journal of Structural Engineering, ASCE*, Vol.117, no.6, June, pp.1703-1717.

[15]   Bachmann, H. and Thürlimann, B.(1965), "Versuche über das Plastische Verhalten von Zweifeldrigen Stahlbetonbalken," *Serie A, Institut für Baustatik, Eidgenössische Technische Hochschule,* Zürich, Bericht Nr. 6203-1, Juli, 131 pp.

[16]   Baker, A.L.L. and Amarakone, A.M.N.(1964), "Inelastic Hyperstatic Frames Analysis," Flexural Mechanics of Reinforced Concrete, *ACI Special Publication SP-12*, Miami, Florida, pp.85-136.

[17]   Balakrishnan, S., Elwi, A.E. and Murray, D.W.(1988), "Effect of Modeling on NLFE Analysis of Structures," *Journal of Structural Engineering, ASCE*, Vol.114, no.7, July, pp.1467-1487.

[18]   Balakrishnan, S. and Murray, D.W.(1988), "Concrete Constitutive Model for NLFE Analysis of Structures", *Journal of Structural Engineering, ASCE*, Vol.114, no.7, July, pp.1449-1466.

[19]   Balint, P.S. and Taylor, H.P.J.(1972), "Reinforcement Detailing of Frame Corner Joints with Particular Reference to Opening Corners," *Technical Report 42.462*, Cement and Concrete Association, London, England, February, 16 pp.

[20]   Bathe, K.J. and Ozdemir, H.(1975), "Elastic-Plastic Deformation Static and Dynamic Analysis," *Computers and Structures*, Vol.6, no.2, April, pp.81-92.

[21]   Bazant, Z.P. and Oh, B.H.(1983), "Crack Band Theory for Fracture of Concrete," *Materials and Structures/Research and Testing* (RILEM, Paris), Vol.16, no.93, July, pp.155-177.

[22]   Bazant, Z.P. and Oh, B.H.(1984), "Deformation of Progressively Cracking Reinforced Concrete ," *ACI Journal*, Vol.81, no.3, May-June, pp.268-278.

[23]   Bazant, Z.P., Pan, J. and Pijaudier-Cabot, G.(1987a), "Softening of Reinforced Concrete Beams and Frames," *Journal of Structural Engineering*, Vol.113, no.12, December, pp.2333-2347.

[24]   Bazant, Z.P., Pan, J. and Pijaudier-Cabot, G.(1987b), "Ductility, Snapback, Size Effect, and Redistribution in Softening Beams or Frames," *Journal of Structural Engineering*, Vol.113, no.12, December, pp.2348-2364.

[25]   Bell, J.C. and Elms, D.G.(1971), "A Finite Element Approach to Post Elastic Slab Behaviour," Cracking, Deflection and Ultimate Load of Concrete Slab Systems, *ACI Special Publication SP-30*, Detroit, Michigan, pp.325-344.

[26]   Bergan, P.G.(1980), "Solution Algorithms for Nonlinear Structural Problems," *Computers and Structures*, Vol.12, no.4, Oct., pp.497-509.

[27]   Berwanger, C.(1975), "Effect of Axial Load on the Moment-Curvature Relationship of Reinforced Concrete Members," Reinforced Concrete Columns, *ACI Special Publication, SP-50*, Detroit, Michigan, pp.263-288.

[28] Birnstiel, C. and Iffland, J.S.B.(1980), "Factors Influencing Frame Stability," *Journal of the Structural Division, ASCE*, Vol.106, no.ST2, pp.491-504.

[29] Bjorhovde, R., Colson, A. and Brozzetti, J.(1990), "Classification System for Beam-to-Column Connections," *Journal of Structural Engineering, ASCE*, Vol.116, no.11, November, pp.3059-3076.

[30] Blaauwendraad, J.(1972), "Realistic Analysis of Reinforced Concrete Framed Structures," *Heron*, Vol.18, no.4, 31 pp.

[31] Blaauwendraad, J. and De Groot, A.K.(1983), "Progress in Research on Concrete Plane Frames," *Heron*, Vol.28, no.2, 59 pp.

[32] Blomeier, G.A.(1968), "Effect of Yielding of Restraints on Slender Concrete Columns in Braced Frames," *Ph.D. Thesis*, University of Texas at Austin, August, 218 pp.

[33] Braam, C.R.(1990), "Control of Crack Width in Deep Reinforced Concrete Beams," *Heron*, Vol.35, no.4, 105 pp.

[34] Breen, J.E.(1962), "The Restrained Long Concrete Column as a Part of a Rectangular Frame," *Ph.D. Thesis*, University of Texas at Austin, June, 228 pp.

[35] Breen, J.E.(1964), "Computer Use in Studies of Frames with Long Columns," Flexural Mechanics of Reinforced Concrete, *ACI Special Publication SP-12*, Miami, Florida, pp.535-556.

[36] Breen, J.E., MacGregor, J.G. and Pfrang, E.O.(1972), "Determination of Effective Length Factors for Slender Concrete Columns," *ACI Journal*, Vol.69, no.11, Nov., pp.669-672.

[37] Bridge, R.Q. and Pham, L.(1987), "Safety Indices for Reinforced Concrete Beam-Columns," *Civil Engineering Transactions*, Institution of Engineers, Australia, Vol.CE29, no.1, February, pp.40-46.

[38] Broms, B. and Viest, I.M.(1958), "Ultimate Strength Analysis of Long Hinged Reinforced Concrete Columns," *Journal of the Structural Division, ASCE*, Vol.84, no.ST1, January.

[39] Bull, F.B. and Sved, G.(1964), *Moment Distribution in Theory and Practice*, Pergamon Press, United Kingdom, 294 pp.

[40] Burnett, E.F.P. and Jajoo, R.P.(1971), "Reinforced Concrete Beam-Column Connection," *Journal of the Structural Division, ASCE*, Vol.97, no.ST9, September, pp.2315-2335.

[41] Burnett, E.F.P. and Trenberth, R.J.(1972), "Column Load Influence on Reinforced Concrete Beam-Column Connection," *ACI Journal*, Vol.69, no.2, February, pp.101-109.

[42] Burnett, E.F.P. and Yu, C.W.(1964), "Reinforced Concrete Linear Structures at Ultimate Load," Flexural Mechanics of Reinforced Concrete, *ACI Special Publication SP-12*, Miami, Florida, pp.29-47.

[43] Campbell, T.I. and Kodur, V.K.R.(1990), "Deformation Controlled Nonlinear Analysis of Prestressed Concrete Continuous Beams," *PCI Journal*, Vol.35, no.5, Sept.-Oct., pp.42-55.

[44] Carreira, D.J. and Chu, K.-H.(1986), "Stress-Strain Relationship for Reinforced Concrete in Tension," *ACI Journal*, Vol.83, no.1, Jan.-Feb., pp.21-28.

[45] Carse, A. and Behan, J.E.(1980), "Static Chord Modulus of Elasticity of High Strength Concrete in Uniform Compression and Flexure," *Tenth ARRB Conference*, University of Sydney, Vol.10, Pt.3, Materials and Structures, 25-29 August, pp.46-56.

[46] Chajes, A. and Churchill, J.E.(1986), "Nonlinear Frame Analysis by Finite Element Methods," *Journal of Structural Engineering, ASCE*, Vol.113, no.6, June, pp.1221-1235.

[47]   Chang, W.F.(1967), "Inelastic Buckling and Sidesway of Concrete Frames," *Journal of the Structural Division, ASCE*, Vol.93, no.ST2, April, pp.287-300.

[48]   Chapra, S.C. and Canale, R.P.(1988), *Numerical Methods for Engineers*, MacGraw-Hill, 839 pp.

[49]   Cichon, C.(1984), "Large Displacement In-Plane Analysis of Elastic-Plastic Frames," *Computers and Structures*, Vol.19, no.5/6, pp.737-745.

[50]   Clark, L.A. and Spiers, D.M.(1978), "Tension Stiffening in Reinforced Concrete Beams and Slabs Under Short Term Load," *Technical Report 42-521*, Cement and Concrete Association, London, July, 19 pp.

[51]   Coates, R.C., Coutie, M.G. and Kong, F.K.(1980), *Structural Analysis*, 2nd Edition, Van Nostrand Reinhold (UK), 579 pp.

[52]   Cohn, M.Z. and Petcu, V.A.(1963), "Moment Redistribution and Rotation Capacity of Plastic Hinges in Redundant Reinforced Concrete Beams," *Indian Concrete Journal*, Vol.37, no.8, August, pp.282-290.

[53]   Collins, M.P. and Mitchell, D.(1987), *Prestressed Concrete Basics*, 1st Edition, Canadian Prestressed Concrete Institute, Ottawa, 614 pp.

[54]   Connor, J.J., Logcher, R.D. and Chan, S.C.(1968), "Nonlinear Analysis of Elastic Frame Structures," *Journal of the Structural Division, ASCE*, Vol.94, no.ST6, June, pp.1525-1547.

[55]   Corderoy, H.J.B.(1978), "Analysis of Slender Reinforced Concrete Frames by SONLA," *Civil Engineering Monograph*, no. C.E.78/1 ST.E., New South Wales Institute of Technology, Australia.

[56]   Corley, W.G.(1966), "Rotational Capacity of Reinforced Concrete Beams," *Journal of the Structural Division, ASCE*, Vol.92, no.ST5, October, pp.121-146.

[57]   Cranston, W.B.(1965), "A Computer Method for Inelastic Analysis of Plane Frames," *Technical Report TRA 386*, Cement and Concrete Association, London, England, March, 38 pp.

[58]   Crisfield, M.A.(1980), "The Automatic Non-linear Finite Element Analysis of Stiffened Plates and Shallow Shells," *Proceedings, Institution of Civil Engineers*, London, Vol.69, Part 2, pp.891-909.

[59]   Crisfield, M.A.(1981), "A Fast Incremental/Iterative Solution Procedure that Handles 'Snap Through'," *Computers and Structures*, Vol.13, pp.55-62.

[60]   Darvall, P. LeP.(1982), "Critical Softening Parameters and Full-Range Analysis for Indeterminate Beams," *Research Report no.2/1982*, Dept. of Civil Engineering, Monash University, 25 pp.

[61]   Darvall, P. LeP.(1984), "Critical Softening of Hinges in Portal Frames," *Journal of Structural Engineering, ASCE*, Vol.110, no.1, January, pp.157-162.

[62]   Darvall, P. LeP. and Mendis, P.A.(1985), "Elastic-Plastic-Softening Analysis of Plane Frames," *Journal of Structural Engineering, ASCE*, Vol.111, no.4, April, pp.871-888.

[63]   de Araujo, J.M.(1989), "Optimization of Newton-Raphson Methods in RC Nonlinear Analysis," *Computers and Structures*, Vol.33, no.3, pp.735-741.

[64]   De Donato, O. and Maier, G.(1972), "Mathematical Programming Methods for the Inelastic Analysis of Reinforced Concrete Frames Allowing for Limited Rotation Capacity," *International Journal for Numerical Methods in Engineering*, Vol.4, no.3, May-June, pp.307-330.

[65]   Drysdale, R.G. and Mirza, M.S.(1974), "A Computer Analysis of Deflection of Statically Indeterminate Concrete Structures," Deflections of Concrete Structures, *ACI Special Publication SP-43*, Detroit, Michigan, pp.179-203.

[66]   Ehsani, M.R. and Wight, J.K.(1984), "Reinforced Concrete Beam-to-Column Connections Subjected to Earthquake-Type Loading," *Proceedings, Eighth World Conference on Earthquake Engineering*, San Francisco, Vol.6, pp.421-428.

[67]   El-Metwally, S.E. and Chen, W.F.(1988), "Moment-Rotation Modeling of Reinforced Concrete Beam-Column Connections," *ACI Structural Journal*, Vol.85, no.4, July-Aug., pp.384-394.

[68]   El-Metwally, S.E. and Chen, W.F.(1989a), "Load-Deformation Relations for Reinforced Concrete Sections," *ACI Structural Journal*, Vol.86, no.2, March-April, pp.163-167

[69]   El-Metwally, S.E. and Chen, W.F.(1989b), "Nonlinear Behaviour of R/C Frames," *Computers and Structures*, Vol.32, no.6, pp.1203-1209.

[70]   EN 1992 Eurocode EC2: Design of Concrete Structures, *European Committee for Standardisation*, draft version.

[71]   Ernst, G.C., Smith, G.M., Riveland, A.R. and Pierce, D.N.(1973), "Basic Reinforced Concrete Performance Under Vertical and Lateral Loads," *ACI Journal*, Vol.70, no.4, April, pp.261-269.

[72]   Espion, B.(1986), "Nonlinear Analysis of Framed Structures with a Plasticity Minded Beam Element," *Computers and Structures*, Vol.22, no.5, pp.831-839.

[73]   Evans, R.H. and Marathe, M.S.(1968), "Microcracking and Stress-Strain Curves for Concrete in Tension," *Materials and Structures/Research and Testing* (RILEM, Paris), Vol.1, no.1, Jan.- Feb., pp.61-64.

[74]   Ferguson, P.M. and Breen, J.E.(1966), "Investigation of the Long Concrete Column in a Frame Subjected to Lateral Loads," Symposium on Reinforced Concrete Columns, *ACI Special Publication SP-13*, Detroit, Michigan, pp.75-119.

[75]   Fey, T.(1966), "Approximate Second-Order Analysis of Reinforced Concrete Frames," *Bauingenieur*, Vol.41, no.6, June, pp.231-238.

[76]   Ford, J.S.(1977), "Behaviour of Concrete Columns in Unbraced Multipanel Frames," *Ph.D. Thesis,* University of Austin at Texas, December, 340 pp.

[77]   Ford, J.S., Chang, D.C. and Breen, J.E.(1981a), "Behaviour of Concrete Columns Under Controlled Lateral Deformation," *ACI Journal*, Vol.78, no.1, Jan.-Feb., pp.1-20.

[78]   Ford, J.S., Chang, D.C. and Breen, J.E.(1981b), "Experimental and Analytical Modeling of Unbraced Multipanel Concrete Frames," *ACI Journal*, Vol.78, no.1, Jan.-Feb., pp.21-35.

[79]   Ford, J.S., Chang, D.C. and Breen, J.E.(1981c), "Behaviour of Unbraced Multipanel Concrete Frames," *ACI Journal*, Vol.78, no.2, March-April, pp.99-115.

[80]   Fraser, D.J.(1983), "Evaluation of Effective Length Factors in Braced Frames," *Canadian Journal of Civil Engineering*, Vol.10, no.1, March, pp.18-26.

[81]   Furlong, R.W.(1963), "Long Columns in Single Curvature as a Part of Concrete Frames," *Ph.D. Thesis*, University of Texas at Austin, June, 170 pp.

[82]   Furlong, R.W. and Ferguson, P.M.(1966), "Tests of Frames with Columns in Single Curvature," Symposium on Reinforced Concrete Columns, *ACI Special Publication SP-13*, Detroit, Michigan, pp.55-73.

[83]   Ghoneim, G.A.M. and Ghali, A.(1982), "Nonlinear Analysis of Concrete Structures," *Canadian Journal of Civil Engineering*, Vol.9, no.3, September, pp.489-501.

[84]   Gilbert, R.I. and Warner, R.F.(1978), "Tension Stiffening in Reinforced Concrete Slabs," *Journal of the Structural Division, ASCE*, Vol.104, no.ST12, December, pp.1885-1900.

[85]   Gopalaratnam, V.S. and Shah, S.P.(1985), "Softening Response of Plain Concrete in Direct Tension," *ACI Journal*, Vol.82, no.3, May-June, pp.310-323.

[86]   Goto, Y.(1971), "Cracks Formed in Concrete Around Deformed Tension Bars," *ACI Journal*, Vol.68, no.4, April, pp.244-251.

[87] Goto, Y. and Chen, W.-F.(1987), "Second-Order Elastic Analysis for Frame Design," *Journal of Structural Engineering, ASCE*, Vol.113, no.ST7, July, pp.1501-1519.

[88] Graff, E. and Eisenberger, M.(1991), "Non-linear Analysis of Framed Structures with Axial Constraints," *Computers and Structures*, Vol.38, no.3, pp.345-351.

[89] Gunnin, B.L., Rad, F.N. and Furlong, R.W.(1977), "A General Nonlinear Analysis of Concrete Structures and Comparison with Frame Tests," *Computers and Structures*, Vol.7, no.2, pp.257-265.

[90] Gupta, A.K. and Maestrini, S.R.(1990), "Tension-Stiffness Model for Reinforced Concrete Bars," *Journal of Structural Engineering, ASCE*, Vol.116, no.3, March, pp.769-790.

[91] Hall, A.S.(1969a), "Joint Deformation in Building Frames," *Civil Engineering Transactions,* Institution of Engineers, Australia, Vol.CE11, no.1, pp.60-62.

[92] Hall, A.S.(1969b), "Deformation and Stresses within Joints of Plane Frames," *UNICIV Report no.R-51*, University of New South Wales, Australia, August, 12 pp.

[93] Hand, F.R., Pecknold, D.A. and Schnobrich, W.C.(1973), "Nonlinear Layered Analysis of RC Plates and Shells," *Journal of Structural Engineering, ASCE*, Vol.99, no.ST7, July, pp.1491-1505.

[94] Hawkins, N.M.(1970), "The Bearing Strength of Concrete for Strip Loadings," *Magazine of Concrete Research*, Vol.22, no.71, June, pp.87-98.

[95] Healey, D.M.(1993), "Influence of Method of Loading on Deflections and Ductility of Concrete Flexural Members," *M.Eng.Sci.*, draft version, University of Adelaide, Australia.

[96] Hellesland, J., Choudhury, D. and Scordelis, A.C. (1985), "Non-linear Analysis and Design of RC Bridge Columns Subjected to Imposed

Deformations," *Report no. UCB/SESM-85/03*, Dept. of Civil Engineering, University of California, Berkeley, California, April, 305 pp.

[97]   Hobbs, R.E. and Jowharzadeh, A.M.(1978), "An Incremental Analysis of Beam-Columns and Frames Including Finite Deformations and Bilinear Elasticity," *Computers and Structures*, Vol.9, no.3, pp.323-330.

[98]   Hognestad, E.(1951), "A Study of Combined Bending and Axial Load in Reinforced Concrete Members," *Bulletin no.399,* University of Illinois Engineering Experimental Station, November, 128 pp.

[99]   Holzer, S.M., Somers, A.E. and Bradshaw, J.C.(1979), "Finite Response of Inelastic RC Structures," *Journal of Sructural Engineering, ASCE*, Vol.105, no.ST1, January, pp.17-33.

[100] Hsu, C.-T.T., Mirza, M.S. and Sea, C.S.S.(1981), "Nonlinear Analysis of Reinforced Concrete Frames," *Computers and Structures*, Vol.13, no.1-3, June, pp.223-227.

[101] Hughes, B.P. and Chapman, G.P.(1966), "The Complete Stress-Strain Curve for Concrete in Direct Tension," *RILEM Bulletin* (Paris), New Series no.30, March, pp.95-97.

[102] Ingraffea, A.R., Gerstle, W.H., Gergely, P. and Saouma, V.(1984), "Fracture Mechanics of Bond in Reinforced Concrete," *Journal of Sructural Engineering, ASCE*, Vol.110, no.4, April, pp.871-890.

[103] Isaacson, E. and Keller, H.B.(1966), *Analysis of Numerical Methods*, John Wiley and Sons, 541 pp.

[104] Jennings, A.(1968), "Frame Analysis Including Change of Geometry," *Journal of the Structural Division, ASCE*, Vol.94, no.ST3, March, pp.627-644.

[105] Jiang, D.H., Shah, S.P. and Andonian, A.T.(1984), "Study of the Transfer of Tensile Stresses by Bond," *ACI Journal*, Vol.81, no.3, May-June, pp.251-259.

[106] Jofriet, J.C. and McNiece, G.M.(1971), "Finite Element Analysis of Reinforced Concrete Slabs," *Journal of the Structural Division, ASCE*, Vol.97, no.ST3, March, pp.785-806.

[107] Kam, T.Y.(1988), "Large Deflection Analysis of Inelastic Plane Frames," *Journal of the Structural Engineering," ASCE*, Vol.114, no.1, January, pp.184-197.

[108] Kang, Y.-J. and Scordelis, A.C.(1980), "Nonlinear Analysis of Prestressed Concrete Frames," *Journal of the Structural Division, ASCE*, Vol.106, no.ST2, February, pp.445-462.

[109] Kao, R.(1974), "A Comparison of Newton-Raphson Methods and Incremental Procedures for Geometrically Nonlinear Analysis," *Computers and Structures*, Vol.4, no.5, Oct., pp.1091-1097.

[110] Kayal, S.(1984), "Finite Element Analysis of RC Frames," *Journal of Structural Engineering, ASCE*, Vol.110, no.12, December, pp.2891-2908.

[111] Kemp, E.L. and Wilhelm, W.J.(1979), "Investigation of the Parameters Influencing Bond Cracking," *ACI Journal*, Vol.76, no.1, January, pp.47-71.

[112] Kent, D.C. and Park, R.(1971), "Flexural Members with Confined Concrete," *Journal of the Structural Division, ASCE*, Vol.97, no.ST7, July, pp.1969-1990.

[113] Kenyon, J.M. and Warner, R.F.(1992), "Refined Analysis of Non-Linear Behaviour of Concrete Structures," *Research Report no.97*, Department of Civil Engineering, University of Adelaide, August, 14 pp.

[114] Kenyon, J.M. and Warner, R.F.(1993), "Refined Analysis of Non-Linear Behaviour of Concrete Structures," *Civil Engineers Transactions*, Institution of Engineers, Australia, Vol. CE35, no.3, August, pp.213-220.

[115] Kgoboko, K.(1987), "Collapse Behaviour of Non-ductile Partially Prestressed Concrete Bridge Girders," *M.Eng.Sci. Thesis*, University of Adelaide, November, 338 pp.

[116] Klink, S.A.(1985), "Actual Elastic Modulus of Concrete," *ACI Journal*, Vol.82, no.5, Sept.-Oct., pp.630-633.

[117] Kotsovos, M.D.(1987), "Consideration of Triaxial Stress Conditions in Design: A Necessity," *ACI Structural Journal*, Vol.84, no.3, May-June, pp.266-273.

[118] Kotsovos, M.D. and Newman, J.B.(1981), "Effect of Boundary Conditions upon the Behaviour of Concrete Under Concentrations of Load," *Magazine of Concrete Research*, Vol.33, no.116, September, pp.161-170.

[119] Kroenke, W.C., Gutzwiller, M.J. and Lee, R.H.(1973), "Finite Element for Reinforced Concrete Frame Study," *Journal of the Structural Division, ASCE*, Vol.99, no.ST7, July, pp.1371-1390.

[120] Kulicki, J.M. and Kostem, C.N.(1974), "Inelastic Analysis of Reinforced Concrete Beam Columns," *IABSE, Reports of the Working Commission*, BD 16, Quebec, pp.71-78.

[121] Kupfer, H.B. and Gerstle, K.H.(1973), "Behaviour of Concrete Under Biaxial Stresses," *Journal of the Engineering Mechanics Division, ASCE*, Vol.99, no.EM4, August, pp.853-866.

[122] Kupfer, H.B., Hilsdorf, H.K. and Rusch, H.(1969), "Behaviour of Concrete Under Biaxial Stress," *ACI Journal*, Vol.66, no.8, August, pp.656-666.

[123] Lai, S.-M.A., and MacGregor, J.G.(1983), "Geometric Nonlinearities in Unbraced Multistory Frames," *Journal of Structural Engineering, ASCE*, Vol.109, no.11, November, pp.2528-2545.

[124] Lai, S.-M.A., MacGregor, J.G. and Hellesland, J.(1983), "Geometric Nonlinearities in Nonsway Frames," *Journal of Structural Engineering, ASCE*, Vol.109, no.12, December, pp.2770-2785.

[125] Lazaro, A.L. and Richards, R.(1973), "Full-Range Analysis of Concrete Frames," *Journal of the Structural Division, ASCE*, Vol.99, no.ST8, August, pp.1761-1783.

[126] L'Hermite, R.(1955), "Idées actuelles sur la technologie due béton," *Documentation Technique du Bâtiment et des Travaux Publics*, Paris.

[127] Lin, C-S. and Scordelis, A.C.(1975), "Nonlinear Analysis of RC Shells of General Form," *Journal of the Structural Division, ASCE*, Vol.101, no.ST3, March, pp.523-538.

[128] Link, R.A., Elwi, A.E. and Scanlon, A.(1989), "Biaxial Tension Stiffening due to Generally Oriented Reinforcing Layers," *Journal of Engineering Mechanics, ASCE*, Vol.115, no.8, August, pp.1647-1662.

[129] Liu, T.C.Y, Nilson, A.H. and Slate, F.O.(1972), "Stress-Strain Response and Fracture of Concrete in Uniaxial and Biaxial Compression," *ACI Journal*, Vol.69, no.5, May, pp.291-295.

[130] Livesley, R.K. and Chandler, D.B.(1956), *Stability Functions for Structural Frameworks*, Manchester University Press.

[131] Lutz, L.A.(1970), "Analysis of Stresses in Concrete Near a Reinforcing Bar Due to Bond and Transverse Cracking," *ACI Journal*, Vol.67, no.10, October, pp.778-787.

[132] Lutz, L.A. and Gergely, P.(1967), "Mechanics of Bond and Slip of Deformed Bars in Concrete," *ACI Journal*, Vol.64, no.11, November, pp.711-721.

[133] Ma, S.Y.A. and May, I.M.(1986), "The Newton-Raphson Method Used in the Non-Linear Analysis of Concrete Structures," *Computers and Structures*, Vol.24, no.2, pp.177-185.

[134] MacGregor, J.G.(1979), "Out-of-plumb Columns in Concrete Structures," *Concrete International,*" Vol.1, no.6, June, pp.26-31.

[135] MacGregor, J.G. and Barter, S.L.(1966), "Long Eccentrically Loaded Concrete Columns Bent in Double Curvature," Symposium on Reinforced Concrete Columns, *ACI Special Publication SP-13*, Detroit, Michigan, pp.139-156.

[137] MacGregor, J.G., Breen, J.E. and Pfrang, E.O.(1970), "Design of Slender Concrete Columns," *ACI Journal*, Vol.67, no.1, January, pp.6-28.

[138] MacGregor, J.G. and Hage, S.E.(1977), "Stability Analysis and Design of Concrete Frames," *Journal of the Structural Division, ASCE*, Vol.103, no.ST10, October, pp.1953-1970.

[139] MacGregor, J.G., Oelhafen, U.H. and Hage, S.E.(1975), "A Re-Examination of the EI Value for Slender Columns," Reinforced Concrete Columns, *ACI Special Publication SP-50*, Detroit, Michigan, pp.1-40.

[140] Mallett, R.H. and Marcal, P.V.(1968), "Finite Element Analysis of Nonlinear Structures," *Journal of the Structural Division, ASCE*, Vol.94, no.ST9, September, pp.2081-2105.

[141] Martin, H.C.(1966), "On the Derivation of Stiffness Matrices for the Analysis of Large Deflection and Stability Problems, " *Proceedings, Conference on Matrix Methods in Structural Mechanics*, Wright-Patterson Air Force Base, Ohio, Oct. 26-28, 1965, AFFDL TR 66-80, pp.697-716.

[142] Martin, H.C. and Carey, G.F.(1973), *Introduction to Finite Element Analysis*, MacGraw-Hill, 386 pp.

[143] Martin, I. and Olivieri, E.(1966), "Tests of Slender Reinforced Concrete Columns Bent in Double Curvature," Symposium on Reinforced Concrete Columns, *ACI Special Publication SP-13*, Detroit, Michigan, pp.121-138.

[144] Massicotte, B., Elwi, A.E. and MacGregor, J.G.(1990), "Tension-Stiffening Model for Planar Reinforced Concrete Members," *Journal of Structural Engineering, ASCE*, Vol.116, no.11, November, pp.3039-3057.

[145] Mattock, A.H.(1969), "Diagonal Tension Cracking in Concrete Beams with Axial Forces," *Journal of the Structural Division, ASCE*, Vol.95, no.ST9, September, pp.1887-1900.

[146] Mayfield, B., Kong, F.-K. and Bennison, A.(1972), "Strength and Stiffness of Lightweight Concrete Corners," *ACI Journal*, Vol.69, no.7, July, pp.420-427.

[147] Mayfield, B., Kong, F.-K., Bennison, A. and Davies, J.C.D.T.(1971), "Corner Joint Details in Structural Lightweight Concrete," *ACI Journal*, Vol.68, no.5, May, pp.366-372.

[148] McAdie, R.L., Resende, L. and Martin, J.B.(1987), "Nonlinear Stability Analysis of Framed Structures by Finite Elements," *The Civil Engineer in South Africa*, Vol.29, May, pp.165-174.

[149] Meek, J.L.(1991), *Computer Methods in Structural Analysis*, E & FN Spon, 503 pp.

[150] Meinheit, D.F. and Jirsa, J.O.(1981), "Shear Strength of R/C Beam-Column Connections," *Journal of the Structural Division*, Vol.107, no.ST11, Nov., pp.2227-2243.

[151] Mendis, P.A.(1986), "Softening of Reinforced Concrete Structures," *Ph.D. Thesis*, Monash University, Australia, 358 pp.

[152] Mendis, P.A. and Darvall, P. LeP.(1988), "Stability Analysis of Softening Frames," *Journal of Structural Engineering*, Vol.114, no.5, May, pp.1057-1072.

[153] Menn, C.(1974), "Simple Method for Determining the Ultimate Load for Slender Compression Members," *IABSE, Reports of the Working Commission*, BD 16, Quebec, pp.137-144.

[154] Mirza, S.M. and Houde, J.(1979), "Study of Bond Stress-Slip Relationships in Reinforced Concrete," *ACI Journal*, Vol.76, no.1, January, pp.19-46.

[155] Mo, Y.L.(1986), "Moment Redistribution in Reinforced Concrete Frames," *ACI Journal*, Vol.83, no.4, July-Aug., pp.577-587.

[156] Monnier, Th.(1970), "The Moment-Curvature Relation of Reinforced Concrete," *Heron*, Vol.17, no.2, 101 pp.

[157] Moucessian, A. and Campbell, T.I.(1988), "Prediction of the Load Capacity of Two-Span Continuous Prestressed Concrete Beams," *PCI Journal*, Vol.33, no.2, March-April, pp.130-151.

[158] Neville, A.M.(1981), *Properties of Concrete*, 3rd Edition, Longman Scientific and Technical, 779 pp.

[159] Ngo, D. and Scordelis, A.C.(1967), "Finite Element Analysis of Reinforced Concrete Beams," *ACI Journal*, Vol.64, no.3, March, pp.152-163.

[160] Nilson, A.H.(1968), "Nonlinear Analysis of Reinforced Concrete by the Finite Element Method," *ACI Journal*, Vol.65, no.9, September, pp.757-766.

[161] Nilson, A.H.(1972), "Internal Measurement of Bond Slip," *ACI Journal*, Vol.69, no.7, July, pp.439-441.

[162] Nilsson, I.H.E.(1965), "Undersökning av Vingmurshörn," *Publikation 65:3*, Institutionen för Konstruktionsteknik Betongbyggnad, Chalmers Tekniska Högskola, Göteborg, Sweden, September, 39 pp.

[163] Nilsson, I.H.E.(1968), "Ramhörn av armerad Betong med positivt moment. Försöksrapporter 1-4," *Rapport 66:2, 67:1, 68:2, 68:3*. Institutionen for Konstruktionsteknik Betongbyggnad, Chalmers Tekniska Högskola, Göteborg, Sweden, May.

[164] Nilsson, I.H.E.(1969a), "Ks 60 - armerade ramhörn med positivt moment. Försöksrapport 5," *Rapport 69:1*, Institutionen för Konstruktionsteknik Betongbyggnad, Chalmers Tekniska Högskola, Göteborg, Sweden, October, 46 pp.

[165] Nilsson, I.H.E.(1969b), "Ramhörn av armerad betong med positivt moment. Konstruktiv utformning av ramhörn med dragen insida," *Rapport 11:1969*, Rapport från Byggforskningen, Stockholm, 46 pp.

[166] Nilsson, I.H.E.(1973), "Reinforced Concrete Corners and Joints Subjected to Bending Moment," *Document D7:1973*, National Swedish Building Research, Stockholm, Sweden, 249 pp.

[167] Nilsson, I.H.E. and Losberg, A.(1976), "Reinforced Concrete Corners and Joints Subjected to Bending Moment," *Journal of the Structural Division, ASCE*, Vol.102, no.ST6, June, pp.1229-1254.

[168] Niyogi, S.K.(1974), "Concrete Bearing Strength - Support, Mix, Size Effect," *Journal of the Structural Division, ASCE*, Vol.100, no.ST8, August, pp.1685-1702.

[169] Noguchi, H.(1981), "Nonlinear Finite Elements Analysis of Reinforced Concrete Beam-Column Joints," *IABSE, Reports of the Working Commission*, BD 34, Delft, pp.639-654.

[170] Oelhafen, U.H.(1974), "Accuracy of Simple Design Procedures for Concrete Columns," *IABSE, Reports of the Working Commission*, BD 16, Quebec, pp.93-115.

[171] Okamura, H., Pagay, S.N., Breen, J.E. and Ferguson, P.M.(1967), "Elastic Frame Analysis - Corrections Necessary for Design of Short Concrete Columns in Braced Frames," *ACI Journal*, Vol.67, no.11, November, pp.894-897.

[172] Oran, C.(1973), "Tangent Stiffness in Plane Frames," *Journal of the Structural Division, ASCE*, Vol.99, no.ST6, June, pp.973-985.

[173] Oran, C. and Kassimali, A.(1976), "Large Deformations of Framed Strutures Under Static Loading and Dynamic Loads," *Computers and Structures*, Vol.6, no.6, Dec., pp.539-547.

[174] Pagay, S.N., Ferguson, P.M. and Breen, J.E.(1970), "Importance of Beam Properties on Concrete Column Behaviour," *ACI Journal*, Vol.67, no.10, October, pp.808-815.

[175] Park, R. and Paulay, T.(1975), *Reinforced Concrete Structures*, Wiley, New York, 769 pp.

[176] Park, R., Priestly, M.J.N. and Gill, W.D.(1982), "Ductility of Square-Confined Concrete Columns," *Journal of the Structural Division, ASCE,* Vol.108, no.ST4, April, pp.929-950.

[177] Parme, A.L.(1966), "Capacity of Restrained Eccentrically Loaded Long Columns," Symposium on Reinforced Concrete Columns, *ACI Special Publication SP-13,* Detroit, Michigan, pp.325-367.

[178] Pfrang, E.O., Seiss, C.P. and Sozen, M.A.(1964), "Load-Moment-Curvature Characteristics of Reinforced Concrete Cross Sections," *ACI Journal,* Vol.61, no.7, July, pp.763-778.

[179] Phillips, D.V. and Zienkiewicz, O.C.(1976), "Finite Element Non-linear Analysis of Concrete Structures," *Proceedings, Institution of Civil Engineers,* London, Vol.61, Part 2, March, pp.59-88.

[180] Powell, G.H.(1969), "Theory of Nonlinear Elastic Structures," *Journal of the Structural Division, ASCE,* Vol.95, no.ST12, December, pp.2687-2701.

[181] Przemieniecki, J.S.(1985), *Theory of Matrix Structural Analysis,* Dover Publications, New York, 468 pp.

[182] Rad, F.N.(1972), "Behaviour of Single Story Two-Column Reinforced Concrete Frames Under Combined Loading," *Ph.D. Thesis,* University of Austin at Texas, December, 295 pp.

[183] Rad, F.N. and Furlong, R.W.(1980), "Behaviour of Unbraced Reinforced Concrete Frames," *ACI Journal,* Vol.77, no.4, July-Aug., pp.269-278.

[184] Raphael, J.M.(1984), "Tensile Strength of Concrete," *ACI Journal,* Vol.81, no.2, March-April, pp.158-165.

[185] Riks, E.(1979), "An Incremental Approach to the Solution of Snapping and Buckling Problems," *International Journal of Solids and Structures,* Vol.15, pp.524-551.

[186] Riva, P. and Cohn, M.Z.(1990), "Engineering Approach to Nonlinear Analysis of Concrete Structures," *Journal of Structural Engineering, ASCE*, Vol.116, no.8, August, pp.2162-2186.

[187] Rosenblueth, E.(1965), "Slenderness Effects in Buildings," *Journal of the Structural Division, ASCE*, Vol.91, no.ST1, February, pp.229-252.

[188] Saafan, S.A.(1963), "Nonlinear Behaviour of Structural Plane Frames," *Journal of the Structural Division, ASCE*, Vol.89, no.ST4, August, pp.557-579.

[189] Scanlon, A. and Murray, D.W.(1974), "Time-Dependent Reinforced Concrete Slab Deflections," *Journal of the Structural Division, ASCE*, Vol.100, no.ST9, September, pp.1911-1924.

[190] Skettrup, E., Strabo, J., Andersen, N.H. and Brøndum-Nielsen, T.(1984), "Concrete Frame Corners," *ACI Journal* , Vol.81, no.6, Nov.-Dec., pp.587-593.

[191] Smith, R.G. and Bridge, R.Q.(1984), "Slender Braced Reinforced and Prestressed Concrete Columns- a Comparative Study," *Research Report no.R472*, School of Civil and Mining Engineering, University of Sydney, April, 15 pp.

[192] Soliman, M.T.M. and Yu, C.W.(1967), "The Flexural Stress-Strain Relationship of Concrete Confined by Rectangular Transverse Reinforcement," *Magazine of Concrete Research*, Vol.19, no.61, December, pp.223-238.

[193] Somerville, G. and Taylor, H.P.J.(1972), "The Influence of Reinforcement Detailing on the Strength of Concrete Structures," *The Structural Engineer*, Vol.50, no.1, January, pp.7-19.

[194] Somes, N.F.(1966), "Moment-Rotation Characteristics of Prestressed Concrete Members. Stages I: Rectangular Sections," *Technical Report TRA 398*, Cement and Concrete Association, London, England, September, 80 pp.

[195] Stevens, L.K.(1967), "Elastic Stability of Practical Multi-Storey Frames," *Proceedings, Institution of Civil Engineers*, London, Vol.36, pp.99-117.

[196] Sved, G.(1988), "A Non-iterative Solution of the Axial Force-Moment-Curvature Problem for Rectangular Reinforced Concrete Sections, " *11th Australasian Conference on the Mechanics of Structures and Materials*, University of Auckland, pp.105-107.

[197] Swann, R.A.(1969), "Flexural Strength of Corners of Reinforced Concrete Portal Frames," *Technical Report TRA 434*, Cement and Concrete Association, London, England, November, 15 pp.

[198] Taylor, H.P.J.(1974), "The Behavior of In Situ Concrete Beam-Column Joints," *Technical Report 42.492*, Cement and Concrete Association, London, England, May, 32 pp.

[199] Tse, D. and Darvall, P.LeP.(1988), "Softening Hinges in Reinforced Concrete Beams," *Research Report No. 3/1988*, Dept. of Civil Engineering, Monash University, 110 pp.

[200] Turner, M.J., Dill, E.H., Martin, H.C. and Melosh, R.J.(1960) "Large Deflections of Structures Subjected to Heating and External Loads," *Journal of the Aero/Space Sciences*, Vol.27, no.2, February, pp.97-106.

[201] van den Beukel, A.(1977), "Non-linear Analysis of Concrete Members," *Heron*, Vol.22, no.2, 24 pp.

[202] van Mier, J.G.M.(1987), "Examples of Non-linear Analysis of Reinforced Concrete Structures with DIANA," *Heron*, Vol.32, no.3, 147 pp.

[203] Vanderbilt, M.D.(1974), *Matrix Structural Analysis*, Quantum Publishers, 397 pp.

[204] Virdi, K.S.(1977), "A New Technique for Moment-Thrust-Curvature Calculations for Columns in Biaxial Bending," *Sixth Australasian Conference on Mechanics of Structures and Materials*, University of Canterbury, New Zealand, pp.307-313.

[205] Virdi, K.S. and Dowling, P.J.(1976), "The Ultimate Strength of Biaxially Restrained Columns," *Proceedings, Institution of Civil Engineers*, London, Vol.61, Part 2, March, pp.41-58.

[206] Warner, R F.(1969), "Biaxial Moment Thrust Curvature Relations," *Journal of the Structural Division, ASCE*, Vol.95, no.ST5, May, pp.923-940.

[207] Warner, R.F.(1975), "Segmental Analysis for Non-linear Concrete Frames," *Fifth Australasian Conference on Mechanics of Structures and Materials*, University of Melbourne, August, pp.535-548.

[208] Warner, R.F.(1993), "Non-linear Design of Concrete Structures," *Thirteenth Australasian Conference on Mechanics of Structures and Materials*, University of Wollongong, July, pp.913-920.

[209] Warner, R.F. and Lambert, J.H.(1974), "Moment-Curvature-Time Relations for Reinforced Concrete Beams," *IABSE, Publications*, Vol.34-I, Zürich, pp.181-203.

[210] Warner, R.F. and Yeo, M.F.(1984), "Collapse Behaviour of Concrete Structures with Limited Ductility," *Research Report no.R61*, Department of Civil Engineering, University of Adelaide, January, 23 pp.

[211] Warner, R.F. and Yeo, M.F.(1986), "Ductility Requirements for Partially Prestressed Concrete," *Partial Prestressing from Theory to Practice*, Vol.II, Martinus Nijhoff Publishers, pp.315-326.

[212] Wen, R.K. and Rahimzadeh, J.(1983), "Nonlinear Elastic Frame Analysis by Finite Element," *Journal of Structural Engineering, ASCE*, Vol.109, no.8, August, pp.1952-1971.

[213] Wong, K.W.(1989), "Non-linear Behaviour of Reinforced Concrete Frames," *Ph.D. Thesis*, University of Adelaide, Australia, August, 359 pp.

[214] Wong, K.W. and Warner, R.F.(1990), "Middle Tier Analysis and Design of Slender Concrete Columns," *Twelfth Australasian Conference on the*

Mechanics of Structures and Materials, Queensland University of Technology, pp.163-168.

[215]   Wong, K.W., Yeo, M.F. and Warner, R.F.(1987), "Collapse Behaviour of Reinforced Concrete Frames," *Research Report no.R78A,* Department of Civil Engineering, University of Adelaide, August, 34 pp.

[216]   Wong, K.W., Yeo, M.F. and Warner, R.F.(1988), "Non-linear Behaviour of Reinforced Concrete Frames," *Civil Engineering Transactions,* Institution of Engineers, Australia, Vol.CE30, no.2, July, pp.57-65.

[217]   Wong, K.W., Yeo, M.F. and Warner, R.F.(1990), "Collapse Behaviour and Strength of Slender Concrete Frames," *Proceedings, George Sved Symposium,* University of Adelaide, May, pp.394-408.

[218]   Wood, B.R., Beaulieu, D. and Adams, P.F.(1976a), "Column Design by *P*-Delta Method," *Journal of the Structural Division, ASCE,* Vol.102, no.ST2, February, pp.411-427.

[219]   Wood, B.R., Beaulieu, D. and Adams, P.F.(1976b), "Further Aspects of Design by *P*-Delta Method," *Journal of the Structural Division, ASCE,* Vol.102, no.ST3, March, pp.487-500.

[220]   Yuan, R.L., McLelland, G.R. and Chen, W.F.(1982), "Experiments on Closing Reinforced Concrete Corners," *Journal of the Structural Division, ASCE,* Vol.108, no.ST4, April, pp.771-779.

[221]   Zienkiewicz, O.C.(1977), *The Finite Element Method in Engineering Science,* 2nd. Edition, McGraw-Hill, 787 pp.

CORRIGENDA

Ph D Thesis

J M Kenyon, 30 July 1994

Page 28   In the third sentence, "control" to read once.

Page 47   In line 4, "degress" to read "degrees".

Page 59   Second paragraph third sentence, delete "... much stronger and stiffer than the columns." and replace with "... much stronger than the columns under no axial thrust."

Page 61   After the last sentence of the second paragraph, add the following sentence: "Section details for this test beam are given in Appendix D and also in Figure 3.16."

Page 61   Delete the second sentence of the third paragraph, and replace with "It should also be noted the maximum moment and curvature from the published experimental results correspond to a steel strain of 200 microstrains. Actual load deformation response for this beam, or any of the other test beams by Clark and Spiers, at levels of steel strain beyond 200 microstrains was not mentioned."

Page 75   Delete the first sentence of the third paragraph, and replace with "In the numerical model for bond-slip behaviour developed by Ingraffea *et al.* (1984), secondary radial cracking was considered the dominant mechanism in bond-slip."

Page 76   Third sentence after "E_c = elastic modulus;" insert "I_* = moment of inertia of the cracked section;".

Page 79   Delete the second sentence of the second paragraph, and replace with "Good correlation was obtained with results of reinforced concrete test specimens."

Page 90   Delete the third sentence of the first paragraph, and replace with "Ford, Chang and Breen (1981a) have also used a value of 0.95 for the ratio of

concrete strength in a member of a horizontally cast beam or frame to the mean strength of a plain concrete cylinder test."

Page 91   Delete the second sentence of the first paragraph, and replace with "For the present study, the strength determined by the splitting test was chosen because it was considered to give the best estimate of tensile strength in a beam or frame subjected to in-plane bending actions."

Page 92   Delete the first sentence of the fourth paragraph, and replace with "Similar to the model developed by Gupta and Maestrini (1990), the tension softening portion is linear."

Page 92   Delete the first sentence of the fifth paragraph, and replace with "The strain at which tension stiffening is no longer effective is given by $\gamma_t \varepsilon_{cr}$."

Page 95   Delete the third sentence of the first paragraph, and replace with "Although this may occur, the proposed model has been modified, as in Figure 3.22, to include a discontinuity at a strain value of $10\varepsilon_{cr}$ to give better correlation."

Page 105   Line 1, "beams" to read "beam".

Page 110   Line 5, "representive" to read "representative".

Page 110   Line 6, "3.40" to read "3.39".

Page 110   Line 12, "3.41" to read "3.40".

Page 110   In the first sentence of the fourth paragraph, insert "within the span" after "... moment and curvature".

Page 115   Line 2, delete "its effect" and replace with "any influence".

Page 129   Delete the third sentence of the first paragraph, and replace with "However, as noted by Somerville and Taylor (1972), at very low percentages of steel, tensile concrete tends to contribute mainly to overall strength."

Page 133   In the second sentence, delete "... delay the formation of diagonal cracks" and replace with "... resist internal stresses as cracks developed."

Page 135   Delete the second sentence of the fifth paragraph, and replace with "It is also worth considering the performance of joggled splices within column lengths."

Page 152   Line 16, delete "not".

Page 240   In the first sentence of the second paragraph, insert "are" after "strength" and before "prediction".

Page 241   Delete the third sentence of the third paragraph, and replace with "In the calculation of N_{uot}, any contribution of the tensile concrete is ignored."

Page 242   Line 7, delete ", and is done so".

Page 255   Line 2, "aslo" to read "also".

Page 288   Delete the third sentence of the second paragraph.